T-cell Checkpoint Pathways Modulate Cell Cycle and Steroid Resistance in T-cell Acute Lymphoblastic Leukaemia

Yuzhe Shi

Student No: 150182377

Thesis submitted to the Faculty of Medical Sciences

In partial fulfilment of the requirements for the degree of

Doctor of Philosophy

2019

Supervisor: Dr. Frederik W van Delft,

Dr. Anja Krippner-Heidenreich

Prof. Olaf Heidenreich

Wolfson Childhood Cancer Research Centre, Northern Institute for Cancer research, Newcastle University, NE1 7RU, United Kingdom

Abstract

T-cell Acute Lymphoblastic Leukaemia (T-ALL) results from the malignant transformation of immature T cells with hallmarks of differentiation blockage and expansive proliferation. The checkpoints during T-cell development are provided by the pre-T-Cell Receptor (pTCR) for β-selection and T-Cell Receptor (TCR) for positive and negative selection. Recurrent gene lesions in proximity to pTCR/TCR are found in T-ALL, such as *NOTCH1, FBXW7* and *PTEN*. Kinases of the pre-B-cell receptor signalling have been validated as drug targets in B-ALL. Whether any critical components of T-cell checkpoint pathways, such as Lymphocyte-specific non-receptor tyrosine Kinase (LCK), play a comparable role in T-ALL remains unclear. A targeted shRNA screen against central components of the pTCR/TCR signalling complex in T-ALL cell lines *in vitro* and primary cells *in vivo* identified an essential role for LCK in cell proliferation and leukaemia propagation. Knockdown of LCK in the cell lines SUPT1, CUTLL1 and MOLT4 revealed a substantial growth defect over time. This was further validated in a competitive assay using MOLT4 *in vivo*, in which control cells outcompeted LCK knockdown cells in mouse bone marrow, spleen and liver. Phenotypically, knockdown or inhibition of LCK by dasatinib (DAS) impaired cell proliferation by inducing G_0/G_1 arrest in T-ALL cell lines and patient-derived xenografts (PDXs) with only trivial induction of apoptosis. The sensitivity of T-ALL cell lines to DAS significantly correlated with LCK activation ($pY394^{LCK}$/LCK). Several cell lines and PDXs were glucocorticoid-resistant *in vitro*. Interestingly, T-ALL cells were re-sensitised to dexamethasone (DEX) after LCK knockdown. Correspondingly, DAS reinforced DEX-induced apoptosis. Drug matrix analyses of ten T-ALL cell lines and six PDXs revealed a significant enrichment of DEX/DAS synergy at clinically relevant concentrations. A murine phase Ⅱ-like clinical trial of ten T-ALL PDXs confirmed that DEX/DAS significantly impaired leukaemia engraftment. Engraftment of human leukaemia cells in spleen, bone marrow, and liver was substantially decreased in the DEX/DAS group compared with control or single-drug therapy. In addition, DEX/DAS significantly reduced CNS infiltration of leukaemia cells. The presented research outcomes highlight the crucial role of LCK in T-ALL proliferation and propagation. LCK inhibitor DAS, in conjunction with DEX, reverses steroid resistance and significantly reduces leukaemia propagation *in vivo*. The DEX/DAS combination might provide a novel therapeutic strategy for refractory and relapsed T-ALL patients.

Acknowledgement

I would like to give my sincere thanks to my supervisors, Frederik van Delft, Anja Krippner-Heidenreich and Olaf Heidenreich for teaching me the most valuable traits of being a scientist – curiosity and integrity. Frederik came up with the hypothesis of my project and helped to direct the path of how this project moved forward. He appreciated my efforts and supported me in every circumstance. He also devoted a lot of time to read my thesis and improve my academic writing. During my PhD, Anja was always there to help me since the 1st day of my arrival in Newcastle. She taught me research techniques without any conservation and helped me to develop connections to others. She also encouraged me to raise questions and participate in public discussions. Many thanks to Olaf for reassuring me when part of my project was published first by others. He inspired me to perform the *in vivo* study in a state-of-art phase Ⅱ-like murine clinical trial. From him, I learned that I need to keep updated of the latest breakthrough and be brave of taking risks sometimes. All these supports and encouragements from my supervisors helped me to build my self-confidence as a scientist and inspired me to pursue an academic career that one day I could become one of them.

I want to acknowledge people who contributed directly to my projects, Melanie Beckett and Helen Blair, as they taught me mouse regulations/techniques and helped me to process almost every mouse in this study. Melanie spent enormous time with me in CBC to give me moral support. Thanks to Ricky Tirtakusuma for always being a good lab buddy for me, Sirintra Nakjang, Amir Enshaei, and Martina Finetti for helping me doing bioinformatics analysis. Further thanks to all the OTH group members, particularly, Asmida Isa, Milene Dalmina, Katarzyna Szoltysek and Hasan Issa who helped me in the day-to-day lab and shared positivity during tea breaks to cheer me up. They taught me how to collaborate and work in groups.

A huge thank you to China Scholarship Council for providing the full scholarship for my PhD study. Finally, I would like to thank my parents for their love and support throughout the years. Special thanks to my husband Kimi for always supporting me in my career goals and being a shoulder to cry on whenever needed.

Contents

List of Figures

List of Tables

List of abbreviations

Abbreviation	Full Term
3AC	3-α-aminocholestane
ABL1	ABL proto-oncogene 1, non-receptor tyrosine kinase
ACTR	nuclear receptor coactivator 3
AF10	MLLT10 histone lysine methyltransferase DOT1L cofactor
AKT	AKT serine/threonine kinase 1
AML	acute myeloid leukaemia
ATM	ATM serine/threonine kinase
BACH2	BTB domain and CNC homolog 2
BAG-1	BCL2 associated athanogene 1
B-ALL	B-cell acute lymphoblastic leukaemia
BCL11B	BAF chromatin remodeling complex subunit BCL11B
BCL2	BCL2 apoptosis regulator
Bcl-XL	Bcl2-like 1
BCR	BCR activator of RhoGEF and GTPase
BHLH	basic helix loop-helix
BIM	BCL2 like 11
BLK	BLK proto-oncogene, Src family tyrosine kinase
BLNK	B cell linker
BTK	Bruton tyrosine kinase
CALM	phosphatidylinositol binding clathrin assembly protein
CASP1	caspase 1
CBL	Cbl proto-oncogene
CBP	phosphoprotein membrane anchor with glycosphingolipid microdomains 1
CCND3	cyclin D3
CD19	CD19 molecule
CD2	CD2 molecule
CD44	CD44 molecule (Indian blood group)
CDKN2A	cyclin dependent kinase inhibitor 2A
CLL	chronic lymphocytic leukaemia
CML	chronic myeloid leukaemia
c-MYC	MYC proto-oncogene, bHLH transcription factor
CNS	central nervous system
CREB	cAMP responsive element binding protein
CREBBP	CREB binding protein
CSK	C-terminal Src kinase
CSL	RBPJ, recombination signal binding protein for immunoglobulin kappa J region

CTCF	CCCTC-binding factor
DEX	Dexamethasone
DL4	delta-like 4
DN	double negative
DNM2	dynamin 2
DP	double positive
EED	embryonic ectoderm development
EEF1A	eukaryotic translation elongation factor 1 alpha 1
EFS	event-free survival
EML1	EMAP like 1
ENL	MLLT1 super elongation complex subunit
ERBB4	erb-b2 receptor tyrosine kinase 4
ERG	ETS transcription factor ERG
ERK	mitogen-activated protein kinase 1
ETP	early T-cell precursor leukaemia
ETV6	ETS variant 6
EZH2	enhancer of zeste 2 polycomb repressive complex 2 subunit
FBXW7	F-box and WD repeat domain containing 7
FGR	FGR proto-oncogene, Src family tyrosine kinase
FKBP-51/52	FKBP prolyl isomerase 4
FOXO1	forkhead box O1
FOXP1	forkhead box P1
FYN	FYN proto-oncogene, Src family tyrosine kinase
GATA3	GATA binding protein 3
GCs	glucocorticoids
GM-CSF	granulocyte macrophage-colony stimulating factor
GR	Glucocorticoid Receptor
GREs	Glucocorticoid Responsive Elements
GSIs	Gamma-secretase inhibitors
GSK3B	glycogen synthase kinase 3 beta
H3K27	histone 3 lysine 27
HATs	histone acetyltransferases
HCK	HCK proto-oncogene, Src family tyrosine kinase
HD	heterodimerisation domain
HDAC	Histone deacetylases
HES1	hes family bHLH transcription factor 1
HOP	HOP homeobox
HOX	homeobox
HOXA	homeobox A cluster
HOXB	homeobox B cluster
HOXC	homeobox C cluster

HOXD	homeobox D cluster
HRAS	HRas proto-oncogene, GTPase
HSC	Hematopoietic stem cells
Hsp90	heat shock protein 90
HSPC	hematopoietic stem and progenitor cells
ICN	NOTCH intracellular domain
IFN-α	interferon alpha 1
IGF1R	insulin like growth factor 1 receptor
IKZF1	IKAROS family zinc finger 1
IL7	interleukin 7
IL7R	interleukin 7 receptor
INPP5D	inositol polyphosphate-5-phosphatase D
IRF4	interferon regulatory factor 4
ITAMs	immunoreceptor tyrosine-based activation motifs
ITK	IL2 inducible T cell kinase
IκBα	NFKB inhibitor alpha
JAK1	Janus kinase 1
JAK3	Janus kinase 3
JMML	juvenile myelomonocytic leukaemia
KDM6A	lysine demethylase 6A
KLF13	Kruppel like factor 13
KRAS	KRAS proto-oncogene, GTPase
LAIR1	leukocyte associated immunoglobulin like receptor 1
LAT	linker for activation of T cells
LCK	LCK proto-oncogene, Src family tyrosine kinase
LIM	PDZ and LIM domain 5
LMO	LIM only domain
LMO1	LIM domain only 1
LMO2	LIM domain only 2
LMO3	LIM domain only 3
LMO4	LIM domain only 4
lncRNA	long non-coding RNAs
LRP	LDL receptor related protein
LYL1	LYL1 basic helix-loop-helix family member
LYN	LYN proto-oncogene, Src family tyrosine kinase
MCL1	MCL1 apoptosis regulator, BCL2 family member
MEK	mitogen-activated protein kinase kinase 7
MHC I	major histocompatibility complex I
miRNA	small non-coding RNA molecules of about 22 nucleotides
MLL	lysine methyltransferase 2A
mTOR	mechanistic target of rapamycin kinase

MYB	MYB proto-oncogene, transcription factor
MYC	MYC proto-oncogene, bHLH transcription factor
NCOA1	nuclear receptor coactivator 1
NF1	neurofibromin 1
NLRP3	NLR family pyrin domain containing 3
NPC	nuclear pore complex
NR3C1	nuclear receptor subfamily 3 group C member 1
NRAS	NRAS proto-oncogene, GTPase
NUP214	nucleoporin 214
P/CAF	lysine acetyltransferase
p300/CBP	E1A binding protein p300/CREBBP, CREB-binding protein
PARP1	poly(ADP-ribose) polymerase 1
PDCD4	programmed cell death 4
PECAM1	platelet and endothelial cell adhesion molecule 1
PEST	polypeptide enriched in proline, glutamate, serine and threonine domain
PHF6	PHD finger protein 6
PI	Propidium Iodide
PI3K	phosphatidylinositol-4,5-bisphosphate 3-kinase
PI3KAP1	Phosphoinositide-3-kinase adaptor protein 1
PIP3	phosphatidylinositol-3,4,5-trisphosphate
PLCγ2	phospholipase C gamma 2
PRC2	polycomb-repressive complex 2
pTCR	pre T-Cell Receptor
PTEN	phosphatase and tensin homolog
PTPN11	protein tyrosine phosphatase non-receptor type 11
PTPN2	protein tyrosine phosphatase non-receptor type 2
PTPN6	protein tyrosine phosphatase non-receptor type 6
PTPRC	protein tyrosine phosphatase receptor type C
RAG1/2	recombination activating 1/2
RUNX1	runt related transcription factor 1
SAHM1	
SERCA	Sarco/endoplasmic reticulum calcium ATPase
SFKs	Src family kinases
SH2	Src Homology 3
SH3	Src Homology 2
SLC	Surrogate Light Chain
SLP76	lymphocyte cytosolic protein 2
SP	single positive
SRC	SRC proto-oncogene, non-receptor tyrosine kinase
STAT5	signal transducer and activator of transcription 5

STIL	STIL centriolar assembly protein
SUZ12	SUZ12 polycomb repressive complex 2 subunit
SYK	spleen associated tyrosine kinase
TAL	transaldolase 1
TAL1	TAL bHLH transcription factor 1, erythroid differentiation factor
T-ALL	T-cell acute lymphoblastic leukaemia
TCF12	transcription factor 12
TCF3	transcription factor 3
TCF3	transcription factor 3
TCR	T cell receptor
TCRA	T cell receptor alpha locus
TCRB	T cell receptor beta locus
TKI	tyrosine kinase inhibitor
TLX1	T cell leukaemia homeobox 1
TLX3	T cell leukaemia homeobox 3
TNFα	tumour necrosis factor
TYK2	tyrosine kinase 2
UBTF1	upstream binding transcription factor
VCP	valosin-containing protein
YES	YES proto-oncogene 1, Src family tyrosine kinase
ZAP70	zeta chain of T cell receptor associated protein kinase 70
ZEB2	zinc finger E-box binding homeobox 2

Chapter 1

Introduction

1 T-cell Development

1.1.1 Origins of Thymus-setting Progenitors

The classic haematopoiesis model proposes that all blood cells arise from haematopoietic stem cells (HSC) ($Lin^{-}SCA1^{+}KIT^{hi}FLT3^{-}$) which situate in the bone marrow with self-renewal and multipotent ability. A step further in differentiation from HSC generates multipotential progenitors (MPP) ($Lin^{-}SCA1^{+}KIT^{hi}FLT3^{+}$) which remain multipotent but lack self-renewal capacity. MMP in turn generate common lymphoid progenitors (CLPs) ($Lin^{-}SCA1^{low}KIT^{low}IL\text{-}7R\alpha^{hi}FLT3^{hi}$) and common myeloid progenitors (CMPs) ($Lin^{-}IL\text{-}7R\alpha^{-}SCA1^{-}KIT^{hi}Fc\gamma R^{low}CD34^{+}$). In this classic hierarchical model, all lymphocytes are derived from CLPs, including T-cell progenitors in the thymus (Rothenberg and Taghon, 2005).

The thymus has been known to be crucially important for T-cell development since 1967 (Miller and Osoba, 1967). This review concluded leukocytes were produced from thymus and migrated to lymph nodes and peripheral blood. However, adult thymus cannot support progenitors to self-renew in the long-term. Mice post-irradiation (thymus was shielded from irradiation) receiving a bone marrow transplantation showed that equilibration between thymic progenitors and bone marrow chimerism only lasted for six to eight weeks (Scollay et al., 1986). Constant supply of T-cell progenitors from the bone marrow to the thymus is indispensable for T-cell development (Frey et al., 1992).

However, the precise origin and characterisation of thymus-setting progenitors (TSP) remains incomplete. Several studies have provided new evidence that TSPs originate from not only CLPs, but also HSCs and MPPs (Bhandoola and Sambandam, 2006) (Figure 1).

CLPs were originally considered as precursors to B-, T- and NK (natural killer) cell lineages (Kondo et al., 1997). The understanding of CLPs has increased after identification of the crucial role of Notch1 in T-cell development. Notch1 is a cell surface transmembrane receptor that controls cell communication and cell fate (Lai, 2004). Overexpression of constitutively activated Notch1 in mice disrupted B-cell development and led to CLPs developing to DP (double positive) thymocytes in the bone marrow (Pui et al., 1999). On the contrary, inactivation of Notch1 resulted in a T-cell development defect at early stages as well as increased B-cell lineage cells in the

thymus (Radtke et al., 1999). The presence or absence of Notch1 controls CLP differentiation towards T-lineage or B-lineage. A subset of pro/pre-B cells has been shown to have the differentiation potential towards T cells by efficiently migrating to the thymus when placed in the bloodstream. They express $B220^{+}CD19^{-}$IL-7R$\alpha^{+}KIT^{-/low}$, and are labelled CLP-2 (Martin et al., 2003). With the development of single-cell assays, the concept has been challenged that each CLP has equal potential to differentiate to the B, T, NK or DC (dendritic cell) lineage. Studies in the murine foetal liver have shown lack of evidence of CLPs restrained in lymphoid lineage only (Katsura, 2002) and the loss of B-cell lineage potential of CLPs before seeding to the thymus (Kawamoto et al., 2000). Therefore, the commitment of progenitors to T cell lineage may occur independently of B cell lineage, thus other populations in the bone marrow may have the capacity to seed in the thymus and commit to the T cell lineage (Figure 1).

Direct intrathymic injection in mice was used for comparing the efficiency of T-cell production by different bone marrow progenitors. DP thymocyte production was maintained more than 4 weeks after intrathymic injection of HSCs and MPPs whilst thymopoiesis by CLPs only lasted for less than 4 weeks, suggesting HSCs and MPPs were more efficient than CLPs (Allman et al., 2003). Another CLP-independent source of TSPs are a rare population of circulating progenitors with LSK phenotype ($Lin^{-}SCA1^{+}KIT^{hi}$) in blood (HSCs and MPPs). On the contrary, CLPs could not be found in the blood, suggesting that CLPs might not be the physiological T cell progenitors because of its absence in the circulation (Schwarz and Bhandoola, 2004).

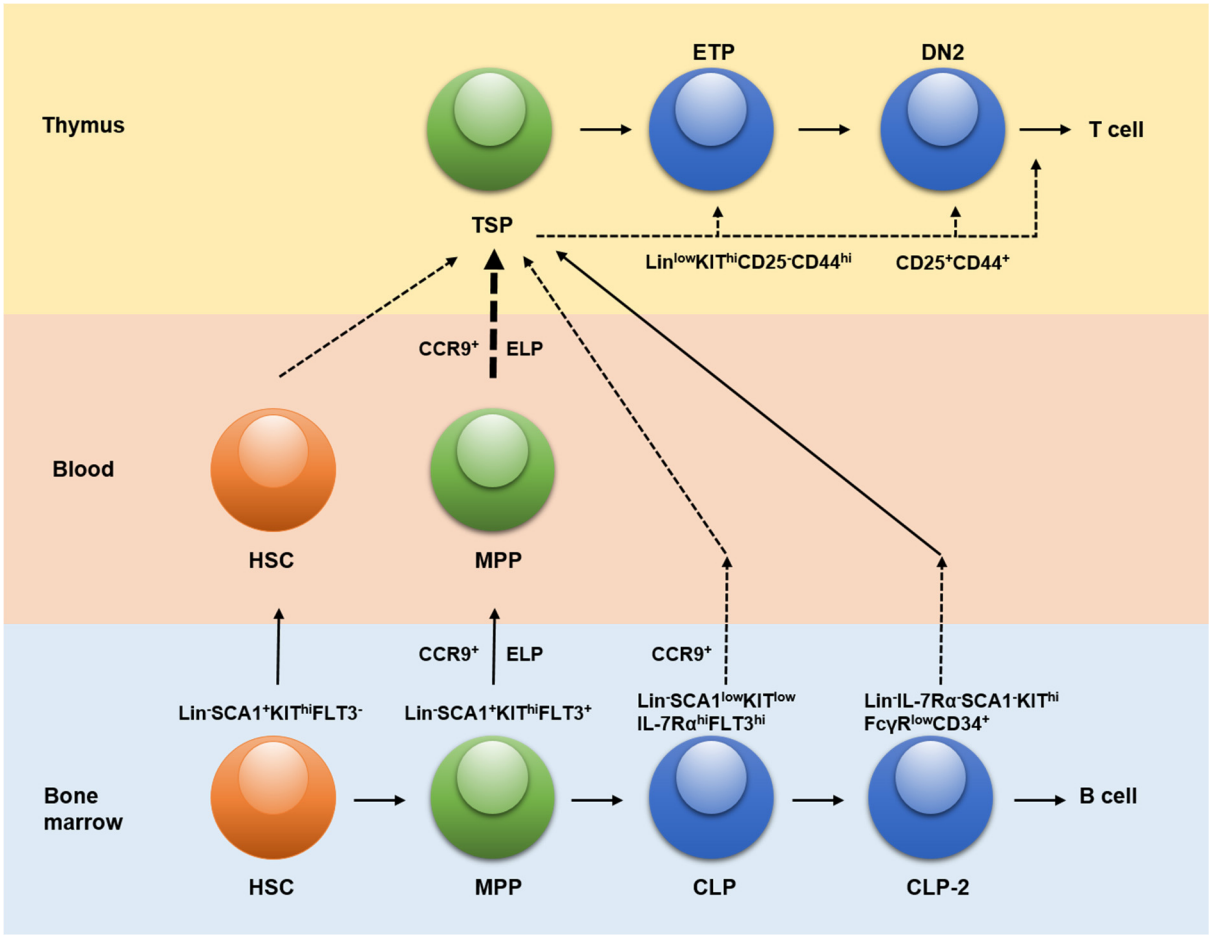

Figure 1. Origins of thymic-setting progenitors. In the bone marrow, haematopoietic stem cells (HSC) differentiate into mutipotential progenitors (MPP), common lymphoid progenitors (CLP and CLP-2). B-cell development occurs in the bone marrow. The cell surface markers of each subset are shown in the diagram; Lin (Lineage), SCA1 (stem-cell antigen 1), KIT (CD117, mast/stem cell growth factor receptor), FLT3 (fms-related tyrosine kinase 3), IL-7Rα (interleukin 7 receptor α), FcγR (fragment C gamma receptor) and CD34 (cluster differentiation 34). In the classic haematopoiesis model, CLP and CLP-2 seed in the thymus and become thymus-settling progenitors (TSP). However, CLP-independent routes to T cells also exist. The HSC and MPP cells can circulate in the blood and seed in the thymus. A subset of MPPs express RAG1/2 termed as early lymphoid progenitors (ELP). Some MPPs also express CC-chemokine receptor 9 (CCR9) and can be the origin of TSP. In the thymus, TSP cells undergo differentiation into early T-cell progenitors (ETP) and double negative (DN) thymocytes. ETPs are very similar to DN1 (CD25^{-}CD44^{+}) and differentiate into DN2 stage (CD25^{+}CD44^{+}). The complete T-cell development continues in the thymus and will be discussed in the next section. Dotted/dashed arrows represent less well characterised trafficking pathways; solid arrows depict clearly defined origins of TSP. The diagram was modified from (Bhandoola and Sambandam, 2006).

Bone marrow LSK progenitors were also investigated to establish if they could seed in the thymus. As previously described, HSCs were efficient in thymopoiesis when direct injected to the thymus (Allman et al., 2003). However, intravenous transfer of HSC subsets into irradiated mice and subsequent re-transplantation of thymic cells in secondary recipients demonstrated that only T, NKT, NK and B-lineages, but not myeloid-lineage, can be generated in the secondary transplanted mice, suggesting that HSCs either failed to self-renewal once settled in the thymus or HSCs could not seed in the thymus efficiently (Mori et al., 2001). Characterisation of MMPs in bone marrow showed low levels of IL-7Rα (interleukin 7 receptor α) mRNA expression (Adolfsson et al., 2005), and a subset of MMPs expressing RAG1/2 (recombination activating 1/2) were found as early lymphoid progenitors (ELP) (Igarashi et al., 2002). Reported candidate genes expressed by MMPs that might direct progenitors settling in the thymus and expansion after thymic seeding are CCR9 (CC-chemokine receptor 9) (Benz and Bleul, 2005), CCR7 (Krueger et al., 2010), IL-7Rα and FLT3 (fms-related tyrosine kinase 3) (Sambandam et al., 2005).

TSPs settle down in the thymus and develop to early T-cell progenitors (ETP), which contain lineage potentials of B-cell, T-cell, NK-cell, myeloid-cell and DC (King et al., 2002). ETPs are defined minimally as $Lin^{low}CD25^{-}KIT^{hi}$ and found to compose 0.01% of murine thymus (Bhandoola et al., 2007). The surface protein CD4 was found on more than 50% of ETPs. Other lineage markers including CD8 were also found in ETPs at low surface expression levels (Michie et al., 1998).

1.1.2 T-cell Development in the Thymus

In the thymus, ETPs differentiate into CD4 and CD8 double negative (DN) cells, double positive (DP) and single-positive (SP) cells. The murine DN cells are divided into four stages by differentially expressing CD25 and CD44 (DN1 ($CD25^{-}$, $CD44^{+}$), DN2 ($CD25^{+}$, $CD44^{+}$), DN3 ($CD25^{+}$, $CD44^{-}$), DN4 ($CD25^{-}$, $CD44^{-}$)). Although ETPs express CD4 and other lineage surface proteins at certain levels, they are CD25 negative and CD44 highly expressing cells, and are considered a fraction of DN1 cells (c-Kit^{hi} DN1 cells) (Sambandam et al., 2005).

Transcription factors

The T-cell specification process relies on expression of transcription factors such as GATA3 (GATA binding protein 3), TCF-1 (T-cell factor 1, also known as T-cell specific transcription factor 7, TCF7) and BCL11B (BAF chromatin remodelling complex subunit).

TCF-1 and GATA3 are rate-limiting factors that regulate early-T cell development (Ting et al., 1996; Verbeek et al., 1995). TCF-1 is induced by Notch1 signalling and it increases T-cell specification transcription factors such as GATA3, BCL11B and TCR (T-cell receptor) components, such as LCK (lymphocyte-specific non-receptor tyrosine kinase), LAT (linker for activation of T cells), CD3γ, and CD3δ (Weber et al., 2011). GATA3 recruits and regulates different genomic sites depending on T-cell development stages (Wei et al., 2011). For example, GATA3 is upregulated in DN1 stage and occupies binding sites of genes associated with stem cells and progenitors. GATA3 dissociates from these sites during T-cell commitment (Zhang et al., 2012). GATA3 knockout embryonic stem (ES) cells were used to investigate its function in T-cell development. Without GATA3, early thymocyte development was completely blocked in contrast to normal development of mature erythroid, myelomonocytic cells and B cells (Ting et al., 1996). It seems that GATA3 regulates T-cell development with a dose-dependent effect. In the earliest ETP stage, lack of GATA3 showed deficiency in development (Hosoya et al., 2009). However, overexpression of GATA3 in bone marrow or thymocyte progenitors did not enhance T-cell development but activated non-T programs (Taghon et al., 2007).

Early development arrest at the DN2-DN3 stages was shown after BCL11B inactivation (Li et al., 2010a). BCL11B is involved in β-selection of $\alpha\beta$ T cells (Wakabayashi et al., 2003) but not $\gamma\delta$ T cells. Deletion of BCL11B disabled T-cell lineage but switched differentiation to NK-like cells (Li et al., 2010b). During DN2 to DN3 transition, multiple genes associated with stem cells or progenitors are downregulated whilst genes involved in T-cell commitment are upregulated as governed by BCL11B (Li et al., 2010a).

Signalling pathway

Notch1 and IL-7 receptor signalling control T cell lineage commitment and development in early T-cells (Radtke et al., 1999).

Notch1 is a cell surface transmembrane receptor that controls cell communication and cell fate through mediating cell proliferation, survival, metabolism and differentiation in all animal species (Lai, 2004). For T-cell development, the generation of ETPs and subsequent differentiation of DN cells requires Notch signalling. An *in vitro* stromal-free model showed T-cell commitment can be initiated by Notch1 and cytokines alone (Ikawa et al., 2010). Lack of NOTCH1 leads to T-cell development arrest at the DP stage (Radtke et al., 1999).

Four Notch receptors (Notch1/2/3/4) have been described as well as several ligands, namely Jagged1/2 (Jag1/2) and Delta 1/3/4 (Dll1/3/4). Studies have shown that Notch ligands are provided by the thymus microenvironment, such as Dll1, which is expressed in thymic blood vessels, Dll4 is secreted from thymic epithelial cells (TECs) in the subcapsular and outer cortical regions and Jag1/2 are limited to thymic medulla and inner cortex (Gonzalez-Garcia et al., 2012). The intracellular Notch domain (ICN) is cleaved by ADAM (a disintegrin and metalloprotease) and γ-secretase after ligand activation. It translocates to the nucleus and transforms the transcriptional repressor CSL (RBPJ, recombining binding protein suppressor of hairless) to become an activator by recruiting p300/CBP (E1A binding protein p300/CREBBP, CREB-binding protein) and MAML1 (mastermind-like 1) (Kopan and Ilagan, 2009). The bHLH protein Hey and Hes, CD25, pTα, c-Myc (myc avian myelocytomatosis viral oncogene homolog), cyclin D1, p21Waf and IL7-Rα *are* direct targets of Notch (Reizis and Leder, 2002).

Notch1 signalling controls T-cell development prominently via enhancing T-cell specification and expansion (De Smedt et al., 2002; Garcia-Peydro et al., 2006). In the hybrid human-mouse foetal thymus organ culture (FTOC) model, inhibition of Notch1 signalling by an inhibitor at various concentrations demonstrated that in human thymopoiesis, enhancing Notch1 signalling gradually suppresses B, myeloid/DC and NK cell lineages (De Smedt et al., 2005). The cellular expansion of T-cell progenitors governed by Notch1 signalling is via IL-7R expression (Gonzalez-Garcia et al., 2009). Notch1 has been shown to replace the transcription factor PU.1 (SPI1, Spi-1 proto

oncogene) at the *Il7ra* promoter in CLP thereby driving the expression of IL-7Rα (Anderson et al., 2002).

IL-7 and its receptor IL-7R are essential for T-cell development and homoeostasis. IL-7R is composed of the common cytokine receptor γ (γc) and the IL-7 specific α chain. IL-7 stimulation results in heterodimerisation of IL-7Rα and γc and subsequent IL-7R signalling pathway. Through JAK/STAT, PI3K (phosphatidylinositol 3-kinase), and MAPK downstream pathways, IL7-R signalling activates Bcl-2, Mcl-1, Ccnd1 (cyclin D1) and c-Myc to induce cell proliferation and promote T-cell differentiation (Li et al., 2006).

IL-7R expression is dynamically regulated through the process of T-cell development. It is up-regulated in ETP stage and grossly increased until DN2 stage. IL-7R is critical for DN2 progenitors to survive and undergo expansion in the intrathymic pool (Akashi et al., 1998). The TCRγδ lineage T cells are controlled by IL-7R signalling to let the TCRγ locus undergo rearrangement at the DN2 stage (Durum et al., 1998). In concordance with this, higher IL-7R expression in DN2 cells results in biased differentiation to the TCRγδ T cells (Kang et al., 2001). The expression of IL-7R needs to be terminated at the DN3 stage to allow the β-selection process which is controlled by the pre-T cell Receptor (pTCR). Reduction of IL-7R signalling is also required for the upregulation of transcription factor BCL11B which drives the complete αβ T-cell development (Li et al., 2010a). Later, after the SP stage, IL7-R is restored on the cell surface to support homeostatic proliferation of matured $CD4^+$ or $CD8^+$ cells in the peripheral (Schluns et al., 2000).

1.1.3 T-cell Checkpoint Pathways in T-cell Development

In an *in vitro* human thymopoiesis model, Notch1 and IL-7R signalling termination is required for the completion of αβ T-cell development (Li et al., 2010a). At the DN3 stage, Notch1 signalling induces *pTα* expression via the transcriptional activator of ICN/CSL/MAML1 binding to the *PTCRA* enhancer (Reizis and Leder, 2002). pTα dimerises with a successfully rearranged TCRβ chain. Together with other CD3 molecules they form a pTCR (pre-T cell receptor) complex on the cell surface. This complex is critical for the β-selection checkpoint at DN3 stage which only allows cells with the successful expression of pTCR to proliferate and survive, whereas thymocytes without pTCR expression will undergo cell death. After β-selection, cells will further differentiate to the DN4 stage (Figure 2).

The pTCR signalling promotes cell cycle progression, proliferation, survival and allelic exclusion of β chain rearrangement. Specifically, the pTCR complex consists of disulfide-linked pTα and TCRβ, associated with two heterodimers, CD3ε/CD3γ and CD3ε/CD3δ. This complex further associates with CD3ζ (von Boehmer and Fehling, 1997). All these components, except the pTCRα chain, are shared with the TCR. At the DP stage, *TCRα* is fully rearranged and expressed. This encourages the formation of the mature TCR, to replace pTCR on the cell surface, upon which selected cells gain proliferative and survival advantages (Aifantis et al., 2008). The TCR complex plays a central role in adaptive immunity through signalling processes that dictate T cell fate during late development and upon exposure to antigen.

The only structural difference between TCR and pTCR is the α-chain component, TCRα or pTCRα respectively. These two components are encoded by two distinct genes. The human *PTCRA* is located on chromosome 6, has four mRNA isoforms, of which three isoforms are predicted to result in pTα protein expression. On the contrary, the human *TCRα* locus is located on chromosome 14q11.2 (including the variable, joining and constant regions).

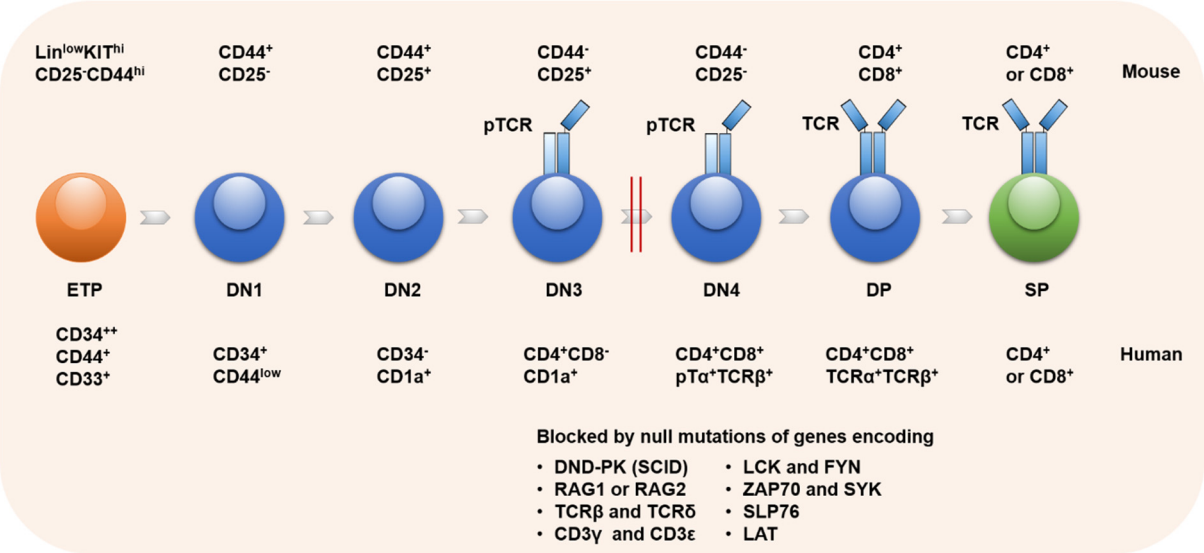

Figure 2. Developmental stages of T-cells in the thymus. The developmental stages from HSC, double negative (DN), double positive (DP) to single positive (SP) cells are shown. The cell surface markers including pTCR and TCR of each development stage of mouse and human are shown on the top and bottom respectively. At the DN3 stage, the pTCR (pre-T-cell receptor) is formed with a correctly rearranged TCRβ chain, pTα chain, and CD3 molecules. This receptor is essential for β-selection in T cell development, which provides the pro-survival and differentiation signals to develop into DN3 and DN4 cells. In the DP development stage, the rearranged TCRα chain replaces the pTα chain and forms a mature TCR (T-cell receptor). Thymocytes are positively selected when the TCR has modest affinity for MHC molecules, and negatively selected when the TCR is strongly activated by self-MHCs in the thymus. T-cell development is entirely or partially blocked when T-cell specification genes are depleted, such as RAG1/2, TCRβ and δ, CD3γ and CD3ε, LCK and FYN, ZAP70 and SYK, SLP76 as well as LAT. The diagram was modified from (von Boehmer, 2005) and (Gonzalez-Garcia et al., 2012). Overexpression of wild-type Lck or a constitutively activated mutant Lck^{Y505F} induces tumorigenesis in mouse models (Abraham et al., 1991).

The *PTCRA* gene encodes for a single-pass transmembrane protein, which is only expressed in immature T cells. Previous studies demonstrated that the activation of pTCR is ligand independent in contrast to that of TCR (Yamasaki and Saito, 2007). The TCR is uniformly distributed on the cell membrane and re-locates to lipid rafts upon ligand binding (Schamel and Reth, 2007). However, the pTCR translocates autonomously into lipid rafts caused by the palmitoylation of juxtamembraneous cysteine residues (Saint-Ruf et al., 2000), where it forms oligomers and induces CD3 and LCK phosphorylation without any ligand stimulation. pTCR and TCR signalling share the same downstream pathways and activate similar transcription factors. Upon TCR stimulation, LCK phosphorylates CD3ζ subunits at ITAMs (immunoreceptor tyrosine-based activation motifs), where ZAP70 is recruited to the receptor complex and phosphorylated by LCK. After ZAP70 activation, it phosphorylates LAT resulting in the recruitment of SLP76 (SH2 domain-containing leukocyte protein of 76kDa), GADS (GRB2-related adaptor downstream of Shc), GRB2 (growth factor receptor-bound protein 2), ADAP (adhesion and degranulation promoting adaptor protein) and NCK1 (SH2/SH3 adaptor protein). These proteins form a microcluster which recruits and activates PLCγ1 (phospholipase Cγ1), ITK (IL-2-inducible T cell kinase) and VAV1 (vav guanine nucleotide exchange factor 1). PLCγ1 enhances the intracellular calcium flux by catalysing PtdIns(4,5)P2 to DAG (diacylglycerol) and InsP3 (inositol (1,4,5)-trisphosphate) which further activates RAS-RAF-ERK and Calcineurin-NFAT pathways (Figure 3).

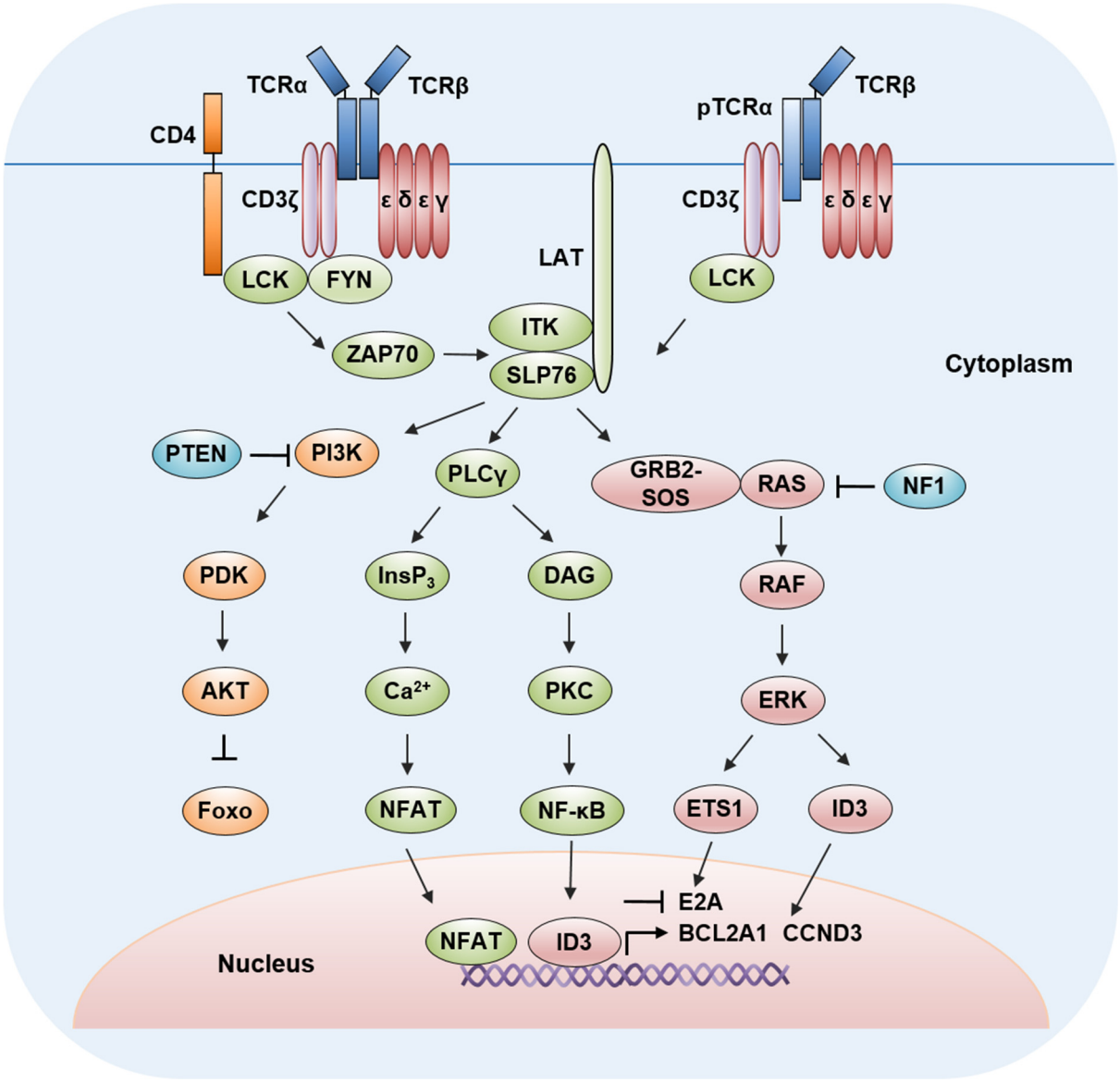

Figure 3. A schematic diagram of pTCR/TCR signalling. For the aim of this illustration, the pTCR/TCR pathways are drawn in the same cell. However, immature thymocytes only express pTCR, which is constitutively activated. Mature T cells express TCR on the cell surface. Upon binding with MHC molecules, CD4-associated LCK is recruited to the TCR complex, which subsequently activates CD3ζ, ZAP70 and downstream signalling. Both pTCR and TCR can activate the PI3K pathway, ERK pathway, PLCγ1-NFAT pathway and NF-κB signalling, resulting in gene expression which regulates T-cell survival, proliferation, and differentiation. This diagram is modified from (Brownlie and Zamoyska, 2013).

1.1.4 LCK

1.1.4.1 LCK Structure and Regulation

The crystal structure of LCK was discovered in 1994 (Eck et al., 1994; Sicheri and Kuriyan, 1997). *LCK* is located at chromosome 1 and encodes for a protein of 56 kDa. Like other Src family kinases (SFKs) (for example LYN, BLK, FGR, HCK, SRC, FYN, and YES), the N-terminal of LCK is myristoylated and palmitoylated allowing its localisation in the lipid rafts of the plasma membrane. The SH3 and SH2 domains regulate its interaction with other proteins. The kinase domain has an autophosphorylation function and the capacity to phosphorylate downstream targets, such as CD3ζ and ZAP70. It also contains a regulatory C-terminal tail. Two phosphorylation sites were identified to be essential in LCK kinase activity. The phosphor-tyrosine 394 moiety represents an active site in the kinase domain. The phosphor-tyrosine 505 functions as an inhibitory site for LCK regulation located in the C-terminal tail. A structurally closed conformation, that prevents LCK activation, can be created by intramolecular (SH2) and intermolecular (SH3) interactions (Figure 4).

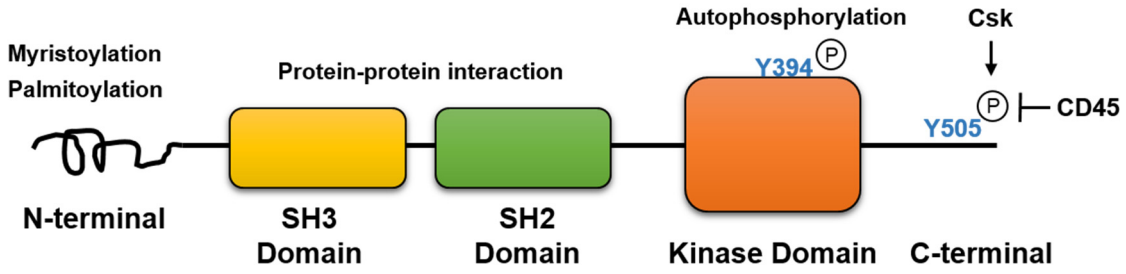

Figure 4. Schematic protein structure of LCK. The N-terminal of LCK can be myristoylated and palmitoylated. The SH3 and SH2 domains are for intramolecular and intermolecular interactions. An autophosphorylation site Y394 locates in the kinase domain. The C-terminal tail contains the Y505 regulatory site, whose phosphorylation is governed by Csk and CD45. The diagram was modified from (Ku et al., 2015).

In the absence of TCR stimulation, the Y505 residue of LCK is phosphorylated therefore inhibiting LCK activity. In contrast, in the case of pTCR or activated TCR signalling and association with CD4 or CD8, LCK is auto-phosphorylated at Y394 allowing the transmission of downstream signalling (Figure 5). CD45 (PTPRC, protein tyrosine phosphatase receptor type C) positively regulates LCK activity by removing

p-LCK^{Y505} (Hermiston et al., 2003), while CSK (C-terminal Src kinase) reduces LCK activity as it phosphorylates LCK^{Y505}.

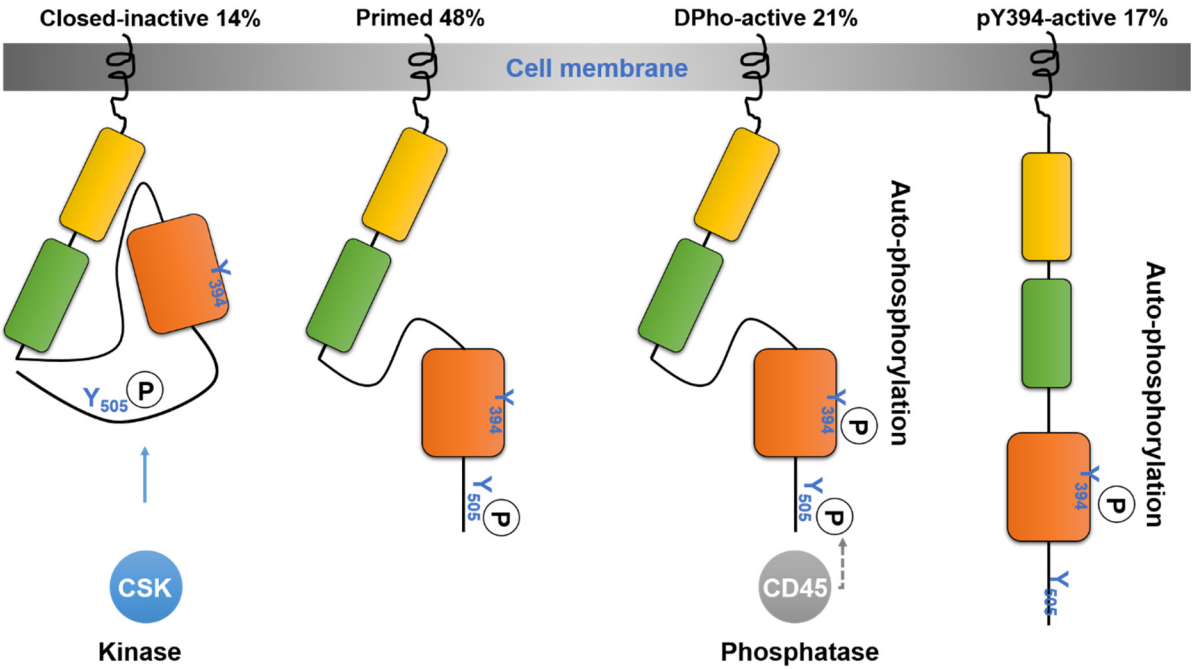

Figure 5. Phosphorylation and structure conformation determine LCK activity. The closed-inactive form of LCK accounts for 14% of total LCK in the cells, which is due to CSK phosphorylating Y505 and intramolecular interactions resulting in a closed formation. The primed LCK (48%) has an open confirmation to allow the kinase domain being released from intramolecular inhibition. However, it remains phosphorylated at Y505. The DPho-active status of LCK, of which both tyrosine sites (Y505 and Y394) are phosphorylated, accounts for 21%. The phosphatase CD45 dephosphorylates Y505 and enforces the full activation of LCK (pY394-activated LCK 17%). The diagram was modified from (Ku et al., 2015).

New evidence proposes that LCK is constitutively activated in T cells, and this activity is controlled both by phosphorylation at Y394 for activation and Y505 for inhibition, as well as structure conformation (Figure 5). CSK phosphorylating Y505^{LCK} and the intramolecular interactions result in a closed formation of LCK, which accounts for 14% of total LCK in the cells. The primed LCK (48%) has an open conformation to allow the kinase domain to be released from intramolecular inhibition. However, it remains phosphorylated at Y505. LCK autophosphorylates Y394 to activate itself. Therefore, after priming, both tyrosine sites are phosphorylated. This is so-called DPho-active status (21%). The phosphatase CD45 dephosphorylates Y505 and enforces the full activation of LCK (pY394-activated LCK 17%) (Nika et al., 2010).

CD45 is a plasma-membrane spanning phosphatase estimated to occupy 10% of T-cell surface (Thomas, 1989). Unlike CD45 in B lymphocytes, there are multiple splicing isoforms in T cells. Transgenic expression of a constitutively activated form of LCK (LCK^{Y505F}) into $CD45^{-/-}$ thymocytes can restore cell differentiation (Seavitt et al., 1999). There is also evidence showing that CD45 affects the activating tyrosine 394. In $CD45^{-/-}$ mice, LCK activity was enhanced and these cells had hyper-responsiveness to TCR stimulation. However, no spontaneous autoimmunity or lymphoproliferation was observed. This is partially due to activated SFKs recruiting other negative regulatory phosphatases to attenuate signalling strength, such as PTPN6 (SHP-1, protein tyrosine phosphatase non-receptor type 6), PTPN11 (SHP-2, protein tyrosine phosphatase non-receptor type 11), and INPP5D (SHIP-1, Inositol polyphosphate-5-phosphatase D). As a primary surface phosphatase expressed in nucleated hematopoietic cells, CD45 also dephosphorylates other SFKs, JAK1 (Janus kinase 1), JAK2, and TYK2 (tyrosine kinase 2) where they play critical roles in BCR (B-cell receptor), IL-3, and IFN-α signalling pathways (Huntington and Tarlinton, 2004).

In T cells, CSK phosphorylates the regulatory tyrosine 505 of LCK. It is constitutively associated with p-PAG1 (CBP, phosphoprotein membrane anchor with glycosphingolipid microdomains 1), a lipid raft-associated protein, which can be disrupted after TCR stimulation. In this case CSK is released from the plasma membrane, leaving LCK in sustained activation (Torgersen et al., 2001).

1.1.4.2 LCK Function in Normal T Cells

It seems that all stages of T-lymphocyte development and function involve LCK.

The T-cell specific SFK family members are LCK and FYN (FYN proto-oncogene), which are not fully redundant despite their structurally and functionally similarities. In fact, several unique features of LCK and FYN are observed in T cells, including differential expression in different development stages, signalling pathways, localisation and specific interaction with proteins. 1) A key feature of SFKs is the myristoylation of glycine and palmitoylation of cysteine at N-terminals, which allows SFKs to attach to plasma membranes (e.g. Lck) or centrosomal and mitotic structures (e.g. Fyn) (Ley et al., 1994). Increasing expression of lipid raft-associated Lck, rather than non-raft associated Lck, ameliorates Fyn activation (Filipp et al., 2004). 2) pTCR signalling is shown to be only affected in Lck-deficient mice, rather than Fyn-deficient mice, resulting in a T-cell differentiation block at the DN3 stage and grossly reduced thymic subpopulations (Appleby et al., 1992; Molina et al., 1992; Stein et al., 1992). Notably, in *Lck*$^{-/-}$ mice, it seems that Fyn could substitute Lck to generate DP cells before the age of 2 weeks. However, thymocytes failed to undergo expansion and failed to correctly create TCRβ rearrangements and CD5 expression in the time of more than 2 weeks (Molina et al., 1998). On the contrary, the thymocyte development in Fyn$^{-/-}$ mice is relatively healthy, indicating the essentiality of Lck in pTCR signalling. The N-terminal domains, rather than the kinase domains, highlight the essential role of Lck. This is supported by experiments where artificially expressed Fyn with Lck N-terminal sequences could restore thymocyte development. This is not the case when the N-terminal residue of Lck is replaced with Fyn N-terminal sequences (Lin et al., 2000). Moreover, a dominant negative (DN) Lck could diminish pTCR signalling, but Fyn DN mutants failed to do so (Cooke et al., 1991; Levin et al., 1993). 3) By using an *Lck*-doxycycline-inducible (*Lck*^{ind}) background and *Lck*$^{-/-}$ and/or *Fyn*$^{-/-}$ mouse models, Seddon and Zamoyska found that both Lck and Fyn are required for the survival of peripheral T cells. However, after withdrawing doxycycline which would stop *Lck*^{ind} (inducible LCK) expression, the naïve T cells of *Lck*^{ind} x *Lck*$^{-/-}$ mice (only Fyn expresses) failed to proliferate, while naïve T cells from *Lck*^{ind} to *Fyn*$^{-/-}$ mice (only Lck expresses) can undergo homeostatic proliferation as usual. This demonstrates the essentiality of Lck in thymocyte survival and proliferation while Fyn failed to restore naïve T cells homeostatic proliferation (Seddon et al., 2000; Seddon and Zamoyska, 2002a;

Seddon and Zamoyska, 2002b). Lck has a unique role in regulating T cell differentiation and function.

In mature T-cells, LCK associates with CD4 or CD8 via cysteine-mediated interactions (Turner et al., 1990). In terms of DP cells differentiating into SP cells, Lck activity regulates positive selection and CD4 or CD8 commitment. Artificial modification of the extracellular domain of CD4 into CD8 did not alter CD4 lineage development, even though these cells recognise MHC I class (Seong et al., 1992). Transgenic manipulation of Lck activity determines CD4 commitment (high Lck activity) or CD8 commitment (low Lck activity) (Hernandez-Hoyos et al., 2000; Legname et al., 2000). In conditional $Csk^{-/-}$ mice, hyperactivated Lck caused all T cells to develop into CD4 cells regardless of pTCR, TCR or MHC class status (Schmedt et al., 1998). Taken together, these studies indicate that Lck controls CD4 versus CD8 lineage development. It may be that Lck propagates sustained signalling which is necessary to allow thymocytes to commit to the CD4 lineage. However, both Lck and Fyn can produce a short duration of signal that is sufficient for CD8 differentiation (Zamoyska et al., 2003).

1.1.5 ZAP70

Another essential tyrosine kinase in pTCR and TCR signalling is ZAP70 (zeta chain of T cell receptor associated protein kinase 70). Upon oligomerisation of pTCR and activation of TCR, ITAMs of CD3 bind to the SH2 domains of ZAP70, releasing its auto-inhibitory status. ZAP70 belongs to the SYK (spleen tyrosine kinase) family and has two SH2 domains, two linker regions called interdomain A and B and a kinase domain. The phosphorylation sites Y315 and Y319 are considered to be auto-inhibitory phosphorylation sites. Y to A mutagenesis of both sites result in higher basal kinase activity (Brdicka et al., 2005). Upon activation of TCR, the phosphorylation of Y493 in the catalytic domain results in full activation of ZAP70. Both LCK and ZAP70 itself can phosphorylate Y493. ZAP70 mutant Y493F can impair the downstream signalling of TCR; however, it does not influence the binding of LCK (Mege et al., 1996). In the early 90s, patients with ZAP70 deficiency were found to lack $CD8^+$ cells while their $CD4^+$ cells fail to respond to antigens. Cell line studies underlined these results. Loss of ZAP70 leads to the deficiency of functional T-cells due to the lack of $CD4^+CD8^+$ DP

cells and a defect in TCR signalling transduction (Williams et al., 1998). It is reported that SYK plays redundant roles in pTCR signalling. Double knockout of ZAP70 and SYK leads to a complete block in β-selection at the DN3 stage. ZAP70 is critically involved in 33% of B-cell derived Chronic Lymphocytic Leukaemia (CLL). ZAP70 promotes BCR signalling independent of its kinase activity but functions as an adaptor protein. Overexpression of ZAP70 SH2 domain enhances the calcium flux in response to stimulation of BCR (Chen et al., 2008).

1.1.6 Tonic TCR Signalling

The resting, naïve, T cells keep circulating in secondary lymphoid tissues, in which the tonic TCR signalling governed by SFKs provides survival or maintenance signals. It has been shown that Lck constitutively phosphorylates ITAMs of approximately 35% of TCR zeta (ζ) motifs in murine thymocytes and lymph node derived T cells (van Oers et al., 1993). Also, ZAP-70 has been shown to specifically associate with phosphorylated TCRζ (Pitcher et al., 2003; van Oers et al., 1993). One explanation for the phosphorylation of TCRζ in resting cells is to prime T cells to facilitate an immediate response towards antigens, which is most likely due to the constitutively autophosphorylated Lck or Fyn (Stefanova et al., 2002). The long-term survival of naïve T-cells is dependent on SFKs, TCR and the co-receptor CD4 as demonstrated previously by overexpression of an inducible Lck in *Lck*$^{-/-}$ and/or *Fyn*$^{-/-}$ mice (Zamoyska et al., 2003). Together, Lck-TCRζ-ZAP70 facilitates T-cell survival through low-level signals.

1.1.7 Glucocorticoid Receptor in T-cell Development

The Glucocorticoid Receptor (GR) belongs to the steroid receptor superfamily which includes receptors for thyroid hormone, vitamin D3, retinoic acid, and several orphan receptors. The GR resides in the cytosol before the occupation of its ligands – glucocorticoids (GC). Dexamethasone (DEX) is a particularly potent synthetic glucocorticoid *in vitro* and *in vivo*. Upon activation, GR disassociates from its cytoplasmic complex and translocates to the nucleus. In the nucleus, GR homodimers bind to Glucocorticoid Responsive Elements (GRE) of corresponding genes acting as enhancer or transcriptional repressor. GR interacts with other nuclear factors including

AP-1 (JUN, Jun proto-oncogene) (Yang-Yen et al., 1990), NF-κB (nuclear factor kappa B) (Scheinman et al., 1995), CREB (cAMP responsive element binding protein) (Imai et al., 1993), STAT3 and STAT5 (Stocklin et al., 1996). As GR interacts with several histone acetyltransferases (HATs) such as NCOA1 (nuclear receptor coactivator 1), ACTR (NCOA3, nuclear receptor coactivator 3), p300/CBP and P/CAF (KAT2B, lysine acetyltransferase), it could enhance gene transcription by chromatin remodelling (Shibata et al., 1997). Also, post-translational modification plays a role in GR regulation such as phosphorylation by cyclin/CDK (cycline dependent kinase 4) complexes and ERK2 (Krstic et al., 1997).

A significant role of GC has been found in T cell development in the thymus. T-cells are generally sensitive to GC associated-apoptosis as well as TCR activation-induced programmed cell death. When both stimuli occur simultaneously, T-cells are protected from apoptosis as demonstrated by specific lysis assays and DNA fragmentation (Sionov et al., 2008). The so-called mutual antagonism model proposes thymocytes undergo cell death (death by neglect) when low TCR avidity cannot counteract GC in the thymus, whilst increasing TCR avidity can overcome GC-induced apoptosis (positive selection) allowing T cells to survive and continue differentiation (Ashwell et al., 2000). Thymic epithelial cells (TEC) secrete GC, which might originate from thymocyte to epithelial cell contact (Pazirandeh et al., 1999). This model that GC is required to antagonise apoptotic signals derived via the pTCR, as well as the mature αβ TCR, is supported by several studies (Teh et al., 1988; Vacchio and Ashwell, 1997). In an *in vivo* model, where the immature thymocytes specifically expressed GR-antisense transcripts, low expression of GR led to decreasing thymus size and the number of DP cells suggesting GR signalling is indispensable for thymocyte development. This loss of mature T cells was partially through activation-induced cell death governed by TCR (Garvin et al., 1990; King et al., 1995).

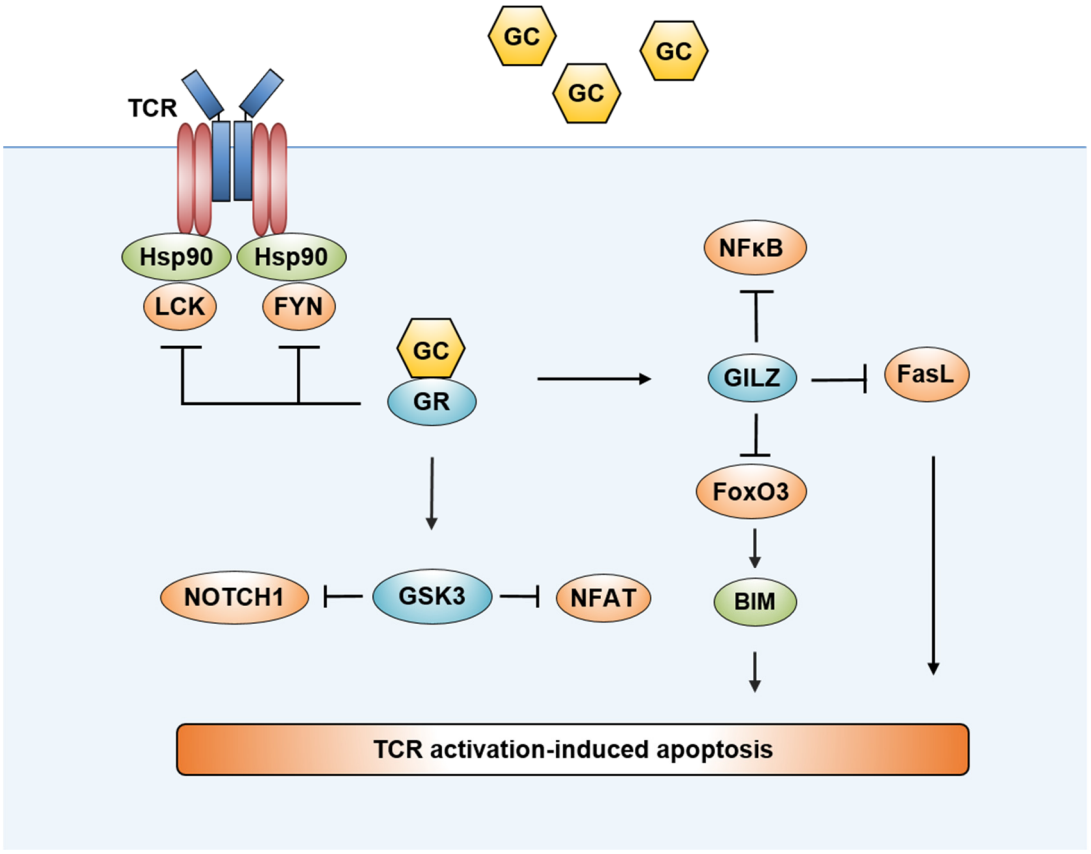

Figure 6. GC antagonises TCR activation induced apoptosis during T-cell development. GC inhibits TCR-signalling by displacing LCK and FYN from the TCR complex. GC-induced GSK3 attenuates TCR downstream NFAT signalling and NOTCH1 function. The GR targeted gene GILZ (glucocorticoid-induced leucine zipper) antagonises BIM expression by repressing FoxO3 and inhibits TCR-induced apoptosis by preventing FasL and NFκB expression. The diagram was modified from (Sionov et al., 2008).

Upon GC-binding with GR, the non-genomic effects of GC rapidly inhibit TCR-signalling by displacing LCK and FYN from the TCR complex (Lowenberg et al., 2006), and GC-induced GSK3 (glycogen synthase kinase 3) attenuates TCR downstream NFAT signalling and NOTCH1 function (Woodgett and Ohashi, 2005). The delayed response of genomic effects of GC also plays a crucial role in antagonising TCR-induced cell death. The GR targeted gene GILZ (glucocorticoid-induced leucine zipper) antagonises BIM (BCL2 like 11) expression by repressing FoxO3 (forkhead box O3) (Asselin-Labat et al., 2004). GILZ also inhibits TCR-induced apoptosis by preventing FasL and NFκB expression (Ayroldi et al., 2001; D'Adamio et al., 1997) (Figure 6).

It has been over 65 years since glucocorticoids were first used to treat patients with inflammation and autoimmune diseases. Immunosuppression by GC is achieved through interference with the expression of a variety of GR-activated genes in T cells, such as IL-2 (interleukin 2) (Northrop et al., 1992; Paliogianni et al., 1993), IL-1β (interleukin 1 beta) (Zhang et al., 1997), IL-6 (interleukin 6), IL-8 (interleukin 8), TNFα (tumour necrosis factor), and GM-CSF (Tobler et al., 1992). Another consequence of GC is induction of lymphocyte cell death through activation of the intrinsic apoptotic pathway. As a transcriptional regulator, GR-targeted genes directly or indirectly regulate cell death. Unlike the activation-induced cell death in T cells which is through TCR-FasL/Fas receptor activated Caspase-8, the common path of GR-induced cell death is Caspase-9-induced apoptosis (Jamieson and Yamamoto, 2000). Also, the fact that a transcriptionally inactive form of the GR could still induce apoptosis suggests the existence of an alternative mechanism through which GR affects nuclear proteins that are required for cell survival (Helmberg et al., 1995) (Reichardt et al., 1998). Apart from the genomic function, GCs also suppress immune response effectively through GR by rapidly inducing signal transduction. Studies in GR-mutant mice, where GR is defective for transcriptional activity, has proven its non-genomic actions (Van Laethem et al., 2001).

1.2 T-cell Acute Lymphoblastic Leukaemia

T-cell acute lymphoblastic leukaemia (T-ALL) is an aggressive blood cancer derived from the malignant transformation of T cell progenitors, and mainly develops in children and adolescents but also arises in adults. T-ALL accounts for 10-15% of paediatric and 25% of adult ALL cases. Characteristically T-ALL is more common in males than in females (Ferrando et al., 2002). The clinical symptoms are often characterised by high peripheral blood cell counts, high circulating numbers of blast cells, mediastinal mass and central nervous system (CNS) involvement. In UKALL2003, 12% T-ALL patients developed CNS disease while only 5% B-ALL patients showed CNS disease. In T-ALL and B-ALL, CNS2 (< 5 white blood cell (WBC) in the cerebrospinal fluid (CSF) with blasts) was observed in 8 and 4.7%, and CNS3 (≥ 5 WBC in the CSF with blasts) in 4.4 and 0.62% respectively (Data obtained in house, courtesy of Anthony Moorman).

The vast improvement in prognosis for T-ALL in children in recent years is achieved by intensive therapy, consisting of multi-agent combination chemotherapy, resulting in 5-year event-free survival (EFS) for paediatric and adult patients of 80% and 50%, respectively (Pui et al., 2008). Despite the significant improvements in the treatment of T-ALL, approximately 25% of children and 50% to 70% of adults with this disease succumb to treatment-resistant illness. Moreover, the high dose treatment can lead to severe acute toxicities, and short or long-term side effects are observed in many patients. Notably, the outcome for relapsed T-ALL remains extremely poor (Bhojwani and Pui, 2013).

T-ALL are classified in five phenotypic subtypes based on different stages of T-cell ontogeny. The ETP-ALL accounts for 15% of T-ALL cases with a poorer prognosis compared with typical T-ALL. The characterisation of ETP-ALL is $CD3^-$, $CD1a^-$, $CD5^{-/low}$, $CD4^-$, $CD8^-$, but frequently expressing myeloid lineage marker CD33 or stem cell markers CD117 and CD34. (Coustan-Smith et al., 2009). The European Group for the Immunological characterization of leukaemias (EGIL) proposed T-ALL into pro-T ($cCD3^+$, $CD7^+$), pre-T/immature ($cCD3^+$, $CD7^+$ and $CD5/CD2^+$), cortical T-ALL ($cCD3^+$, $sCD3^{+/-}$, $CD1a^+$, $CD2^+$, $CD5^+$, $CD7^+$, $CD34^-$), and mature T-ALL ($cCD3^+$, $sCD3^+$, $CD1a^-$, $CD2^+$, $CD5^+$, $CD7^+$, $CD34^-$). The cortical T-ALL subgroup has the best prognosis (Raetz and Teachey, 2016).

T-ALL is generally associated with clonal chromosomal translocations and other genetic or epigenetic abnormalities, which lead to differentiation arrest, uncontrolled growth and clonal expansion. These genetic abnormalities are usually classified as Type A and B lesions, with Type A lesions representing the initiating cancer mutation and Type B lesions required to lead to full-blown leukaemia in a multistep model.

1.2.1 Type A Oncogenic Gene Lesions in T-ALL

Genomic and transcriptomic studies have identified major genetic abnormalities in T-ALL cases that involve promoter and enhancer element of TCR genes and transcription factor genes associated with development, including Homeobox genes and bHLH genes (Figure 7). Discovery of these oncogenic proteins by using a combination of gene analysis strategies such as Giemsa banding (G-banding), fluorescent in situ hybridization (FISH), array comparative genomic hybridization

(aCGH), RNA-sequencing (RNA-Seq) and whole genome sequencing (WGS) are crucial for the classification of T-ALL subtypes.

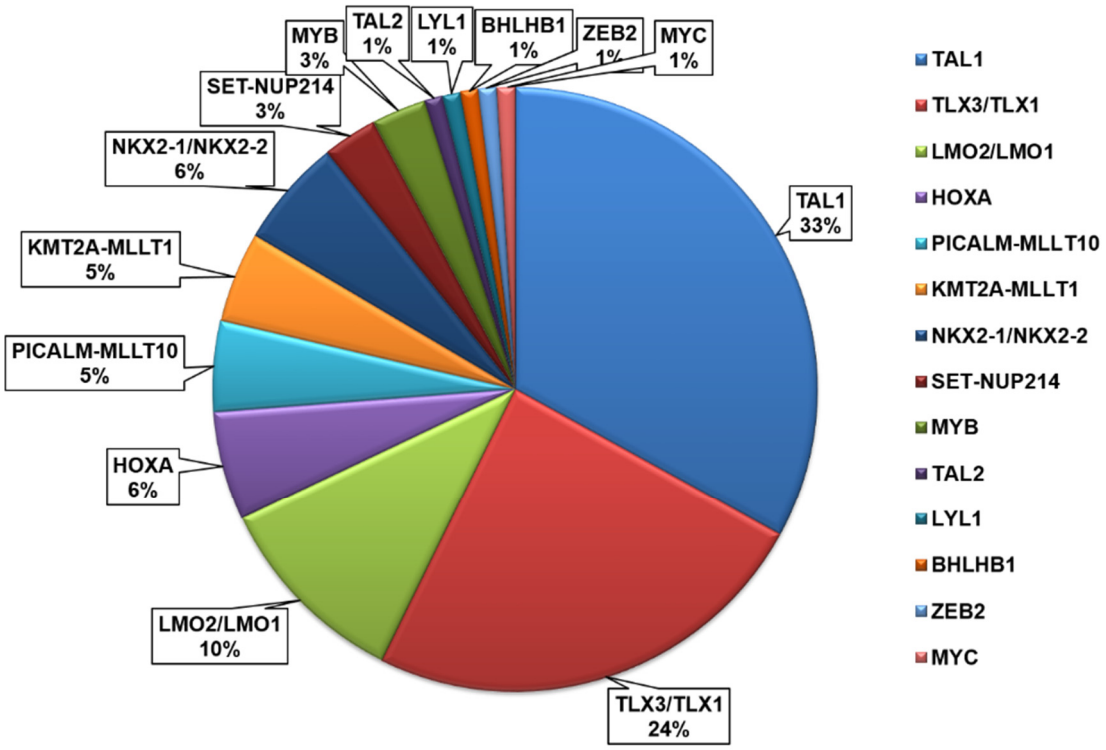

Figure 7. The classification of paediatric T-ALL. 33% of T-ALL cases have TAL1-associated gene aberrations. The frequency of TLX1 or TLX3 aberrations is 5% and 20% respectively. LMO2 and LMO1 accounts for 10% of T-ALL cases. The other major gene aberrations are HOXA (6%), PICALM-MLLT10 (also known as CALM-AF10, 5%), KMT2A-MLLT1 (also known as MLL-ENL, 5%), NKX2-1 (5%), NKX2-2 (1%), SET-NUP214 (3%), MYB (3%), TAL2 (1%), LYL1 (1%), BHLHB1 (1%), ZEB2 (< 1%) and MYC (1%). Data obtained from (Belver and Ferrando, 2016). TAL, T-cell acute lymphoblastic leukaemia protein 1; TLX, T-cell leukaemia homeobox; LMO, LIM domain only; HOXA, homeobox A; PICALM, phosphatidylinositol-binding clathrin assembly protein; KDMT2A, histone-lysine N-methyltransferase 2A; NKX2, NK2 homeobox; NUP214, nucleoporin 214; LYL1, lymphoblastic leukaemia associated haematopoiesis regulator 1; BHLHB1, basic helix-loop-helix protein1; ZEB2, zinc finger E-box binding homeobox 2. This diagram was made according to (Girardi et al., 2017).

Homeobox genes

The Homeodomain-containing proteins can be divided into two types: class I HOX genes and class II orphan HOX genes.

The class I contains four distinct members, namely HOXA, HOXB, HOXC and HOXD. A large-scale gene expression analysis has identified and characterised that only the HOXA cluster is associated with T-ALL (Soulier et al., 2005). HOXA9 and HOXA10 are crucial genes involved in T-ALL pathogenesis (Abate-Shen, 2002). HOXA gene expression can be upregulated by translocation with the *TCRB* or *TCRG* loci in 3% T-ALL cases. The dysregulated expression of HOXA is also found in T-ALLs with translocations of KMT2A-MLLT1 (MLL-ENL) (Rubnitz et al., 1996), PICALM-MLLT10 (CALM-AF10) (Asnafi et al., 2003), and SET-NUP214 (Van Vlierberghe et al., 2008).

Members of class II orphan HOX genes are *TLX1* (T-Cell Leukaemia Homeobox 1, HOX11) and *TLX3* (T-Cell Leukaemia Homeobox 3, HOX11L2).The oncogenic role of TLX1 in T-ALL is due to the translocation of the strong enhancers of *TCRA* (t(10;14)(q24;q11)), *TCRB* (t(7;10)(q35;q24)) or *TCRD* (t(10;14)(q24;q11)) leading to overexpression of *TLX1*. Forced TLX1 expression in Notch-activating mouse models results in development arrest at the cortical stage (Rakowski et al., 2011). TLX1 dysregulated expression leads to malignant features such as increased cell proliferation, downregulation of anti-apoptotic genes, induction of aneuploidy and deletions of tumour suppressor genes such as *BCL11B*, *PTPN2* (Kleppe et al., 2011), *WT1* (Tosello et al., 2009) and *PHF6* (Van Vlierberghe et al., 2010) during T-cell transformation (De Keersmaecker et al., 2010). The transcription signatures and directly regulated genes of TLX1 and TLX3 are broad overlapping (Della Gatta et al., 2012). TLX3 high expression can be detected in 20-25% paediatric T-ALL patients and 5% in adult T-ALL patients (Belver and Ferrando, 2016). Unlike TLX1, TLX3 is frequently translocated to the *BCL11B* locus (t(5;14)(q35;q32)), which is highly expressed during T-cell differentiation (Ballerini et al., 2002). The high level of TLX3 is associated with relapse of T-ALL, suggesting that monitoring the expression of TLX3 is vital for the treatment of T-ALL and risk assessment (Silverman et al., 2001).

Class II bHLH proteins

The third subtype of TALL is characterised by activation of the basic helix-loop-helix (bHLH) proteins TAL1 (T-cell acute lymphoblastic leukaemia protein 1, SCL), LYL1 (lymphoblastic leukaemia-derived sequence 1) and LIM-only (LMO) domain genes.

The activation of TAL1, through chromosomal translocation t(1;14)(p32;q11), t(1;7)(p32;q34) or interstitial deletion of 1p32, is the most common type A lesion in childhood T-ALL (Begley and Green, 1999), which accounts for up to 34% of all T-ALL cases (Girardi et al., 2017). In only 3% of these cases, this is related to activation by the *TCR* locus, whereas the rest of cases are associated with an interstitial deletion that places TAL1 under the control of the *STIL* (SCL/TAL1 interrupting locus) gene promoter. It was recently shown that mutations in TAL1 upstream noncoding sites lead to *de novo* binding sites for MYB (MYB proto-oncogene, transcription factor), recruiting CBP, RUNX1, GATA3 and itself to form a super-enhancer promoting *TAL1* gene expression in a subset of T-ALL patients (5%) (Mansour et al., 2014; Sanda et al., 2012). A variety of studies have been done to demonstrate the function of TAL1 in the transgenic mouse model and whether its expression could lead to leukaemogenesis. Firstly, no leukaemia occurs by using a bone marrow mouse model which overexpresses TAL1 (Elwood and Begley, 1995). Similarly, transgenic mice with expression of TAL1 driven by the *CD2* promoter do not develop leukaemia (Curtis et al., 1997). Furthermore, overexpression of TAL1-STIL fusion gene cannot induce leukaemia in transgenic or knock-in mouse models (Cheng et al., 2007). These results indicate that additional genetic abnormalities or signalling pathways are essential for the full development of leukaemia. However, it has also been reported that transgenic mice which express TAL1 driven by the *LCK* (LCK proto-oncogene, p56lck) promoter develop T-ALL in 80% of these mice (Condorelli et al., 1996). In a study which investigated whether TAL1 induced leukaemia through TCF3/TCF12, it was observed that leukaemia accelerated in Tal1/Tcf3$^{+/-}$ and Tal1/Tcf12$^{+/-}$ mice, indicating that TAL1 transformed thymocytes due to the repression of TCF3/TCF12 (O'Neil et al., 2004). Also, TRIB2 (tribbles pseudokinase 2) and NKX3-1 which are necessary for T-ALL proliferation have been shown to mediate TAL1 oncogenic activity (Kusy et al., 2010; Sanda et al., 2012).

LYL1 gene is another member of the class II bHLH transcription factor family. The LYL1 gene was discovered in close juxtaposition with the *TCRB* locus as part of the t(7;19)(q35;p13) chromosomal translocation causing T-ALL (Mellentin et al., 1989). The gene product of LYL1 plays a crucial role in cell proliferation, especially in haematopoiesis (Baer, 1993). To illustrate the oncogenic role of LYL1, transgenic mice have been created with LYL1 driven by the *EEF1A* (eukaryotic translation elongation factor 1 alpha) promoter. 30% of mice exhibited B-cell and T-cell leukaemia. These results indicate that LYL1 has an active role not only in B-cell leukaemia but also in T-cell leukaemia (Zhong et al., 2007).

The LIM domain family consists of four DNA-binding proto-oncogenic proteins, such as LMO1, LMO2, LMO3 and LMO4. The function of LMO1 and LMO2 in T-ALL is studied extensively. LMO1 was found in 1% T-ALL cases with the chromosomal translocation t(11;14)(p15;q11) and t(7;11)(q34;p15). LMO2 was upregulated as a consequence of interstitial deletion del(11)(p12p13), t(11;14)(p13;q11) or t(7;11)(q35;p13) accounting for approximately 10% of T-ALL cases (Boehm et al., 1991). Several transgenic mouse models have been developed to investigate the roles of LMO1 and LMO2 in the induction of T-ALL. Both LMO1 and LMO2 transgenic mice develop leukaemia with a long latency of 10 months, suggesting these two genes are essential but are not sufficient for the leukaemia development (Chervinsky et al., 1999). LMO proteins are frequently co-expressed with TAL1 or LYL1 in T-ALL (Ferrando et al., 2002). Although LMO proteins do not directly interact with DNA, the multiprotein complexes including LMO and TAL1/LYL1 disturb downstream gene expression through binding to DNA directly and displacing important transcriptional regulators required for T-cell differentiation (Larson et al., 1996).

Chimaeric fusion proteins

Fusion proteins found in T-ALL result from chromosomal translocations, involving ABL1 associated proteins, KMT2A-MLLT1 (also known as MLL-ENL) (HOXA group) and PICALM-MLLT10 (also known as CALM-AF10) (HOXA group) fusion proteins.

Examples of ABL1 associated fusion proteins are ETV6-ABL1, EML1-ABL1 and NUP214-ABL1. *ETV6* (ETS variant 6) is located on 12p13 and occurs rearranged due to the chromosomal translocation t(9;12)(q34;p13). This translocation occurs with very low frequency in patients.

EML1 (Echinoderm microtubule-associated protein-like 1) is a ABL1 fusion partner in EML1-ABL1 resulting from the translocation t(9;14)(q34;q32). The complex chromosomal rearrangements with three chromosomal breaks leading to the formation of the EML1-ABL1 fusion gene explains the low frequency in patients (Van Limbergen et al., 2001). EML1-ABL1 shows increased tyrosine kinase activity and is sensitive to imatinib, an ABL1 kinase inhibitor, which provides the possibility to treat this type of T-ALL with tyrosine kinase inhibitor (TKI) (De Keersmaecker et al., 2005).

NUP214 (nucleoporin 214) is located at the nuclear pore complex (NPC) which is important for nucleocytoplasmic transport. The NUP214-ABL1 fusion protein can be found in 6% of T-ALL. It is also associated with the expression of TLX1 and TLX3 (Graux et al., 2004), and thought to be subclonal in most cases. Again, it is sensitive to imatinib providing a new approach to treat this type of T-ALL by targeting the tyrosine kinase. Surprisingly, unlike BCR-ABL1 where the coiled-coil domain of BCR facilitates BCR-ABL1 proteins to form a tetramer which is constitutively activated in the cytoplasm, it is the nuclear pore localisation function of NUP214, rather than its coiled-coil motifs, which is crucial for NUP214-ABL1 to fully induce T-cell leukaemia (De Keersmaecker et al., 2008).

KMT2A is the mixed lineage leukaemia gene located on chromosome 11q23. KMT2A-MLLT1 fusion occurs upon chromosomal translocation at t(11;19)(q23;p13.3). PICALM (clathrin-assembly protein) forms the PICALM-MLLT10 fusion protein as a result of the t(10;11)(p12;q21) chromosomal translocation. It is associated with both ALL and AML. This protein can be found in approximately 10% of T-ALL patients with the malignancy only in the γδ T-cell lineage. The mechanism of induction of T-ALL through CALM-AF10 expression is poorly understood (Asnafi et al., 2003). NUP214

and CALM-AF10 aberrations are also associated with high frequency of corticosteroid resistance and dismal survival rates (Ben Abdelali et al., 2013; Ben Abdelali et al., 2014).

The cryptic del(9)(q34.11q34.13) deletion was identified in T-ALL patients resulting in a fusion protein SET-NUP214. In the GRAALL (French Group for Research on Adult Acute Lymphoblastic Leukaemia) 2003 and 2005 trials, 6% of cases (11 patients) harboured a SET-NUP214 fusion. Ten out of eleven patients were TCRγδ T-ALLs and associated with poor response to corticosteroid (Ben Abdelali et al., 2014). This subgroup is characterised by high expression of HOXA genes. Knockdown of this fusion gene in a SET-NUP214 positive T-ALL cell line LOUCY significantly impaired HOXA expression and cell proliferation (Van Vlierberghe et al., 2008).

1.2.2 Type B Genetic Aberrations and Their Role in Oncogenesis

The type B genetic aberrations are factors cooperating with type A gene lesions in T-ALL development. Their functions include roles in cell signalling, cell cycle control, tumour suppression and chromatin remodelling. Many critical type B genetic aberrations contribute to T-ALL development. It is beyond the scope of this thesis to discuss all genetic aberrations, but frequently recurring lesions affecting NOTCH1, PTEN, IL-7R, and NRAS will be discussed. Dysregulation of these genes is crucial for the proliferative and survival advantage of leukemic blast cells and has led to the development of therapeutic strategies aimed at inhibition of Notch, PI3K and MEK signalling.

NOTCH1

The oncogenic role of NOTCH1 was first discovered as part of the t(7;9)(q34;q34.3) chromosomal translocation found in less than 1% of human T-ALL patients (Ellisen et al., 1991). However, activating mutations of NOTCH1 occur in more than 60% of T-ALL cases indicating the crucial role of NOTCH1 in T-ALL development (Weng et al., 2004). A bone marrow reconstitution assay of cells with forced expression of a nuclear form of NOTCH1 (a constitutively active intracellular form of NOTCH1 (ICN)) was performed in lethally irradiated BALB/cByJ mice. Rapid T-cell leukaemia progression was shown in 50% of transplanted animals indicating NOTCH1 may specifically transform T cells (Pear et al., 1996). Notch signalling is activated by DLL4 which is expressed by thymic epithelial cells. Ectopic expression of DLL4 in T-cells resulted in T-ALL in mouse models (Xiong et al., 2013).

Two significant regions are mutated in NOTCH1; HD (heterodimerisation domain) and PEST domain (polypeptide enriched in proline, glutamate, serine and threonine domain). HD mutations are found in exon 26 and 27 which affect NOTCH1 activation on the cell surface and the release of ICN. The variations in the HD domain result in the increase of S3 cleavage (Figure 8) and the production of ICN. PEST domain mutations are found in exon 34 which influence the half-life of ICN. The deletions of the PEST domain lead to extended half-life of ICN1 (Gupta-Rossi et al., 2001). In 187 paediatric T-ALL cases, 58% of cases were discovered with HD and/or PEST

mutations; 27% had HD mutations, 15% had PEST mutations, and 16% had both HD and PEST mutations (Ferrando and Look, 2000).

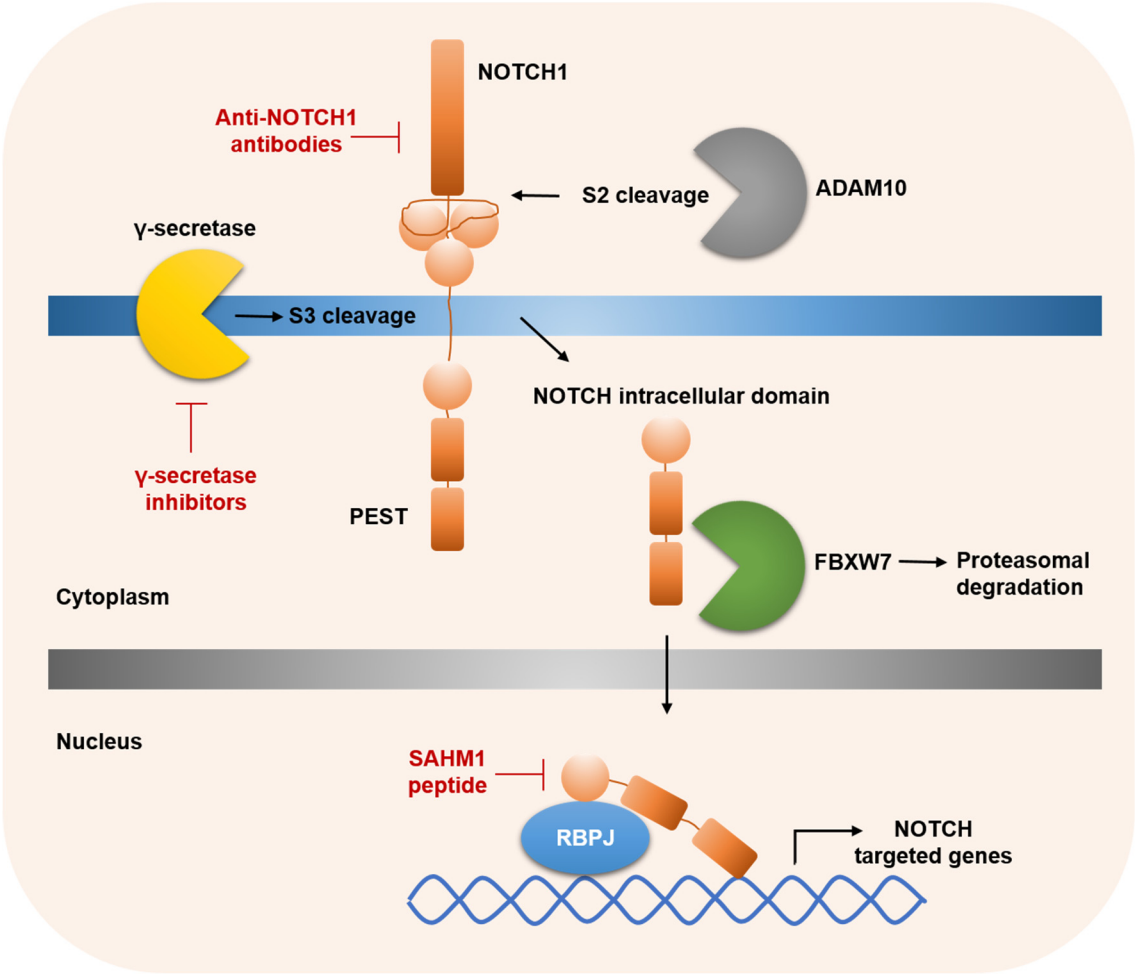

Figure 8. Schematic diagram of Notch signalling. The Delta-like (DL4) ligand is expressed by the thymic stromal cells. After activation by DL4, NOTCH1 undergoes S2 cleavage (by ADAM10) and S3 cleavage (by γ-secretase) which releases ICN (NOTCH intracellular domain). It can translocate to the nucleus and activate the expression of NOTCH target genes. FBXW7 (F-box and WD repeat domain containing 7) is a negative regulator of NOTCH1. FBXW7 works as an E3 ubiquitin ligase to lead to ubiquitin-mediated degradation of ICN. Several effective approaches to block Notch signalling are indicated; (1) anti-NOTCH1 antibodies to bind the extracellular domain, (2) γ-secretase inhibitors to inhibit the S3 cleavage of NOTCH1, and (3) SAHM1 (stapled α-helical peptide derived from mastermind-like 1) peptide to disrupt the transcriptional complex. The diagram was modified from (Van Vlierberghe and Ferrando, 2012).

As Notch signalling is pivotal in T-ALL pathogenesis, loss of function of negative regulators of NOTCH1 is seen in T-ALL patients. The proteasomal degradation of NOTCH1 is mediated by FBXW7 (F-box and WD repeat domain containing 7) (O'Neil et al., 2007). Inactivating mutations of FBXW7 resulting in increased level of NOTCH1 were identified in 8-30% of T-ALL cases (Thompson et al., 2007).
The induction of Notch-mediated leukaemia is dependent on pTCR signalling, since overexpression of ICN fails to induce leukaemia in the absence of pTCR signalling (Allman et al., 2001). MYC is a direct target of NOTCH1 and shares many targeted genes of NOTCH1. Both NOTCH1 and MYC enhance anabolic pathways of nucleotide and amino acid metabolism, protein translation and ribosome biosynthesis (Palomero et al., 2006). Another critical downstream transcriptional factor of NOTCH1 in T-ALL is HES1 (Hes Family bHLH Transcription Factor 1), which regulates PI3K, NF-κB signalling and suppresses pro-apoptotic factor PUMA. Many T-ALL-specific long noncoding RNA (lncRNA) were identified to be regulated by NOTCH1. A NOTCH1 downstream lncRNA LUNAR1 was shown to promote leukaemia growth via enhancing IGF1 (insulin-like growth factor 1) signalling (Trimarchi et al., 2014).

Activated Notch signalling represents a therapeutic target in T-ALL. GSIs (Gamma-secretase inhibitors) prevent the cleavage of NOTCH by γ-secretase to decrease the formation of ICN thereby blocking Notch signalling (Figure 8). However, lack of specificity and side-effects are common problems of GSIs (Knoechel et al., 2014). This led to the development of other inhibitors to specifically target the Notch pathway for the treatment of T-ALL. SAHM1, a stapled peptide, inhibits the Notch1 signalling explicitly to halt the progression of leukaemia and also has proved to be effective in a murine model (Moellering et al., 2009).

PTEN

PTEN (phosphatase and tensin homolog) is an important negative regulator of the PI3K signalling pathway, which is essential for cell proliferation, survival, growth, migration and metabolism. Activation of PI3K results in the production of phosphatidylinositol triphosphate (PIP3) which activates the key downstream molecule AKT (AKT serine/threonine kinase, PKB). AKT is the principal mediator in the PI3K pathway which promotes proliferation via the regulation of several factors involved in cell cycle control, such as GSK3β, FoxO1 and $p27^{Cip1}$. The activated AKT can induce the phosphorylation of mTOR (mechanistic target of rapamycin) and activate anti-apoptosis transcriptional factors (Cantley, 2002).

The activation of the PI3K/AKT pathway was detected in 15% of T-ALL patients in which 13% was accounted for by *PTEN* deletions or mutations, and 2% characterised by AKT activating mutations (Zuurbier et al., 2012). Moreover, several mouse models have shown that mice transplanted with PTEN-deficient or PTEN-mutant HSCs develop AML and T-ALL but not B-ALL, suggesting a significant function of PTEN in lineage fate determination and leukemogenesis (Zhang et al., 2006). Pten deficiency induced leukemogenesis was significantly impaired after the ablation of Raptor which is a regulatory-associated component of mTOR complex, suggesting Akt/mTOR signalling was the primary oncogenic driver of Pten-loss-evoked leukemogenesis (Kalaitzidis et al., 2012). The analysis of primary T-ALL samples illustrates a crucial role for PI3K/AKT/mTOR in the progression of T-ALL and provides novel therapeutic targets in T-ALL (Gutierrez et al., 2009). The mTOR inhibitor rapamycin induces apoptosis in paediatric T-ALL cells and re-sensitises chemo-resistance to doxorubicin and dexamethasone (Batista et al., 2011).

IL-7R

Crosslinking of IL-7 and IL-7R initiates IL-7R signalling through recruitment of JAK1 and JAK3 and increase of their kinase activity. IL-7R phosphorylates STAT5 (signal transducer and activator of transcription 5) which then translocates to the nucleus and finally induces target gene expression.

Recent studies show that Notch signalling can upregulate the PI3K pathway through the enhancement of IL7R expression, which is a direct transcriptional target of NOTCH1 (Gonzalez-Garcia et al., 2012). IL-7R enhances the PI3K/AKT/mTOR in T-ALL (Gonzalez-Garcia et al., 2009). A somatic gain-of-function mutation in IL-7R was discovered in 10% of T-ALLs resulting in the activation of JAK/STAT signalling (Zenatti et al., 2011). The activation mutations of JAK1 and JAK3 were found in 4-18% and 7% T-ALL cases respectively (Belver and Ferrando, 2016). Three missense mutations of JAK1 (A634D, R724H and R879C) result in oncogenic upregulation of multiple downstream pathways such as STAT1, STAT5, AKT and ERK (MAPK, mitogen-activated protein kinase) (Flex et al., 2008). Another member of the JAK family, TYK2, was found to be important in some T-ALL cases through the STAT1 and BCL2 axis. Small-molecule inhibitors against TYK2 (JAK inhibitor I and AG490) induced T-ALL cell death (Sanda et al., 2013). Loss of PTPN2 was identified in approximately 6% of T-ALL cases, resulting in the activation of JAK1 and STAT5 (Kleppe et al., 2011).

Nowadays, several pieces of data have shown activated IL7R pathway via mechanisms other than genetic mutations in IL-7R, JAK or STAT5 genes. In the ETP subtype, a point mutation V265G was found in DNM2 resulting in Dynamin 2 loss of function and decreased clathrin-mediated IL-7R internalisation. High IL-7R density on the surface led to enhanced IL-7 signalling in leukaemic stem cells (Tremblay et al., 2016). In another ETP-ALL case, a t(2;14)(q22;q23) translocation leading to the overexpression of ZEB2 (zinc finger E-box binding homeobox 2) was found to induce hyperactivated STAT5. An IL7R-blocking antibody or JAK1/2 inhibitor Ruxolitinib could effectively prevent ZEB2 overexpression induced T-ALL in mice (Goossens et al., 2015).

These findings indicate that the activation of IL-7R is associated with progression of T-ALL and offers a novel therapeutic target. Recent treatments have been developed based on chemical inhibition of JAK/STAT5 signalling components, such as the JAK1/2 inhibitor ruxolitinib and JAK3 inhibitor tofacitinib (Meyer and Levine, 2014).

NRAS

The MAPK/ERK pathway, also known as the RAS-RAF-MEK-ERK pathway, is critical in the regulation of cell division and growth. Three distinct RAS genes are known; KRAS (KRAS proto-oncogene, GTPase), NRAS (Neuroblastoma RAS viral oncogene homolog) and HRAS (HRas proto-oncogene, GTPase). Even though RAS activation mutations are rare in T-ALL (5-10% of cases), it is shown that constitutive activation of ERK1 and ERK2 was found in 38% of cases (Martelli et al., 2012). Upstream of MEK/ERK signalling are several pathways, for example IL-7, IL-9 and pTCR/TCR signalling (Brownlie and Zamoyska, 2013). It is notable that in a study with a cohort of 131 ALL patients, highly phosphorylated ERK1 and ERK2 correlated with high white blood cell counts and less response to steroids and negatively associated with the expression of CD34 antigen (Gregorj et al., 2007). In leukaemia and lymphoma, NRAS mutations are two to three times more frequent than mutations in other RAS members. Studies have shown that transplantation of $NRAS^{G12D}$ bone marrow into recipient mice resulted in 100% T-ALL (Wang et al., 2011). A similar outcome was seen for K-RAS^{G12D}. Aggressive T-ALL or T-cell lymphoma was seen in recipient mice after the bone marrow transplantation of conditional knock-in K-RAS^{G12D} mice. Half of these mice with T-ALL-like disease also acquired Notch1 mutations which were hypersensitive to γ-secretase inhibitors (Kindler et al., 2008).

One of the downstream molecules of MAPK/ERK2 is ERG (v-ets avian erythroblastosis virus E26 oncogene homolog). The phosphorylation site S283 of ERG is regulated by MAPK/ERK2, which is specifically highly phosphorylated in AML and T-ALL cells rather than HSPCs (hematopoietic stem and progenitor cells) (Huang et al., 2016). Transgenic ERG mice also developed T-ALL, and knockdown of ERG inhibited cell proliferation in the human T-ALL cell line MOLT4 (Thoms et al., 2011). Adverse outcomes are shown for T-ALL patients with higher ERG expression (overall survival high ERG 26% vs low ERG 58%) (Baldus et al., 2006).

1.2.3 Epigenetic Factors and Non-coding RNAs in T-ALL

Epigenetic factors

Approximately 56% of paediatric T-ALL cases have epigenetic mutations with the most prevalent mutations in *PHF6* (the plant homeodomain protein 6) and PRC2 (polycomb-repressive complex 2) components *EZH2* (enhancer of zeste 2 polycomb repressive complex 2 subunit), *SUZ12* (SUZ12 polycomb repressive complex 2 subunit) and *EED* (embryonic ectoderm development).

PHF6 inactivation mutations were found in 16% of paediatric T-ALL and 38% of adult T-ALL (Belver and Ferrando, 2016). Its epigenetic regulator function involves a wide variety of interactions with post-translationally modified histones, double-stranded DNA, nucleosome remodelling deacetylase (NuRD) complex, RNA polymerase 1 (UBTF1), ribosome RNA and DNA, as well as DNA damage checkpoint kinase ATM (ataxia telangiectasia mutated) (Girardi et al., 2017).

Dysregulation of H3K27 (histone 3 lysine 27) methylation caused by defects in PRC2 is found in 25% of paediatric T-ALL patients resulting from loss-of-function mutations and deletions in *EZH2*, *EED* and *SUZ12* (Belver and Ferrando, 2016). PRC2 acts as a tumour suppressor by competing with NOTCH1 to recruit lysine demethylase KDM6B (JMJD3, Jumonji D3), which leads to the activation of NOTCH1-targeted genes (Ntziachristos et al., 2012). Therefore, loss of PRC2 activity and NOTCH1 activation mutations are frequently co-occurring.

Contrary to the oncogenic role of KDM6B, another H3K27me3 histone demethylase KDM6A (UTX, ubiquitously transcribed tetratricopepetide repeat X-linked protein) was found as a tumour suppressor in T-ALL. Around 5-15% of T-ALL cases have loss-of-function mutations of KDM6A (Ntziachristos et al., 2014). However, this concept was challenged by a study where KDM6A was shown to be hijacked by TAL1 to remove H3K27 methylation and activate genes in TAL1$^+$ patients specifically (Benyoucef et al., 2016).

The discovery of alterations in epigenetic regulators in T-ALL paves the way for developing epigenetic inhibitors as new therapies for T-cell malignancies.

Micro-RNAs and long noncoding RNAs

The increased understanding of miRNAs (small non-coding RNA molecules of about 22 nucleotides) and lncRNAs (long noncoding RNAs) allows us to identify and study T-ALL pathogenesis-related non-coding sequences.

The miRNAs miR-19b, miR-20a, miR-26a, miR-92, and miR-223 are pro-tumourigenic as they downregulate gene expression of *IKZF1*, *PTEN*, *BIM*, *PHF6*, *NF1* and *FBXW7* (Mavrakis et al., 2011). On the contrary, a tumour suppressive role for miRNA was also found, exemplified by miR-193b. The downregulation of miR-193b in T-ALL causes MYB and MCL1 overexpression (Mets et al., 2015). Dicer1 (ribonuclease III), which cleaves pre-miRNA into miRNA, was found to be essential in Notch-mediated T-ALL progression. Dramatic apoptosis of T-ALL cells after the loss of Dicer1 strongly indicates Dicer1-processed miRNAs support leukaemia cell survival. The profiling of Dicer processed miRNAs identified aberrant expression of miR-21 in T-ALL which prevents apoptosis induction of leukaemia cells via suppression of Pdcd4 (programmed cell death 4) (Junker et al., 2015).

NOTCH1 regulates many T-ALL-specific long noncoding RNA (lncRNA), such as lncRNA LUNAR1, which promotes leukaemia growth via enhancing IGF1 signalling (Trimarchi et al., 2014).

1.3 T-cell Checkpoint Pathways in Malignancies

Although several critical signalling pathways are essential in T-ALL development, there is still limited knowledge about the role of individual key signalling components. In an RNAi-assisted screen to identify proteins providing survival advantages in T-ALL, ITK (IL-2 inducible T-cell kinase), ZAP70, LCK and FYN have been found (Sanda et al., 2013). These proteins are critical members of the pTCR or TCR signalling pathways. The *PTCRA* gene is highly expressed in more than 50% of T-ALL patients (Bene et al., 1995). These findings suggest that pTCR/TCR signalling might have a role in T-ALL development and maintenance. However, extensive research in elucidating the role of pTCR/TCR signalling in T-ALL has not yet been conducted.

1.3.1 LCK in Leukaemia

The tumour forming capacity of Lck has been investigated in genetically modified mouse models. Overexpression of wild-type Lck or a constitutively activated mutant Lck^{Y505F} in DBA/2 x C57BL6/J F2 murine zygotes led to a specific high expression of Lck in thymus and grossly increased the total phosphotyrosine levels. The physiological Lck mRNA levels in thymocytes are approximately 12 pg/µg total RNA. A two-fold increase of Lck mRNA in Lck^{Y505F} mice resulted in large thymic lymphoid tumours with an immature phenotype ($CD3^-$, $CD4^-$, $CD8^{-/low}$). This was in line with the fact that Lck^{Y505F} could transform NIH 3T3 fibroblasts *in vitro* (Marth et al., 1988). Wildtype Lck is also capable of transforming thymocytes with a 6-fold increase in mRNA levels. This time, more mature T cells ($CD3^{low}$, $CD4^{-/low}$, $CD8^{low}$) were observed compared with Lck^{Y505F} transgenic mice. The cells derived from both transgenic mouse models can continue to grow *in vitro* without the addition of growth factors. Overall, Lck overexpression induces tumorigenesis in mouse models (Abraham et al., 1991).

Notably, LCK plays a significant oncogenic role in a human T-ALL cell line HSB-2 cells. HSB-2 cells are double negative T-cells with a t(1; 7)(p34; q34) translocation, placing *LCK* under the control of the *TCRB* promoter. Moreover, *LCK* carries four mutations; (1) the V28L point mutation, which is located within the CD4/CD8 binding domain. This only creates a weak LCK oncogenic ability in fibroblast cells, but could be important in T-cells since it may affect the binding of CD4/CD8, (2) the second mutation was characterised by the insertion of three additional amino acids QKP (Gln-Lys-Pro)

between the SH2 and C-terminal catalytic domains. The inhibitory function of the SH2 domain relies on its binding with phosphorylated Y505 of the kinase domain. This QKP insert might stabilise the alignment of the phosphorylated Y505 residue and the SH2 domain, which disrupts the negative regulation of phosphorylated Y505 and produces a constitutively active LCK. Last but not least, two-point mutations (3) A353V and (4) P447L with unknown function can synergise with the QKP insert to promote fibroblast transformation. Together these mutations result in a 10-fold higher activity of LCK compared to other T-ALL cells. In normal T cells, LCK is down-regulated at the transcriptional level after T cell activation. However, when translocated under the control of *TCRB* in the t(1;7)(p34;q34) translocation, the high expression of *LCK* in HSB-2 cells counteracts the repression of *LCK* transcription leading to constitutive activation (Wright et al., 1994).

Recent studies report that NOTCH1 can activate AKT through LCK to upregulate anti-apoptotic genes in T cells. This suggests cooperation between NOTCH1 and LCK in leukaemogenesis (Sade et al., 2004). Another research study has shown that CCND3 can cooperate with NOTCH1 through the pTCR-LCK axis (Sicinska et al., 2003).

Moreover, LCK was shown to be crucial in BCR signalling in CLL. Firstly, varied levels of LCK expression in 39 CLL primary samples were identified. When stimulating CLL cells with IgM, LCK high-expressing cells showed more activation of CD79a, ERK, AKT and IKK phosphorylation, which could be reversed by siLCK or a specific LCK inhibitor (Pyrrolo(2,3-d)pyrimidine substituent) when used in excess of 1 μM concentration (Talab et al., 2013).

1.3.2 Other SFKs in Haematological Malignancies

An ever-increasing body of evidence highlights the role and influence of SFKs in haematological malignancies. For example, in CML (Chronic Myeloid Leukaemia), the dysregulated expression or activation of HCK, LYN and FYN has been shown; 1) the phosphorylation of several cellular proteins such as WAS (WASP actin nucleation promoting factor), BTK, HSP90, PKCδ (protein kinase C delta) and CSK in Ph^+ (Philadelphia-positive) CML leukaemic cells is mediated by SFKs (Rubbi et al., 2011); 2) LYN and HCK directly phosphorylate BCR-ABL1, after their activation by BCR-ABL1, to form a positive feedback loop; 3) SFKs act as a scaffold protein to bridge

BCR-ABL1 and STAT5 resulting in cell survival (Ban et al., 2008); 4) overexpression of HCK and LYN correlated with therapy resistance (Mahon et al., 2008; Pene-Dumitrescu and Smithgall, 2010). Inhibition of SFKs induced apoptosis in imatinib or nilotinib resistant CML (Gamas et al., 2009; Gioia et al., 2011). Similar to their role in CML, LYN, HCK and FGR appear to be involved in BCR-ABL1$^+$ B-ALL. The activation of HCK is shown to be induced by BCR-ABL1 in malignant B cells (Hu et al., 2004).

The SFK LYN is predominantly expressed in B-cells and has also been implicated in CLL. An aberrant LYN-HSP90 cytosolic complex causes the constitutive activity of LYN in CLL cells. Disruption of this LYN-HSP90 interaction by the HSP90 inhibitor geldanamycin was toxic to CLL cells (Trentin et al., 2008). STAT3 and MCL-1 expression can be upregulated by LYN, as well as the activation of CD40 signalling through LYN to increase anti-apoptotic mediators, such as NF-κB, BCL2 and MCL-1 (Contri et al., 2005; Tibaldi et al., 2011).

Oncogenic transformation of myeloid cells to AML requires the activity of SFKs, such as LYN, HCK and FGR (Duong et al., 2013). SFKs have been shown to promote AML progenitor proliferation and survival via MAPK and PI3K/AKT pathways as well as increased expression of anti-apoptotic proteins. Hyper-activated LYN is found in 76% of primary AML cells (Roginskaya et al., 1999), in which LYN strongly binds to FLT3-ITD and links it to STAT5 to activate anti-apoptotic targets, such as BCL2 and BCL-xL (Okamoto et al., 2007). In CBL (Cbl proto-oncogene, E3 Ubiquitin-Protein Ligase) mutated AMLs, the ubiquitin-mediated degradation of FYN was hindered resulting in overactivity (Bandi et al., 2009; Dos Santos et al., 2013).

CSK, the negative regulator of LCK, constitutively binds to PAG1. Upon TCR activation, PAG1 is released from the plasma membrane together with CSK allowing the full activation of LCK (Torgersen et al., 2001). In a study of high-resolution genome profiling of 40 childhood ALLs, a case of a microdeletion (8q21.13) affecting PAG1 was found. About 10% of near-haploid ALL has PAG1 homozygous deletions indicating its oncogenic role in lymphoid malignancies (Holmfeldt et al., 2013).

1.3.3 LCK Inhibitor - Dasatinib

Dasatinib (DAS) is a potent dual kinase inhibitor targeting ABL1 and SFKs. Dasatinib was approved by US FDA and EU in 2009 for CML and Ph^+ ALL patients with chemotherapy or imatinib resistance (Squibb, 2009). Although it was initially designed to target the oncogenic fusion protein BCR-ABL1, it was also found to inhibit activated SFKs, such as LCK and FYN, as well as block anti-CD3 induced tyrosine phosphorylation (Schade et al., 2008). In MRC compound-screening, at 0.1 μM, DAS inhibited 100% activity of ABL1, 99% activity of Src and Lck; at 1 μM, DAS treatment led to 0% activity of ABL1, DDR2, and 1% activity of Lck (obtained from Kinase Profiling Inhibitor Database, MRC PPU international Centre for Kinase Profiling).

Though both dasatinib and imatinib are potent BCR-ABL1 inhibitors, the chemical structures are very different. Imatinib can only bind with the inactive conformation of BCR-ABL1. The activation loop in the imatinib-bound ABL1 folds back to the ATP-binding site leading to an inhibitory conformation. In this form, Phe^{382} in the DFG (Asp-Phe-Gly) motif point toward ATP-binding site. On the contrary, both the active and inactive conformations of BCR-ABL1 were found to be inhibited by dasatinib. The Phe^{382} of dasatinib-bound ABL1 is buried in a hydrophobic pocket which is not accessible by ATP. This is typically found in activated kinases (Tokarski et al., 2006).

Using a dose of 60-120 mg/m^2 once daily, the C_{max} (maximum plasma concentration) of dasatinib in patients was reached within 0.5 - 6 hours, and the half-life of dasatinib is around 2 to 5 hours in paediatric Ph^+ CML patients (Zwaan et al., 2013). In a study of patients who received 140 mg once or 70 mg twice daily, around 5 - 28% of dasatinib was shown to cross the blood brain barrier to penetrate the CNS (Porkka et al., 2008).

Since several SFKs have been demonstrated to play a role in many types of leukaemia, dasatinib has been explored for its efficacy in CML, JMML (Juvenile MyeloMonocytic Leukaemia), AML, and CLL. When examining a Nilotinib-resistant CML cell line K562NR, dasatinib was shown to effectively inhibit Lyn and induce apoptosis (Okabe et al., 2011). JMML harbouring CBL mutations is associated with hypersensitivity of monocytic cells to GM-CSF (granulocyte macrophage-colony stimulating factor), which is driven by Src and Lyn. Dasatinib treatment in JMML patient samples decreased GM-CSF induced growth, demonstrating its efficacy in JMML *in vitro* (Bunda et al., 2013). Dasatinib was also found to selectively inhibit AML

progenitor cells by inhibition of LYN, HCK and FGR. The secondary engraftment capacity of dasatinib-treated AML stem cells is dramatically decreased (Dos Santos et al., 2013).

1.4 pBCR Signalling and Its Role in BCP-ALL

The pre-B cell receptor (pBCR) is essential for B cell development in providing a checkpoint in the bone marrow (Figure 9). The composition of pBCR is a correctly rearranged Igμ, SLC (Surrogate Light Chain; V_{preB} and *λ5*), CD79A (Igα) and CD79B (Igβ). Knock-out studies showed that SLC knockout mice, either V_{preB} or *λ5*, have a differentiation block and an accumulation of pro-B cells.

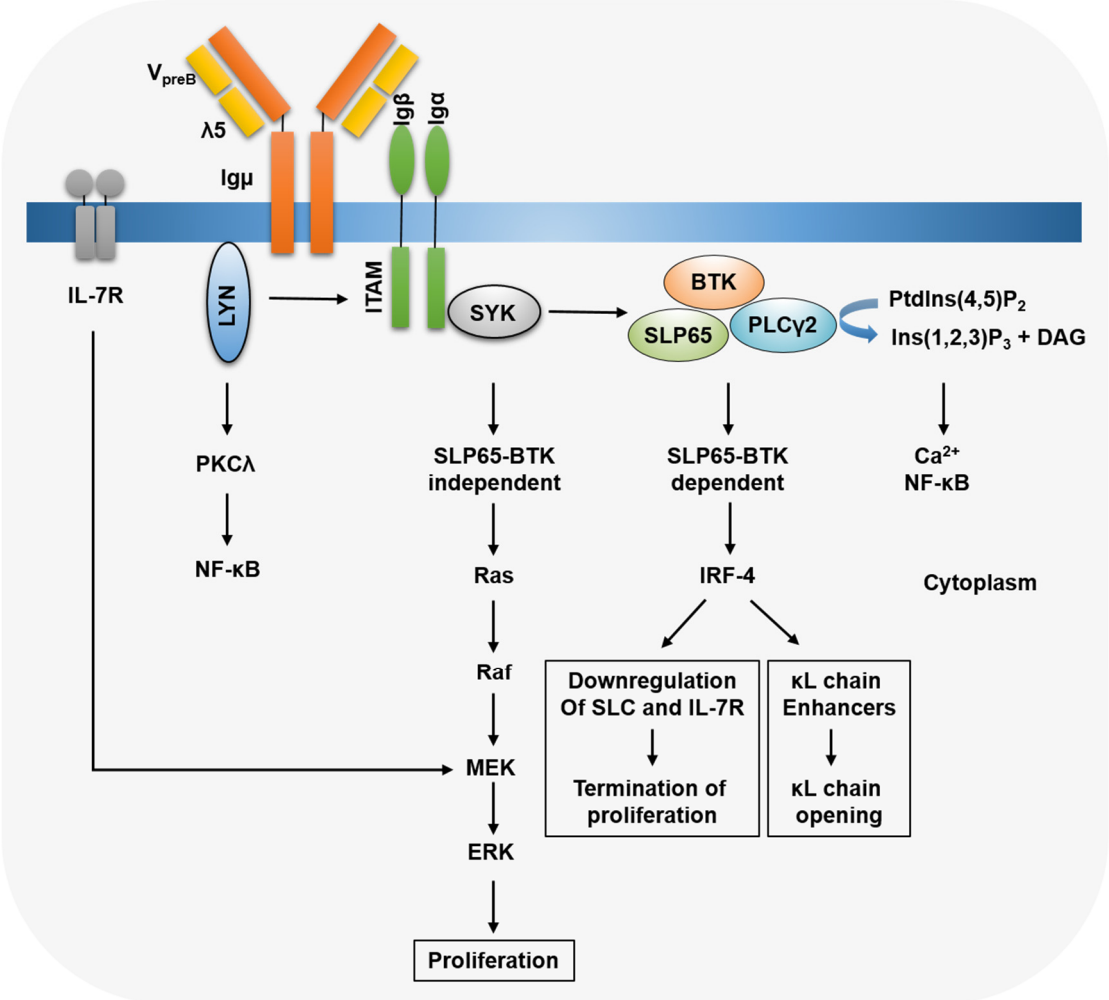

Figure 9. A diagram depicting pBCR signalling. The pre-B cell receptor (pBCR) is composed of V_{preB}, λ5, Igμ, Igα (CD79a) and Igβ (CD79b). The pBCR activates the Lyn-Syk-SLP65 axis to regulate NF-κB signalling, MAPK signalling and Ca^{2+} pathway. The diagram was modified from (Hendriks and Middendorp, 2004).

Whether the pBCR is ligand-dependent or aggregates autonomously on the plasma membrane initiating the signalling pathway is still not clear. The non-immunoglobulin part of SLC λ5 is positively charged and facilitates pBCR aggregation and interaction with various proteins. Clustered pBCR complexes facilitate the phosphorylation of CD79A-CD79B (Igα - Igβ) by SFKs. This further recruits and phosphorylates SYK to amplify the signal since it can phosphorylate neighbouring pBCR as a positive feedback mechanism (Hendriks and Middendorp, 2004).

The pBCR itself functions as a tumour suppressor gene. Evidence comes from studies in Ph^+ B-ALL, in which BCR-ABL1 suppresses pBCR expression (Trageser et al., 2009). Re-introduction of a functional rearranged Igμ reduces cancer cell growth in ALL with a non-functional Igμ (Klein et al., 2004). SYK can be phosphorylated by SFKs or autophosphorylated. It has been shown that SYK plays an oncogenic role in pBCR signalling since overexpression of SYK leads to pre-B cell proliferation and rearrangement of *IgL* (Wossning et al., 2006). Overexpression of SYK results in leukaemic transformation *in vivo* (Wossning et al., 2006). SFKs and SYK also activate PI3K signalling by phosphorylating CD19 and PI3KAP1 (Phosphoinositide-3-kinase adaptor protein 1). The downstream molecule of SYK is BLNK (B cell linker, also called SLP65), which activates PLCγ2, BTK (Bruton tyrosine kinase) and ERK signalling pathway. The BLINK-BTK-PLCγ2 axis downregulates *λ5* by activating Aiolos (IKZF3) to terminate pBCR function and promote *Igκ* (the κ chain of IgL) rearrangement by inducing the expression of *IRF4* (interferon regulatory factor 4). BLNK seems to suppress leukaemia progress since the deficiency of BLNK promotes B-ALL cell growth by elevating the autocrine IL-7 and JAK3-STAT5 pathways. Another possible mechanism of BLNK suppressing leukemic transformation is the fact that it inhibits AKT to release FOXO1 and upregulate FOXO1-targeted genes, which switches cell proliferation to cell differentiation (Flemming et al., 2003). FOXO proteins are rapidly degraded in the cytoplasm as a result of AKT phosphorylation, which inhibits FOXO to import into the nucleus. As a transcription factor, FOXO slows down cell cycle progression and induces RAG1/2 expression to promote pre-B cells to differentiate. A truncated form of BLNK is found in BCR-ABL1 ALL. This leads to a reduction in *pBCR* gene expression. Studies have demonstrated that inactivation of FOXO1 reduces its inhibition of *CCND2* and *MYC*. In this way, BLNK antagonises proliferation and promotes differentiation. The other upstream factor of BLNK is IKZF1 (IKAROS family

zinc finger 1). Overexpression of the Ik6 isoform (a dominant negative mutant form of IKZF1) in B-ALL cells leads to BLNK phosphorylation (Y36) and drives leukaemic cells to undergo cell cycle arrest (Trageser et al., 2009).

In summary, the downstream functions of pBCR include: (1) BLNK-BTK independent pathway to activate RAS-RAF-MEK-ERK signalling to promote cell proliferation; (2) BLNK-BTK dependent pathway to negatively regulate λ5 expression to terminate pBCR signalling, facilitate allelic exclusion of Igμ and promote IgL rearrangement by mediating the expression of RAG1/2 (Figure 9).

It has been reported that the aberrant activation of pBCR signalling facilitates B cell transformation. Gene expression studies demonstrate that 13% of B-cell precursor ALL (BCP-ALL) are $pBCR^+$ (Geng et al., 2015). The well-known target genes of pBCR signalling are CDKN2A (cyclin-dependent kinase inhibitor 2A) and p53. The pro-survival signals originating from the pBCR pathway promote BCL6 expression, and it competes with BACH2 (BTB domain and CNC homolog 2) to alter p53 and CDKN2A function, antagonising cell death. Further evidence related to the oncogenic role of pBCR signalling is provided by studies of BTK. In BCR-ABL1 ALL, a BTK mutant which lacks kinase activity, works as a scaffold protein to facilitate BCR-ABL1 mimicking pBCR signalling to provide continual pro-survival signals to leukaemic cells (Trageser et al., 2009).

A dual role for SYK has been found by the Markus Müchen group in 2015. The intrinsic mechanism of B cell negative selection also exists in B-ALL. The activation of BCR signalling caused by BCR-ABL1 is tightly regulated by inhibitory receptors PECAM1 (platelet and endothelial cell adhesion molecule 1), CD300A and LAIR1 (leukocyte-associated immunoglobulin-like receptor 1), which recruit phosphatases PTPN6 and INPP5D to negatively regulate BCR signalling. Hyperactivation of SYK is toxic to Ph^+ ALL cells due to mimicking auto-reactive BCR signalling, which forces the leukemic cells to undergo cell death. This provides a new perspective in the treatment of B-ALL by enhancing the BCR pathway to simulate the auto-reactive BCR signalling (Chen et al., 2015).

Several drugs targeting pBCR signalling provides novel treatments for B-ALL, including the dual approach to target SYK: 1) the molecular inhibitor PRT062607 which

diminishes SYK activity and blocks oncogenic pBCR signalling, 2) inhibitors against INPP5D such as 3AC (3-α-aminocholestane) resulting in SYK hyperactivation (Chen et al., 2015). Other drug targets such as Ibrutinib and Idelalisib are used to target BTK and PI3K respectively in BCP-ALL (Rickert, 2013).

1.5 Glucocorticoid Resistance and Underlying Mechanisms

The synthetic GCs, dexamethasone and prednisone, are essential as first-line chemotherapy in treating ALL. However, glucocorticoid-resistance (GC-resistance) remains a considerable issue in the clinic (Inaba and Pui, 2010). The inadequate response to GCs after seven days of initial therapy significantly associates with therapy failure and high-risk of relapse (Dordelmann et al., 1999). The molecular mechanisms of GC-induced cell death can be influenced at multiple levels, such as GR isoforms and its stability, GR interacting chaperone proteins, signalling pathways proximal to the GR, GR downstream apoptotic-related proteins, transcription factors, as well as epigenetic regulations.

1.5.1 GR Isoforms and GR-interacting Proteins

Two decades ago, a study (Leung et al., 1997) reported glucocorticoid resistance resulting from aberrant expression of GR isoforms. The human GR is composed of a classic α isoform and a transcriptionally inactive β isoform (Bamberger et al., 1995). GRβ differs from GRα in the C-terminal residues by alternative using of Exon 9β rather than 9α, which lacks the ability to bind GCs. Both isoforms are expressed in the cells. However, GRβ resides in the nucleus constitutively. Overexpression of GRβ inhibits GR transcription activity in a dominant negative fashion. One example of this is patients with GC-resistant asthma, who have more GRβ expressed in peripheral blood mononuclear cells (Leung et al., 1997). However, this association was debated by several groups, when they demonstrated that instead of a specific GR isoform, it was the low expression of total GR which was associated with steroid resistance (Haarman et al., 2004; Lauten et al., 2003; Tissing et al., 2005a).

Two independent studies tried to evaluate the components of the GR-multiprotein complex in steroid resistance in ALL. The mRNA levels of various chaperones such

as Hsp90 (heat shock protein 90), Hsp70, Hsp40, BAG-1 (BCL2 associated athanogene, also called RAP46), HOP (HOP homeobox), FKBP-51, and FKBP52 were measured and suggested that these proteins were of minor importance for GC resistance (Lauten et al., 2003; Tissing et al., 2005b).

1.5.2 Signalling Pathways Involved in Steroid Resistance

Overexpression of ICN (NOTCH) induces GC resistance in DP thymocytes (Deftos et al., 1998). The Notch signalling inhibitor (γ-secretase inhibitor) reverses GC-resistance in CUTLL1, a cell line characterised by an activating *NOTCH1* translocation. In addition, it restored *NR3C1* (GR, nuclear receptor subfamily 3 group C member 1) and *BCL2L11* gene expression after DEX treatment (Real et al., 2009). The transcriptional repressor HES1 is controlled by NOTCH1 and binds to the promoter of NR3C1 and negatively regulates its expression in T-ALL. Knockdown of HES1 increased NR3C1 protein level and sensitised dexamethasone response (Real et al., 2009).

It has been extensively studied that inhibition of IL-7 signalling sensitises DEX response in T-ALL. Steroid resistance-related mutations in JAK1 and KRAS were identified by targeted sequencing of paired diagnostic and remission patient samples. This study showed that hyperactivated IL-7 signalling upregulates expression of the anti-apoptotic proteins MCL1 and BCL-xL, and inhibits GSK3β and BIM through its downstream ERK and AKT pathways (Li et al., 2016).

In T-ALL, AKT has been shown to directly phosphorylate the serine 134 residue of GR, retaining its localisation in the cytoplasm, therefore blocking the activation and translocation of GR after ligand stimulation. Consistent with this finding, dexamethasone in combination with MK2206 (an AKT inhibitor) facilitates GR translocation, induces a greater degree of apoptosis, and reduces leukaemia engraftment *in vivo* (Piovan et al., 2013). Recently, a study has shown that the Akt inhibitor (Akt inhibitor IV) *in vivo* causes severe hepatotoxicity. Furthermore it was shown that Akt2, rather than Akt1, actively phosphorylated FoxO3a inhibiting Bim expression as well as driving GC resistance in T-ALL (Xie et al., 2019).

The first association of RAS mutations with GC resistance was published in 2013, where the authors identified infants with RAS mutations were less sensitive to prednisone in a cohort of 109 infant ALLs (Driessen et al., 2013). KRAS mutations have been identified at a low level in subpopulations of diagnostic samples, which may confer steroid-resistant relapse (Irving et al., 2014). The combination of dexamethasone and Selumetinib (MEK inhibitor) has been shown to synergise in RAS pathway mutated ALL (Matheson et al., 2019). This combination is currently tested in an early phase clinical trial SeluDex (UK, 2018).

1.5.3 Mechanism of TCR Signalling on GC-induced Apoptosis

During T-cell development, TCR signalling antagonises GC-induced apoptosis via multiple mechanisms, but mainly via ERK, AKT and Calcineurin/NFAT pathways. GC-induced apoptosis relies on GSK3 activation and BIM expression (Kfir-Erenfeld et al., 2010).

TCR signalling activates ERK signalling pathway after stimulation which antagonises GC-induced apoptosis (Figure 10). On one hand, ERK phosphorylates GSK3β at Thr43, which facilitates RSK1 (ribosomal protein S6 kinase A1) inactivation of GSK3β by phosphorylating $Ser9^{GSK3\beta}$ (Ding et al., 2005). On the other hand, ERK promotes BIM degradation via proteasome pathway by phosphorylation of BIM_{EL} (Ley et al., 2003). The murine Fas-negative cell line 2B4.11 was used for the investigation of how TCR signalling rescues cells from GC-induced apoptosis. The downstream Ras/MEK/ERK cascade, rather than PI3K/AKT cascade, was shown to be essential in preventing GC-induced cell death (Jamieson and Yamamoto, 2000).

GR translocation and GR-targeted genes were investigated under conditions of TCR activation alone or in presence of DEX. T-cell activation did not directly influence intracellular localisation of GR and transcription of GR-targeted genes (Zacharchuk et al., 1990). The Calcineurin/NFAT pathway is activated by TCR stimulation. Inhibitionof Calcineurin by Cyclosporin A (CsA) effectively blocked the activation of NFAT signalling pathway, therefore reducing the antagonism between TCR activation-induced and DEX-induced apoptosis. The mechanism of by which Calcineurin antagonises GC-induced apoptosis is unclear, but may be related to NFAT targeted

genes (Zhao et al., 1995). TCR antagonises GC-induced apoptosis also through AKT signalling, which often inhibits GSK3 function by phosphorylation (Sade et al., 2004).

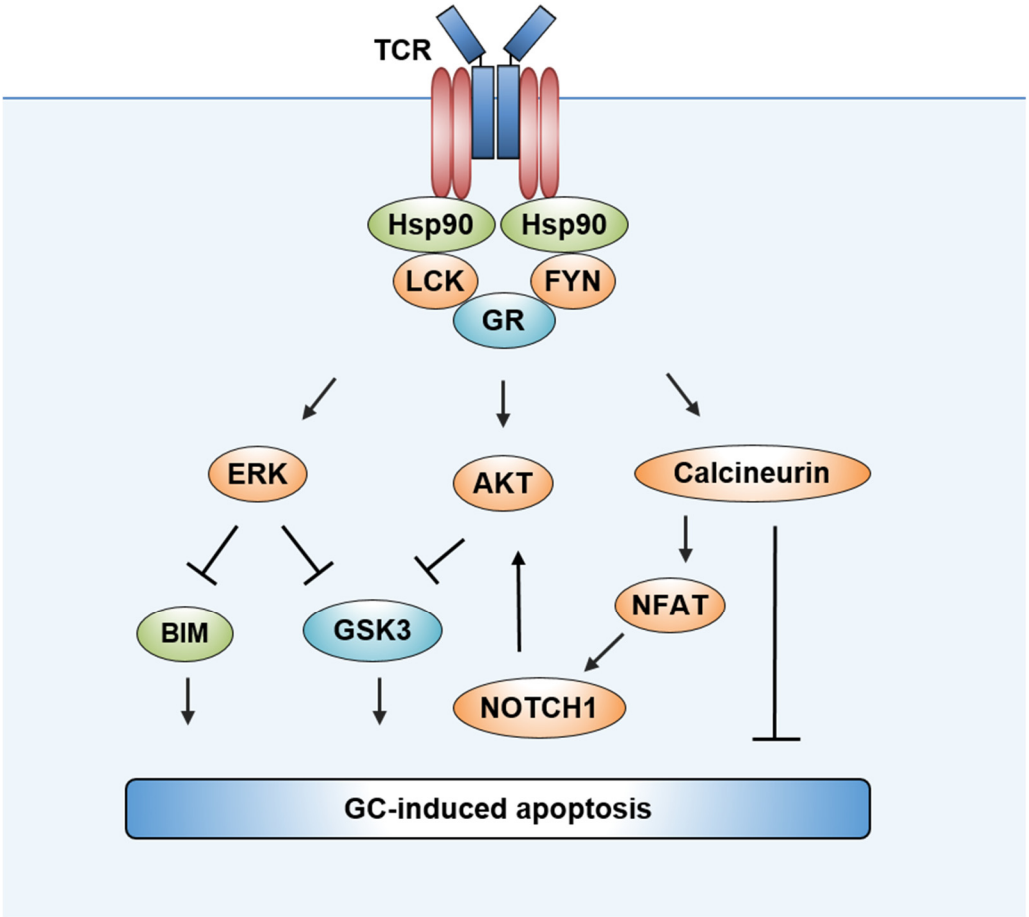

Figure 10. Known mechanisms of how TCR signalling antagonises GC-induced apoptosis in normal T cells. GC-induced apoptosis relies on BIM and GSK3. TCR signalling activates ERK, which then inhibits BIM via phosphorylation and GSK3 function. AKT, another downstream molecule of TCR signalling, phosphorylates GSK resulting in GSK inactivation. The TCR activated Calcineurin-NFAT pathway also antagonises GC-induced apoptosis. NOTCH1 can be upregulated by TCR signalling, which promotes AKT inhibition of GSK3. Taken together, TCR signalling antagonises GC-induced apoptosis. The diagram was modified from (Sionov et al., 2008).

The full activation of a T-cell requires interactions of TCR-MHC as well as costimulatory molecules (CD28/CTLA4 and B7-1 and/or B7-2). The majority of thymocytes undergo apoptosis during T-cell development due to physiological levels of GCs. However, this can be blocked by the interaction of CD28 and B7 (Wagner et al., 1996). The blockade of GC-induced apoptosis by TCR activation allows thymocytes to survive in the thymus.

One microarray study of a murine T lymphoma cell line (DEX-sensitive) demonstrated that Lck expression was downregulated by DEX (Harr et al., 2010). Further investigation indicated that DEX affected Lck phosphorylation, protein expression and its downstream calcineurin pathway. Knockdown of Lck by shRNA or inhibition of Lck by dasatinib synergised with DEX to inhibit TCR signalling. Reduction in ZAP70, LAT, SLP-76, and p-MEK1/2, as well as an increase in Annexin V^+ cells and caspase-3 activity were seen after Lck inhibition (Harr et al., 2010). As LCK is highly expressed in CLL, this study was expanded to include primary CLL cells. DEX did not affect LCK protein or phosphorylation levels due to the fact that these CLL cells were resistant to DEX. However, GC sensitivity and apoptosis were enhanced by concurrent use of dasatinib (Harr et al., 2010).

1.5.4 GR Downstream Apoptotic-related Proteins

Bcl-2 expression negatively correlates with GC sensitivity during T cell development. DP cells are more sensitive to GC compared with SP cells, which have higher expression of Bcl-2 (Cohen and Duke, 1984) (Hockenbery et al., 1991). In GC-sensitive ALL PDXs, GR inhibits MYB resulting in the downregulation of BCL2 expression. However, in GC-resistant samples, BCL2 is highly expressed due to sustained MYB activity (Jing et al., 2015). Rapamycin (mTOR inhibitor) was shown to increase prednisolone sensitivity via MCL1 inhibition. The AKT-MCL1 axis, but not the AKT-BCL2/BCL-xL pathway, was inhibited by rapamycin, and it restored BIM function in B-ALL cells (Wei et al., 2006).

The gene BAG-1 was the first GR-interacting protein to be cloned from a cDNA expression library in 1995 (Zeiner and Gehring, 1995). It binds to GR at the hinge region and inhibits GR in its trans-activation of apoptosis-related genes. Mouse S49.1 cells became resistant to GC-induced apoptosis after BAG-1 overexpression, while sensitivity to GC was restored after rapamycin treatment which downregulated BAG-1 (Kullmann et al., 1998).

By correlating prednisolone sensitivity *in vitro* with gene expression microarrays in a cohort of 444 patients, researchers from St. Jude Children's Research Hospital highlighted the importance of CASP1 (Caspase1) for GC resistance. Prednisolone

resistance was induced by overexpression of CASP1. GR was cleaved at the transactivation domain by CASP1, which can be reversed by RNA interference of CASP1 (Paugh et al., 2015).

1.5.5 Transcription Factors and Epigenetic Regulations

In BCP-ALL patients, mutations in CREBBP (CREB binding protein) resulting in a defective histone acetyltransferase domain have been identified in patients who experienced induction-treatment failure. Notably, the dysregulated targets of CREBBP include many GC-regulated genes. *In vitro* testing of vorinostat demonstrated GC-resistant T-ALL cell lines were sensitive to HDAC inhibition, providing a potential new therapy for GC-resistant ALL (Mullighan et al., 2011). More recently, by comparing open chromatin domains of lymphocytes and non-lymphoid cell types, as well as GC-associated transcriptome and epigenome, lymphocyte-specific open chromatin domains (LSOs) were identified. In GC-sensitive cells, DNA regions such as promoters and enhancers with lymphocyte-specific chromatin access were unmethylated (enhancers) and bound to CTCF (CCCTC-Binding Factor). Subsequently, after GC stimulation, the GR translocated to the nucleus and bound adjacent to CTCF at enhancer regions facilitating the formation of an active and accessible loop to initiate transcription of specific genes, such as *BCL2L11*. On the contrary, the same regions were highly methylated in GC-resistant cells similar to non-lymphoid cell types. Without lymphocyte-specific chromatin access, the association of CTCF and DNA looping after GR incorporation was inhibited which caused silencing of GR-targeted genes including pro-apoptotic gene *BCL2L11* (Jing et al., 2018).

1.6 Hypothesis and Aims

T-ALL represents approximately 15% of paediatric ALL. Although the prognosis is generally good, cure is achieved by intensive chemotherapy often accompanied by acute and chronic side effects. The prognosis for relapsed T-ALL remains extremely poor (Bhojwani and Pui, 2013). These patients represent an unmet medical need and urgently require an improved understanding of the mechanisms underlying T-ALL drug resistance and novel targeted therapies.

The checkpoints during T-cell development are provided by the pTCR during β-selection and TCR in positive/negative selection (Li and Rudensky, 2016). According to their established roles in normal thymocyte development, namely to govern life-death decisions and promote survival and proliferation, it seems reasonable to suggest that aberrant pTCR and TCR signalling might be critically involved in transforming thymocytes into cancer cells and/or remain involved in T-ALL progression. Currently known gene lesions in T-ALL such as *NOTCH1, FBXW7/CBL, PTPRC, PI3K/AKT, RAS* and *NF1*, are situated proximally, distally or around the pTCR and TCR signalling complex, and might affect pTCR/TCR signalling activity.

The oncogenic role of pBCR signalling in BCP-ALL has been established and has been validated as a valid drug target to treat leukaemia (Rickert, 2013). pTCR/TCR signalling is similar to pBCR-signalling, as they share multiple downstream signalling pathways. Moreover, their functions in lymphocyte development are highly analogous (Reth and Brummer, 2004).

The T-cell specific SFK, namely LCK, is a central molecule in pTCR/TCR signalling transduction. A critical role for LCK has already been shown in Chronic Lymphoblastic Leukaemia in enhancing the oncogenic role of BCR signalling (Harr et al., 2010). The role of LCK in T-ALL has however not yet been studied.

My **hypothesis** is that the pTCR/TCR signalling pathway, or components thereof, provide proliferative and survival advantage to malignant T-cells and, thus, might represent a novel drug target.

My **aims** are to explore the functional role of pTCR/TCR pathway elements in T-ALL cellular behaviour and drug resistance, as well as to investigate their value as novel drug targets. To accomplish this several main approaches are used: (1) shRNA screening to investigate the role of different components of the pTCR/TCR signalling complex in the maintenance of T-ALL, (2) The top hit of the shRNA screen, i.e. LCK, was further studied for its dependency of the proliferation/survival of T-ALL cells after gene modulation of LCK or use of dasatinib to study, (3) Development of a novel and highly-efficient drug combinations for T-ALL by using drug matrixes in a panel of T-ALL cell lines and primary cells, (4) Translation of findings into immunocompromised mouse models to validate LCK essentiality and a combination drug efficacy.

Chapter 2

Materials and Methods

2.1 Patient Samples

2.1.1 Patient Samples

The patient-derived material was collected as part of diagnostic investigations of patients at the Great North Children's Hospital, Department of Paediatric Haematology and Oncology, Newcastle upon Tyne, United Kingdom. The material was collected and stored with informed consent obtained from all subjects in accordance with the Declaration of Helsinki. Samples with explicit written consent for *in vivo* studies were requested from the Newcastle Biomedicine Biobank, Newcastle University, United Kingdom and used according to approvals given by the Newcastle Biomedicine Biobank (NHB application NHB-008) and the local institutional review board Newcastle & North Tyneside Ethics Committee (REC reference: 07/H0906/109) (Table 1).

UPN	Gender Time point	Sub-groups	Deletion	PDX No.	Cytogenetics
L809	Male diagnosis	TAL1	CASP8AP2	T-ALL14	46, XY, del(6)(q13q23) Extra RUNX1 signal [11%]
L903	Female diagnosis	TAL1	CDKN2A, CDKN2B, MTAP	T-ALL5	46, XX STIL-TAL1
L907	Male diagnosis	TAL2		T-ALL22	46,XY TCRA/D-TAL2
L963	Male diagnosis	nk		T-ALL9	46, XY, r(5)(p14q23) del(7)(q22)
L970	Male diagnosis	TLX3	WT1	T-ALL12	t(5;14)(q35;q32) BCL11B-TLX3
LK203	Female diagnosis	TCRA-LMO2	CDKN2A PTEN TCRA	T-ALL3	46, XX biallelic loss 14q11.2 14q32.33 an interstitial deletion of TCRA or unbalanced TCRA rearrangement with unknown partner gene
LK214	Male diagnosis	TAL1	CDKN2AC DKN2B	T-ALL1	cryptic interstitial deletion of SIL (1p32) SIL-TAL1 polyploid
LK080	Male relapse	nk		T-ALL13	46,XY
LK287	Male diagnosis	TAL1		T-ALL26	46, XY, del(6)(q14~16q23) STIL-TAL1 FIP1L1-PDGFRA
LK290	Male diagnosis	KMT2A	CDKN2A	T-ALL32	46, XY t(11;19)(q23;p13.3) KMT2A-MLLT1

Table 1. Details of patient samples used in this project to generate PDXs. The unique patient number (UPN), (PDX T-ALL ID used in this study), gender and disease status, characterised oncogenes and deletions and cytogenetics are shown.

2.1.2 Generation of Patient-Derived Xenograft

Patient-derived xenografts (PDX) were harvested from the NOD.Cg-Prkdc^{scid}Il2rg^{tm1wjl}/SzJ (NSG) mice after the engraftment of patient samples. In this study, patient samples (usually 1x10^6 or 2 x10^6 cells per mouse) were intrafemoral injected into NSG mice. Peripheral blood samples may be taken by tail bleeding used for leukaemia engraftment staining. Mice were weighed weekly and monitored daily. Once they showed signs of illness, enlarged spleens (can be seen as a darker area through the skin when scruff handling of mice), or weight loss >15% for three consecutive days, they were humanely killed by a schedule 1 method (dislocation of the neck). Bone marrow and spleen samples were collected. Spleen samples were homogenized through a cell strainer and bone marrow samples were harvested by flushing the lumens with PBS or crushing bones with a pestle and mortar with PBS.

2.2 Tissue Culture

2.2.1 T-ALL Cell Lines

SUPT1, CUTLL1, MOLT4, Jurkat, HPB-ALL and CCRF-CEM were cultured in RPMI1640 (Roswell Park Memorial Institute 1640, Sigma Aldrich#R8758, Dorset UK) with 10% FBS (ThermoFisher#10500-064, Paisley UK). HSB-2, KOPT-K1, ALLSIL, DU528 and MOLT16 were cultured in RPMI1640 with 20% FBS (Table 2). All cell line were cultured in a 5% CO_2 and humidified atmosphere at 37°C. All T-ALL cell lines used in this study were authenticated by STR (Short Tandem Repeat) profiling analysis (NewGene, Newcastle upon Tyne, UK).

2.2.2 Other Cell Lines

Human embryonic kidney 293T cells (293T) are cultured in DMEM (Dulbecco's modified Eagle's medium, Sigma Aldrich#D6171, Dorset UK) with 10% FBS, 2 mM L-Glutamine (Sigma Aldrich#G7513, Dorset UK) and 1 mM Sodium Pyruvate (Sigma Aldrich#S8636, Dorset UK). The murine stroma cell line OP9-DL1 used in these studies was kindly provided by Professor Sophie Hambleton, Newcastle University, United Kingdom and is subject to a Material Transfer Agreement between Sunnybrook Health Sciences Centre, Toronto, Canada and Newcastle University, United Kingdom. OP9-DL1 cells were cultured in MEMα (Minimum Essential Medium α, ThermoFisher#12561056, Paisley UK) with 20% FBS.

Cell line	Age Gender	ATCC DSMZ	Dise-ase	TCR status	Muta-tion	Deletion	Cytogenetics
SUPT1	8 Male relapse	CRL 1942	T-LBL	pTCR+ TCRαβ-		CDKN2B CDKN2A	t(7;9)(q34;q34.3) *TRB-NOTCH1/TAN1* Inv(14)(q11q32) *TRAD-IGH*
CUTLL1	14 Male relapse		T-NHL	TCRαβ+	P53		t(7;9)(q34;q34) *TRB-NOTCH*
HPB-ALL	14 Male diagnosis	ACC 483	T-ALL	TCRαβ+		IFNB CDKN2B CDKN2A	t(5;14)(q35;q32.2) *HOX11L2/TLX3-BCL11B* pseudodiploid with 8% polyploidy
HSB-2	11 Male	ACC 435	LS ALL	TCRαβ-	LCK^{V28L} LCK^{A353V} LCK^{P447L}		t(1;7)(p34;q34) *LCK-TRB* submicroscopic del(1)(p32) *STIL-TAL1(SIL-SCL)* pseudodiploid with 4% polyploidy
MOLT4	19 Male relapse	CRL 1582 ACC 362	T-ALL	TCRαβ- pTCR+	NRAS P53 PTEN TYK2	CDKN2A	hypertetraploid
Jurkat	14 Male relapse	TIB 152	T-ALL	TCRαβ+	P53 PTEN	IFNA CDKN2B CDKN2A	pseudodiploid
MOLT16	5 Female relapse	ACC 29	T-ALL	TCRαβ+	P53 PTEN	CDKN2B CDKN2A	t(8;14)(q24;;q11) *MYC-TRAD,* submicroscopic del(1)(p32) *SIL-TAL1/SCL fusion* near-diploid
KOPT-K1	6 Male		T-NHL	TCRαβ-		CDKN2A	t(11;14)(p13;q11) *LMO2/TTG2-TRD*
DU.528	16 Male diagnosis		T-ALL	TCRαβ-			t(1;14)(p32;q11) *TAL1/SCL-TRD*
ALLSIL	17 Male relapse	ACC 511	T-ALL	TCRαβ-		IFNA IFNB CDKN2B CDKN2A RB1	t(10;14)(q24;q11) *TLX1/HOX11-TRAD NUP214-ABL1* hypertetraploid
CCRF-CEM	3 Female relapse	CCL 119 ACC 240	LS ALL	TCRαβ+	P53 KRAS	IFNA IFNB CDKN2A	submicroscopic del(1)(p32) *SIL-TAL1/SCL* t(5;14)(q35.1;q32.2) *NKX2-5-BCL11B* near-tetraploid

Table 2. Details of T-ALL cell line used in this study. The origin of cell lines are listed (age, gender, diagnosis/relapse, ATCC or DSMZ ID, diseases). Characteristics of cell lines showed as TCR expression, gene mutation, deletion and cytogenetics. Abbreviations: T-LBL (T-cell lymphoblastic lymphoma), T-NHL (T-cell non-Hodgkin Lymphoma), LS (lymphosarcoma).

2.2.3 The Co-culture of PDX Cells

PDXs were co-cultured *in vitro* with OP9-DL1 in StemSpan Serum-Free Expansion Medium II (STEMCELL#09655 Cambridge UK) medium supplemented with 20% FBS, human IL-7 (interleukin 7, 10 µg/ml) (PeproTech#200-07, London UK) and SCF (stem cell factor, 100 µg/ml) (PeproTech#300-07, London UK). The feeder cell line OP9-DL1 was seeded in 12-well plates (0.45 x 10^4 cells/well) (Corning#3513, NY USA) one day before seeding PDX cells. Cell counts and viability were checked under the microscope by Trypan blue solution (Sigma Aldrich, Dorset UK) for both PDXs and feeder cells. The proliferation of PDXs was estimated by cell counts and/or cell cycle staining (see Ch2.10.2) once a week.

2.3 Plasmids and Cloning

The shRNA plasmids were based on the pLKO5d.SFFV.eGFP backbone (kindly provided by Jan-Henning Klusmann, MHH Hannover (Schwarzer et al., 2017)). Oligonucleotides encoding for the shRNA were designed by myself, synthesised by Sigma Aldrich, phosphorylated by T4 PNK (Polynucleotide kinase, Thermo Scientific, Paisley UK), annealed at a 95°C heat block slowly cooling down to room temperature. The pLKO5d.SFFV.eGFP vector was digested using BsmB1 (Esp3I ThermoFisher, Paisley UK) and purified by agarose gel and Qiagen Gel Extraction Kit (ID 28706, Valencia CA). Ligation of the annealed oligonucleotides with the digested vector results in a new construct that will target the respective gene products (Figure 11).

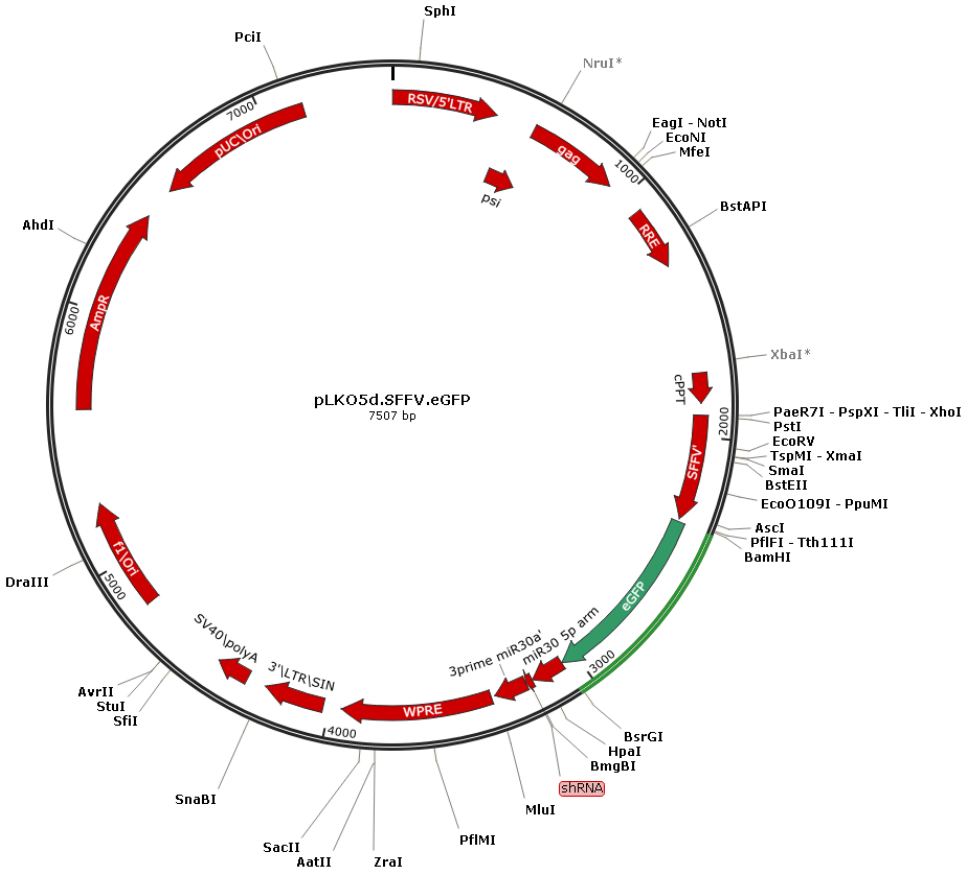

Figure 11. The schematic diagram of pLKO5d.SFFV.eGFP plasmid. RRE, Rev response element enhances titre by increasing packaging efficiency of full-length viral genome; 5' LTR, 5' long terminal repeat; 3' SIN LTR, 3' self-inactivating LTR for increased lentivirus safety; SFFV promoter, spleen focus-forming virus promoter; eGFP, enhanced Green fluorescent protein.

2.4 Lentivirus Production and Cell Transduction

2.4.1 Lentivirus Production

Lentivirus was generated in 293T cells. One day before co-transfection with a second-generation lentiviral vector pMD2.G and pCMV ΔR8.91 (Bomken, Buechler et al. 2013), 1 x 10^6 293T cells were seeded per 10 cm plate (Corning, USA). For co-transfection, 5 µg pMD2.G, 15 µg pCMVR Δ8.91 and 20 µg of the lentiviral vector were mixed to a final volume of 500 µl containing 0.25 M $CaCl_2$. This solution was slowly mixed with 500 µl 2xHeBS (0.28 M NaCl, 0.05 M HEPES, 1.5mM Na2HPO4, pH 7.0) drop by drop. After thorough mixing, the mixture was left for 30-40 mins at room temperature. The 1 ml transfection mix was gently dropped onto a 293T monolayer of 25-35% confluency. On the 3rd day, the cells were carefully washed once with PBS,

and fresh cell culture medium was added. After culturing the cells for 72 hours, the supernatant containing lentivirus was harvested and filtered through a 0.45 µM Syringe Filter (StarLab, UK).

The filtered lentivirus was either added directly to T-ALL cells or concentrated to improve the transduction efficiency. Lentivirus was centrifuged by ultra-centrifuge centrifugation (Beckman Coulter Optima XE-100, IN, USA) of 26,500 x g at 4°C for two hours and re-suspended in an appropriate volume of 100 µl – 500 µl cell culture medium.

2.4.2 Transduction of T-ALL Cells

T-ALL cells were seeded in 48-well plates with 1 – 2 x 10^6 cells per well and transduced in the presence of 0.1% polybrene (8 µg/ml final) by spinfection at 900 x g for 50 mins. After spinfection the cells were cultured, and the next day the majority of the lentiviral and polybrene containing supernatant was removed from the cells, before the addition of fresh RPMI1640 and transfer of cells to a 24-well plate. The transduction efficiency was measured by flow cytometry 6 days post-transduction.

2.5 Targeted shRNA Screening

2.5.1 Library Preparation

A library of short hairpin RNA (shRNA) targeting *PTCRA*, *LCK*, *FYN*, *ZAP70*, *CD3E* and *LAT* was generated (Table 3). Positive and negative controls comprising 18 shRNAs were selected based on in-house RNAi screens in different types of cancers. All shRNAs cloned into pLKO5d.SFFV.eGFP vectors were verified using Sanger sequencing (Source Bioscience, Nottingham UK).

	Gene	Oligo Sequences 5' → 3'
1F	shFYN#1	AGCGACCGATTGATAGAAGACAATGATAGTGAAGCCACAGATGTATCATTGTCTTCTATCAATCGGG
1R		GGCACCCGATTGATAGAAGACAATGATACATCTGTGGCTTCACTATCATTGTCTTCTATCAATCGGT
2F	sh#FYN2	AGCGAAAGACAATGAGTACACAGCAATAGTGAAGCCACAGATGTATTGCTGTGTACTCATTGTCTTC
2R		GGCAGAAGACAATGAGTACACAGCAATACATCTGTGGCTTCACTATTGCTGTGTACTCATTGTCTTT
3F	shFYN#3	AGCGAATAGAGATCTGCGATCAGCAATAGTGAAGCCACAGATGTATTGCTGATCGCAGATCTCTATG
3R		GGCACATAGAGATCTGCGATCAGCAATACATCTGTGGCTTCACTATTGCTGATCGCAGATCTCTATT
4F	shLCK#1	AGCGACGGAATTATATTCATCGTGACTAGTGAAGCCACAGATGTAGTCACGATGAATATAATTCCGC
4R		GGCAGCGGAATTATATTCATCGTGACTACATCTGTGGCTTCACTAGTCACGATGAATATAATTCCGT
5F	shLCK#2	AGCGACACATGTCTTGTACATGTGTATAGTGAAGCCACAGATGTATACACATGTACAAGACATGTGC
5R		GGCAGCACATGTCTTGTACATGTGTATACATCTGTGGCTTCACTATACACATGTACAAGACATGTGT
6F	shLCK#3	AGCGACCCATCTACATCATCACTGAATAGTGAAGCCACAGATGTATTCAGTGATGATGTAGATGGGC
6R		GGCAGCCCATCTACATCATCACTGAATACATCTGTGGCTTCACTATTCAGTGATGATGTAGATGGGT
7F	shPTCRA#1	AGCGCGCAGATGACTGAGAACATTAATAGTGAAGCCACAGATGTATTAATGTTCTCAGTCATCTGCT
7R		GGCAAGCAGATGACTGAGAACATTAATACATCTGTGGCTTCACTATTAATGTTCTCAGTCATCTGCG
8F	shPTCRA#2	AGCGACAGCACAGGCCTGGTGCTCAATAGTGAAGCCACAGATGTATTGAGCACCAGGCCTGTGCTGG
8R		GGCACCAGCACAGGCCTGGTGCTCAATACATCTGTGGCTTCACTATTGAGCACCAGGCCTGTGCTGT
9F	shPTCRA#3	AGCGCAGGGTCTTACCTCAGCAGTTATAGTGAAGCCACAGATGTATAACTGCTGAGGTAAGACCCTT
9R		GGCAAAGGGTCTTACCTCAGCAGTTATACATCTGTGGCTTCACTATAACTGCTGAGGTAAGACCCTG
10F	shZAP70#1	AGCGCGGCGTAGATCACCAGAATAAATAGTGAAGCCACAGATGTATTTATTCTGGTGATCTACGCCT
10R		GGCAAGGCGTAGATCACCAGAATAAATACATCTGTGGCTTCACTATTTATTCTGGTGATCTACGCCG
11F	shZAP70#2	AGCGAGCCCTGTCCCTCATCTATGGGTAGTGAAGCCACAGATGTACCCATAGATGAGGGACAGGGCG
11R		GGCACGCCCTGTCCCTCATCTATGGGTACATCTGTGGCTTCACTACCCATAGATGAGGGACAGGGCT
12F	shZAP70#3	AGCGCCGGCCAGAAGCCCTACAAGAATAGTGAAGCCACAGATGTATTCTTGTAGGGCTTCTGGCCGT
12R		GGCAACGGCCAGAAGCCCTACAAGAATACATCTGTGGCTTCACTATTCTTGTAGGGCTTCTGGCCGG
13F	shLAT#1	AGCGCCCATGGAGTCCATTGATGATTTAGTGAAGCCACAGATGTAAATCATCAATGGACTCCATGGA
13R		GGCATCCATGGAGTCCATTGATGATTTACATCTGTGGCTTCACTAAATCATCAATGGACTCCATGGG
14F	shLAT#2	AGCGCCAGTGTGGCGAGCTACGAGAATAGTGAAGCCACAGATGTATTCTCGTAGCTCGCCACACTGT
14R		GGCAACAGTGTGGCGAGCTACGAGAATACATCTGTGGCTTCACTATTCTCGTAGCTCGCCACACTGG
15F	shLAT#3	AGCGCCCTCAGATAGTTTGTATCCAATAGTGAAGCCACAGATGTATTGGATACAAACTATCTGAGGA
15R		GGCATCCTCAGATAGTTTGTATCCAATACATCTGTGGCTTCACTATTGGATACAAACTATCTGAGGG
16F	shCD3E#1	AGCGCACCAGAAGATGCGAACTTTTATAGTGAAGCCACAGATGTATAAAAGTTCGCATCTTCTGGTT
16R		GGCAAACCAGAAGATGCGAACTTTTATACATCTGTGGCTTCACTATAAAAGTTCGCATCTTCTGGTG
17F	shCD3E#2	AGCGAGGGCAAGATGGTAATGAAGAATAGTGAAGCCACAGATGTATTCTTCATTACCATCTTGCCCC
17R		GGCAGGGGCAAGATGGTAATGAAGAATACATCTGTGGCTTCACTATTCTTCATTACCATCTTGCCCT
18F	shCD3E#3	AGCGACCCTCTTGCCAGGATATTTATTAGTGAAGCCACAGATGTAATAAATATCCTGGCAAGAGGGC
18R		GGCAGCCCTCTTGCCAGGATATTTATTACATCTGTGGCTTCACTAATAAATATCCTGGCAAGAGGGT
19F	shRPL9#1	AGCGCGCCCAGAAAGATGAATTAATCTAGTGAAGCCACAGATGTAGATTAATTCATCTTTCTGGGCT
19R		GGCAAGCCCAGAAAGATGAATTAATCTACATCTGTGGCTTCACTAGATTAATTCATCTTTCTGGGCG
20F	shRPL9#2	AGCGAACATTGAGCTTGTTTCAAATTTAGTGAAGCCACAGATGTAAATTTGAAACAAGCTCAATGTC
20R		GGCAGACATTGAGCTTGTTTCAAATTTACATCTGTGGCTTCACTAAATTTGAAACAAGCTCAATGTT
21F	shRPS29#1	AGCGCTCCGTCAGTACGCGAAGGATATAGTGAAGCCACAGATGTATATCCTTCGCGTACTGACGGAA
21R		GGCATTCCGTCAGTACGCGAAGGATATACATCTGTGGCTTCACTATATCCTTCGCGTACTGACGGAG
22F	shRPS29#2	AGCGACGGCACGGTCTGATCCGGAAATAGTGAAGCCACAGATGTATTTCCGGATCAGACCGTGCCGG

22R		GGCACCGGCACGGTCTGATCCGGAAATACATCTGTGGCTTCACTATTTCCGGATCAGACCGTGCCGT
23F	shCD19#1	AGCGCGCTCAAGACGCTGGAAAGTATTAGTGAAGCCACAGATGTAATACTTTCCAGCGTCTTGAGCT
23R		GGCAAGCTCAAGACGCTGGAAAGTATTACATCTGTGGCTTCACTAATACTTTCCAGCGTCTTGAGCG
24F	shCD19#2	AGCGCCCCCACCAGGAGATTCTTCAATAGTGAAGCCACAGATGTATTGAAGAATCTCCTGGTGGGGT
24R		GGCAACCCCACCAGGAGATTCTTCAATACATCTGTGGCTTCACTATTGAAGAATCTCCTGGTGGGGG
25F	shTRPM7#1	AGCGCGCCCTGACGGTAGATACATTATAGTGAAGCCACAGATGTATAATGTATCTACCGTCAGGGCT
25R		GGCAAGCCCTGACGGTAGATACATTATACATCTGTGGCTTCACTATAATGTATCTACCGTCAGGGCG
26F	shTRPM7#2	AGCGCGCTGCAGATCTGCTAGCGTATTAGTGAAGCCACAGATGTAATACGCTAGCAGATCTGCAGCT
26R		GGCAAGCTGCAGATCTGCTAGCGTATTACATCTGTGGCTTCACTAATACGCTAGCAGATCTGCAGCG
27F	shKLHL7	AGCGCGCAGTTGGCTCTATAGTTTATTAGTGAAGCCACAGATGTAATAAACTATAGAGCCAACTGCT
27R		GGCAAGCAGTTGGCTCTATAGTTTATTACATCTGTGGCTTCACTAATAAACTATAGAGCCAACTGCG
28F	shDDB2	AGCGAGGAGATATCATGCTCTGGAATTAGTGAAGCCACAGATGTAATTCCAGAGCATGATATCTCCC
28R		GGCAGGGAGATATCATGCTCTGGAATTACATCTGTGGCTTCACTAATTCCAGAGCATGATATCTCCT
29F	shSESN2	AGCGCGGAGGGAGTATTAGATTATAATAGTGAAGCCACAGATGTATTATAATCTAATACTCCCTCCT
29R		GGCAAGGAGGGAGTATTAGATTATAATACATCTGTGGCTTCACTATTATAATCTAATACTCCCTCCG
30F	shERGIC3	AGCGACCTTCAAGAACCCAGATACTATAGTGAAGCCACAGATGTATAGTATCTGGGTTCTTGAAGGC
30R		GGCAGCCTTCAAGAACCCAGATACTATACATCTGTGGCTTCACTATAGTATCTGGGTTCTTGAAGGT
31F	shFLG	AGCGCGGATATAGACCACAACAAGAATAGTGAAGCCACAGATGTATTCTTGTTGTGGTCTATATCCA
31R		GGCATGGATATAGACCACAACAAGAATACATCTGTGGCTTCACTATTCTTGTTGTGGTCTATATCCG
32F	RUNX1/ETO	AGCGAAACCTCGAAATCGTACTGAGATAGTGAAGCCACAGATGTATCTCAGTACGATTTCGAGGTTC
32R		GGCAGAACCTCGAAATCGTACTGAGATACATCTGTGGCTTCACTATCTCAGTACGATTTCGAGGTTT
33F	shPTEN#1	AGCGAAGGCGCTATGTGTATTATTATTAGTGAAGCCACAGATGTAATAATAATACACATAGCGCCTC
33R		GGCAGAGGCGCTATGTGTATTATTATTACATCTGTGGCTTCACTAATAATAATACACATAGCGCCTT
34F	shPTEN#2	AGCGCCACGACGGGAAGACAAGTTCATAGTGAAGCCACAGATGTATGAACTTGTCTTCCCGTCGTGT
34R		GGCAACACGACGGGAAGACAAGTTCATACATCTGTGGCTTCACTATGAACTTGTCTTCCCGTCGTGG
35F	shPTEN#3	AGCGACCAGCTAAAGGTGAAGATATATAGTGAAGCCACAGATGTATATATCTTCACCTTTAGCTGGC
35R		GGCAGCCAGCTAAAGGTGAAGATATATACATCTGTGGCTTCACTATATATCTTCACCTTTAGCTGGT
36F	shNTC	AGCGATCTCGCTTGGGCGAGAGTAAGTAGTGAAGCCACAGATGTACTTACTCTCGCCCAAGCGAGAG
36R		GGCACTCTCGCTTGGGCGAGAGTAAGTACATCTGTGGCTTCACTACTTACTCTCGCCCAAGCGAGAT

Table 3. Oligonucleotide sequences of the targeted shRNA screen library comprising of 36 shRNAs. Both forward (5'→ 3' starting with AGCG) and reverse (5'→ 3' starting with GGCA) sequences are shown. Three shRNAs per gene targeting *FYN, LCK, PTCRA, ZAP70, LAT* and *CD3E* as well as *PTEN* have been used.

All plasmids were equally pooled together before generating lentiviral shRNA library. The non-concentrated virus was titrated on T-ALL cell lines (50 - 500 µl) and the transduction was performed as described above (Chapter 2.4.2). Transduction efficiency was estimated by GFP expression analysed by flow cytometry using a BD FACS Calibur (BD Biosciences, Wokingham UK). Cells transduced by approximately 20 - 30% were selected to reduce the risk of multiple integrations (Fehse et al., 2004). Samples were collected at baseline, day 16, 30 and 40 for the *in vitro* screen.

T-ALL PDXs (L963, LK203 and LK080) were transduced with concentrated lentivirus (2 x 10^6 cells were transduced with virus that were concentrated from 30 ml supernatant). Baseline samples (2 days after transduction) were taken before PDXs were injected into NSG mice (2 x 10^6 cells per mouse). Mice were kept until they began to exhibit clinical signs which necessitated humane killing. Spleen and bone marrow samples were harvested by homogenising material through a cell strainer with PBS or by flushing the lumens with PBS, respectively.

Genomic DNA (gDNA) was extracted using a DNeasy Blood&Tissue Kit (Qiagen#69504, Manchester UK). In general, cell pellets were suspended in 180 µl ATL buffer. After mixing with 20 µl proteinase K, samples were incubated at 56°C for 1h with occasionally vortexing to disperse the sample. Later add 200 µl Buffer AL and vortex again. 200 µl ethanol (96-100%) was added and mixed thoroughly to yield a homogeneous solution. The mixture was transferred into the DNeasy Mini spin column. After centrifugation (8000 g for 2 mins), Buffer AW1 was added to the column with a new collection tube. Finally, gDNAs were eluted in distilled water.

The gDNA was quantified by Nanodrop ND-1000 (Thermo Scientific, Paisley UK). Library amplification was performed using 1xPhusion GC-rich buffer, 200 µM of each dNTPs, 0.5 µM NGS-F3 primer, 0.5 µM reversed indexed primer, 0.04U/µl Phusion Hot Start II DNA polymerase (ThermoFisher#F549L, Paisley UK) and 825 ng gDNA per reaction (50 µl per reaction). The resulting amplicons were analysed by agarose gel (agarose, Sigma; O'RangeRuler Ladders and GeneRuler 1kb DNA Ladder, ThermoFisher) and purified by QIAGEN Gel Extraction Kits (ID 28706, Valencia CA). Pooled amplicons were sequenced by next-generation sequencing (NGS) (Illumina MiSeq) at Newcastle University Genome Core Facility.

2.5.2 NGS Bioinformatics Analysis

The NGS bioinformatics analysis were done by Sirintra Nakjang from Bioinformatics Support Unit (Newcastle University). Raw sequencing reads were trimmed at both ends up to the locations of barcode sequence before aligning to the reference shRNA barcodes using Bowtie2 (Langmead and Salzberg, 2012) with a zero mismatch tolerance. An in-house script was used to extract read counts from aligned sequence

files. Differential representation analyses of aligned read counts from different screen datasets were performed as described in Dai et al. using edgeR (Dai et al., 2014; Robinson et al., 2010). In brief, read counts were normalised to adjust for library size differences across samples. The likelihood ratio test method based on generalised linear models (GLM) framework in edgeR was used to test for differential representation of shRNA barcodes.

For screen data from cell lines, time-course differential representation analysis with replicates was performed to identify shRNAs with changes in their abundance over time (days 0, 16, 30 and 40). The analysis was performed for each cell line independently. Depletion of shRNAs over time was allocated a negative slope of the regression line, whereas enrichment of shRNAs was allocated a positive slope.

For the primograft LK203 *in vitro* screen dataset, we treated samples from different time points (day 16 and day 30 with/without mesenchymal stem cell) as non-baseline samples and tested for differential representation between the baseline samples and non-baseline samples.

To control for unwanted variation (e.g. biological, technical) between samples derived from the *in vivo* screen dataset, the RUVg approach was employed to estimate factors of unwanted variation under the assumption that our negative controls (i.e. non targeted control (NTC) and shRNA targeting RUNX1/ETO) had constant representation across samples (Risso et al., 2014).

To adjust for this unwanted bias, the estimated factors of unwanted variation as well as the covariate of interest were both included in the model for differential representation analysis which was performed on upper-quartile normalised counts using the GLM approach from edgeR as described above. In this dataset, we tested for differential representation between baseline samples and samples either from spleen or bone marrow separately.

2.6 RNA Extraction and Quantitative Real-Time PCR

RNA was extracted from 5 x 10^6 cells by using the RNeasy Mini Kit (Qiagen#74106, Manchester UK) and working after the manufactory recommendations. Briefly, cells were collected at 500 g for 3 mins and lysed in RLT buffer with 1% β-mercaptoethanol.

The cell lysates were transferred to the QIAshredder column and centrifuged at 8000 g for 2 mins. The flow-through was mixed with 70% Ethanol and moved to the RNeasy mini-spin column. After the centrifugation, the flow-through was discarded, and the column was washed twice with RW1 and RPE buffer respectively. Finally, the column was dried off by centrifugation at maximum speed for 2 mins. The RNA was dissolved in RNase-free water and eluted from the column by centrifugation at 8000 g for 2 mins.

The cDNA was synthesised using RevertAid H Minus First Strand cDNA Synthesis Kit (Thermo scientific#1631, Paisley UK). Briefly, 200 - 1000 ng of RNA was mixed with 1 µl of the random hexamer. RNase-free water was used to make a total volume of 12 µl. They were incubated at 70°C for 5 mins and cooled down to 4°C using the Applied Biosystems thermocycler (GeneAmp PCR system 2700, ThermoFisher, Paisley UK). A master mix which contained 4 µl MMLV buffer (5x), 2 µl dNTP, 1 µl RNase inhibitor and 1 µl MMLV RT enzyme for each sample was prepared. Eight µl of the master was mixed with each sample and PCR tubes were incubated in the thermocycler at 42°C for 60 mins followed by an incubation at 70°C for 10 mins.

For quantitative real-time PCR (qRT-PCR), the Applied Biosystems ViiA 7 (ThermoFisher, Paisley UK) was used. The template cDNA (20 µl of the cDNA synthesis reaction) was diluted in 80 µl ddH2O. The primers for qRT-PCR (Table 4) were ordered from Sigma Aldrich (Dorset UK). Relative mRNA expression was expressed as 2^{-DCt} (Livak and Schmittgen, 2001).

Gene	Sequence 5' → 3'
LCK-F	CACGCTGCTCATCCGAAATG
LCK-R	ACCAGGTTGTCTTGCAGTGG
PTCRA-F	TGGATGCCTTCACCTATGGC
PTCRA-R	AAGCCTCTCCTGACAGATGC
ZAP70-F	GAACTTTGTGCACCGTGACC
ZAP70-R	CTGAGCGGGCAGTGTAGTAG
FYN-F	TACCCAGGCATGAACAACCG
FYN-R	GTTGGTACTGGGGCTCTGTC
GILZ-F	CATGGAGGTGGCGGTCTA
GILZ-R	TTACACCGCAGAACCACCAG

Table 4. The qRT-PCR primers used in this study. The primer sequences were designed by myself using NCBI (National Centre for Biotechnology Information) Primer-BLAST specifically for *LCK, PTCRA, ZAP70, FYN* and *GILZ.*

2.7 Protein Assays

2.7.1 SDS-PAGE and Western Blot

5 x 10^6 cells were harvested, and the pellets were resuspended in Laemmli buffer (32.9 mM Tris-HCl pH 6.8, 13.15% glycerol, 1.05% SDS, 0.005% bromophenol blue, 5% β-mercaptoethanol). After sonication (QSonica#Q125, CT, USA), protein samples (20-30 µg per lane) were loaded and electrophoresed in 8% PAGE gel to run for 90-120 mins at 100 V. Proteins were transferred on to methanol activated Polyvinylidene difluoride (PVDF) membrane (Merck Millipore#IPVH00010, Watford, UK). After the transfer, the membrane was blocked with 5% milk or BSA (Fisher Bioreagents#BP9702, Loughborough, UK). The membrane was incubated with primary antibodies overnight at concentrations recommended by the antibody datasheets. The following primary antibodies were used: LCK (#2984, clone D88), p-SRC (Tyr416) (#6943, clone D49G4), p-LCK (Tyr505) (#2751), p-PLCγ1 (Tyr783) (#2821), PLCγ1 (#5690, clone D9H10) (all purchased from Cell Signalling), GAPDH (Cat#5G4, clone 6C5, Hytest, Finland) and Clathrin (BD Biosciences, Wokingham, UK). On the 2nd day, blots were washed and incubated with respective secondary antibodies from Dako (CA, USA) for 1 hour: Goat Anti-Mouse IgG HRP (P0447), Goat Anti-Rabbit IgG (P0448). For developing blots, Immobilon Western Chemiluminescent HRP Substrate (Millipore#WBKLS0500, Watford, UK) and ChemiDoc MP Imaging System with Image Lab Software (Bio-Rad, Watford, UK) have been used.

2.7.2 Reverse Phase Protein Array

The Reverse Phase Protein Array (RPPA) protocol was obtained from Edinburgh University. CUTLL1, MOLT4 and SUPT1 cells (1 x 10^7 cells) were pelleted (300xg, 5 mins), washed once with ice cold PBS and resuspended in 700 µl Lysis buffer (1% Triton X-100, 50 mM HEPES, pH 7.4, 150 mM NaCl, 1.5 mM $MgCl_2$, 1 mM EGTA, 100 mM NaF, 10 mM sodium pyrophosphate, 10% glycerol, containing freshly added 1 mM Na3VO4, protease and phosphatase inhibitors from Roche. A homogenous lyses of the cells was ensured by pipetting the lysates up and down and vortexing of the samples for 15 seconds followed by an incubation on ice for 30 mins and repeated vortexing. The cell lysate was centrifuged at 15,000 rpm for 10 mins at 4°C. The supernatant was carefully collected, 10 µl was used for protein quantification; 100 µl

was used for total cell lysate; the rest of samples were shipped on dry ice to the Protein/Antibody Microarray Facility of Edinburgh University.

For protein quantification Protein Assay (5x) (Cat#500-0006, Bio-Rad, Watford, UK) was used. Briefly, dilute one part 5x assay buffer with four parts of distilled water. Samples for a standard curve was generated using 2 mg/ml BSA dilutions (0, 0.05, 0.1, 0.15, 0.2, 0.3, 0.4 mg/ml) in 100 µl PBS each. Cell lysates were diluted in PBS (1:10 or 1:20) to a final volume of 100 µl, and 1 ml of 1x Protein Assay Buffer was added to each sample. Samples were loaded in a 96-well plate in quadruplicates and the absorbance readings at 595 nm were acquired by the POLARstar Omega plate reader (BMG LABTECH, Bucks, UK). Data was analysed in Mircosoft Excel and protein concentrations were calculated from the BSA standard curve.

2.8 Competitive Assay

2.8.1 *In vitro* Competitive Assay in T-ALL Cell Lines

In vitro T-ALL cells (1 x 10^6) were transduced with shRNA lentiviral supernatant (500 µl). Transduction efficiencies as demonstrated by GFP expression were determined by flow cytometry at day 6. On the same day, 5 x 10^6 cells were mixed with parental cells to generate approximately 50% GFP expression. The exact percentage was determined again after mixing by flow cytometry. These cells were cultured for 4 - 6 weeks and the GFP expression was assessed every three days. A relative GFP expression of 1 denotes a mixture of 50% GFP+ cells with 50% parental cells (ratio 1:1). Graphs were generated by using GraphPad Prism (version 6, CA, USA).

2.8.2 Competitive Assay of MOLT4 and Jurkat Engraftment *in vivo*

MOLT4 cells were transduced with either pLKO5d.SFFV.RFP657-shNTC (kindly provided by O Heidenreich) or pLKO5d.SFFV.eGFP-shLCK#3. After six days, the GFP and RFP expression were determined by flow cytometry, and cells were mixed to give a 1:1 ratio of RFP:GFP. In total, 1 x 10^7 cells were injected intrafemorally into five NSG mice. Twenty-six days post-injection mice showed signs of ill health and were humanely euthanised. Samples were collected from bone marrow, spleen and liver. Fluorescence expression levels were determined by using flow cytometry. The

RFP:GFP ratio was calculated to assess cell composition after leukaemia propagation *in vivo*.

The *in vivo* competitive assay of Jurkat cells was performed with pLKO5d.SFFV.eGFP empty vector transduced cells. Approximately 95% of these cells were GFP^+, thus GFP positivity was used as a marker for the presence of Jurkat cells derived from mouse samples. To compare the LCK effects on leukaemia propagation *in vivo*, cells were transduced with pLKO5d.SFFV.RFP657-shNTC and pLKO5d.SFFV.dTomato-shLCK#3. Similar to MOLT4, cells were mixed and had an equal distribution of RFP and dTomato before injection into five NSG mice. All five mice were harvested 22 days after injection due to 11-19% of weight loss. Spleen and bone marrow samples were collected as described above and assessed by flow cytometry.

2.9 siRNA to Knockdown LCK in PDXs

The siRNAs against LCK were adapted from the core sequences of shLCK#3 and purchased from Sigma Aldrich (Dorset, UK). Lyophilsed sense and antisense siLCK strand were reconstituted in hybridisation buffer (25 mM HEPES, 100 mM NaCl, pH 7.5) at a final concentration of 100 µM, mixed 1:1 equal molar quantity of and hybridised by initial incubation at 95°C followed by a slow cooling down to room temperature.

Oligo	Length	Sequence (5'-3')
siLCK	21	CCAUCUACAUCAUCACUGA[dT][dT]
siLCK_as	21	UCAGUGAUGAUGUAGAUGG[dT][dT]

Table 5. siLCK sequences. The lengths of both LCK siRNAs are 21 nucleotides with 19-base core sequences and 3' dTdT (deoxyribonucleotides) to confer nuclease resistance.

On the day of electroporation, PDX cells were counted and resuspended at 2 x 10^7 (for the 1st electroporation) or 1x10^7 (for the 2nd and 3rd electroporation) density in 4 mm gap width electroporation cuvettes (Cat#450135, BTX Molecular Delivery Systems™). Cells were electroporated sequentially three times with siLCK and siCtrl (siRUNX1/ETO provided by O Heidenreich) at 350V and 10 ms with 2 pauses. Cell

cycle analysis was performed on day 3, 6 and 9. LCK knockdown levels were measured by flow cytometry after the intracellular staining of LCK and p-SRC.

2.10 Flow Cytometry

2.10.1 Intracellular PhosFlow Staining

For each sample, 3 x 10^6 cells were harvested for intracellular staining of LCK and pSRC and transferred into three FACS tubes (BD#352054, Wokingham, UK). Cells were washed once with cold PBA (PBS, 1% BSA and 0.05% NaN_3), fixed in Cytofix Fixation Buffer (BD Biosciences#554655, Wokingham, UK) for 15 mins at 37 degree, washed and permeabilised in PermBuffer III (BD Biosciences#558050, Wokingham, UK) for 30 mins on ice. Cells were left unstained (i) no stain control (mouse serum (Sigma Aldrich#M5905, Dorset, UK)) or were stained with (ii) control IgGs (mouse serum, PE-IgG1 control (R&D#IC200P, Abingdon, UK), Alexa Fluor 647-IgG control (Biolegend#400130, London, UK)) or (iii) LCK/pLCK specific stain (mouse serum, Alexa Fluor 647-LCK (0.38 µl/sample) (BioLegend#628303, London, UK), PE-Src (Y418, 7.5 µl/sample) (BD Biosciences#560094, Wokingham, UK) in a final volume of 50 µl PBA for 45 min on ice in the dark. Cells were washed twice in PBA and fixed in 2% PFA (Paraformaldehyde in PBS (pH=7.4) prepared in-house) and analysed on BD FACSCanto™ II (BD Biosciences, Wokingham, UK).

2.10.2 Cell Cycle Assay

Cell cycle analysis was performed using Propidium iodide (PI, Sigma Aldrich#P4170, Dorset, UK) or Hoechst 33342 (Sigma Aldrich#14533, Dorset, UK) on the BD Calibur or BD FACSCanto™ II. For PI staining, 1 x 10^6 cells were resuspended in 200 µl citrate buffer (0.25 M sucrose, 40 mM sodium citrate, pH 7.6). Subsequently 800 µl staining solution (20 µg/ml PI, 0.5% NP40, 0.5 mM EDTA in PBS, pH 7.2) and 2 µl RNase A (50 mg/ml) were added to the cells. Cells were analysed by flow cytometry immediately. For Hoechst 33342 staining, 1 x 10^6 cells were washed and resuspended in 1 ml cell culture medium containing 10 µl Hoechst 33342 (stock concentration 10 mg/ml). After 15 mins incubation, cells were analysed on the FACSCanto™ II.

2.10.3 Apoptosis Assay

Apoptosis assays were performed using PE-Annexin V and 7-AAD (BD Biosciences#559763, Wokingham, UK) as per manufacturer's instructions or APC-Annexin V (Biolegend#640920, London, UK) and LIVE/DEAD Fixable Aqua (ThermoFisher#L34966, Paisley, UK) on the BD LSRFortessa^{TM} X-20 or Attune NxT (ThermoFisher Invitrogen, Paisley, UK). Briefly, 1 x 10^6 cells were washed twice with cold PBS and resuspended in 1mL 1 x Binding buffer of which 100 µl of sample was transferred to a new tube with the addition of 5 µl Annexin V and 5 µl 7-AAD (or 0.5 µl LIVE/DEAD Fixable Aqua). After 15 mins incubation at room temperature in the dark, samples were taken for flow cytometry analysis.

2.10.4 Mouse Peripheral Blood Staining

For the determination of murine peripheral blood engraftment with human T-ALL blasts, 20 µl of mouse blood samples were incubated with APC-huCD45 (HI30, 10 µl/sample) (BD Biosciences#555485, Wokingham, UK), PE-huCD7 (M-T701, 10 µl/sample) (BD Biosciences#555361, Wokingham, UK) and BV421-mCD45 (30-F11, 2 µl/sample) (BD Biosciences#563890, Wokingham, UK) for 20 mins at room temperature in the dark. Red cells were lysed by using freshly prepared lysis buffer (155 mM NH_4Cl, 12 mM $NaHCO_3$, 0.1 mM EDTA) for 10 mins. Thereafter, LIVE/DEAD Fixable Aqua (ThermoFisher Paisley UK) was added to cells followed by 10 mins incubation in the dark. Finally, the samples were fixed in 2% (PFA) (Paraformaldehyde in PBS (pH=7.4) prepared in-house) and analysed on the BD FACSCanto^{TM} II. The raw data were analysed and visualised using FlowJo (FlowJo_v10, Oregon, USA).

2.10.5 Cell Trace Violet Proliferation Assay

2 x 10^7 L963 cells were incubated with 5 µM Cell Trace Violet (CTV) (ThermoFisher#C34571, Paisley UK) for 20 mins at 37°C. To stop the reaction, FBS was used at the final concentration of 10%. Cells were washed in PBS and reseeded in SFEM II medium with OP9-DL1 cells. Two weeks later, cells were separated from feeder cells by multiple transferring of non-adherent cells over a time period of 4 - 6 hours. BD FACSCanto^{TM} II was used to assess CTV distribution at the excitation / emission of 405/450 nm. Data were interpreted by using FlowJo.

2.11 Drug Matrix Assays

T-ALL cell lines were seeded at 4 x 10^4 and 90 µl per well in 96-well plates (Corning#3598, NY, USA). Dasatinib (0 – 30 µM) (DC Chemicals#302962-49-8, Shanghai, China), Dexamethasone (0 – 15 µM) (Sigma Aldrich, Dorset, UK), MK2206 (0 – 50 µM) (Cat#CAY11593, Cambridge Biosciences, Cambridge, UK), SCH772984 (0 – 50 µM) (Cat#CAY19166, Cambridge Biosciences, Cambridge, UK) were titrated and added to T-ALL cells in a 10 µl volume, and cultured for 72 h in a 37°C cell incubator. Assays were performed in triplicates. Cell proliferation and cytotoxicity were assessed after three days using Cell Counting Kit 8 (CCK-8, NBS Biologicals, Cambridgeshire, UK). The tetrazolium-based substrate was added to each well and the absorbance was measured at OD450 nm in a POLARstar Omega plate reader (BMG LABTECH, Bucks, UK). IC_{50} (half-maximal inhibitory concentration) or GI_{50} (growth inhibition of 50%) values were determined by using the GraphPad Prism software.

To investigate the combined effect of dasatinib and dexamethasone, drug matrix assays were performed using T-ALL cell lines and PDX cells. Cells (4 x 10^4 cells per well for T-ALL cell lines and 8 x 10^4 cells per well for PDX cells in a volume of 80 µl were seeded in 96-well plates. PDXs were expanded *ex vivo* by co-cultured with OP9-DL1 cells for 1-2 weeks. To seed PDX cells for the drug matrix assays, PDXs and feeder cells were harvested by trypsinisation. PDX cells were separated from OP9-DL1 cells by multiple transferals of the non-adherent cells into a new plate as 1-2 hours was sufficient for OP9-DL1 cells to adhere to the plate. Dasatinib (80 nM – 50 µM) and Dexamethasone (0.09 nM – 600 nM) were titrated and added to cells (10 µl each) in 2-dimensions to create a 6 x 10 matrix. After 72 h culturing of the cells, the plates were developed with CCK-8 and read by an Omega plate reader. Cell viability data were analysed for drug-combination synergy by using Combenefit software (v2.021) (Di Veroli et al., 2016).

2.12 Mouse Work

Mice used in this project were bred and housed in the Newcastle University Comparative Biology Centre under specific pathogen-free conditions. A flow hood (FASTER S.r.l, Cornaredo (MI), Italy) was used for sterilised manipulations or experiments. All mouse work was approved and followed Home Office Project License PPL60/4552 and carried out by researchers with Home Office Personal License under the Animal (Scientific Procedures) Act 1986. All mice were humanely killed by a schedule 1 method when they exhibited endpoints as specified by the license.

2.12.1 Toxicitiy Study

A pilot toxicity study in a small number of NSG mice was carried out to explore the maximal tolerant dose of dasatinib in combination with 1 mg/kg dexamethasone. Six healthy mice (three males and three females) were dosed daily (Monday to Friday) with a combined administration of 1 mg/kg dexamethasone and dasatinib by intraperitoneal (IP) injection. Mice were examined and weighed daily upon drug administration. The starting dose of dasatinib was 5 mg/kg. This was increased weekly to 10 mg/kg, 20 mg/kg and 35 mg/kg (set as the highest dose) of dasatinib in combination with 1 mg/kg dexamethasone. At the 3rd week of treatment at 1 mg/kg dexamethasone and 35 mg/kg dasatinib, all six mice lost 10-15% of weights indicating that they could not tolerate this dose. Dosing was stopped, and weights were monitored continuously for ten days.

2.12.2 The Murine Phase II-like Clinical Trial

The power analysis of this *in vivo* study was based on the 'resource equation' approach (Arifin and Zahiruddin, 2017):

$$n = DF/k + 1$$

In this equation, k = number of treatment groups, and n = number of mice per group. The acceptable range of DF (degrees of freedom) is between 10 to 20 (R. Mead, 2012). In this study, we have used a paired T-test. In this case, k is set equal to 2. Therefore, minimum n = 10/2 + 1 = 6; maximum n = 20/2 + 1 = 11. Taken together, the total sample size of this *in vivo* study should be 24 – 44 mice in order to compare

the control vehicle, dasatinib-treated, dexamethasone-treated and drug combination-treated group.

Acute leukaemia PDXs that mimic human randomised clinical trials can characterise drug efficacy and generate potential biomarkers in both treatment-naïve and relapsed/refractory disease (Townsend et al., 2016). Ten PDXs were used for the phase II-like trial *in vivo*. All 10 PDXs were generated from NSG mice which were injected with primary patient samples previously. For each PDX sample, 2 x 10^6 cells were intrafemorally injected into 4 NSG mice each (40 mice in total). The 4 NSG mice derived from one PDX sample were matched for gender and age. Human T-ALL engraftment in mouse peripheral blood was monitored weekly by tail vein bleeds (20 µl blood/mouse) using hCD7/CD45 and mCD45 as marker proteins. The four mice of each PDX were randomised to receive the vehicle, dasatinib alone, dexamethasone alone or combination treatment by intraperitoneal (IP) injection upon engraftment of ≥ 0.5% peripheral blood $hCD45^+/hCD7^+$ cells. Treatment was given for two or three weeks depending on the clinical status of the mice. When any of the four mice displayed signs of ill health or weight loss, all four mice derived from one PDX were sacrificed at the same time to assess leukaemia engraftment in bone marrow, spleen, liver and CNS. Spleen and liver samples were collected by homogenising material through a cell strainer with PBS. Bone marrow samples were collected by flushing the lumens or crushing bones with a pestle and mortar with PBS. Flow cytometry was performed on the BD FACSCantoTM II, and data were analysed by FlowJo. GraphPad Prism was used to visualise the data and statistic was achieved by using RStudio (MA, USA) with a linear mix model. Murine heads were stripped of soft tissues and decalcified in Hilleman and Lee EDTA solution (5.5% EDTA in 10% formalin) for 3 weeks, then trimmed and put in fresh EDTA for 4 days. Samples were processed on a Tissue-Tek VIP processor using a routine overnight 17.5 hour cycle. Following paraffin wax embedding, 2.5µm sections were cut onto Poly-L-silane coated slides. Sections were then stained with Gill's haematoxylin and Putt's eosin (both made in house). Quantification of CNS infiltration was performed using a Hamamatsu Nanozoomer Digital Pathology slide scanner with digital slide management/image analysis software from Slidepath (Dublin).

Chapter 3

Identification of LCK as a Critical Gene in T-ALL

3.1 Introduction

The RNAi screens in T-ALL cells were used for identification of leukaemia vulnerabilities and drug resistance in several studies. In Notch1-induced T-ALL, miR-19 facilitates leukaemia progression *in vivo*. A genome-wide screen comprising of 12,000 shRNAs was performed to identify the targeted genes of miR-19 in murine cell line FL5-12 (Foetal Liver clone 5-12). Several PI3K regulators such as Prkaa1, Pten and PP2A were determined to be suppressed by miR-19. Thus, a novel oncogenic function of miR-19 was identified in T-ALL (Mavrakis et al., 2010). A shRNA knockdown screen was performed in T-ALL cell line DND41 to investigate GSI (γ-secretase inhibitors) resistance. The readout was an array format of cell viability dye. In this screen, they identified the chromatin regulator BRD4 leading to resistance to GSI. The BRD4 inhibitor JQ1 enhanced apoptosis, and the drug combination of GSI-JQ1 effectively reduced primary leukaemias *in vivo* (Knoechel et al., 2014). TYK2 was identified as a critical gene regulating T-ALL survival in a tetracycline-induced shRNA screen targeting 1740 genes in Jurkat, CCRF-CEM and SKW-3 cells. After labelling shRNA-induced cells with Cy3 and un-induced cells with Cy5 and amplification and barcoding gDNA, amplicons were hybridised onto the microarray chip for analysing relative abundances of each population. After identification of TYK2, they also found that the TYK2-STAT1-BCL2 pathway promotes T-ALL survival. TYK2 mutations were discovered in 4 cell lines, and in the other TYK2 dependent cell lines IL-10/IL-10R activated TYK2 (Sanda et al., 2013).

However, these shRNA screens were performed in murine or human T-ALL cell lines *in vitro*. To explore the importance of the pTCR/TCR complex for T-ALL proliferation or survival, targeted shRNA screens were performed not only in four T-ALL cell lines but also in three PDX samples *in vivo*. The shRNA abundance in our study was determined by the state-of-the-art next-generation sequencing, which increases the sensitivity compared with microarray-based approaches (Sims et al., 2011).

3.2 Targeted shRNA Screens in T-ALL Cells

3.2.1 Generation of pLKO shRNA Library

To explore the critical genes of pTCR/TCR signalling for T-ALL cell proliferation or survival, a library targeting six essential components of pTCR/TCR signalling complex: *PTCRA, CD3E, LCK, FYN, ZAP70* and *LAT* were designed. The shRNA library (Figure 12) also contained positive controls (shRNAs targeting *RPL9* and *RPS29* were expected to be lost because cells without ribosome genes could not survive, and shRNAs targeting *PTEN* were supposed to be enriched because *PTEN* is a tumour suppressor in T-ALL) and several negative controls (shRNAs expected to have no change). The negative controls were selected from in-house RNAi screens in various leukaemia subtypes. The core sequences of shRNAs were obtained from Dharmacon (http://dharmacon.horizondiscovery.com). Oligos were cloned into the shRNA expression vector pLKO5d-SFFV-eGFP.

Targets (x3)	Positive controls (x2)	Negative controls	Others (x3)
PTCRA	*RPL9*	*CD19 (x2)*	*PTEN*
LCK	*RPS29*	*TRPM7 (x2)*	
FYN		*KLHL7*	
ZAP70		*DDB2*	
LAT		*ERGIC3*	
CD3ε		*SESN2*	
		FLG	
		RUNX1/ETO	
		NTC	

Figure 12. The composition of targeted shRNA screen library. The shRNA library was composed of 36 constructs including three shRNAs per gene for pTCR/TCR complex genes *PTCRA, LCK, FYN, ZAP70, LAT* and *CD3E*; two shRNAs per gene for depletion positive controls *RPL9* and *RPS29*; eleven shRNAs targeting genes that were unlikely to change as indicated in in-house RNAi screens; and three shRNAs targeting *PTEN* as the enrichment positive controls.

All shRNA sequences were confirmed by Sanger sequencing. Two sequences targeting the gene LCK (namely shLCK#1 and shLCK#3) are shown in Figure 13. The results confirmed the sequences originally ordered. All 36 constructs were confirmed to be successfully generated.

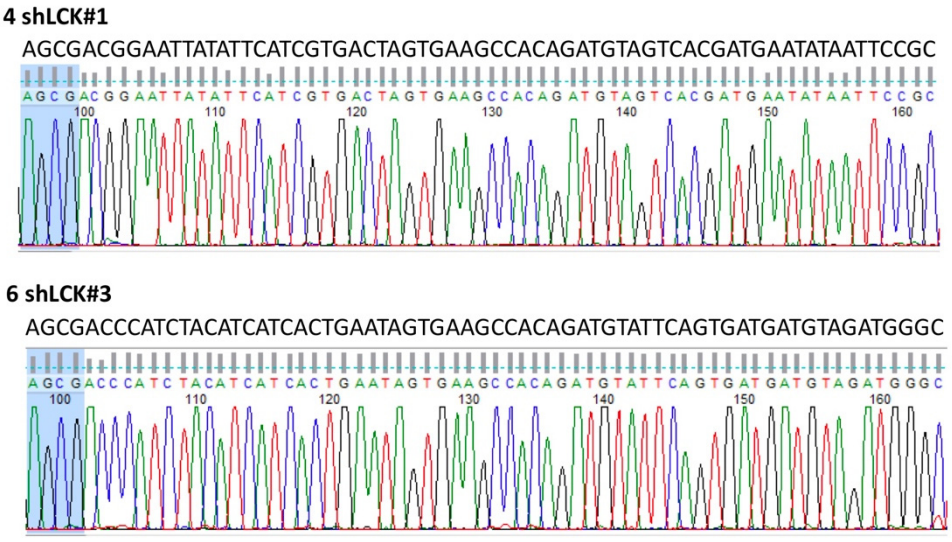

Figure 13. Sanger sequencing results of shLCK#1 and shLCK#3. The chromatogram plots demonstrate the sequence of shLCK#1 and shLCK#3 cloned into the pLKO5d-SFFV-eGFP vector. Top line sequences corresponds to the designed shRNA sequences. Green: Adenine (A); Red: Thymine (T); Blue: Cytosine (C); Black: Guanine (G). The shaded area of AGCG represents the start site of the oligonucleotides.

3.2.2 Primer Design and PCR Condition Optimisation for Genomic DNA Amplification

Previously, our lab has performed shRNA screens using pTRIPZ and pGIPZ backbones. However, T-ALL cell lines are generally difficult to transduce when using pTRIPZ and pGIPZ. Thus, the pLKO5d-SFFV-eGFP backbone was chosen aiming for higher transduction efficiencies for T-ALL cell lines. The amplification primers were designed as follows: the forward primer fitted to the Illumina P5 sequence required for the attachment of the library fragment to the flow cell surface, with an additional sequence needed for binding of the standard Illumina sequencing primer, and a pLKO5d-SFFV-eGFP vector specific binding sequence; the reverse primer included the Illumina P3 sequence, the index sequence, and a vector specific binding sequence (Figure 14). After alignment those two primers which were previously used in the group to the pLKO5d-SFFV-eGFP vector, only the reverse primer could be used to amplify the shRNA region of pLKO5d-SFFV-eGFP. The full list of reverse primers with 89 barcodes is shown in Appendix 1. Three additional forward amplification primers were designed by myself accordingly.

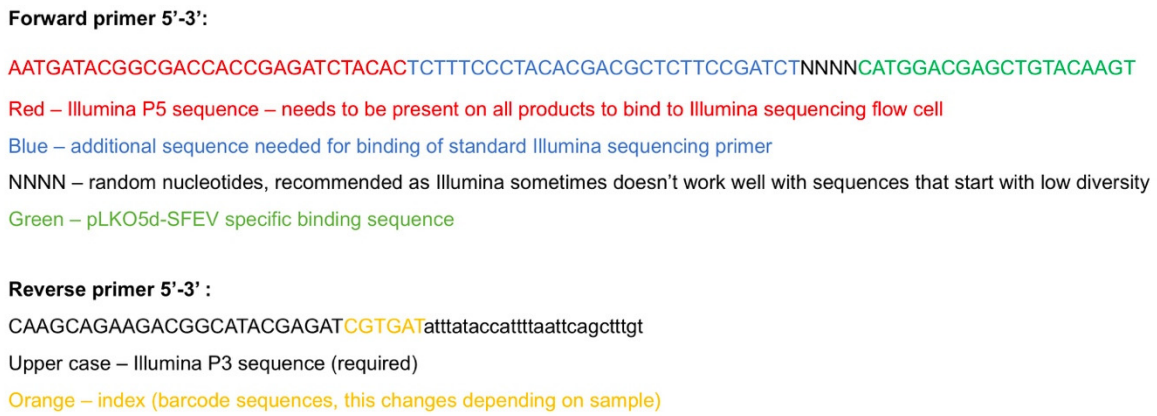

Figure 14. Primer design for shRNA library amplification. The forward primer (newly designed) contains Illumina P5 sequence (red), standard Illumina sequencing binding site (blue), stagger sequences (black) and pLKO5d-SFFV specific binding site (green). The reverse primer contains Illumina P3 sequence (upper case in black), index sequences (orange) and pLKO5d-SFFV binding sites (lower case in black).

To design a forward primer specific for the pLKO5d-SFFV-eGFP vector, the vector sequences were blasted against the human genome (NCBI BLAST Genome (GRCh38.p12 reference, Annotation Release 109)). Primers were created 5' of the shRNA cloning site within the GFP sequence. This was necessary when using the pLKO5d-SFFV-eGFP vector, as there were 153 bp (5') before shRNA hairpin structure overlapping with Homo sapiens chromosome 6. Initially, three primer binding sites were selected and tested for their amplification efficiency. Full primer sequences are shown in Appendix 1. NGS-F1 BS (binding site) and NGS-F3 BS were overlapping and situated closer to the shRNA sequence while NGS-F2 BS was further upstream from the shRNA sequence which would generate a predicted amplification fragment of 863 bp (Figure 15).

Green: GFP sequences
Red: shRNA hairpin
Yellow: final primer binding sequences
Black: Home sapiens chromosome 6 overlap

Figure 15. Design of three primer binding sites for specifical amplification of the pLKO5d-SFFV-eGFP shRNA region. About 150 bp nucleotides 5' of the shRNA region (red) corresponds to a sequence found in Homo sapiens chromosome 6 (black). NGS-F1 BS (red italic, underlined) and NGS-F2 BS (red italic, not underlined) binding sites were closer to the shRNA sequences compared to the NGS-F2 binding site. Final primers used for library amplification are highlighted in yellow (NGS-F3 BS and reverse primer binding site).

The three primer sets (forward primer NGS-F1, NGS-F2, NGS-F3 and the reverse primer) were tested for library amplification efficiency. For this, genomic DNA (gDNA) of CUTLL1 wildtype (WT) cells, CUTLL1-shNTC and MOLT4-shNTC cells was used as PCR template. In the meantime, PCR efficiency under different buffer conditions was also considered. The standard buffer from Phusion High-Fidelity PCR kit was compared with/without the addition of $MgCl_2$ and GC-rich buffer. Overall, all three sets of primers gave specific amplification (expected size of NGS-F1/R 436bp; NGS-F2/R 863bp; NGS-F3/R 433bp) of shRNA integration sites since there was no amplification band in CUTLL1 WT cells. The NGS-F3 gave rise to a brighter DNA amplicon, and GC-rich buffer generated the maximum amount of PCR products (Figure 16). Using the NGS-F2 primer, a PCR fragment was generated which turned out to be too long for MiSeq analysis. This primer was thus not used in further experiments. Thus, the NGS-F3 primer and the GC-rich buffer were used for the library amplification of the targeted shRNA screen.

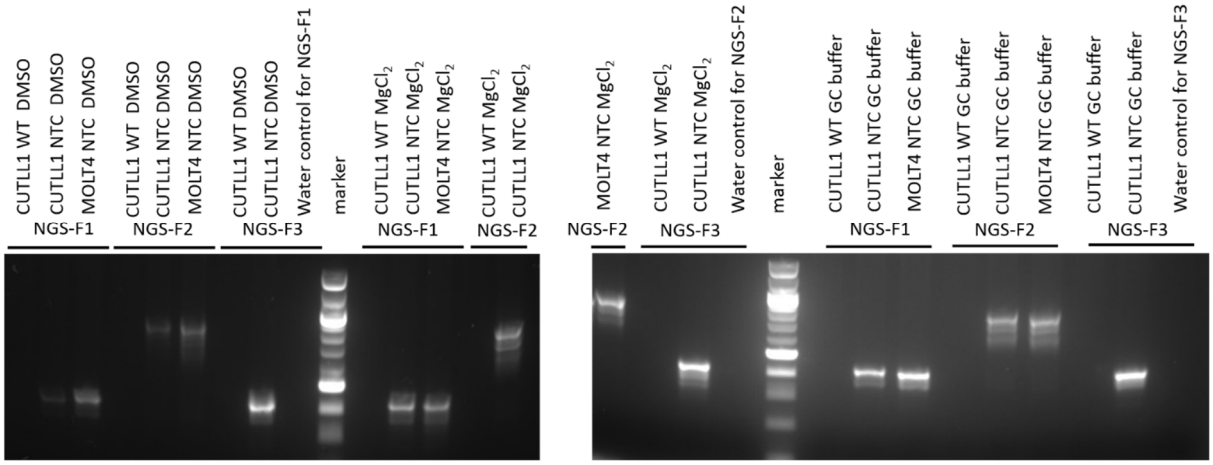

Figure 16. The optimisation of primer sets and PCR buffer conditions. Three newly in-house designed forward primers and a reverse primer were tested. gDNA from CUTLL1 WT, CUTLL1 shNTC and MOLT4 shNTC was used as PCR template. The standard buffer with/without $MgCl_2$ and GC-rich buffer were also tested to compare the amplification efficiency. The amplicons were separated on an agarose gel (2%). Amplicon size NGS-F1/R 436bp; NGS-F2/R 863bp; NGS-F3/R 433bp. Marker, O'RangeRuler Ladders.

Next, the effect of the number of PCR cycles on library amplification was tested. As expected, more thermocycles gave more abundant PCR products (Figure 17). Twenty-three cycles was recommended by the protocol of Thermo Scientific Decode Pooled Lentiviral shRNA Screening Libraries, however, the yield after gel purification was not sufficient for NGS sequencing which requires at least 10 nM (2.6 ng/µl) of the amplicon. Using 27 or 31 PCR cycles, no non-specific amplification of the gDNA was observed. Thus, the library amplification was performed using 31 PCR cycles (Figure 17). After the library amplification, PCR products were purified from the agarose gel. Qubit Fluorometric Quantification was used to assess the yield of DNA fragments after PCR amplification (Appendix 2).

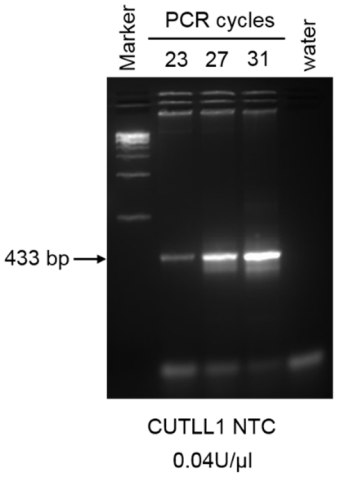

Component	µl per reaction	Final concentration
5xPhusion GC buffer	10 µl	1x
10 mM dNTPs	1 µl	200 µM each
NGS-F3 (100 µM)	0.25 µl	0.5 µM
Reverse Indexed primer (10 µM)	2.5 µl	0.5 µM
gDNA + PCR grade H_2O	35.25 µl	~ 825 ng/reaction
Phusion Hot Start II DNA Polymerase	1 µl	0.04 U/µL
Total	50 µl	

Figure 17. Optimised PCR conditions. The PCR cycles of 23, 27 and 31 were tested with gDNA of CUTLL1 shNTC. A 433bp fragment was generated by the primer set of NGS-F3 and a reverse indexed primer. The fragments were visualised on a 2% agarose gel. PCR conditions are listed in the table. Marker, GeneRuler 1kb DNA Ladder.

3.2.3 Transduction Efficiency of T-ALL Cell Lines in Targeted Screens

Once the 36 shRNA constructs were generated, equal amounts of individual shRNAs were pooled together and lentiviral shRNA libraries were generated. For the targeted screen in T-ALL cell lines (SUPT1, MOLT4, CUTLL1 and HPB-ALL), two independent batches of lentiviral shRNA libraries were produced. Virus titration was performed to optimise for transduction efficiency (Figure 18). High transduction efficiency may result in multiple copies of shRNA in one cell, while low efficiency may cause low library complexity or non-sufficient sequencing depth. Therefore, a range of 20 - 30% transduction efficiency was chosen because this range was reported to give

approximately one shRNA integration site per cell (Fehse et al., 2004). Overall, library 2 transduced HPB-ALL and MOLT4 (22.2% - 65%) better than library 1 (10.2% - 54.8%). Higher transduction efficiencies, as demonstrated by GFP expression, were observed with higher virus concentrations (Figure 18). Finally, HPB-ALL with 50 µl library 1 (20.9%) and 20 µl library 2 (26.2%), and MOLT with 50 µl library 1 (18.1%) and 20 µl library 2 (22.2%) were selected and expanded to proceed with the screening. A similar strategy was used for SUPT1 and CUTLL1 cells. Transduced cells with 20 - 30% efficiency were chosen to continue the targeted shRNA screen.

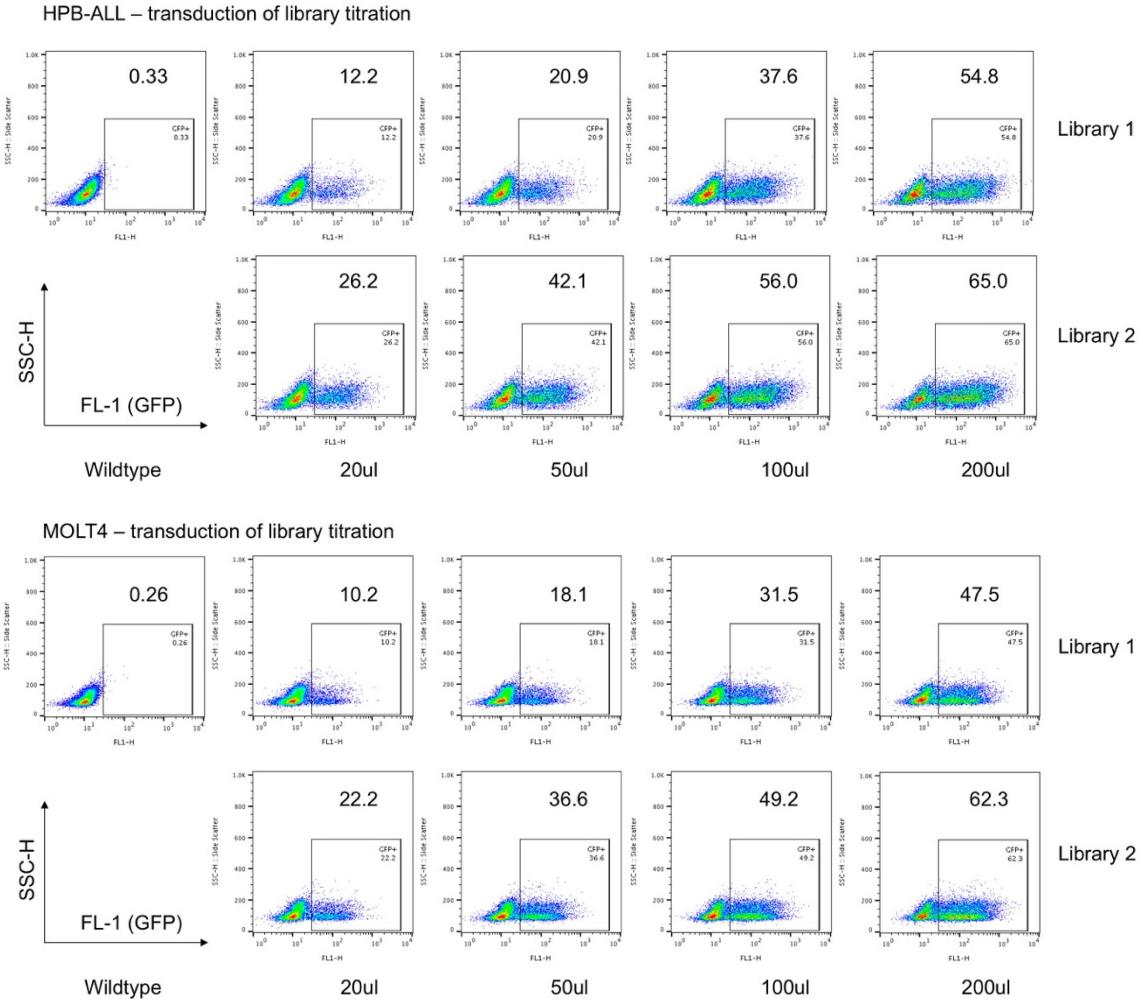

Figure 18. Verification of transduction efficiencies using lentiviral library 1 and 2. HPB-ALL and MOLT4 were transduced with library 1 and 2 using different amounts of non-concentrated virus supernatant (20, 50, 100 and 200 µl). The first column correspond to non-transduced cells. After forward/sideward scatter gating for alive cells, flow cytometry plots were generated showing GFP expression (X-axis); Y-axis, SSC-H. The number in the top right indicates the percentage of GFP^+ cells.

3.2.4 A Targeted Screen in T-ALL Cell Lines Demonstrates the Importance of TCR Components.

The pTCR/TCR complex is composed of pTCRα / TCRα, TCRβ, CD3ε, CD3δ, CD3γ and CD3ζ chains. The TCRα chains undergoes somatic recombination from V(D)J rearrangement after the TCRβ chain. However, the pTCRα is a nonpolymorphic gene that is translated from the *PTCRA* gene. It is reported that *PTCRA* transcript is expressed in 57% of the TCRαβ lineage and 40% of TCRγδ T-ALLs (2003 Blood). Since the pTCR complex, encompassing PTCRA, provides proliferative and survival advantage during normal T-cell development presumably without ligand binding, we focused our intention first on *PTCRA* as a potentially critical gene in T-ALL. After performing qPCR of twelve T-ALL cell lines (Figure 19), four T-ALL cell lines (SUPT1, CUTLL1, MOLT4 and HPB-ALL) with high *PTCRA* expression were chosen to conduct targeted shRNA screens. Karpas 45 was not chosen due to its more demanding nature when cultured and rather low transduction efficiencies.

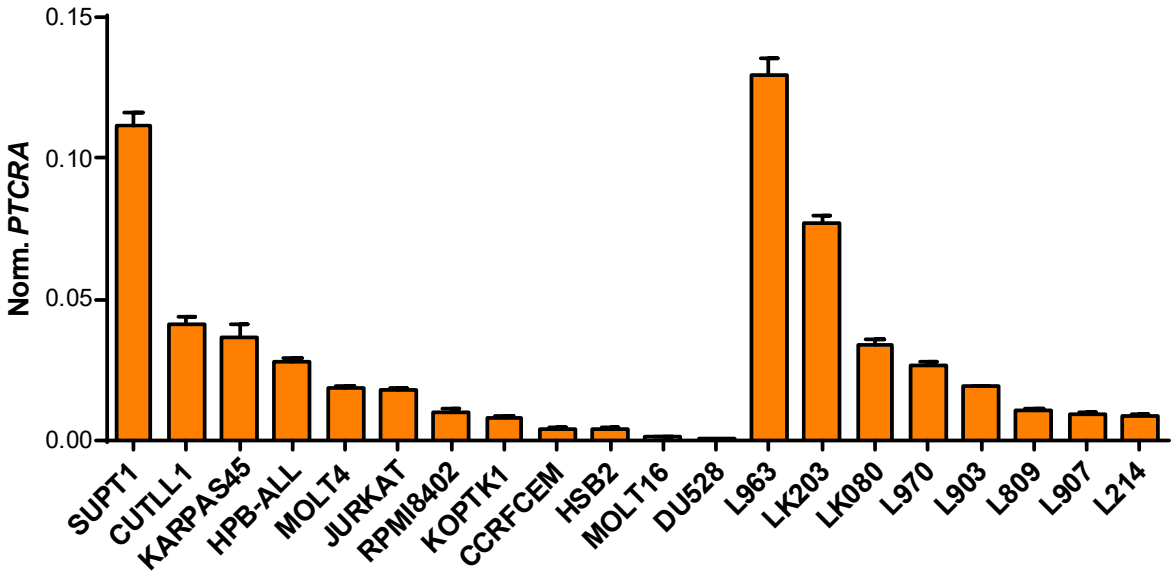

Figure 19. The transcription level of *PTCRA* in a panel of T-ALL cells. *PTCRA* expression was normalised relative to the housekeeping gene *GAPDH*. In T-ALL cell lines, SUPT1, CUTLL1, Karpas 45, HPB-ALL, Jurkat and MOLT4 express high mRNA levels of *PTCRA*. Primary patient samples of L963, LK203, LK080, L970, L903, L809, L907 and L214 were also examined for *PTCRA* expression.

The selected four T-ALL cell lines (SUPT1, CUTLL1, MOLT4 and HPB-ALL) were transduced with lentiviral library. Two independent lentiviral shRNA libraries were prepared, one of them for repetition experiments. Baseline samples were harvested six days after transduction. Cells were continuously cultured and old medium was

replaced by fresh medium every three days. To track shRNA depletion or enrichment over time, samples at day 16, 30 and 40 were harvested. Overall, each cell line had eight samples (two independent samples each at baseline, day 16, day 30 and day 40), with a total sample number of 32. After extraction of gDNA, each sample was barcoded and amplified with different reverse primers (Appendix 1). Each barcoded sample was quantified by Qubit Fluorometer and pooled together accurately to generate the library. This sequencing library included 82 barcoded samples (both T-ALL cell line samples and PDX samples) (Figure 20). The sequencing library was composed of an equimolar pool of 82 samples (2.6 ng/µl, 10nM each). NGS was performed at the Genomic Core Facility in Newcastle University (NCL) and generated 25,000,000 reads which was sufficient for 8000 x coverage. The sequencing reads underwent bioinformatic analyses to determine the accumulation or loss of cell clones. Briefly, raw sequencing reads were trimmed at both ends up to the locations of barcode sequence before aligning to the reference shRNA barcodes. Read counts were extracted from aligned sequence files. Differential representation analyses of aligned read counts from different screen datasets were performed.

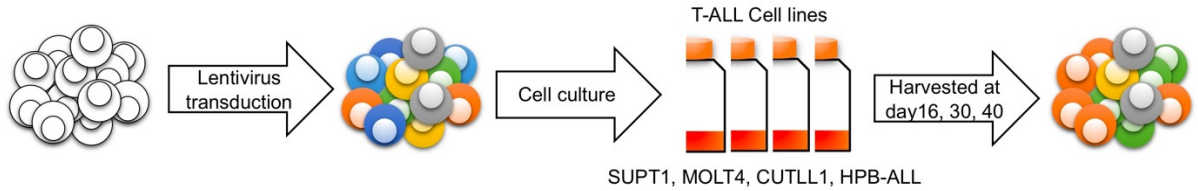

Figure 20. *In vitro* shRNA screen workflow. T-ALL cell lines SUPT1, MOLT4, CUTLL1 and HPB-ALL were transduced with the lentiviral library containing 36 shRNAs and cultured *in vitro*. The gDNA samples were collected at baseline (day 6), day 16, day 30 and day 40. NGS was used to determine shRNA enrichment and depletion.

The analysis in T-ALL cell lines took different time points into consideration, therefore slope was used for the magnitude of the relative change in shRNA abundance over time (16, 30 and 40 days) after *in vitro* propagation. In SUPT1 cells, shRPL9#1, shRPL9#2 and shRPS29#2 targeting ribosome genes were depleted (slope: -0.56, -0.18 and -0.53; p-value: 2×10^{-16}, 0.00034 and 2.7×10^{-17}) while all 3 shRNAs of PTEN were enriched significantly (slope, p-value: shPTEN#1 0.29, 4.8×10^{-6} shPTEN#2 0.28, 3.25×10^{-9} shPTEN#3 0.42, 1.06×10^{-8}), suggesting this screen was successfully conducted as SUPT1 expresses wildtype PTEN which restricts cell proliferation and

loss of PTEN is expected to cause cell proliferation, thus, resulting in an enrichment of cells expressing shPTEN. Secondly, cells expressing shRNAs targeting one of four specific components of the pTCR/TCR complex were significantly depleted: two shRNAs targeting LCK (slope, p-value: shLCK#1 -0.35, 4.5 x 10^{-7} shLCK#3 -0.62, 5.1 x 10^{-13}), two PTCRA targeting shRNAs (slope, p-value: shPTCRA#2 -0.54, 1.08 x 10^{-11} shPTCRA#3 -0.36, 0.000489), one ZAP70 shRNA (slope -0.37; p-value 2.55 x 10^{-8}) and two CD3E shRNAs (slope, p-value: shCD3E#1 -0.24, 9.3 x 10^{-6} shCD3E#2 -0.14, 0.009456) (Figure 21).

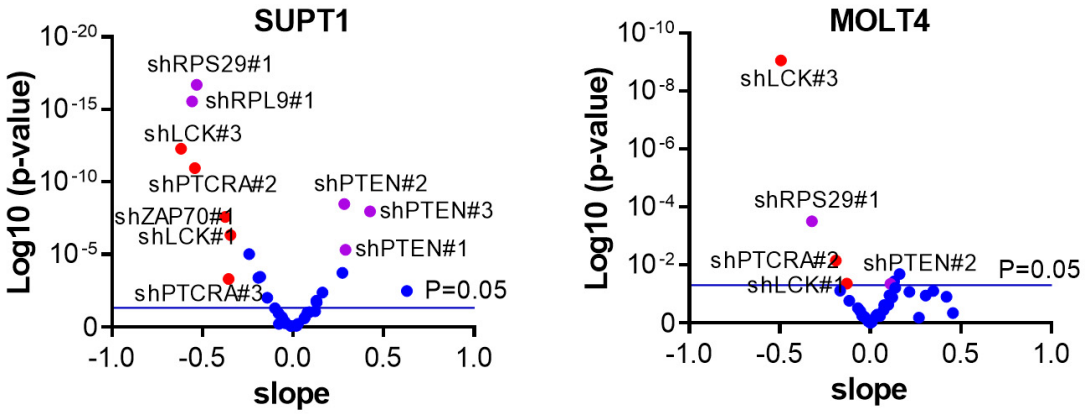

Figure 21. Volcano plots of the targeted shRNA screens in SUPT1 and MOLT4. The magnitude of the relative shRNA change in shRNA abundance over time of SUPT1 (left) and MOLT4 (right) is represented. Depleted (negative slope) and enriched (positive slope) shRNAs from two independent experiments are shown on the X-axis. The Y-axis represents log10 transformed p values. Dots above the line show significance ($p < 0.05$). Red dots indicate significantly depleted shRNAs targeting the pTCR/TCR complex. Purple, positive controls. Raw data are shown in Appendix 3.

The degree of shRNA depletion and enrichment in MOLT4 cells was less pronounced compared with SUPT1 cells. The positive control shRPS29#1 was significantly lost (slope -0.32; p-value 0.0003114). MOLT4 carries a PTEN deletion, therefore no significant enrichment was seen of shPTEN#1 and shPTEN#3. Importantly the depletion of shLCK#1 (slope -0.13; p-value 0.04), shLCK#3 (slope -0.49; p-value 8.6 x 10^{-10}), and shPTCRA#2 (slope -0.19; p-value 0.0069573) were significant, suggesting an essential role of LCK and pTCRα for cell proliferation or survival in MOLT4 cells (Figure 21).

In CUTLL1 cells, all three PTEN shRNAs showed significantly enrichment (slope, p-value: shPTEN#1 0.23, 2.4 x 10^{-17} shPTEN#2 0.11, 4.7 x 10^{-4} shPTEN#3 0.27, 3.17 x 10^{-21}) while the positive control for depletion shRPL9#2 was lost (slope -0.07; p-value 0.016). With regards to pTCR/TCR components, only shLCK#3 (slope -0.36; p-value

1.27 x 10^{-30}) and shZAP70#1 (slope -0.14; p-value 9.67 x 10^{6}) were lost (Figure 22). The shLCK#1 was also lost (slope -0.055), however, not yet statistical significant (p=0.059).

A more pronounced difference was observed in HPB-ALL cells. Similar with SUPT1, three shRNAs targeting PTEN (slope, p-value: shPTEN#1 0.19, 1.25 x 10^{-6} shPTEN#2 0.36, 8.99 x 10^{-15} shPTEN#3 0.32, 1.14 x 10^{-16}) were enriched and shRPL9#1 (slope -1.21; p-value 4.08 x 10^{-22}), shRPL9#2 (slope -0.55; p-value 2.77 x 10^{-14}) and shRPS29#1 (slope -0.16; p-value 5.1 x 10^{-4}) were depleted significantly. All three shRNAs against LCK were lost (slope, p-value: shLCK#1 -0.12, 9.76 x 10^{-4} shLCK#2 -0.17, 4.79 x 10^{-6} shLCK#3 -0.31, 2.41 x 10^{-17}). However, the effect of shRNAs targeting ZAP70 and PTCRA were inconsistent. shZAP70#1 was lost (slope -0.15; p-value 4.9 x 10^{-4}) and shZAP70#3 (slope 0.30; p-value 2.1 x 10^{-10}) was enriched; shPTCRA#2 was lost (slope -0.09; p-value 0.019) and shPTCRA#1 (slope 1.16; p-value 6.5 x 10^{-23}) was enriched. Intriguingly, two shRNAs targeting FYN (slope, p-value: shFYN#1 -0.11, 0.003 shFYN#2 -0.15, 0.001) were identified to be lost only in HPB-ALL cells (Figure 22).

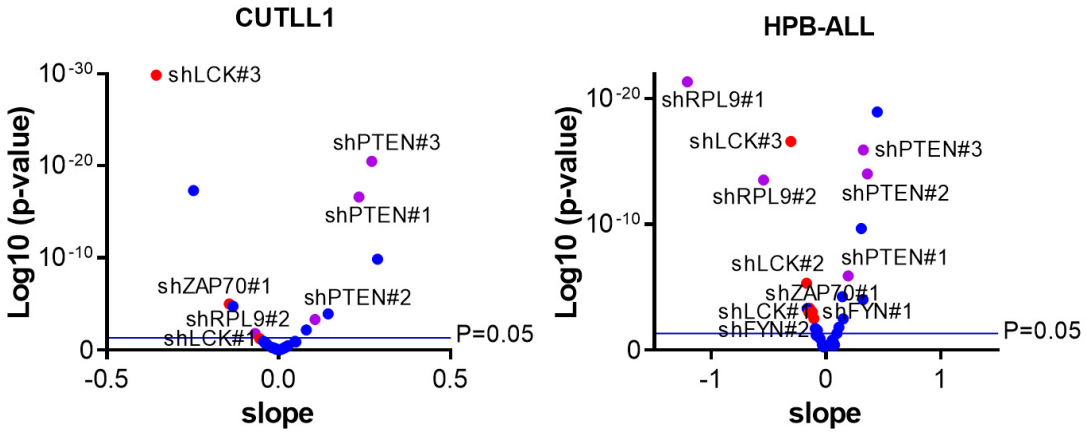

Figure 22. Targeted screen in T-ALL cell lines CUTLL1 and MOLT4. Volcano plots show significantly lost and enriched shRNAs during cell propagation. Depleted (negative slope) and enriched (positive slope) shRNAs are shown on the x-axis. The y-axis represents log10 transformed p values. ShRNAs above the line show significance ($p < 0.05$). Red dots indicate significantly depleted shRNAs targeting the pTCR/TCR complex. Purple, positive controls. Raw data are shown in Appendix 3.

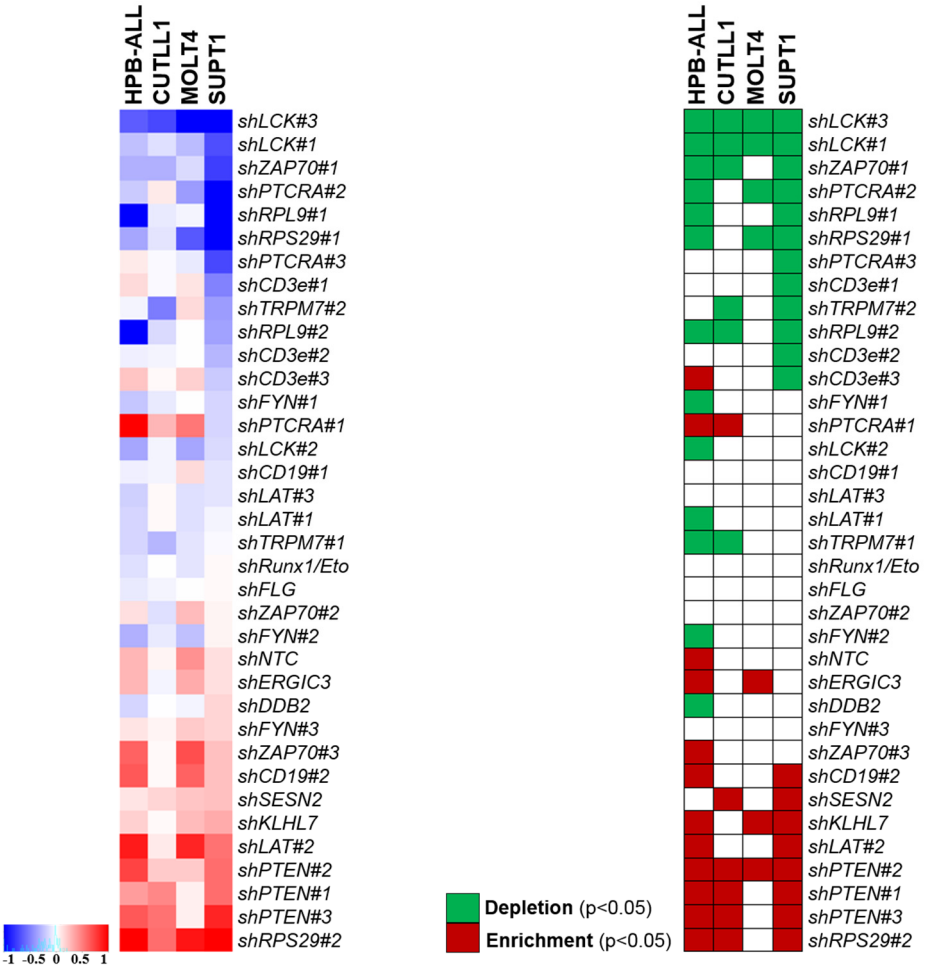

Figure 23. The heatmap summaries shRNAs depletion and enrichment in all four cell lines. Heatmap on the left depicting gains (red; > 0 - (+1) positive slope) or losses (blue < 0 - (-1) negative slope) of shRNA constructs after *in vitro* culture of four cell lines. The right heatmap shows the significance of each shRNA in all four T-ALL cell lines; significant enrichment ($p < 0.05$ red), significant depletion ($p < 0.05$ green), not significant ($p > 0.05$ white).

The targeted shRNA screens in T-ALL cell lines highlighted the significance of pTCR/TCR components in T-ALL cell maintenance. Overall, the screen itself worked well as positive controls behaving precisely as what we expected such as shRNAs shRPL9#1, shRPL9#2 and shRPS29#1 targeting ribosome genes were depleted. SUPT1, CUTLL1, and HPB-ALL cells are PTEN wildtype in which all three shRNAs targeting PTEN were significantly enriched. Consistently, in PTEN null MOLT4 cells, shPTEN#1 and shPTEN#3 were not enriched. The shPTEN#2 was significantly enriched with a slope of 0.1. Designed negative controls such as shRUNX1/ETO, shFLG and shNTC did not undergo depletion or enrichment during the time course.

Across all four cell lines, the most significant change is observed for LCK whose shRNA#3 and #1 showed top 1 and top 2 depletion, suggesting that LCK is essential for cell propagation in T-ALL cell lines (Figure 23).

Some discrepancies could be observed when comparing four cells. They might be explained by (i) insufficient knockdown, e.g. shLCK#2 only showed significant depletion in HPB-ALL cells, but not the other three cell lines. Verification of LCK knockdown of all three shRNAs in CUTLL1 and MOLT4 revealed barely any knockdown of LCK mRNA when using shLCK#2 in CUTLL1 and MOLT4 (Figure 30) suggesting this shRNA is less efficient than the other two shRNAs. The depletion of shLCK#2 in HPB-ALL cells might mean that LCK expression was affected in this particular cell line, however, this requires further validation. Moreover, shZAP70#1 was significantly lost in SUPT1, CUTLL1 and HPB-ALL cells, but no substantial effect was observed by shZAP70#2 and #3. Validation ZAP70 KD *in vitro* in CUTLL1 and MOLT4 cells indicated that only shZAP70#1 reduced *ZAP70* on the transcriptional level (Figure 30). The slope of shZAP70#1 in MOLT4 cells was -0.069, indicating it was lost during the screen. However, the p-value fell just short of statistical significance. This might be due to lower transduction levels in MOLT4 compared with the other three cell lines. In further *in vitro* validation experiments, it was confirmed that knockdown of *ZAP70* by shRNA#1 indeed impaired cell proliferation of MOLT4 (Figure 30).

(ii) Differential expression patterns of pTCRα. The shRNAs targeting *PTCRA* showed different patterns in four T-ALL cell lines. According to our analyses of these T-ALL cell lines, SUPT1 and MOLT4 cells are cells that only express pTCR while CUTLL1 and HPB-ALL express both pTCR and TCR. This might explain why SUPT1 and MOLT4 cells showed depletion of shPTCRA#2 and #3, since they are more dependent on the pTCR signalling complex. On the contrary, CUTLL1 and HPB-ALL might overcome pTCR depletion by compensating through TCR signalling.

(iii) Lack of on-target effect. Two shRNAs each to target ribosome proteins RPL9 and RPS29 as positive controls for this screen were used. Anti-sense sequences were obtained from other gene-editing screens in our lab. As expected, shRPL9#1 and #2 were depleted in all four T-ALL cell lines indicating the essential role of ribosome protein RPL9 in T-ALL cells. However, shRPS29#1 was depleted in HPB-ALL, SUPT1 and MOLT4 while shRPS29#2 was enriched in HPB-ALL, CUTLL1 and SUPT1. This raises the possibility that either shRPS29#2 lack of on-target effects or both shRNAs targeting RPS29 work differently at transcript levels.

(iv) Differences in T cell biology. Several shRNA sequences were obtained from other group members' screens in leukeamic cells, in which knockdown did not affect the leukeamic cell proliferation/engraftment. However, some of these did not behave as proper negative controls in our screens, such as shTRPM7#1 and #2, shSESN2, shERGIC3 and shKLHL7. This is most likely due to differences in T-ALL cell biology compared with other types of leukaemia.

Together, among the six components of the pTCR/TCR complex included in this shRNA screen, depletion of the kinases LCK and ZAP70 indicated a significant and essential role in T-ALL cell maintenance in all four cell lines. In contrast FYN, CD3ε and LAT does not seem to be essential in general as shCD3E was lost only in SUPT1 cells, whilst shFYN showed depletion only in HPB-ALL. Two of LAT shRNAs were not depleted or enriched, whereas the third shRNA of LAT showed enrichment in SUPT1 and HPB-ALL. Overall, it suggests that these three genes are less important for cell proliferation in these four T-ALL cell lines.

3.2.5 Targeted Screens in Patient-Derived Xenografts (PDXs)

The same targeted screen which was performed in T-ALL cell lines (Chapter 3.2.4) was performed in three PDXs L963, LK080 and LK203 as they express higher levels of *PTCRA* at the mRNA level among eight PDXs that I have tested (Figure 19). They were transduced with highly concentrated lentivirus generated from the same library mentioned previously. Transduction efficiencies of L963, LK080 and LK203 were 3%, 5% and 7.5% respectively as demonstrated by GFP positivity. Two days after transduction, baseline samples were harvested in triplicates, cells were washed several times and injected into six NSG mice per PDX. Mice were weighed and monitored twice a week. When leukaemia symptoms were observed, the six mice derived from one patient sample were harvested around the same time. Mice injected with LK203 were harvested 54/56 days after injection and enlarged spleens were observed weighing between 0.55 - 0.74g. Mice with the relapse sample LK080 were harvested 67/68/69 days after injection. The spleen weight was 0.88 - 1.27g for five mice, with one mouse displaying a smaller spleen (0.45g). The patient sample L963 took the longest time to full leukaemia engraftment *in vivo* with a 77/81 day lifespan. The spleens derived from these mice were enlarged with a weight of 0.70 - 1.05g. Bone marrow samples from femurs and tibias were collected and used in NGS analysis. In parallel, PDX LK080 and LK203 were also kept *in vitro* for 30 days. Two samples (day 16 and day 30) were harvested for LK080, and three samples (day 16, day 30 with MSC, and day 30 without MSC) were collected for LK203 after long-term culture. All gDNA was extracted and amplified with barcode primers. The purified amplicons were sequenced in house using NGS.

3.2.5.1 The Targeted shRNA Screen in LK080

Unfortunately the NGS analysis of LK080 both *in vivo* and *in vitro* failed. For the *in vivo* screening of LK080, a large number of shRNAs was represented by very low read counts (< 10), which means many shRNAs in these samples were under sampled due to a few dominant clones in the library (shRNAs with extremely high counts). For example, in mouse 1 and mouse 6, the frequency of shRUNX1/ETO reads was 90.2%, 99.6%, 85.5%, and 98.3% in the spleen and bone marrow cells; mouse 3 had dominant clones containing shZAP70#2, shCD19#1 and shRUNX1/ETO with a total percentage of 87.9% in the spleen and 99.9% in the bone marrow. Similar results were observed in mouse 2, 4 and 5 (Figure 24). Two spleen samples of mouse 2 and 5 failed in gDNA

amplification, which might be indicative of clonal engraftment of non-transduced cells. Overall, these results suggest that LK080 cells might undergo clonal expansion *in vivo*, rendering this sample non-informative in our analysis.

ID	Sample	Index	FYN#1	ZAP70#2	LAT#3	CD19#1	TRPM7#2	RUNX1/ETO	PTEN#1	Total (%)
Mouse 1	Spleen	13						90.2		90.2
Mouse 1	BM	19						99.6		99.6
Mouse 3	Spleen	15		41.2		20.4		26.2		87.9
Mouse 3	BM	21				86.5		13.3		99.9
Mouse 4	Spleen	16					76.0			76.0
Mouse 4	BM	22					83.4			83.4
Mouse 6	Spleen	18						85.5		85.5
Mouse 6	BM	24						98.3		98.3
Mouse 2	BM	20	37.2		31.0				30.1	98.3
Mouse 5	BM	23		36.1		37.7				73.8

Figure 24. Dominant clones of LK080 *in vivo* screening. Mouse ID, sample origin, barcode index and the abundance of some dominant clones in percent (shFYN#1, shZAP70#2, shLAT#3, shCD19#1, shTRPM7#2, shRUNX1/ETO, shPTEN#1) are shown. The abundance of total dominant clones was calculated and listed in the last column.

On the contrary, LK080 *in vitro* screening samples did not show any clonal expansion. All 36 shRNAs were presented in samples from day 16 and day 30, without significant loss of LCK shRNAs in LK080 *in vitro* screening. There was significant depletion of ribosome shRNAs and enrichment of shPTEN shRNAs; however, the fold change (log_2(FC)) was much less compared with LK203 *in vitro* screening (-0.79 - 0.47 in LK080 while -1.3 - 1.05 in LK203 sample), suggesting that LK080 might have less doublings *in vitro* compared with LK203. In addition, the viability of *ex vivo* growing LK080 cells was around 50% only, compared with ≥ 75% for LK203. In summary, the *in vitro* culture of LK080 was not as successful as LK203 in detecting differential shRNA expression, possibly due to less cell cycle divisions and poor viability.

3.2.5.2 The Targeted shRNA Screen in LK203

The samples derived from *in vivo* screening of L963 and LK203 were analysed for their shRNA representation. An intended output of shRNA screens would be an equal distribution and a full presentation of all shRNAs in the baseline samples while depletion of shRNAs targeting gene essentiality of T-ALL cells and enrichment of shRNAs of tumour suppressor genes during leukaemia propagation. First, similar to T-ALL cell lines, the baseline samples of L963 and LK203 showed an equal and homogenous distribution of each shRNA in the library (Figure 25).

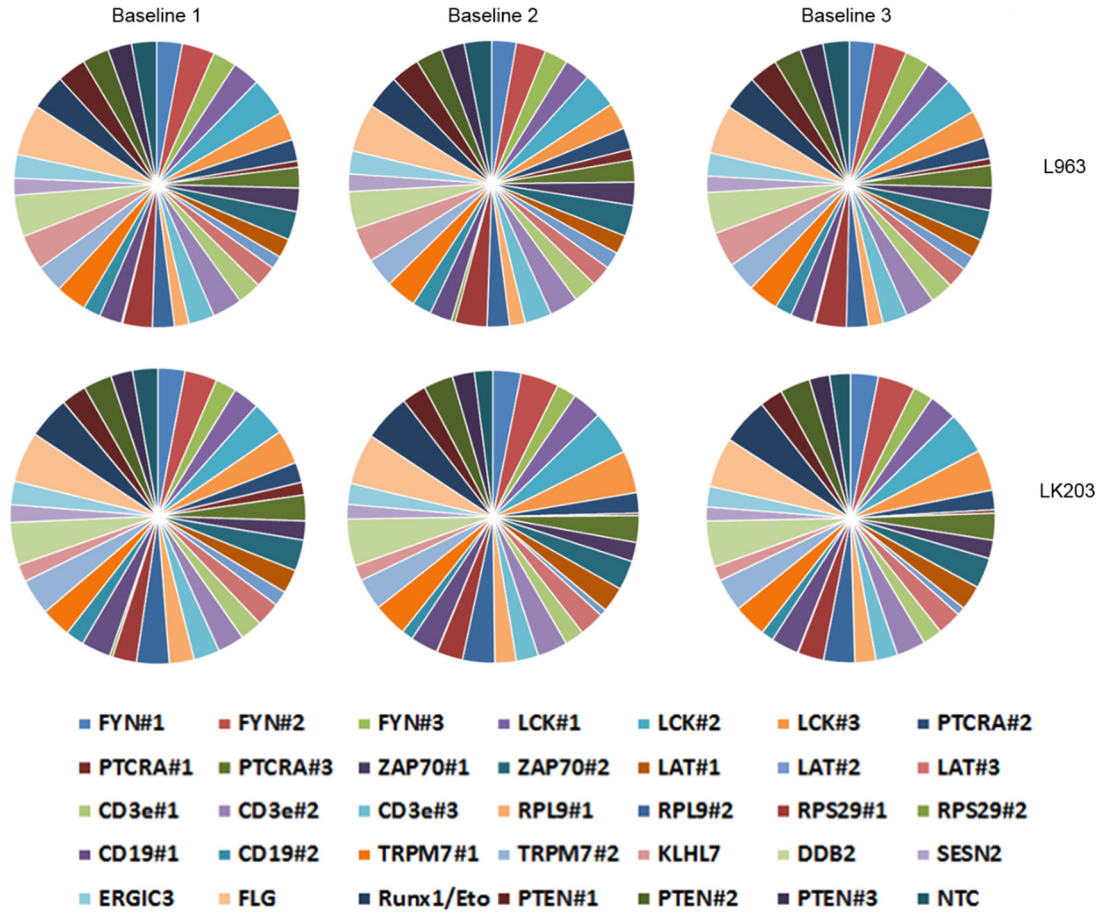

Figure 25. The composition of shRNAs of PDX L963 and LK203 at baselines. There are 36 shRNAs in the targeted shRNA library. Reads from three baseline samples taken 2 days after lentiviral transduction of L963 and LK203 are plotted in pie charts. The distribution of each of the 36 shRNAs is indicated in different colours as shown in the legend.

For the *ex vivo* screen of LK203, after transduction of lentiviral library, LK203 was kept on MSC cells. One sample was collected at day 16, and two more samples were collected at day 30. They were considered as triplicates in the final bioinformatics analysis to perform significance tests. The significantly enriched shRNAs included two shRNAs targeting PTEN (shPTEN#2 Log_2(FC) = 0.5773, p = 0.0322 and shPTEN#3 Log_2(FC) = 0.9738, p = 9 x 10^{-5}). The positive controls targeting ribosome genes which were supposed to be lost, such as shRPL9#1, #2 and shRPS29#1, were significantly depleted in LK203. Intriguingly, three shRNAs targeting LCK were all significantly depleted (shLCK#1 Log_2(FC) = -0.771, p = 0.0012; shLCK#2 Log_2(FC) = -0.679, p = 0.0061; shLCK#3 Log_2(FC) = -0.655, p = 0.0159) in LK203 indicating the importance of LCK for LK203 proliferation *in vitro*. Two shRNAs targeting LAT were significantly lost (shLAT#1 Log_2(FC) = -0.793, p = 0.0015; shLAT#3 Log_2(FC) = -0.815, p = 0.0063) (Figure 26). shZAP70#1 and shPTCRA#2, #3 showed negative slopes, however did not reach significance.

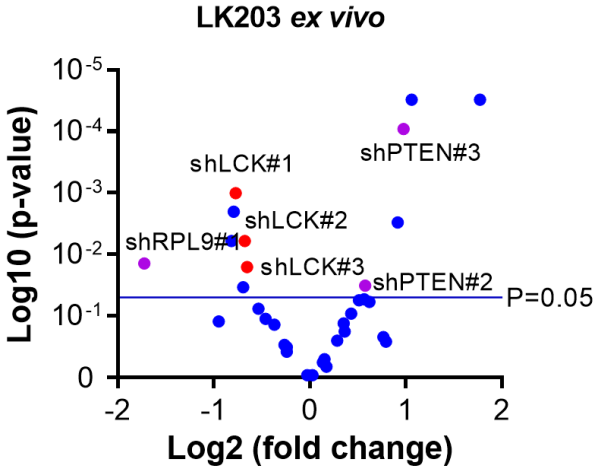

Figure 26. The volcano plot of PDX LK203 *ex vivo* shRNA screen. The Log_2(fold change) is shown on the X-axis while log_{10}(p-value) is shown on the Y-axis. Each dot represents a shRNA. Any shRNAs above the line are significantly enriched or depleted. Red colour demonstrates shLCK#1, shLCK#2 and shLCK#3. Purple, positive controls. Raw data are shown in Appendix 3.

Transduced LK203 was injected into six NSG mice. Bone marrow and spleen samples were collected for NGS analysis. However, in the LK203 *in vivo* shRNA screen, only a few shRNAs showed significant depletion. These shRNAs were ribosome shRNAs (shRPL9#1, #2 and shRPS29#1, #2). No shRNAs showed significant enrichment including PTEN shRNAs. Also, no other shRNAs targeting TCR components were significantly lost or enriched except for shFYN#1 which showed a Log_2(FC) of -3.2 with

significance (p=0.0149). Overall, the *in vivo* shRNA screen of LK203 seems to have less pronounced differences compared to the *in vitro* shRNA screen of LK203. Several aspects were considered in understanding these data: 1) The baseline samples of the LK203 *in vivo* screen had equal shRNA distribution and they were the same baselines as used in the LK203 *in vitro* screen. 2) The LK203 samples derived from the mice showed all 36 shRNAs in all bone marrow and spleen samples, suggesting this PDX did not undergo clonal expansion *in vivo*. All six mice had confirmed leukaemic bone marrow and enlarged spleens (0.55 - 0.74g). There was thus no problem with leukaemia engraftment of this PDX sample. 3) The final reads of the LK203 *in vivo* screen were similar to all other barcoded samples. The average number of reads of 6 mice spleen and bone marrow samples was 283,561, with 312,697 reads for the baseline samples and 293,269 for the *in vitro* screen samples indicating all barcoded samples were equally sequenced. 4) It might be the case that LK203 was dependent on LCK *in vitro* but not *in vivo*. However, with overall less pronounced shRNA fold change and less positive controls behaving as expected such as shPTEN, the conclusion that LCK is dispensable for LK203 *in vivo* does not appear convincing. 5) Last but not least, the *in vivo* shRNA screen analysis was much more challenging as the biological coefficient of variation was over 100%, demonstrating huge variations between samples from different mice. The bioinformatics analysis was performed with the assumption that shNTC and shRUNX1/ETO would have constant representation across all LK203 samples. However, this assumption might not be true for all of the samples. To further investigate this, more thorough bioinformatics analyses are needed, as well as a repetition of the shRNA LK203 screen in additional mice.

3.2.5.3 The Targeted shRNA Screen in L963 in vivo

The *in vivo* shRNA screen was also performed in PDX L963. After thawing (day 0), L963 was transduced with highly concentrated lentiviral shRNA library. Two days later, baseline samples were taken, and remaining cells (1.2 x 10^7 cells) were used to inject into six NSG mice (2 x 10^6 cells per mouse). These mice were harvested due to obvious leukaemia engraftment after 77 days and 81 days. All six spleens were enlarged weighing between 0.7g and 1.05g. After gDNA extraction and amplification, an expected 433 bp band was generated as seen in samples from mouse bone marrow and spleen (Figure 27).

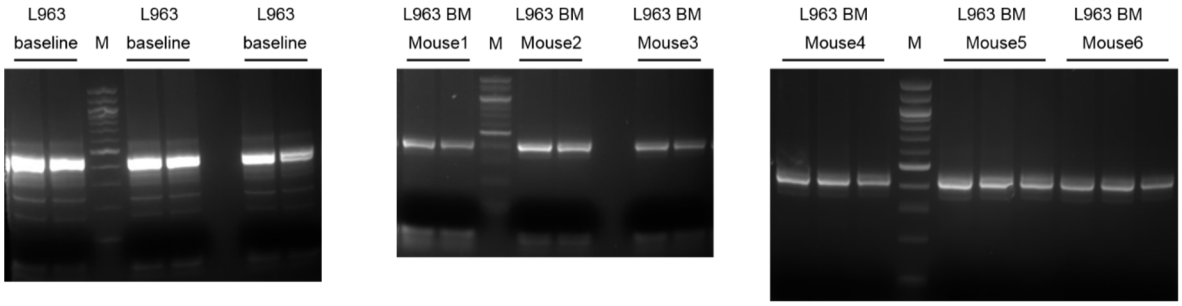

Figure 27. Representative results of gDNA amplification in targeted shRNA screens. gDNA was isolated, amplified with NSG-F3 and reverse barcoded primer. The amplicon was loaded onto agarose gels (2%). The gels show an approx. 400bp band (theoretical size 433bp). These amplicons obtained from L963 samples including three baselines (gDNA of L963 cells before injection into NSG mice), bone marrow samples (BM) from mouse 1, 2 and 3, and bone marrow samples from mouse 4, 5 and 6. M (NEB 100bp DNA Ladder)

In the bone marrow and spleen samples of L963 cells, the positive control shRPL9#1 was significantly depleted (Log_2(FC) = -6.49, p = -0.0017 and Log_2(FC) = -6.10, p = 0.0013 respectively). There was no enrichment of any PTEN shRNAs. However, the dependence of L963 on PTEN is not known at this point. Notably, across all six mice engrafted with L963, shLCK#3 was significantly lost in bone marrow (Log_2(FC) = -8.57, p = 3.01x10^{-7}) and spleen (Log_2(FC) = -8.03, p=2.17 x 10^{-8}) of each individual mouse. However, shLCK#1 only showed a substantial loss in mouse 2, 4 and 5, but not the other three mice (Figure 28).

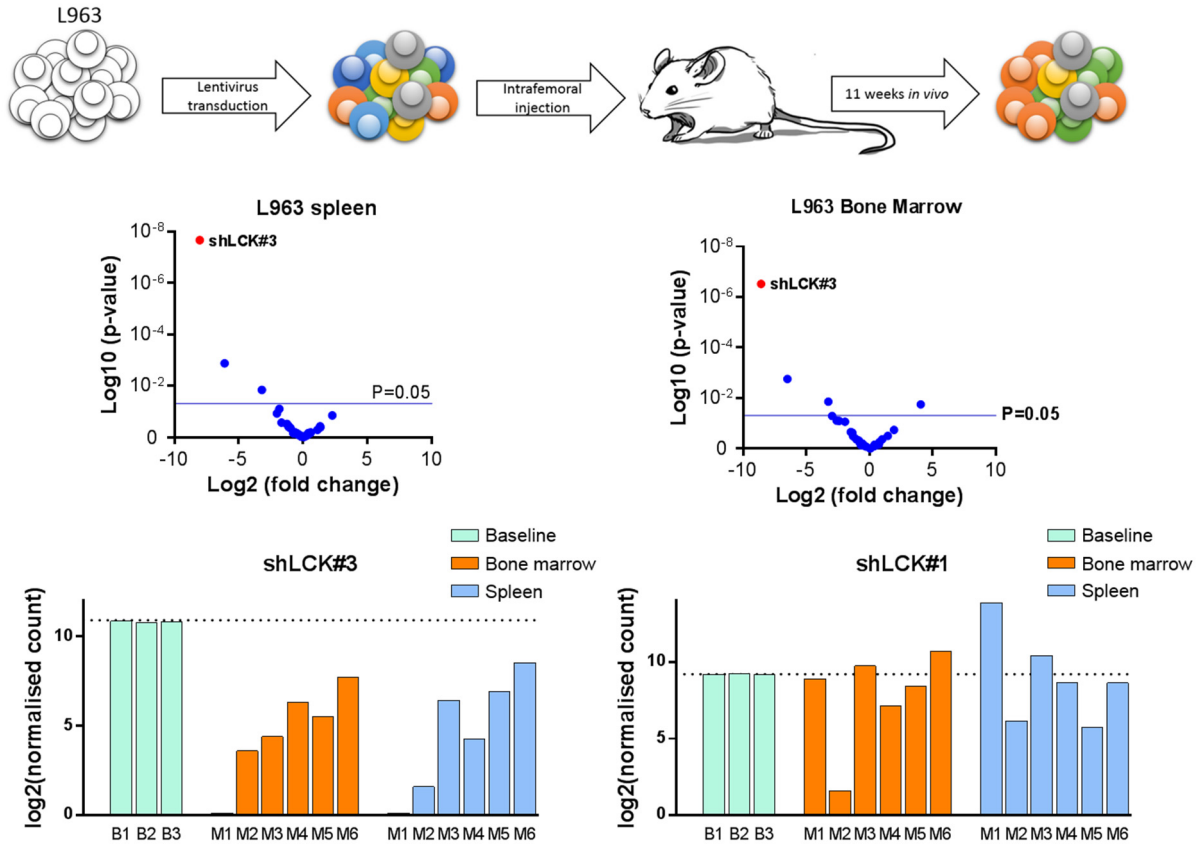

Figure 28. The targeted screen in L963 demonstrates the essential role of LCK *in vivo*.(Top) The *in vivo* screen was performed using L963 as shown in the schematic diagram (n = 1). L963 was transduced with lentiviral shRNA libraries, and intrafemorally injected into 6 NSG mice. Mice were euthanised after 11 weeks due to leukaemia symptoms. Bone marrow and spleen samples were collected. (Middle) Volcano plots are representing the magnitude of the fold change (Log2) in shRNA abundance derived from bone marrow and spleen of L963 on the x-axis. The y-axis represents log10 transformed p values. Dots above the line represent significant shRNAs ($p < 0.05$). The red dot shows shLCK#3. (Bottom) Bar plots of shLCK#3 and shLCK#1 expression in L963 mice. The x-axis shows sample annotations (baseline samples in green columns; bone marrow in orange columns; and spleen samples in blue columns). The y-axis shows the normalised sequencing reads (Log2). Raw data are shown in Appendix 3.

Taken together, similar to the results obtained of T-ALL cell lines, screening data obtained on PDX samples (L963 *in vivo;* LK203 *in vitro)*, indicate that LCK is indispensable for T-ALL propagation both *in vitro* and *in vivo*.

3.3 LCK Deficiency Leads to a Growth Defect Characterised by G_0/G_1 Arrest

3.3.1 Knockdown of LCK, ZAP70 or PTCRA Leads to a Proliferation Defect in T-ALL Cell Lines

To validate the results from the targeted shRNA screens, I performed shRNA knockdown individually targeting LCK, ZAP70, PTCRA and FYN in T-ALL cells. Several negative control shRNAs such as shNTC, shRUNX1/ETO, and shFLG were also included. Cells were transduced with individual shRNA (GFP^+) and mixed with parental GFP negative cells on day 6 to generate approximately 50% GFP expression. They were kept in culture for up to 40 days. The GFP expression was measured every three days to assess the competition of wildtype cells and transduced cells.

All three shRNAs from the targeted library of LCK, ZAP70, PTCRA, and FYN were used in MOLT4 and CUTLL1. The negative control shRNAs (shFLG, shRUNX1/ETO, and shNTC) retained their GFP expression for up to 40 days. Knockdown of FYN by three shRNAs did not influence cell growth in both CUTLL1 (maximal 50% KD) and MOLT4 (maximal 40% KD) (Figure 29). These results were consistent with the targeted shRNA screen results.

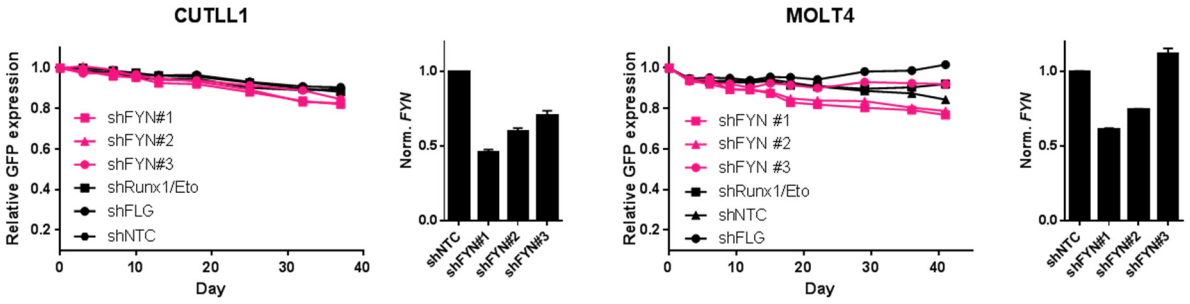

Figure 29. Knockdown of FYN does not affect cell growth in CUTLL1 and MOLT4.Three shRNAs were used to target FYN expression (square shFYN#1; triangle shFYN#2; and circle shFYN#3). Transduced cells were seeded in a 1:1 ratio with non-transduced parental cells (relative GFP expression equals 1.0). Cells were cultured and analysed repetitively for the presence of GFP^+ cells over a time of 40 days for CUTLL1 and MOLT4, respectively. A relative GFP expression of 1 denotes a mixture of 50% GFP^+ cells with 50% parental GFP^- cells (ratio 1:1). The x-axis represents the time (day). The y-axis represents the relative GFP expression of the control shRNA transduced cells (black) and shFYN cells (pink). Knockdown levels of FYN on mRNA level are shown in bar charts.

CUTLL1 did not respond to PTCRA knockdown while all three shRNAs of PTCRA led to slightly growth defect in MOLT4 cells. More importantly, these two cell lines showed

remarkably similar effects for the same LCK and ZAP70 shRNAs. There was no effect after shLCK#2, shZAP70#2 and shZAP70#3 knockdown which can be explained by no reduction of LCK or ZAP70 at transcriptional level. This also explains why these three shRNAs were not significantly depleted in any of the targeted shRNA screen, while other shRNA designed for the same target showed significant depletion. Both shLCK#1 and shLCK#3 reduced LCK expression levels in CUTLL1 and MOLT4, with a more pronounced knockdown of shLCK#3. The growth defects could be correlated with LCK knockdown levels, as shLCK#3 resulted in more growth defect than shLCK#1 (Figure 30). The targeted shRNA screen showed significant depletion of shZAP70#1 in CUTLL1 but not MOLT4 cells. However, shZAP70#1 led to a growth defect in both CUTLL1 and MOLT4 cells in the competitive assay (Figure 30).

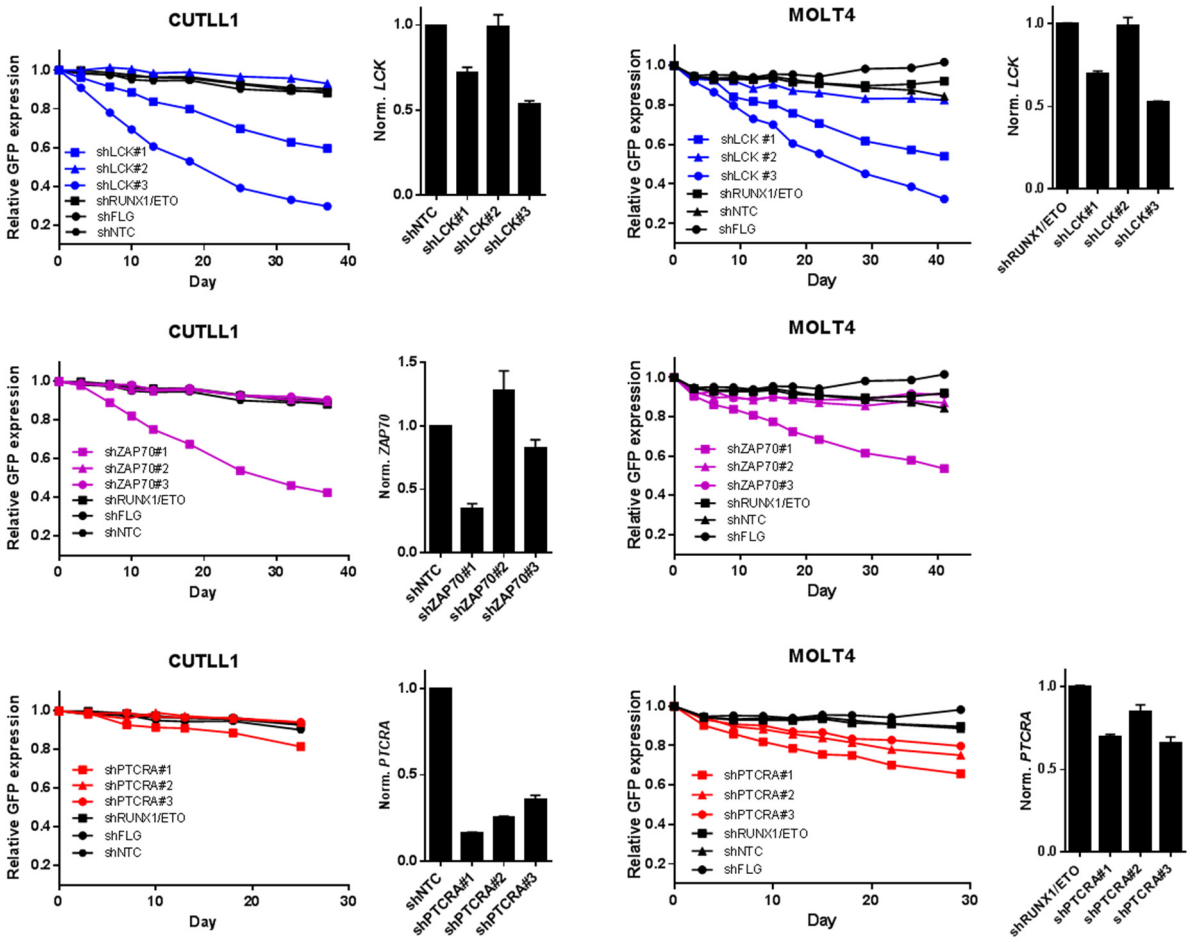

Figure 30. Competitive *in vitro* assays in CUTLL1 and MOLT4 cells. T-ALL cell lines CUTLL1 and MOLT4 were transduced with three shRNAs per gene targeting LCK, ZAP70 and PTCRA and three negative shRNAs. The knockdown levels were determined six days after the transduction by pLKO5d-eGFP constructs. Cells were mixed with parental cells in a 1:1 ratio according to their GFP expression. The GFP expression (blue, LCK shRNAs; purple, ZAP70 shRNAs; red, PTCRA shRNAs; black,

control shRNAs) was measured repetitively and plotted over time (square, shRNA#1; triangle shRNA#2; and circle shRNA#3). The x-axis represents time (days) and the y-axis the relative GFP expression. A relative GFP expression of 1 denotes a mixture of 50% GFP+ cells with 50% parental cells (ratio 1:1). Knockdown levels of targeted genes are shown in bar charts to the right of the competitive assays.

The summarised data of MOLT4 and CUTLL1 are included in (Figure 31). Four more T-ALL cell lines (SUPT1, RPMI8402, HPB-ALL and Jurkat) were tested. Knockdown of LCK (shLCK#3), PTCRA (shPTCRA#1), or ZAP70 (shZAP70#1) all led to proliferation defects in SUPT1 and RPMI8402, but not HPB-ALL cells (Figure 31).

The HPB-ALL results were not consistent with the targeted shRNA screen as LCK was shown to be crucial in HPB-ALL cells in the previous screen. However, shNTC cells lost GFP expression at a similar speed as shLCK knockdown cells. The results are difficult interpret (see discussion).

The competitive assay in Jurkat cells was performed in a different way. Jurkat was transduced with RFP657-shNTC and GFP-shLCK#3. After 6 days after transduction, the fluorescent protein expression was measured. GFP-shLCK#3 cells were seeded in a 1:1 ratio with RFP657-shNTC cells. Mixed cells were cultured and analysed repetitively for the presence of GFP^+ and $RFP657^+$ cells over a time of 10 days. Notably, RFP657-shNTC cells outcompeted GFP-shLCK#3 cells, suggesting that knockdown of LCK affected cell proliferation also in Jurkat (Figure 31). Overall, these data suggest that the protein kinase LCK plays a universal role for cell proliferation and/or survival in nearly all T-ALL cell lines as shown in Figure 31.

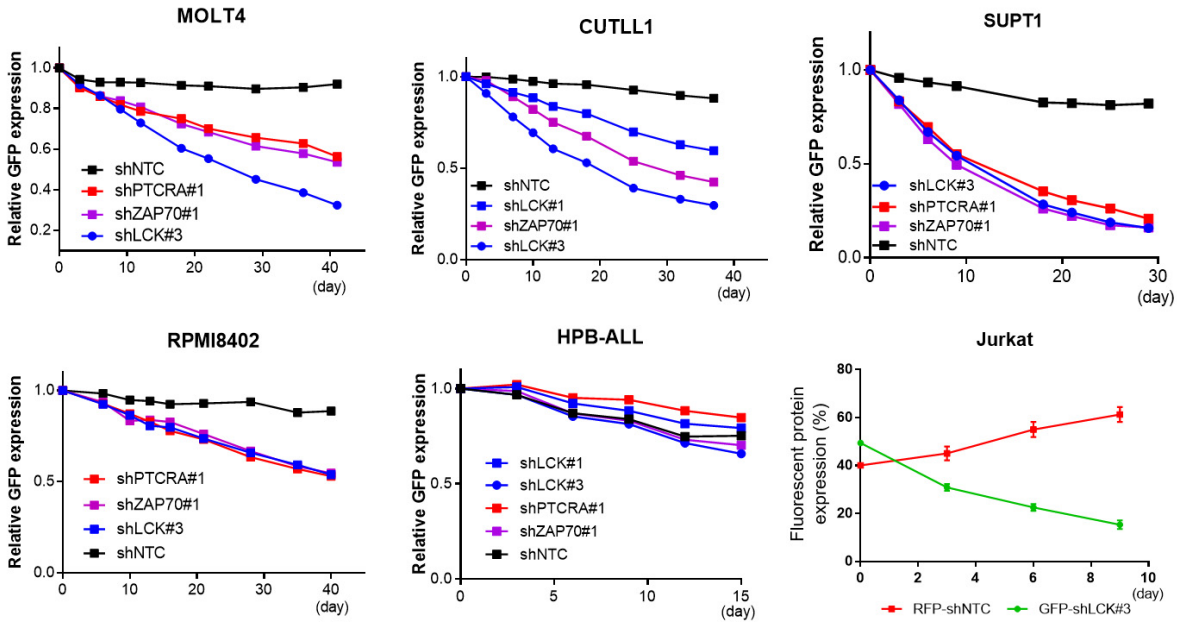

Figure 31. Summary of competitive assays in six T-ALL cell lines. MOLT4, CUTLL1, SUPT1, RPMI8402, and HPB-ALL were transduced with GFP-shRNAs and mixed equally with parental cells. Representative experiments are shown in this figure. The x-axis represents time (days since mixture) and the y-axis shows relative GFP expression. Over a period of 40 days, GFP expression was monitored and plotted after normalisation. shLCK#1, blue square; shLCK#3, blue circle dot; shPTCRA#1, red square; shZAP70#1, purple square; shNTC, black square. For Jurkat cells, after lentiviral transduction, RFP657-shNTC cells were mixed with GFP-shLCK#3 cells in equal numbers. The RFP657 and GFP expression were monitored by flow cytometry and indicated as percentage. The mean of three independent experiments is shown in this figure. Red, shNTC cells; Green, LCK knockdown cells.

3.3.2 Verification of LCK as a Critical Factor for the Maintenance of T-ALL Cells *in vivo*

To further evaluate LCK function in leukaemia progression, *in vivo* competitive assays with MOLT4 and Jurkat cells were performed. For this cells were transduced with RFP657-shNTC and GFP-shLCK (or dTomato-LCK) separately. After six days of transduction, these cells were mixed to generate RFP657:GFP (or dTomato) in a 1:1 ratio. On the same day, five NSG mice per cell line received mixed samples by intrafemoral injection. When mice showed disease-related symptoms or weight loss they were euthanised, and samples were collected to analyse GFP (dTomato) and RFP657 expression (Figure 32).

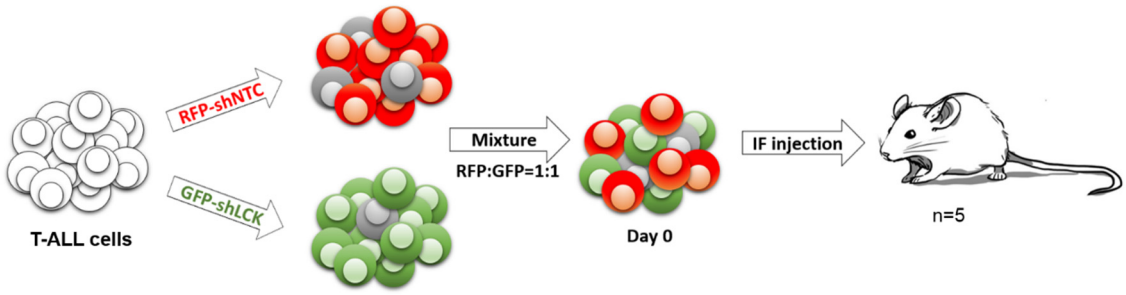

Figure 32. Schematic of *in vivo* competitive assays. MOLT4 cells were lentivirally transduced with either RFP657-shNTC or GFP-LCK. After 6 days of transduction, cells were mixed to generate a mixed sample with RFP657:GFP in a 1:1 ratio. These cells were injected into 5 NSG mice. After leukaemia engraftment and expansion *in vivo*, samples from mice spleen, liver and bone marrow were isolated and used to analyse GFP and RFP657 expression by flow cytometry.

Since transduced MOLT4 cells were not 100% positive for RFP657 or GFP, it was not possible to obtain mixed samples of exactly 50% GFP and 50% RFP657. In this experiment shNTC cells (RFP) and shLCK (GFP) cells represented 41.7% and 39.2% respectively. The remainder 18.7% of cells refers to the non-transduced population. Mice receiving MOLT4 cells lived for 26 days before showing disease-related symptoms such as pale colour, loss of muscle tone or weight loss. MOLT4 cells engraft in the liver, spleen and bone marrow. Spleens were enlarged weighing from 0.14 g to 0.21 g with approximately 3 - 5% of cells being MOLT4. Flow cytometry analysis revealed shNTC cells represented 50.2%, 47.7%, 59.8%, 49.0% and 55.9%, while shLCK cells accounted for 14.9%, 16.6%, 19.4%, 18.0% and 20.6% respectively demonstrating knockdown of LCK leads to population loss when in competition with control shRNA transduced-cells. No liver or bone marrow engraftment was observed

in mouse 1 and mouse 2, however, the engraftment rates for the other three mice were 11 - 15% in the liver and 1.7 - 22% in the bone marrow. Overall, the representation of RFP657-expressing control cells was 56% (mean obtained from mouse 3-5) and clearly outcompeted GFP-shLCK cells with a mean of 22% in all liver derived samples. The bone marrow samples were more heterogeneous as the RFP657 vs GFP ratios and ranged from 58.2% vs 8.5% to 35.4% vs 20.8% (Figure 33).

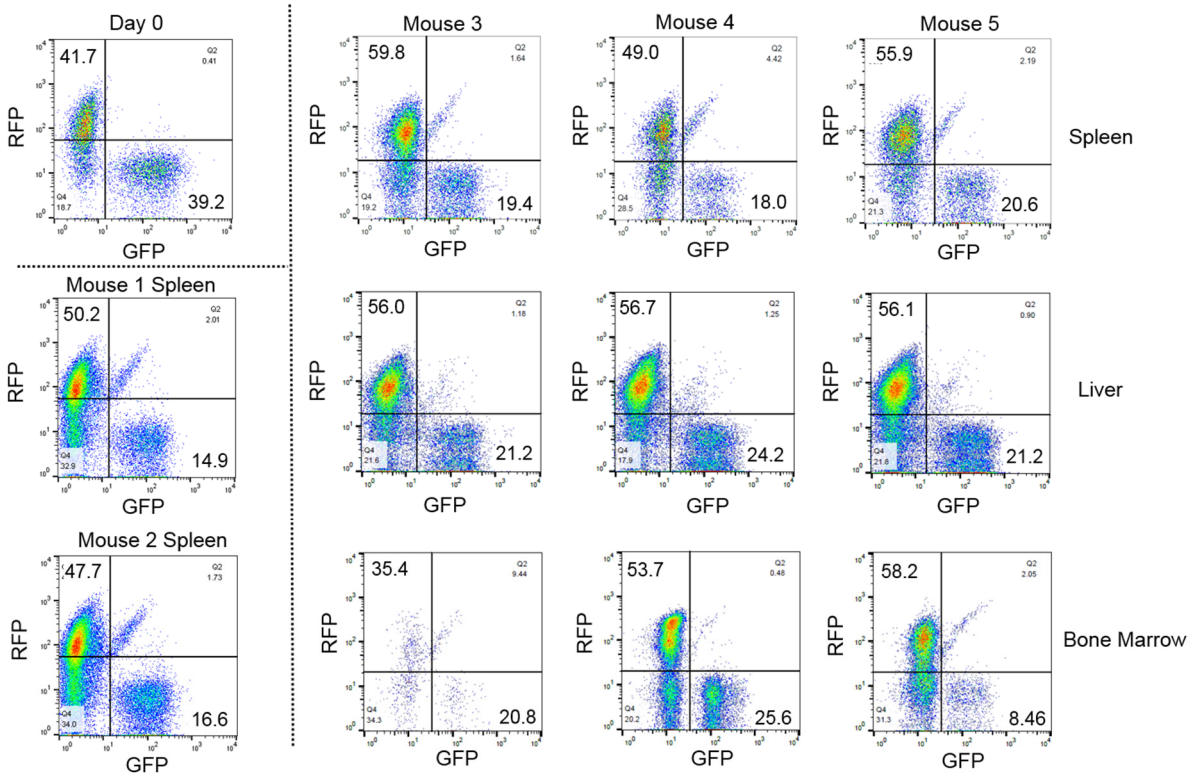

Figure 33. *In vivo* competitive assay with MOLT4 in NSG mice. Expression of GFP and RFP657 was determined on day 0 before injection (cells were mixed after six days post-transduction) and on day 26 after harvesting spleen (n = 5), bone marrow (n = 3) and liver (n = 3) samples from the mice. Y-axis: RFP657; X-axis: GFP. Numbers in up left square and bottom right square represent RFP657 and GFP expression percentages respectively.

In summary, these data show that the RFP657-shNTC MOLT4 cell population outcompeted the GFP-shLCK transduced cell population in all five mice. After cleaning the data for non-transduced cells and comparing RFP657 and GFP expressions to those determined at the injection day (day 0), a significant advantage to engraft and propagate *in vivo* of control shRNA cells compared to LCK knockdown cells in all tissues analysed, the spleen ($p < 0.0001$), BM ($p = 0.0276$) and liver ($p = 0.0003$), can be observed (Figure 34).

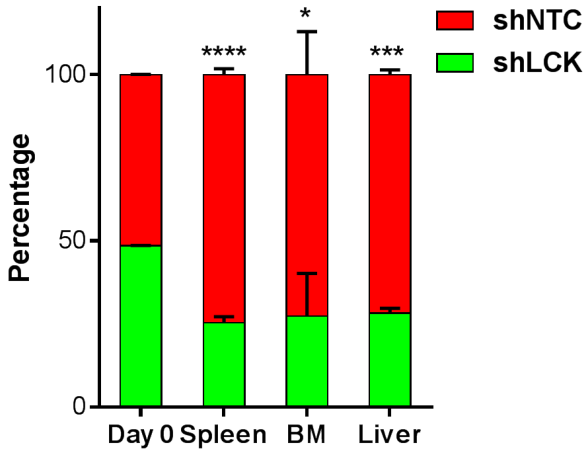

Figure 34. *In vivo* competitive assay with MOLT4 cells. Non-transduced cells were excluded from the analysis. The proportion of shNTC (RFP657) cells and shLCK (GFP) cells is shown in red and green, respectively. Statistical analyses were performed on the proportions of shLCK cells (spleen (n = 5), BM (n = 3), liver (n = 3)) using student t-tests (spleen ($p < 0.0001$), BM ($p = 0.0276$) and liver ($p = 0.0003$)).

The *in vivo* competitive assay using Jurkat cells was performed with pLKO5d-SFFV-eGFP-transduced Jurkat cells. Approximately 95% of these cells express GFP, which was used as a marker for Jurkat cells derived from *in vivo* samples. To compare the LCK effects on leukaemia propagation *in vivo*, cells were transduced with RFP657-shNTC or dTomato-shLCK. They were mixed and had an equal distribution of RFP657 and dTomato before intrafemoral injection into NSG mice. Five NSG mice were used for this experiment, and weight loss, compared with the highest weight, was observed in all five mice (11% - 19%) after 22 days. At that time, spleen and bone marrow samples were collected, although the weights of the spleens were only 0.04 g to 0.08 g.

The engraftment of Jurkat cells in all five NSG mice (LN, RN, BN, NN, 2LN) was generally very poor, with only two mice (BN and 2LN) demonstrating spleen engraftment. However, LN had a leg tumour, and NN possibly showed minor bone

marrow engraftment. When examining RFP657 and dTomato expression, the leg tumour showed RFP657-shNTC population outcompeting the dTomato-shLCK population (shNTC 42.4% vs shLCK 34.8%). Surprisingly, the spleen and bone marrow samples showed different results as LCK knockdown cells were more abundant than control cells (15.9 - 17.2% RFP-shNTC cells; 58.6 - 59.6% dTomato-shLCK cells). At this point, the results were not clear enough to draw any conclusion (Figure 35).

To further elaborate on the question whether shNTC cells outcompete shLCK cells, Jurkat cells from the leg tumour, spleen and bone marrow were kept *in vitro* for five days, as T-ALL cell line Jurkat should proliferate better *in vitro* and quickly become the dominant population in these samples. Flow cytometric analysis was performed and indicated that the GFP populations in the leg tumour and spleen represented 95.4%, 95% and 93.9% of total cells. However, no GFP was detected in the BM sample, suggesting that at least the GFP signal on the harvested day was not a true GFP signal of Jurkat cells, and possibly derived from auto-fluorescent mouse BM cells. Therefore, it is most likely, that none of the five mice showed BM engraftment. Of interest is, that although leukaemia cells had been injected in the femur, they did not engraft in the bone marrow, at least not in the bone marrow derived from femur and tibia that were harvested. To date, the reason for the lost in weight is not clear.

After five days *in vitro* culture, the leg tumour sample was obviously losing the LCK knockdown cell population (shNTC 41.8% vs shLCK 25.3%). In the spleen samples however, there were more shLCK cells than shNTC cells indicating the results from the day of harvest were likely true data. When compared with the composition on harvest day and five days later *in vitro*, the shLCK population started to be outcompeted by control population (59.6% to 56.8 in BN spleen, 58.6% to 52.5% in 2LN spleen) (Figure 35). It is currently not understood how the splenic microenvironment affects LCK knockdown or control cells differently with regards to nutritional requirement and subsequent cell survival. In the tumour sample, shNTC outcompeted shLCK in a similar fashion as in the *in vitro* result. As only one mouse developed a leg tumour, a conclusion can unfortunately not be drawn at this point.

Studies of Jurkat in mouse models often use the intrahepatic or subcutaneous injection, and Jurkat cells form solid tumours growing in the abdominal cavity or under the skin (El Zawily et al., 2017). Using this route of tumour cell application, it is likely that similar results will be obtained as the leg tumour sample that shNTC cells

outcompeted shLCK cells. However, this solid tumour-like orthotropic mouse model does not represent the generally accepted mode of leukaemia modelling.

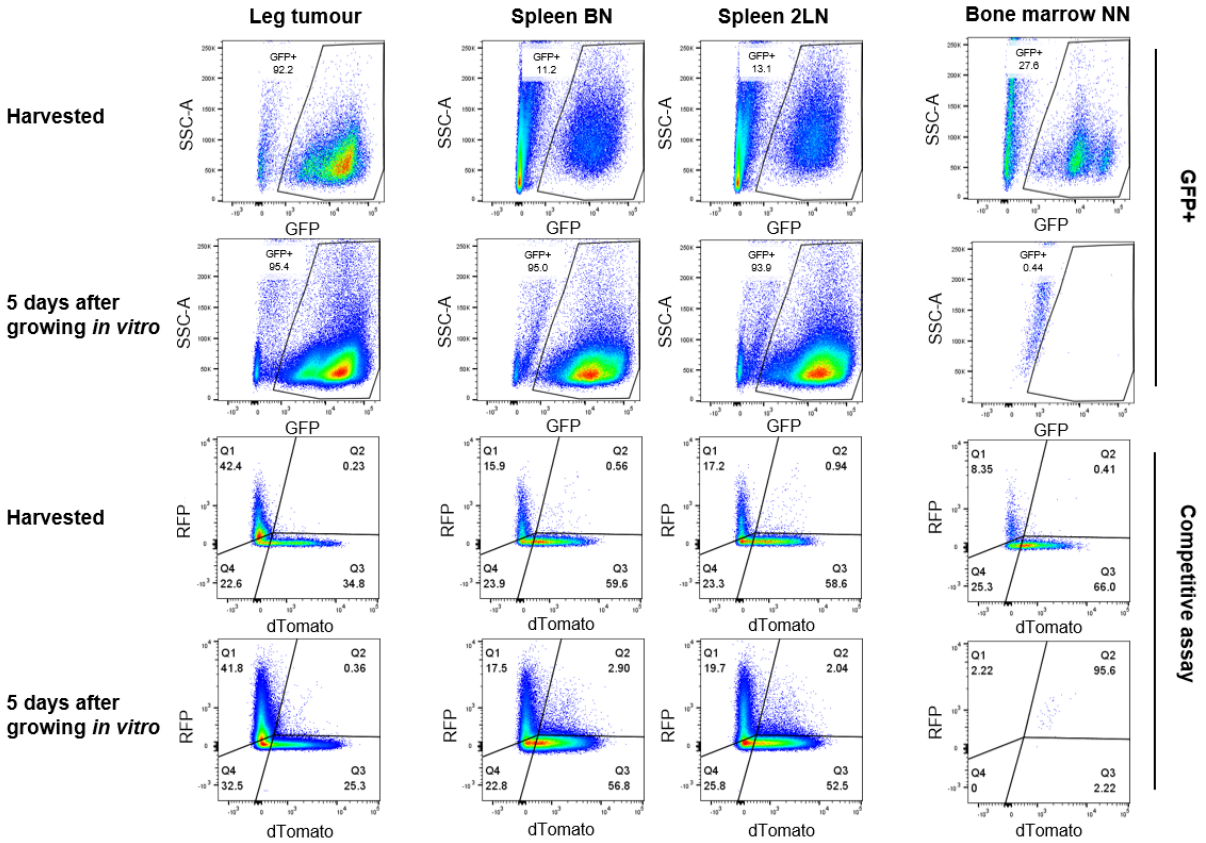

Figure 35. The *in vivo* competitive assay with Jurkat cells.Tissues that showed engraftment of Jurkat (one leg tumour (left), two spleen samples (middle) and one bone marrow sample (right)) were analyse for GFP-expressed Jurkat cells (top). The GFP percentage was used to determine pLKO5d-SFFV-eGFP transduced Jurkat cells. The shNTC (RFP657) and shLCK (dTomato) expression of Jurkat cells are shown in the bottom (competitive assay analysis). Y-axis showed RFP657 expression (shNTC transduced cells in Q1) while X-axis showed dTomato expression (LCK knockdown cells in Q3).The proportion on the day of harvest is shown on row 1 and row 3, while samples followed up *in vitro* for five days are shown in row 2 and row 4.

3.3.3 Knockdown of LCK Induces G_0/G_1 Arrest in T-ALL Cell Lines

To investigate the effects of LCK knockdown in T-ALL cells, cell cycle and apoptosis assays were performed. The apoptosis assay was performed in MOLT4, SUPT1, CUTLL1 and Jurkat using PE-Annexin V and 7-AAD. A mild effect of increasing early apoptosis (Annexin $V^+/7\text{-}AAD^-$) was observed in MOLT4 after LCK knockdown (shNTC, 9%; shLCK 17%); however, this was not shown in CUTLL1, SUPT1 and Jurkat (Figure 36).

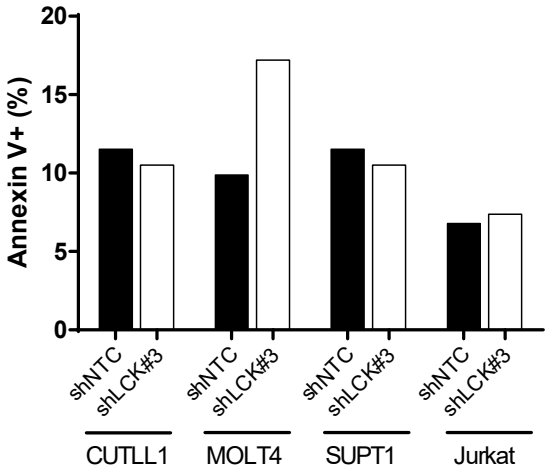

Figure 36. Analysis of cell death induction in T-ALL cell lines after LCK knockdown. Apoptosis assay was performed after six days of transduction with shNTC (black) and shLCK#3 (white) in CUTLL1 (n = 2), MOLT4 (n = 2), SUPT1 (n = 1) and Jurkat (n = 1). Annexin V positivity (%) was shown on the Y-axis referring to the Annexin $V^+/7\text{-}AAD^-$cell poplulation.

Analysis of DNA content revealed that knockdown of LCK using two shRNAs in Jurkat and MOLT4 cells increased the G_0/G_1 phase and decreased S and G_2/M phase compared with shCtrl cells. This was mirrored in SUPT1 cells where LCK loss induces cell cycle arrest (45.5% G_0/G_1 in shCtrl increased to 53.3% in shLCK#3) suggesting that LCK plays a critical role in the G_1/S checkpoint (Figure 37). Overall, these data indicate that LCK promotes T-ALL cell cycle progression since knockdown of LCK leads to a significant increase in the G_0/G_1 phase in all three T-ALL cell lines.

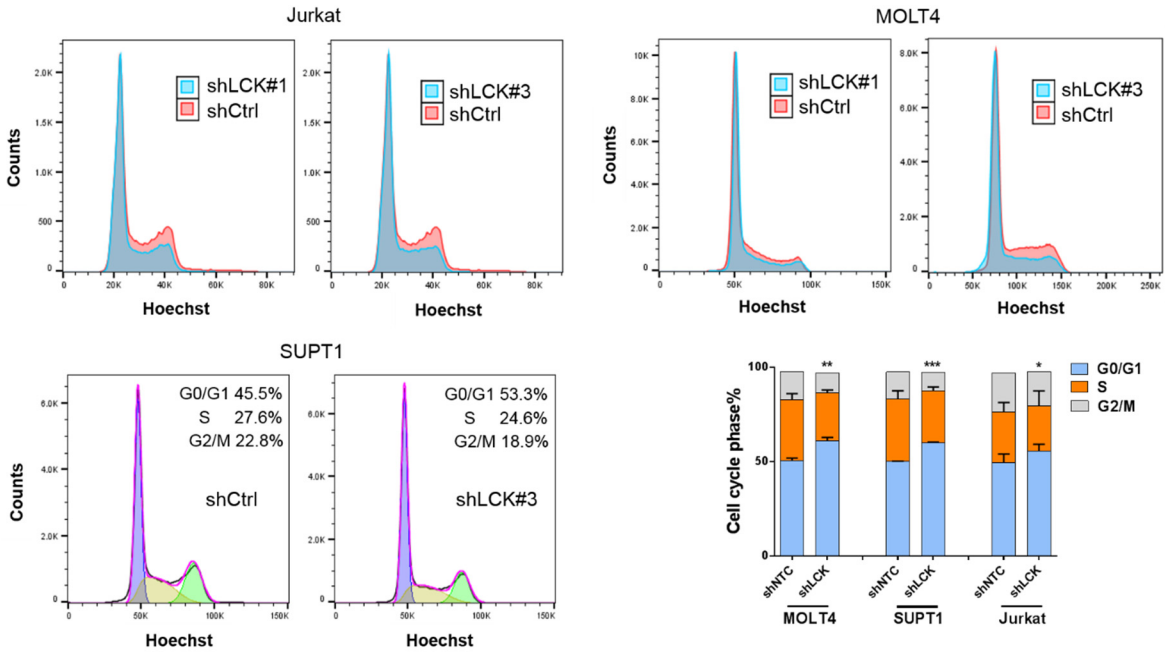

Figure 37. Knockdown of LCK leads to cell cycle arrest. T-ALL cell lines Jurkat and MOLT4 were transduced with shLCK#1 and #3. After 6 days of transduction, the cell cycle was assessed after Hoechst staining by flow cytometry. Both shRNAs targeting LCK (blue) induced G_0/G_1 cell cycle arrest compared with shCtrl (red). SUPT1 cells were transduced with shCtrl and shLCK#3. DNA content was stained with Hoechst and cell cycle analysis was performed in FlowJo. Three independent experiments (n = 3) were summarised in the bar plots with the y-axis representing the cell cycle distribution. * $p \leq 0.05$, ** $p \leq 0.01$, *** $p \leq 0.001$.

3.3.4 Knockdown of LCK in PDXs Leads to Cell Cycle Arrest

3.3.4.1 Knockdown of LCK by shRNA in L963 Leads to the Reduction of Proliferation in vitro

The observation that LCK knockdown induced G_0/G_1 arrest in T-ALL cell lines was studied further in T-ALL PDX cells. L963 cells from the spleen were thawed and co-cultured *in vitro* with mouse OP9-DL1. 1 x 10^7 cells were transduced with highly concentrated lentivirus containing shCtrl or shLCK#3. After six days, GFP expression was assessed by flow cytometry to determine the transduction efficiency, which was 8.0% for shCtrl and 6.4% for shLCK#3 (Figure 38). Cell cycle analysis was performed on GFP positive cells using Hoechst 33342 on day 7, day 13 and day 17 by flow cytometry and manual gating of G_0/G_1, S and G_2/M phases. All LCK knockdown T-ALL cells showed a decrease in S phase over time (Figure 38). To assess LCK knockdown levels, PhosFlow was used to determine p-Y394^{LCK} and total LCK on day 8 and day 13. A substantial knockdown of LCK was seen; namely 45% KD at total LCK protein level and 71% KD at p-Y394^{LCK} level.

Having confirmed that a successful knockdown of LCK in PDX L963 caused cell cycle arrest, a cell proliferation assay using Cell Trace Violet (CTV) was performed. CTV is a cell permeable, stable and well-retained proliferation dye binding to intracellular amines. Upon cell division the dye is divided equally onto the daughter cells, i.e. the intensity of CTV is diluted by half after one cell division. Thus, more cell divisions will lead to peaks of less CTV intensity, which can be assessed by flow cytometry. In this experiment, 2 x 10^7 L963 cells were labelled with 5 µM CTV and split into two wells to receive shCtrl virus and shLCK virus respectively. In total, seven CTV peaks were observed in both samples. However, LCK knockdown cells had fewer cells in later divisions (5 and 6) and more cells in early divisions (1, 2 and 3) compared with shCtrl cells. (shCtrl and shLCK percentages in 0 - 6 divisions: 3.7% vs 3.7%; 6.8% vs 8.0%; 14.7% vs 18.5%; 17.5% vs 20.0%; 17.3% vs 17.9%, 17.4% vs 13.3%; and 8.8% vs 4.0%) (Figure 38). These data demonstrate that LCK is crucial for cell cycle progression and cell proliferation, also in T-ALL PDXs.

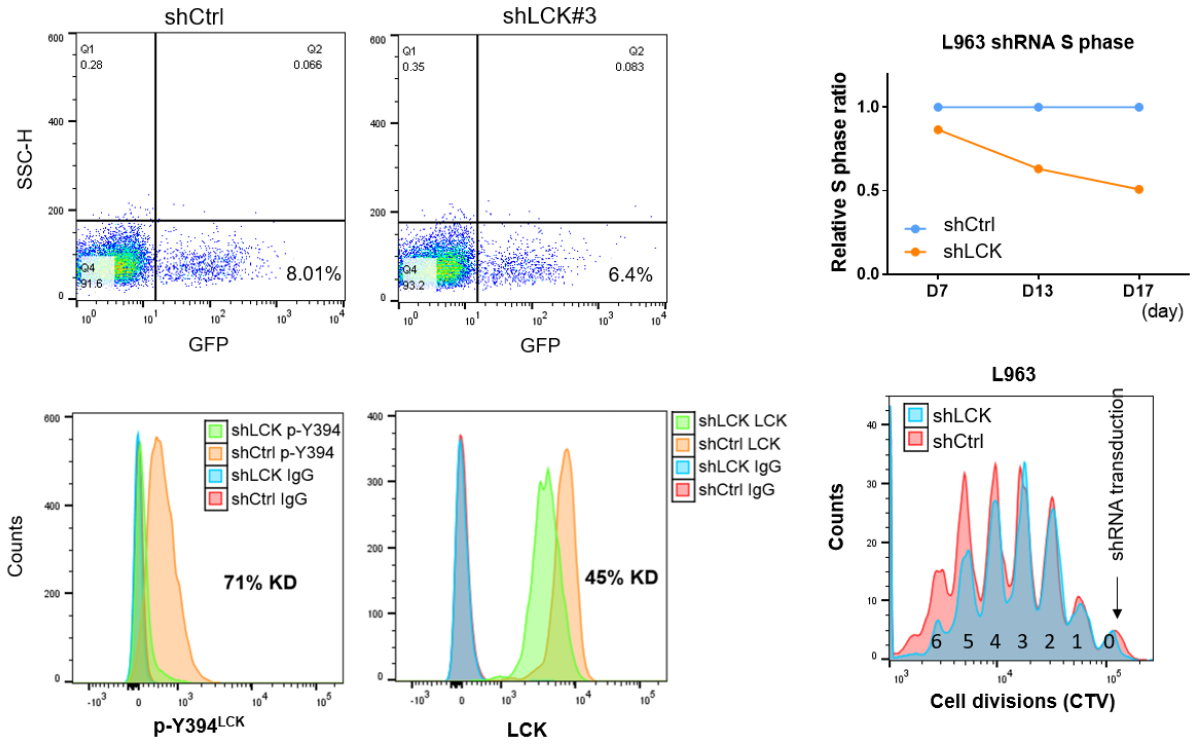

Figure 38. Knockdown of LCK by shRNA in PDX L963 results in proliferation defects. PDX L939 were lentivirally transduced with shCtrl and shLCK#3 expression constructs coexpressing GFP to allow for the assessment of transduction efficiencies (x-axis, GFP expression, y-axis, side scatter height SSC-H). Cell cycle analysis on GFP positive cells was performed on day 7, 13 and 17 after transduction and Hoechst stain by flow cytometry. The S phase of shLCK (orange) was compared with S phase in shCtrl (blue) cells over time. PhosFlow determined LCK knockdown levels and activating p-Y394^{LCK} reduction on day 8. As negative control an isotype control antibody (IgG) was used. Cell Trace Violet (CTV) labelling was used to assess cell proliferation of L963 (n = 1). Cells were labelled with CTV, transduced with shLCK or shCtrl and grown for another two weeks on OP9-DL1 feeder cells. Flow cytometric analysis of the CTV incorporation in GFP positive cells, shLCK (blue) and shCtrl (red), respectively (fluorescence intensities indicate cell divisions 0 - 6) were overlayed.

3.3.4.2 Knockdown of LCK by siRNA in PDX Leads to the Reduction of S Phase

In addition to shRNA lentiviral transduction, siRNA oligonucleotides were designed against LCK allowing for transient knockdown of LCK in T-ALL PDX. LK203 and L963 were electroporated consecutively every three days with 100 nM siRNA under 300 V for 5 ms (3 times). They were kept *in vitro* supported by OP9-DL1 feeder cells. LCK knockdown levels were assessed by flow cytometry on day 4 and day 9 with more pronounced knockdown of LCK observed at the latter time point. A 67% KD of p-Y394^{LCK} and 43% KD of total LCK protein were observed in LK203. L963 had a similar knockdown efficiency to LK203 (Figure 39). Moreover, LK203 proliferated much better *in vitro* with a substantial S phase while the majority of the population of L963 was at G_0/G_1 phase. After three electroporation, PI or Hoechst 33342 were used to determine cell cycle phases. A significant G_0/G_1 arrest was observed in LK203 ($p = 0.004$). A similar effect was shown in L963, however, as L963 initially had a substantial number of cells in G_0/G_1 phase, the increase in cell cycle arrest after LCK knockdown did not reach significance ($p = 0.2039$) (Figure 39).

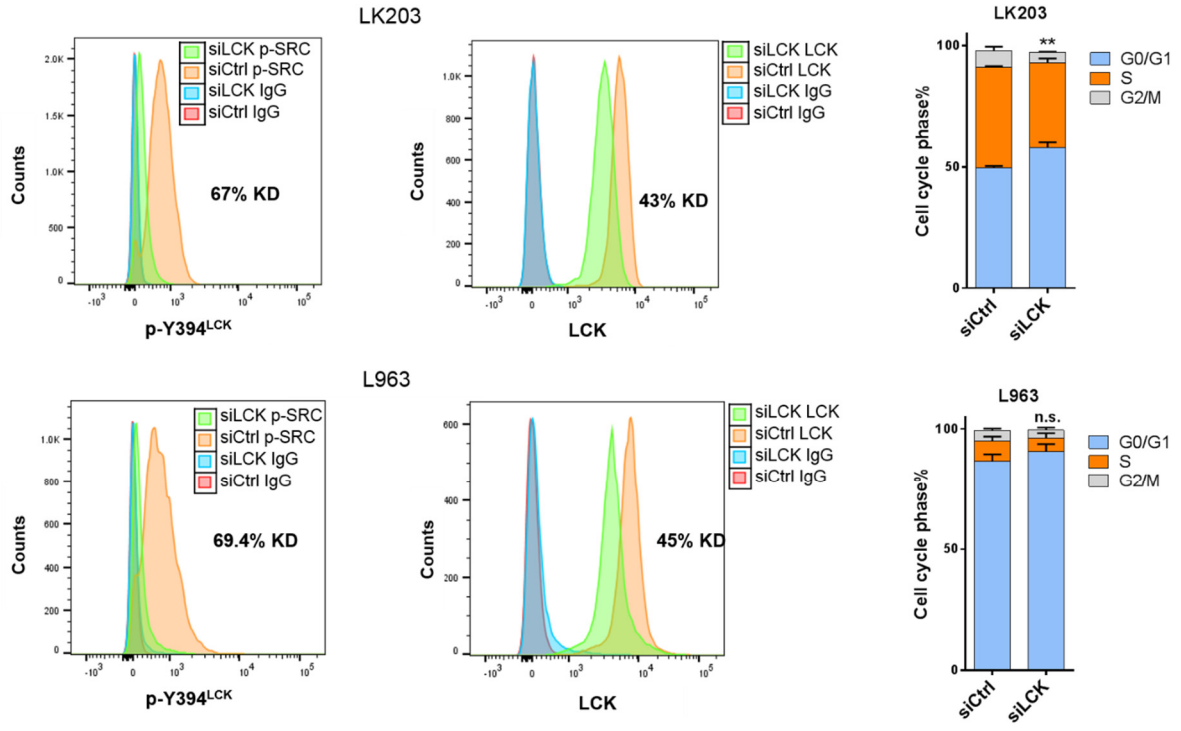

Figure 39. Successful LCK knockdown by siLCK in LK203 and L963 leads to G_0/G_1 arrest. Three consecutively siRNA electroporation were performed in PDX LK203 and L963 to knockdown LCK. As a control siRUNX1/ETO (siCtrl) was used. Total LCK and p-Y394^{LCK} levels were examined by flow cytometry. Cell cycle distributions were determined on day 3, day 6 and day 9. Data were summarised and plotted in bar plots. Statistical analysis were performed on G_0/G_1 phase (n = 3, LK203 ** $p = 0.004$; L963 n.s. $p = 0.2039$).

Chapter 4

Pharmacological Inhibition of LCK by Dasatinib Induces Cell Cycle Arrest in T-ALLs

4.1 Introduction

The kinase activity of LCK is controlled by $pY394^{LCK}$ at the kinase domain for positive regulation and $pY505^{LCK}$ at the cytoplasmic tail for inhibitory effects. In the latest report (Wan et al., 2019) where a FRET-based (Fluorescence resonance energy transfer-based) biosensor for LCK was used in live cells demonstrated that a 60% portion of LCK was pre-activated with phosphorylated Y394 in T-ALL cell line Jurkat. Impairment of this phosphorylation site by the mutation of Y394F led to low levels of LCK aggregation at the plasma membrane and complete abolishment of the basal-level LCK activation (Wan et al., 2019). Activated LCK phosphorylates and activates CD3ζ (ITAMs), ZAP70 (pY493) and PLCγ (pY783), resulting in pTCR/TCR signalling cascades.

Dasatinib (DAS) is a very potent dual ABL/SRC family kinase inhibitor in clinical trials of Philadelphia positive ALL and CML. In MRC (Medical Research Council) compound-screening, DAS effectively inhibits 100% activity of ABL1 and 99% activity of LCK at 0.1 μM and 1 μM. Inhibiting other SFKs (LYN, HCK or FGR) by dasatinib has been shown the efficacy in treating several types of leukaemia, such as JMML, CLL, and AML. In this study, DAS was selected to target LCK clinically.

In healthy T cells (PBMCs, peripheral blood mononuclear cells), dasatinib has been shown to specifically block anti-CD3 induced activation of TCR signalling as demonstrated by reduced pAKT, pERK and CD69 expression (Schade et al., 2008). The successful application of chimeric antigen receptor (CAR) – engineered T cells in advanced malignancies has opened a new era for immunotherapy. However, the side effect -- cytokine release syndrome (CRS) remains a significant clinical challenge (Mestermann et al., 2019). Recently, dasatinib has been shown to act as a pharmacological on/off switch for CAR T cells to minimise CRS. The underlying mechanism is treatment with dasatinib inhibits LCK activation as well as impairs cytokine production and cell proliferation of CAR T cells. Moreover, this inhibitory effect can be fully reversed as dasatinib only halts cell proliferation of CAR T cells without affecting cell viability (Mestermann et al., 2019).

4.2 DAS Abolishes LCK Activation in T-ALL Cell Lines and PDXs

To access the effects of DAS on LCK, western blotting of phospho-LCK was performed on T-ALL cell lines and PDXs treated with control vehicle or DAS for 24 hours. 2 µM DAS was more or less the average IC_{50} values of SUPT1, Jurkat and CUTLL, therefore this concentration was used for T-ALL cell lines. The phosphorylation of both the activation site Y394 and inhibitory site Y505 of LCK was abolished entirely by DAS (2 µM) in SUPT1, MOLT4 and CUTLL1 cell lines. Since LCK activates ZAP70 and PLCγ1 by phosphorylation of Y493 and Y783 respectively (Brownlie and Zamoyska, 2013), the activation status of the LCK downstream targets PLCγ1 and ZAP70 were investigated. Treating cells with DAS led to reduction in p-Y783^{PLCγ1} and p-Y493^{ZAP70} levels in T-ALL cell lines (Figure 40) indicating that DAS diminishes LCK kinase activity. The mode actions of DAS were also explored in T-ALL PDXs. Consistent with T-ALL cell line data, DAS (1 µM) inhibited p-Y394^{LCK} and p-Y505^{LCK} in all PDX tested (LK203, L963, L970, L907, L809 and LK080). In line with cell line data, activating phosphorylation of the downstream lipase PLCγ1 was abolished in PDX LK203, L963, L970 and L907 (Figure 40). Overall, this data indicates that LCK kinase activity is impaired after DAS treatment in both T-ALL cell lines and PDX.

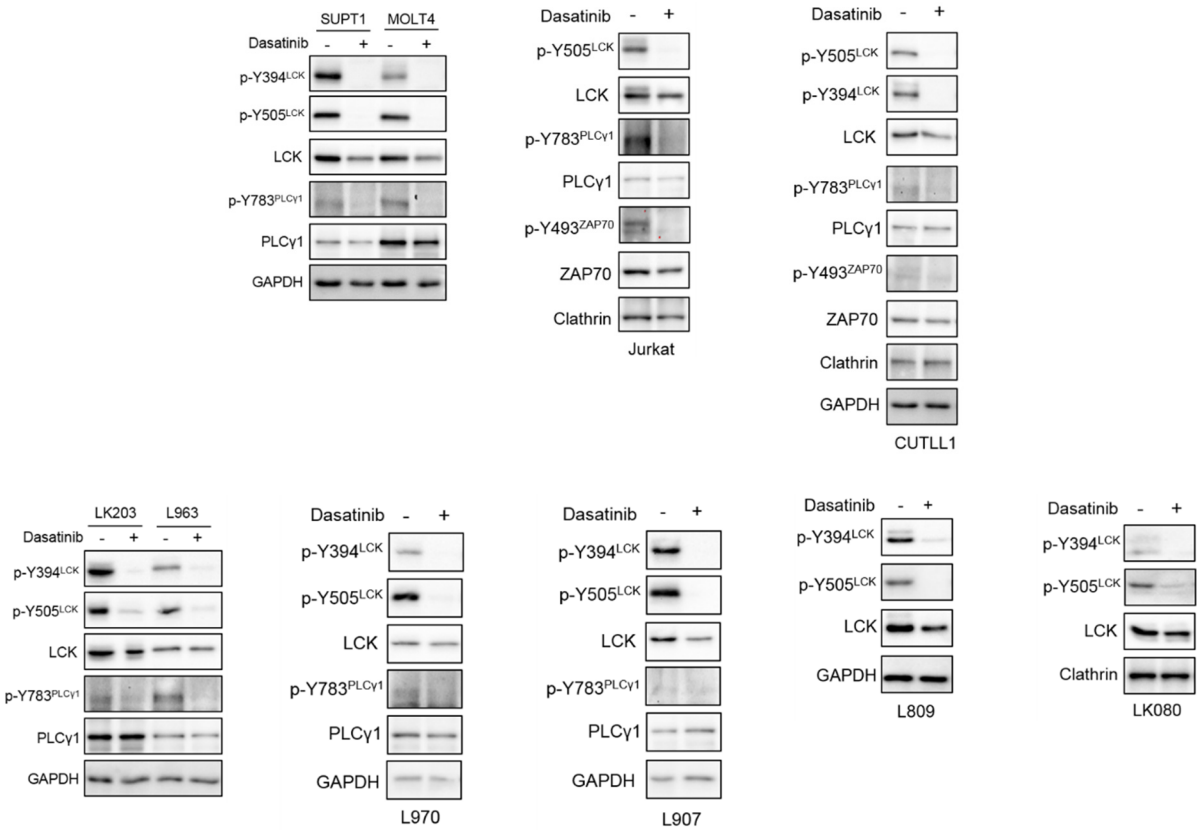

Figure 40. DAS abrogates LCK kinase activity in T-ALL cells. T-ALL cell lines (n = 3) and PDXs (n = 2) were treated with 2 µM and 1 µM DAS respectively for 24 hours. Whole cell lysates were generated and applied to Western Blot analysis. LCK activation (p-Y394) and inhibition (p-Y505), PLCγ activation (p-Y783), ZAP70 activation (p-Y493) and expression was examined using phosphor-specific antibodies. GAPDH or Clathrin served as housekeeping proteins.

The effect of DAS on LCK was also assessed in L963 by PhosFlow. After 24 hour treatment of 1 µM DAS, p-Y394^{LCK} reduced 85%, and total LCK decreased 67% (Figure 41). A decrease of LCK total protein was also observed in other samples by western blotting but not in this PDX (Figure 40) (Disucssion in Chapter 6.2.2.2).

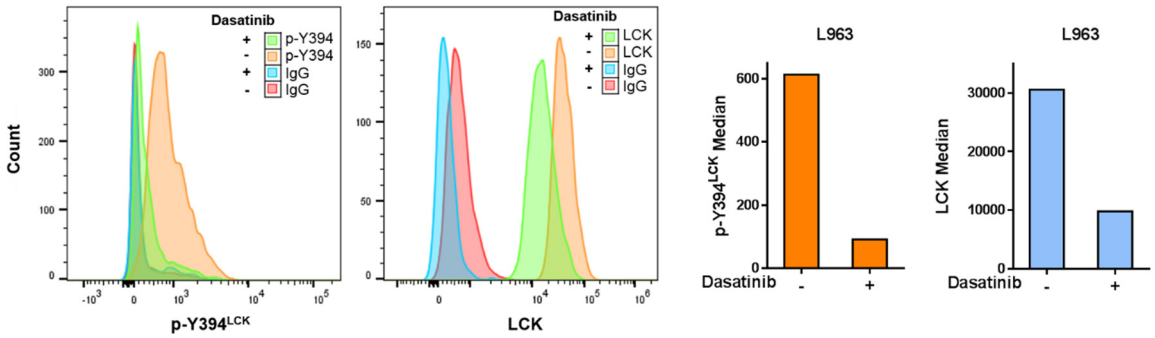

Figure 41. DAS inhibits LCK activation in T-ALL PDX L963. PhosFlow determined LCK activation and protein level in L963 after DAS treatment (1 µM for 24 hours, n = 1) (x-axis represents the distribution of p-Y394^{LCK} (PE) and LCK (Alexa Fluor 647), y-axis shows events (cell counts)). The bar graph displays the median of p-Y394^{LCK} (orange bars) and LCK (blue bars) (x-axis shows control and dasatinib treatment, y-axis represents the median of fluorescence intensity).

4.3 DAS Induces Cell Cycle Arrest in T-ALL

4.3.1 DAS Induces G_0/G_1 Cell Cycle Arrest in T-ALLs

T-ALL cell lines were treated with DAS for 24 hours and cell cycle analyses were performed after staining cells with Hoechst 33342 or PI. Treatment of DAS (2 μM) resulted in a significant G_0/G_1 arrest in MOLT4, SUPT1, and Jurkat. A similar effect was observed in HSB2 and KOPTK1 cells in which 100 nM DAS induced substantial G_0/G_1 cell cycle arrest. MOLT16 showed no significant difference in cell cycle profile after DAS treatment which is consistent with its resistance to DAS compared to other T-ALL cells (Figure 44). Similar studies were expanded to T-ALL PDXs. With 24-hour treatment of DAS (1 μM), LK203, L963 and LK080 showed significant cell cycle arrest (Figure 42). Overall, these data suggest DAS induces cell cycle arrest in T-ALL cells which resembles LCK knockdown effects.

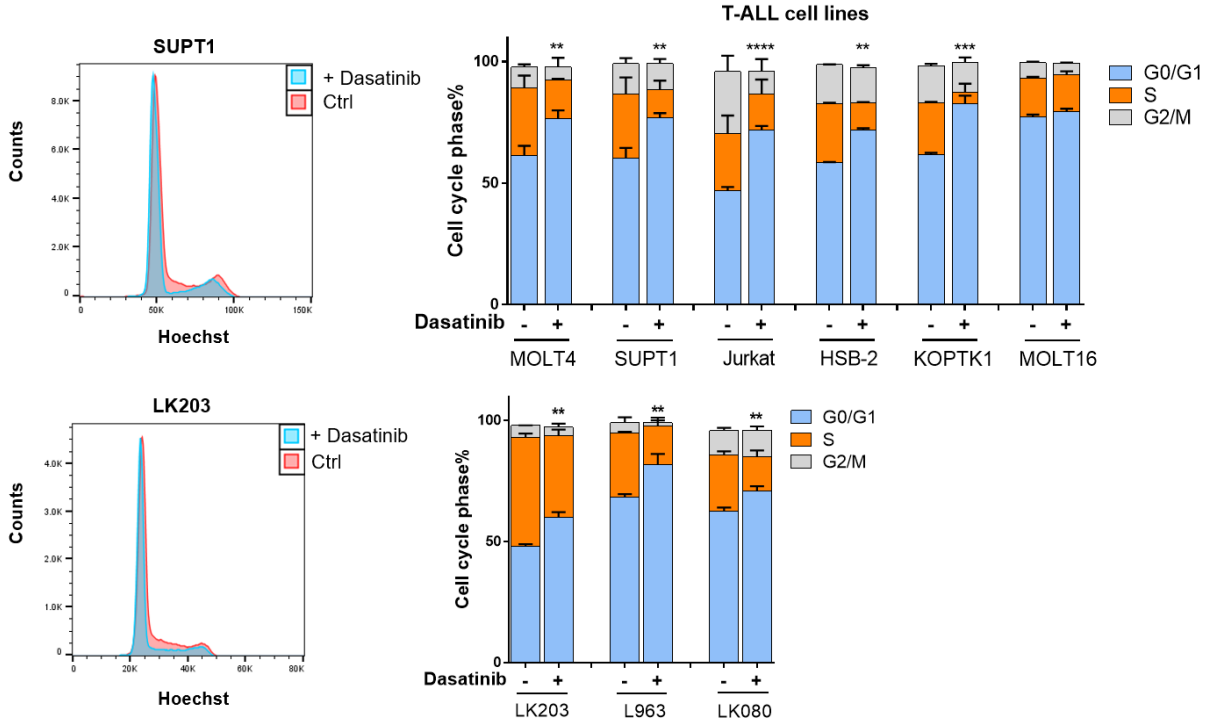

Figure 42. G0/G1 arrest after DAS treatment in T-ALL cell lines and PDXs. T-ALL cell lines and PDXs were treated with 2 μM or 1 μM DAS for 24 hours respectively. Cell cycle status was determined and shown in flow plots (red control; blue DAS-treated, x-axis represents Hoechst distribution (DNA content), y-axis shows events (cell counts)) and bar plots (x-axis shows different samples with or without DAS treatment, y axis represents cell cycle phase (%), blue G_0/G_1 phase; orange S phase; and grey G_2/M phase). Statistical analysis were performed on G_0/G_1 phase (n = 3, * $p \leq 0.05$, ** $p \leq 0.01$, *** $p \leq 0.001$, **** $p \leq 0.0001$).

4.3.2 DAS Induces an G_0 Cell Cycle Arrest in T-ALL Cell Lines

To further evaluate DAS effect on cell cycle arrest, a method to differentiate the G_0 and the G_1 phase was performed in Jurkat, SUPT1 and MOLT4 cells. Hoechst 33342 was used for DNA content measurement while Pyronin intercalate into RNA allowing to separate G_0 and G_1 phases. Cells in G_0 phase are often identified by low RNA content, therefore, this method could distinguish G_0 and G_1 phase.

As little as 200 nM DAS treatment for 24 hours effectively induced G_0 cell cycle arrest in Jurkat (from 2.9% to 17.6%) and SUPT1 cells (from 8.7% to 18.4%). With increasing concentration of DAS treatment, the degree of G_0/G_1 arrest did not further accumulate. Similar findings were observed in MOLT4 cells where DAS increased the G_0 population from 9.5% to 21.1%.

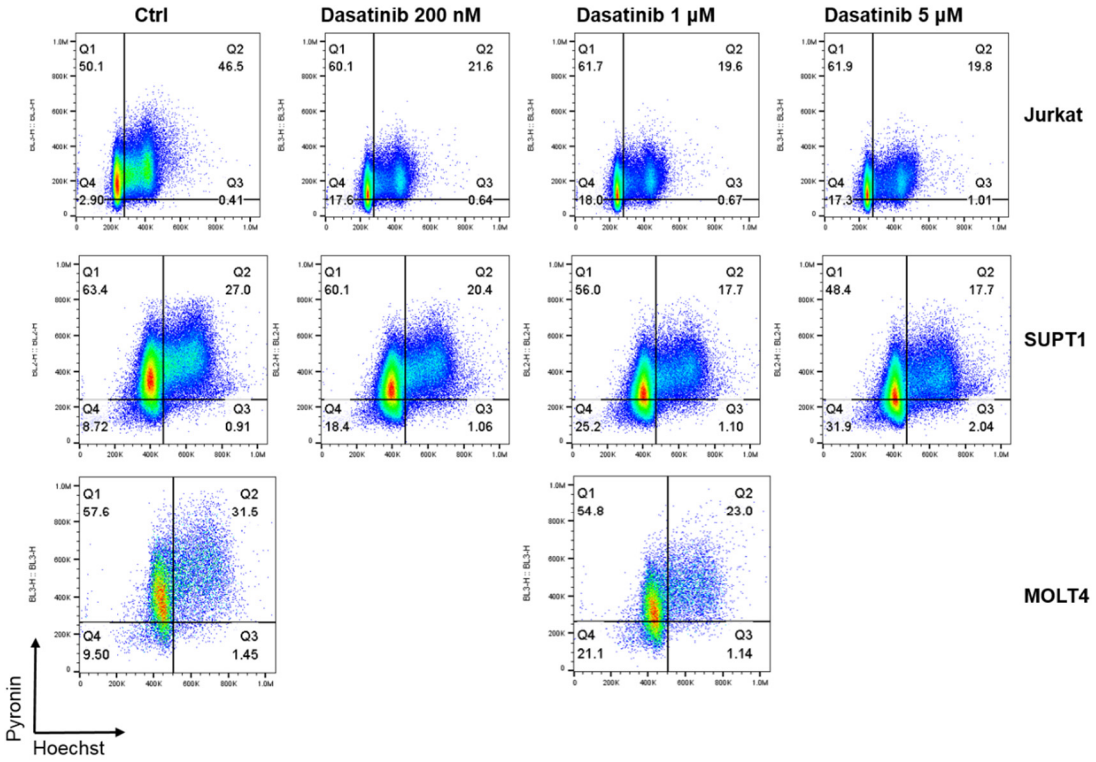

Figure 43. DAS induces a G_0 cell cycle arrest. T-ALL cells Jurkat (n = 2), SUPT1 (n = 2) and MOLT4 (n = 1) were treated with DAS for 24 hours. Increased concentration of DAS was applied to Jurkat and SUPT1 with 200 nM, 1 µM and 5 µM. MOLT4 was treated with 1 µM DAS only. Cells were stained with Hoechst and Pyronin and analysed by flow cytometry. X-axis, Pyronin staining demonstrates RNA content, Y-axis, Hoechst distribution shows DNA content.

4.4 DAS Sensitivity of T-ALL Cell Lines Correlates with LCK Activation

Cytotoxic assays in nine T-ALL cell lines were performed to determine DAS sensitivity. The IC_{50} of DAS was determined by repeated independent experiments. HSB-2 and KOPT-K1 were very sensitive to DAS with an IC_{50} of 5 nM and 20 nM. SUPT1, CUTLL1 and MOLT4 showed an intermediate response to DAS with an IC_{50} of approximately 2 - 5 µM, whilst HPB-ALL, CCRF-CEM, DU528 and MOLT16 were more resistant to DAS with IC_{50} values of approximately 15 µM (Figure 44). At the same time, PhosFlow was used in all cell lines to determine the degree of LCK activation (p-Y394^{LCK}) and expression (LCK). HSB-2 had much higher p-Y394^{LCK} compared with other T-ALL cell lines as it carries a t(1;7)(p34;q34) LCK-TCRB translocation and its survival and proliferation was shown to heavily dependent on LCK (Wright et al., 1994). KOPT-K1 had an intermediate p-Y394^{LCK}/LCK ratio but showed much higher levels of p-Y394^{LCK} by western blotting. Cell lines that expressed the lowest p-Y394^{LCK}/LCK ratio were CCRF-CEM, DU528 and MOLT16. When correlating these two data sets, there was a significant negative linear correlation between DAS IC_{50} and p-Y394^{LCK}/LCK (R^2 = 0.778, p = 0.004; Figure 44). This indicates that T-ALL cell line response to DAS is dependent on LCK activation, suggesting that at least in T-ALL cell lines, the primary target of DAS is LCK.

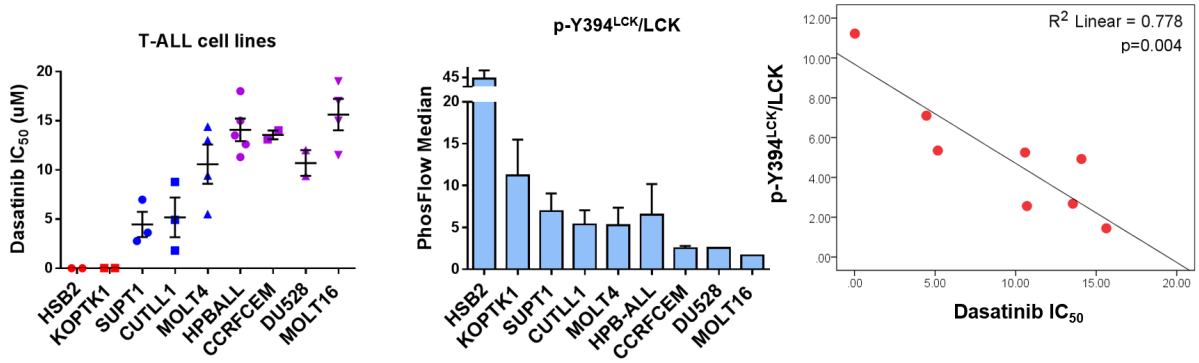

Figure 44. DAS sensitivity correlates with p-Y394^{LCK}/LCK in T-ALL cell lines. The IC_{50} of T-ALL cell lines was plotted on the y-axis (red: hypersensitive cell lines; blue: sensitive cell lines; and purple: resistant cells lines). PhosFlow determined the p-Y394^{LCK}/LCK ratio. The linear correlation analysis was performed in SPSS (R^2=0.778, p=0.004). HSB2 was excluded from this analysis, as the extreme sensitivity to dasatinib was caused by the presence of a unique translocation absent in all other sensitive cell lines.

PDX samples were also used for evaluation of DAS sensitivity. Notably, PDX cells directly used after thawing failed to respond to DAS. As previously shown, DAS acts on cell proliferation by inhibiting cell cycle of T-ALL cells, PDX cells straight from thawing were almost all in G_0/G_1 phase; therefore, the failure in DAS sensitivity was expected. To restore cell cycle progression, PDXs were co-cultured with OP9-DL1 feeder cells *in vitro* for at least one week. For DAS sensitivity assessment, PDX cells were washed and separated from feeder cells through multiple transfers to fresh plates. In general, DAS had clear cytostatic effects with a GI_{50} between 23.8 nM to 6.36 µM on T-ALL PDXs. However, these values did not correlate with pSRC/LCK in PDXs which were analysed in parallel at the day of treatment.

	p-Y394^{LCK}/LCK	lowest viability	Dasatinib GI_{50}
L809	3.361478	28.41	1.035
L963	6.392995	33.69	3.81
LK287	1.483683	54.06	0.02385
LK203	9.176213	47.27	1.398
L903	4.676165	49.39	0.03311
LK080	1.769295	37.62	6.363

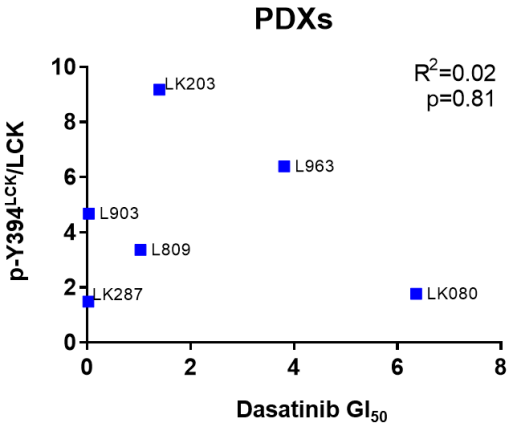

Figure 45. No significant correlation between the DAS GI_{50} and pSRC/LCK was identified in PDXs. Left, the table shows pSRC/LCK, GI_{50}, and maximal inhibition (lowest viability) of PDXs. Right, correlation analysis of pSRC/LCK and GI_{50}. $R^2 = 0.02$, $p = 0.81$.

In this setting, only six PDX samples were evaluated. LK287 was hypersensitive to DAS as this sample has a kinase activating genetic lesion (FIP1L1-PDFGRA). More investigations will be needed to be done to understand genetic aberrations of these PDX samples. Moreover expanding the PDX cohort will be necessary to assess the correlation between DAS sensitivity and LCK activation.

4.5 LCK Downstream Signalling Regulates Cell Cycle Progression

4.5.1 Reverse Phase Protein Array (RPPA) Reveals Downstream Signalling of LCK in CUTLL1 Cells

TCR signalling is known to regulate NFAT, AKT, ERK and NFκB signalling in healthy T cells, but which downstream signalling are more relevant for T-ALL cell proliferation remains less characterised. To address this question, protein lysates from shLCK#3, shZAP70#1 and shCtrl transduced CUTLL1 cells were collected and sent to the protein/antibody microarray facility of the University of Edinburgh for RPPA analysis. In total, 94 antibodies covering TCR signalling, JAK-STAT signalling, MAPK signalling, apoptosis, cell cycle, WNT signalling, P53 signalling and chemokine signalling pathways were used. As expected, the protein expression profiles after LCK knockdown and ZAP70 knockdown were significantly correlated (R^2 = 0.23; $p < 0.0001$). In shZAP70#1 transduced cells, 50% loss of ZAP70 was observed while no changes in ZAP70 expression were seen after shLCK#3 and shCtrl transduction as expected. Unfortunately, LCK antibody was not in the antibody panel, however, shLCK#3 induced the knockdown of pSRC by 60%. Around half of the proteins that were included in this array were significantly downregulated by both LCK knockdown and ZAP70 knockdown ($p < 0.01$). Among these proteins, p-AKT^{Ser473}, p-AKT^{Thr308}, p-ERK1$^{Thr202/204}$, p-ERK2$^{Thr185/187}$, and p-MEK1/2$^{Ser217/221}$ were dramatically downregulated after LCK knockdown (54%, 43%, 62% and 55% respectively) (Figure 46). Similar effects were observed after ZAP70 knockdown but to a lesser extent. This study demonstrates that in the T-ALL cell line CUTLL1, LCK and ZAP70 knockdown leads to downregulation of the AKT and ERK signalling pathways, both situated downstream of TCR signalling.

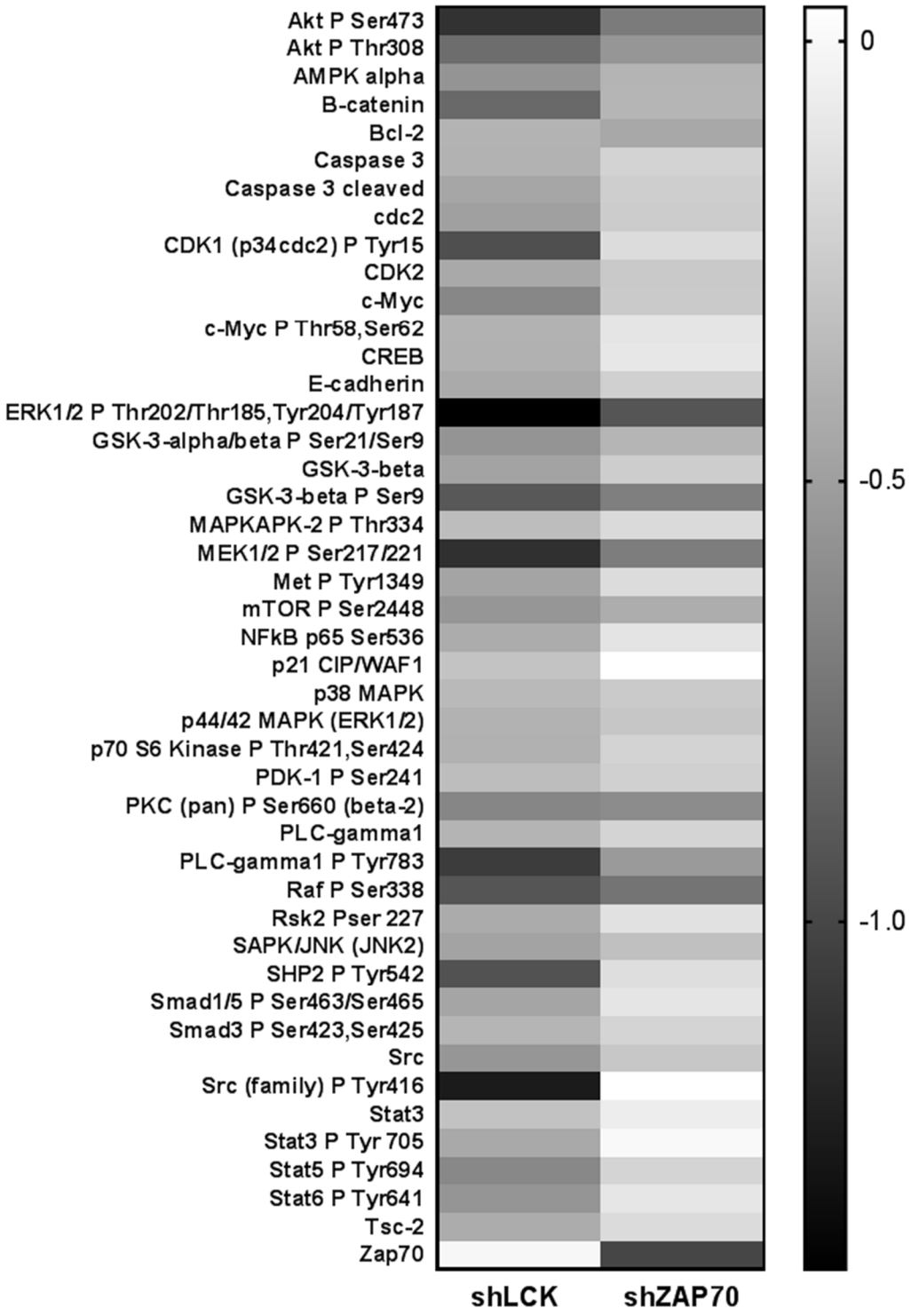

Figure 46. RPPA analysis after LCK and ZAP70 knockdown in CUTLL1 cells. The top 50 downregulated protein targets after LCK and ZAP70 knockdown. Light grey (0 to -0.5): no change to 30% downregulation; dark grey (-0.5 to -1.0 to more): downregulation 30% - 50%; black (< -1.0): downregulation more than 50%.

4.5.2 G_0/G_1 Arrest of shLCK Might Be Due to the Reduction of AKT and/or ERK Signalling

RPPA data suggest that downregulation of AKT and ERK signalling pathways might contribute to cell cycle arrest after LCK knockdown. To verify this hypothesis, the AKT inhibitor MK2206 and the ERK inhibitor SCH772984 were used on T-ALL cell lines. Same amounts of inhibitors were applied to T-ALL cell lines for 24 hours to compare the effect of DAS, MK2206 and SCH772984. After PI staining and cell cycle analysis, a more pronounced cell cycle arrest was observed in DAS treated cells compared with AKT and ERK inhibitor-treated cells. In CUTLL1, Jurkat and MOLT4, both MK2206 and SCH772984 induced G_0/G_1 arrest. But only the AKT inhibitor induced cell cycle arrest in SUPT1 cells. No effect on cell cycle after ERK inhibition was observed at least at this concentration (Figure 47). Cytotoxic assays demonstrated varying responses to the AKT inhibitor MK2206 on T-ALL cell lines, yet a cell cycle arrest was observed in all four cell lines. Consistent with the fact that there is no effect of SCH772984 on the cell cycle of SUPT1 cells, SUPT1 cells are highly resistant to this ERK inhibitor in toxicity studies (Figure 47). These data suggest that T-ALL cell cycle progression is controlled by LCK via at least two downstream signalling pathways, i.e. AKT and ERK signalling.

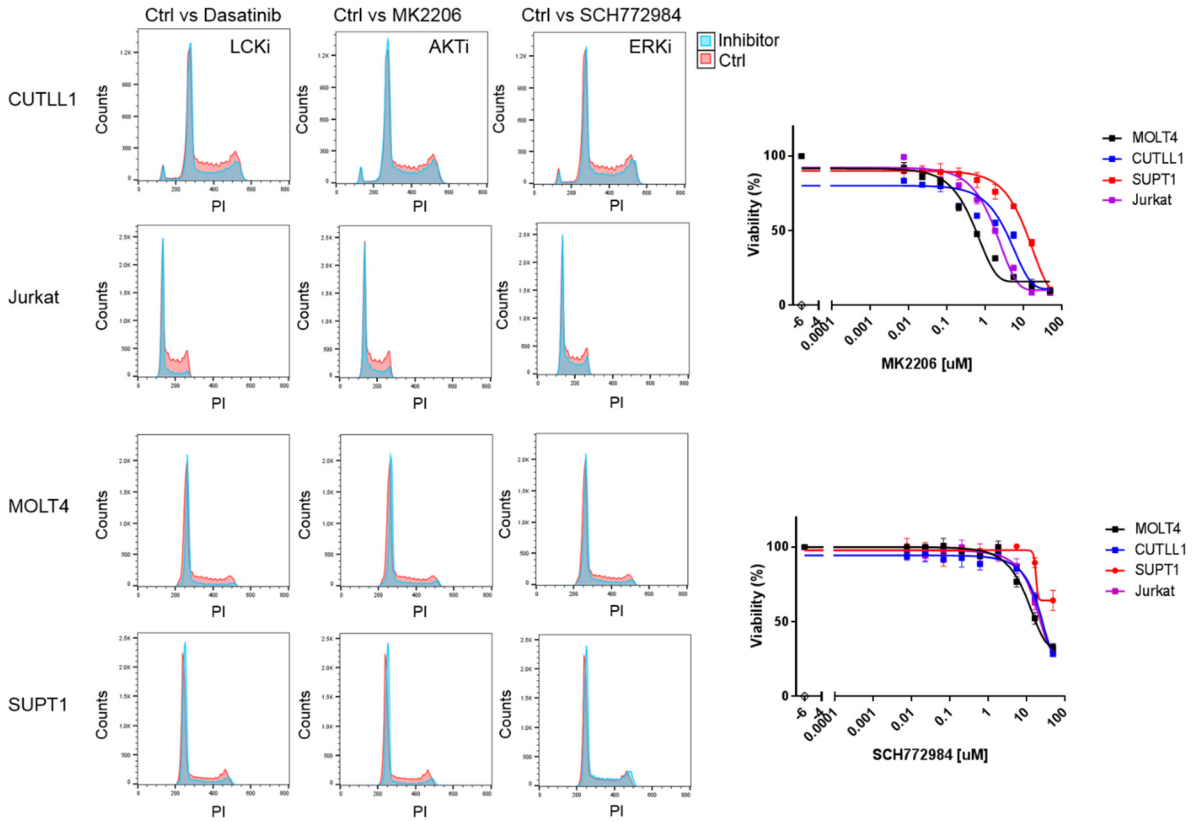

Figure 47. Cell cycle and cytotoxicity analysis of T-ALL cells after LCK, AKT and ERK inhibition. CUTLL1, Jurkat, MOLT4 and SUPT1 were treated with DAS (1.5 µM), MK2206 (1.5 µM) and SCH772984 (1.5 µM) for 24 hours (n = 1). Cell cycle profiles of the vehicle (red) and inhibitor-treated cells (blue) were overlayed. The y-axis represents PI distribution (DNA content), the x-axis represents events (cell counts). The cytotoxicity curves of these four T-ALL cell lines (black, MOLT4; blue, CUTLL1; red, SUPT1; and purple, Jurkat) were determined using a resazurin assay. The y-axis represents the cell viability (%), the x-axis represents the concentration of the AKT inhibitor MK2206 or ERK inhibitor SCH772984 (µM).

Chapter 5

Dasatinib and Dexamethasone Offer a Novel Therapeutic Strategy for T-ALL

5.1 Introduction

DAS leads to cell cycle arrest in T-ALL cell lines and PDX cells indicating that DAS treatment of T-ALL has a cytostatic, rather than cytotoxic effect. In practice, effective eradication of ALL requires combinatorial treatment. We thus investigated potential synergy between DAS and the glucocorticoid dexamethasone (DEX), which is a core component of the first-line multi-agent chemotherapy in treating paediatric ALL. However, 20% of T-ALL patients experience relapse, which is often DEX-resistant. In T-ALL, inhibition of IL-7R signalling or AKT function has been shown to enhance DEX-induced cell death (Li et al., 2016; Piovan et al., 2013).

Acute leukaemia PDX samples can be used in a phase II-like mouse trial that mimics human randomised clinical trials. Such an experiment can reveal drug efficacy and generate biomarkers in both treatment-naïve and relapsed/refractory disease. The benefit of phase II-like clinical trials in mice is to make the comparison between treatment arms very comparable to a human phase-II study since multiple PDXs will be assessed in parallel and any significant data will be more meaningful. It also allows for studying a wide range of heterogeneous biological samples to identify potential drug response biomarkers. In another relevant study, pilot drug studies were designed using an MDM2 inhibitor CGM097 in B-ALL to compare three-versus-three (three mice per treatment arm) and one-versus-one (one mouse per treatment arm) trial settings. Similar results were observed between the two formats indicating the one-mouse-cohort study was sufficient for mouse clinical trials (Townsend et al., 2016).

Leukaemia infiltration into the CNS remains a clinical challenge in curing ALL patients. Most optimal levels of chemotherapy drugs are reduced after the blood-brain barrier; therefore, CNS provides a protected niche for leukaemia cells. Mechanically, ZAP70 has been shown to correlate with CNS in B-ALL while CNS positive T-ALL patients express higher CCR7/CXCR4 (Alsadeq et al., 2017). In UKALL2003, 12% of T-ALL patients develop CNS disease, while only 5% of B-ALL patients show CNS disease. Therefore, to develop a novel drug combination that could reverse DEX-resistance and eradicate leukaemia from CNS is essential for cure.

5.2 LCK Knockdown Cells Are Re-sensitised to DEX

After silencing LCK by shLCK#1 and shLCK#3 in SUPT1 and CUTLL1 cells, the cell viability was measured in the presence of increasing concentrations of DEX (0 - 1699 nM). Wildtype cells (Mock, grey) and control shRNA transduced cells (shCtrl, black) were resistant to DEX while LCK knockdown cells (shLCK#1 in red and shLCK#3 in blue) were sensitive to DEX (Figure 48). In SUPT1 cells, a more pronounced knockdown by shLCK#3, compared with shLCK#1 (Figure 30), led to a more significant effect of re-sensitisation of cells to DEX. These data indicated that LCK inhibition could reverse DEX resistance.

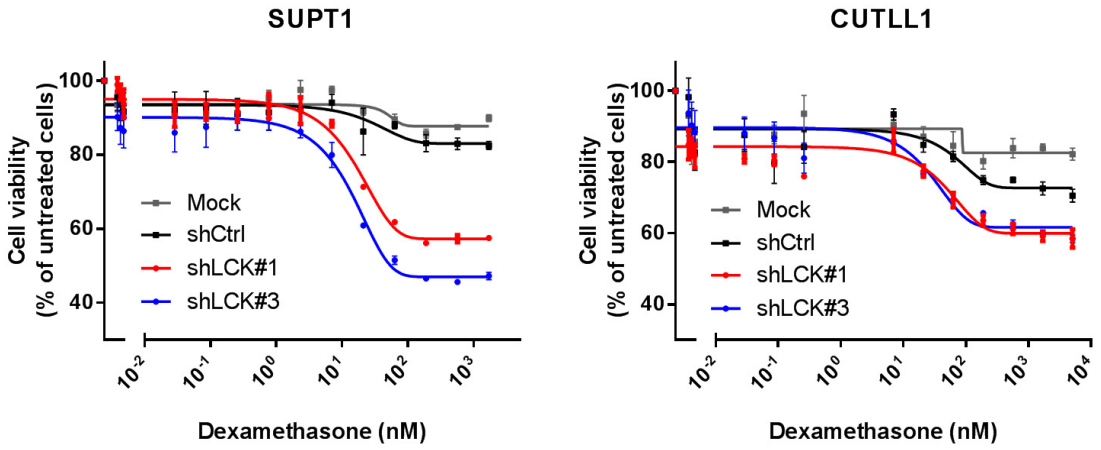

Figure 48. Knockdown of LCK re-sensitises SUPT1 and CUTLL1 to DEX. T-ALL cell lines SUPT1 and CUTLL1 were transduced with shLCK#1, shLCK#3 and shNTC. Cytotoxic assays of DEX were performed in knockdown cells (blue: shLCK#3; red: shLCK#1) and control cells (black: shNTC; grey: mock (wildtype) cells). The x-axis represents DEX concentration (0 - 1699 nM), the y-axis shows cell viability of untreated cells (%).

5.3 Drug Matrix Analysis of DAS and DEX Reveals Synergy in T-ALLs

To further evaluate the relationship between LCK inhibition and DEX response, drug matrix analyses were performed. For each matrix, T-ALL cells were seeded into three 96-well plates. DAS and DEX were titrated in two dimensions. Cell viability was measured by CCK-8 after 72-hour treatment.

5.3.1 Drug Matrix of T-ALL Cell Lines

Ten T-ALL cell lines were used to examine drug interactions of DAS and DEX. DEX was titrated from 0.09 nM – 600 nM in all matrixes. However, DAS was titrated differently according to cell line sensitivity: 0.08 µM – 50 µM for SUPT1 and Jurkat; 0.37 µM – 30 µM for CUTLL1, CCRF-CEM, MOLT16, HPB-ALL and MOLT4; 0.005 nM to 50 nM for HSB2, KOPTK1 and ALL-SIL. These concentration ranges were chosen based on cytotoxicity studies of dasatinib in these cell lines, however, the highest concentration of DAS (30-50 µM) might have potential off-targets in T-ALL cells.

The cell viability of SUPT1 exposed to DEX decreased in the presence of DAS in a concentration-dependent manner. Data were generated in triplicates and imported into Combenefit (Di Veroli et al., 2016) to interrogate drug interaction. This software gave drug synergy (blue) or antagonism (red) based on the Loewe model (Loewe, 1926). There were several synergistic combinations of DEX and DAS in SUPT1 cells indicated by dark blue colour. In order to analyse the significance of the data generated of all ten T-ALL cell lines, a scatterplot was generated indicating significant enrichment of drug synergy in the area (shaded box) of $\log_e$(DEX concentration) from 2.7 to 4.7 (8 - 110 nM) and $\log_e$(DAS concentration) from -1.5 to 1.5 (0.223 - 4.5 µM) (Figure 49). This concentration ranges included the clinically applicable C_{max} of DAS (264 nM) (Liston and Davis, 2017) and DEX (100 nM) (Yang et al., 2008). Thus, DEX and DAS synergises to decrease cell viability at clinical relevant concentrations.

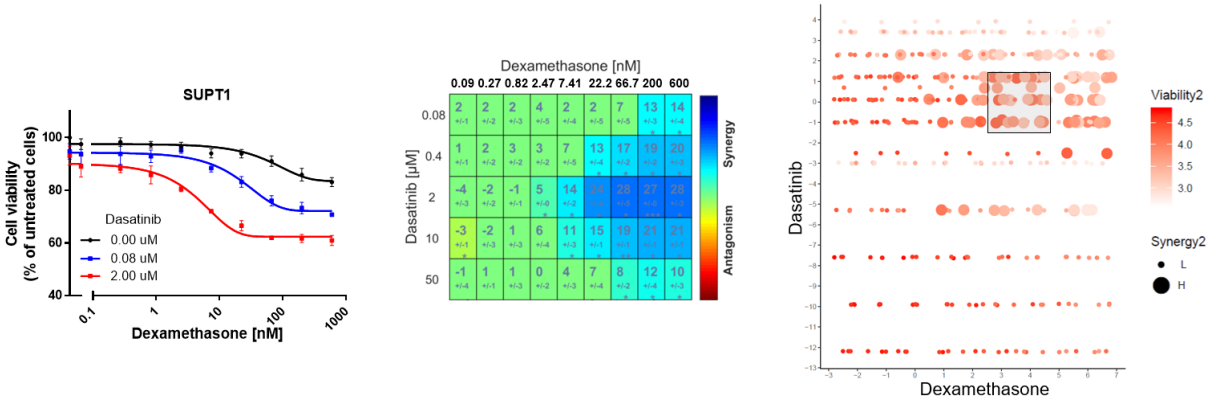

Figure 49. Drug matrix analysis in T-ALL cells demonstrates significant drug synergy, including C_{max} of DAS and DEX. Matrix was plotted in cytotoxicity curves of DEX in the presence of different levels of DAS and the synergy plot from Combenefit. (Left) The cell viability of SUPT1 cells after exposure to DEX (0 - 600 nM) and DAS (black: 0 µM; blue: 0.08 µM; and red: 2 µM) as derived from the drug matrix analysis. (Middle) Drug synergy plot as drawn by Combenefit using DAS (0 - 50 µM) and DEX (0 - 600 nM) on SUPT1 cells. (Right) Combined statistical analysis (by Dr Amir Enshaei) of all drug matrices derived from 10 T-ALL cell lines was performed in RStudio (area of the circles indicate synergy levels; red colour shading: the darker, the higher the cell viability). The x-axis represents the DEX concentration ((log_e(DEX)= -3 – 7; 0 - 600 nM) and the y-axis represents the DAS concentration (log_e(DAS)= -13 – 4; 0.005 nM – 50 µM). The size of the circle represents the level of synergy observed. The shaded grey square highlights drug concentrations resulting in statistically significant drug synergy and loss of cell viability. This grey shaded area includes clinically relevant C_{max} concentrations for both drugs.

5.3.2 Drug Matrix of T-ALL PDXs

Similar studies were performed in T-ALL PDXs. The PDX cells were thawed and co-cultured on OP9-DL1 cells for one week (L903, LK214, and LK809) or several weeks (LK080, L963 and LK203). As no cytotoxic assays of single drug DAS or DEX were performed previously on these PDXs in our laboratory, the range of drug concentrations used in cell lines was applied in the PDX drug matrices. After co-culture, PDX cells were separated from feeder cells by multiple transfers. PDX cells were counted and seeded in three 96-well plates for one drug matrix analysis. DAS and DEX were added in the plates on the same day. Three days later, plates were developed by CCK-8. Data were normalised relative to the control well (0 nM DEX and 0 µM DAS). Combenefit gives both the viability and the degree of synergy as shown in Figure 39. Overall, synergy was observed in all six PDXs, though at variable concentrations of DAS and DEX (Figure 50).

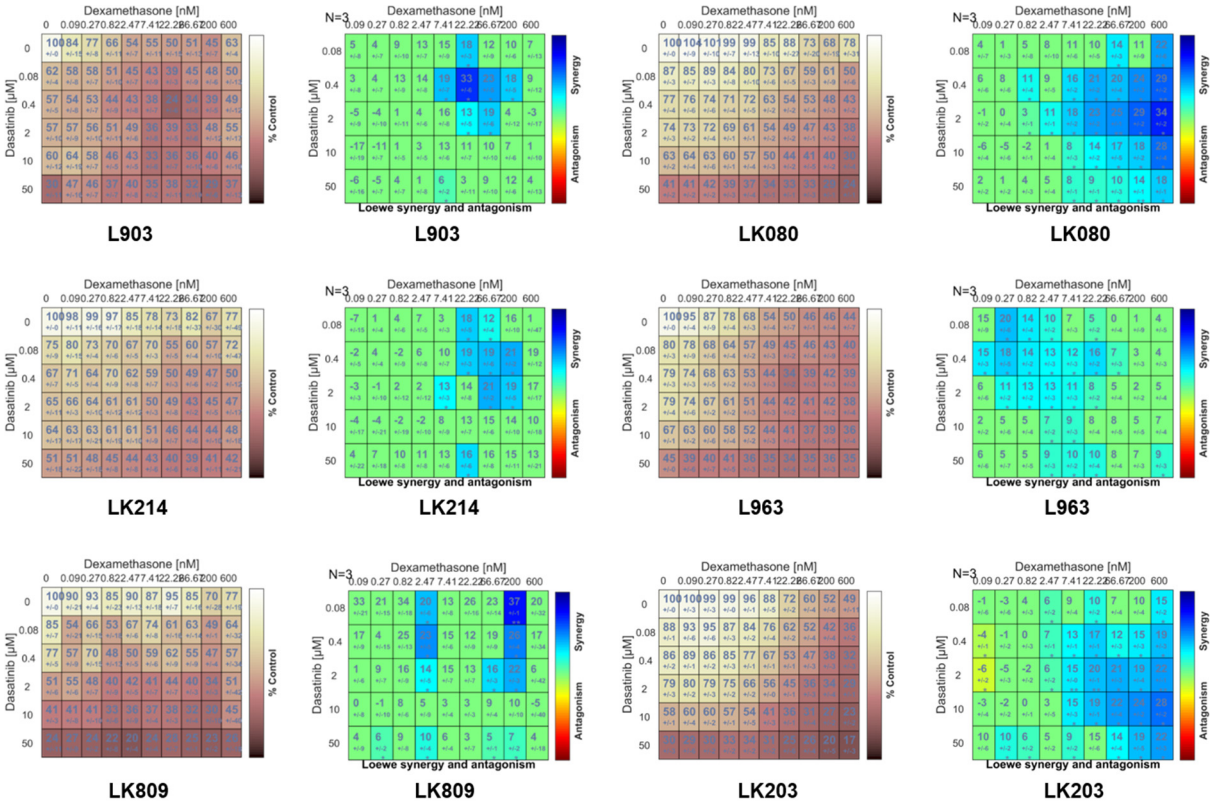

Figure 50. Drug matrix analysis of PDXs. DEX and DAS were titrated in two dimensions in a range of 0 - 600 nM and 0 - 50 µM respectively. CCK-8 measured cell viability after 72-h drug treatments. Data points were analysed by Combenefit and generated synergy plots (blue: synergy; red, antagonism). Viability plots (shaded colours from yellow (more viable) to brown (less viable)).

5.3.3 DAS and DEX Induce Apoptosis

Based on drug matrix assays, DAS and DEX in combination led to a decrease in cell viability, however, whether this was dependent on apoptosis remained an open question. To address this, Annexin V/viability (Live-Dead aqua) staining was conducted in Jurkat cells treated with 2 µM DAS and/or 100 nM DEX after 24 h and 48 h.

Since Jurkat is a DEX-resistant cell line, 100 nM DEX did not induce any cell death. On the contrary, 2 µM DAS induced 6.1% early apoptosis. Furthermore, DAS in combination with DEX led to 14.6% early apoptosis (AnnexinV+/Live-Dead aqua-) without affecting the percentage of dead cells (Live-Dead aqua+; Figure 51). After incubation of cells for another 24 hours, Annexin V staining identified more dead cells in DAS (30.5%), and combination (52.2%) treated samples compared with the control sample (18.0%) (Figure 51). Taken together, this data suggests that the DAS and DEX combination induces increased apoptosis-induced cell death compared to no treatment or single drug (DEX or DAS) treatment in Jurkat.

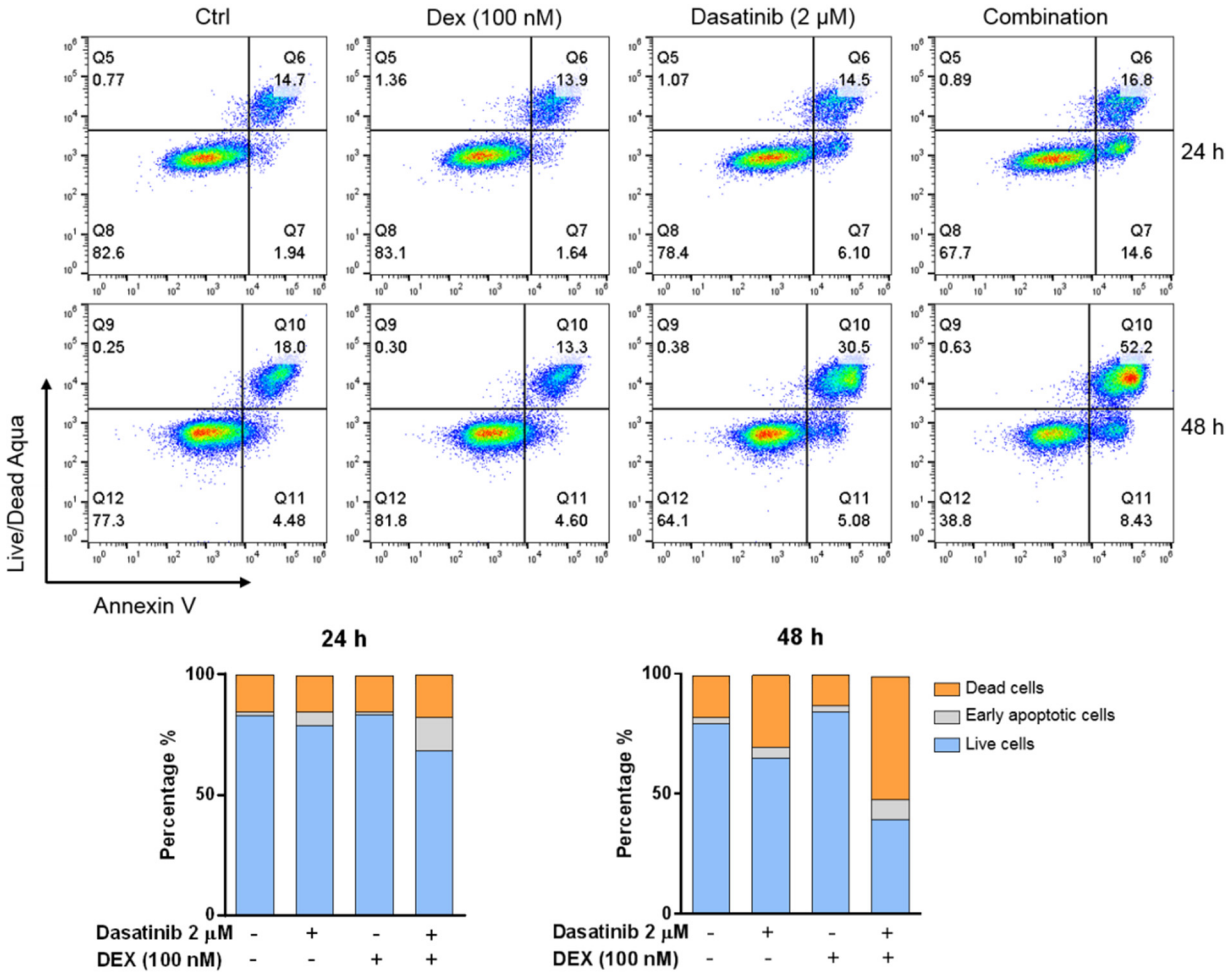

Figure 51. Drug combination of DAS and DEX induces greater apoptosis-induced cell death in Jurkat cells. Jurkat cells were treated with DAS (2 µM) and DEX (100 nM) for 24 hours and 48 hours, respectively (n = 1). Annexin V and Live/Dead Aqua separated the live cells (bottom left, Annexin V^- $Aqua^-$), apoptotic cells (bottom right, Annexin V^+ $Aqua^-$) and dead cells (top right, Annexin V^+ $Aqua^+$). The bar graph shows the proportion of live cells (blue, AnnexinV^- $Aqua^-$), early apoptotic cells (grey, Annexin V^+ $Aqua^-$) and dead cells (orange, Annexin V^+ $Aqua^+$) under drug treatment as determined by flow cytometry and indicated in dot plots.

5.4 A Phase II-like Trial in Mice Confirms the Synergy between DAS and DEX

5.4.1 Toxicity Study of the Combination of DAS and DEX *in vivo*

Our lab has previously used DEX in *in vivo* mouse models. Based on these experiments, the appropriate dosing of DEX in NSG mice was established as 1 mg/kg. At this concentration, it will reach a mouse plasma level of 100 nM which is similar to the C_{max} in patients (Yang et al., 2008). However, for DAS, several pieces of literature have published on DAS doses *in vivo* where they applied from 5 mg/kg to 50 mg/kg. This however did not help to predict the suitable dosing for drug combinations of DAS and DEX.

Therefore, a pilot toxicity study was performed in a small number of NSG mice to explore the maximal tolerated dosing of DAS in combination with 1 mg/kg DEX. Six healthy NSG mice (three males and three females) were dosed daily (Monday to Friday) with one single combined dose of 1 mg/kg DEX and DAS by intraperitoneal (IP) injection. Mice were examined and weighed daily. The starting dose of DAS was 5 mg/kg. The dose was increased to 10 mg/kg, 20mg/kg and 35mg/kg in the following weeks. While this experiment was ongoing, a study was published showing combination dosing of DEX (5 mg/kg) and DAS (35 mg/kg) *in vivo* (Serafin et al., 2017). Thus, the DAS dosing was set according to this study and evaluated how many weeks the mice would tolerate this drug regimen. Using DEX 1 mg/kg and DAS 35 mg/kg mice lost weight during drug treatment within the accepted range of 10%. On the 3rd week, all six mice lost around 10 - 15% of weight indicating that they could not tolerate this dose any longer. In particular, NN (m) reached 15.3% weight loss, thus dosing was stopped on that day. It regained weight and the dosing was restarted. Weight monitoring was continued for more than 10 days after dosing finished. Overall, mice gained weight gradually after stopping drug treatment and were back at their original

weight around 12 days later. Mouse NN (f) had to be euthanised as it showed 15% weight loss for three consecutive days (Figure 52). In summary, our pilot study indicated that the maximum tolerated dosing for NSG mice is 35 mg/kg DAS with 1 mg/kg DEX for in total three weeks.

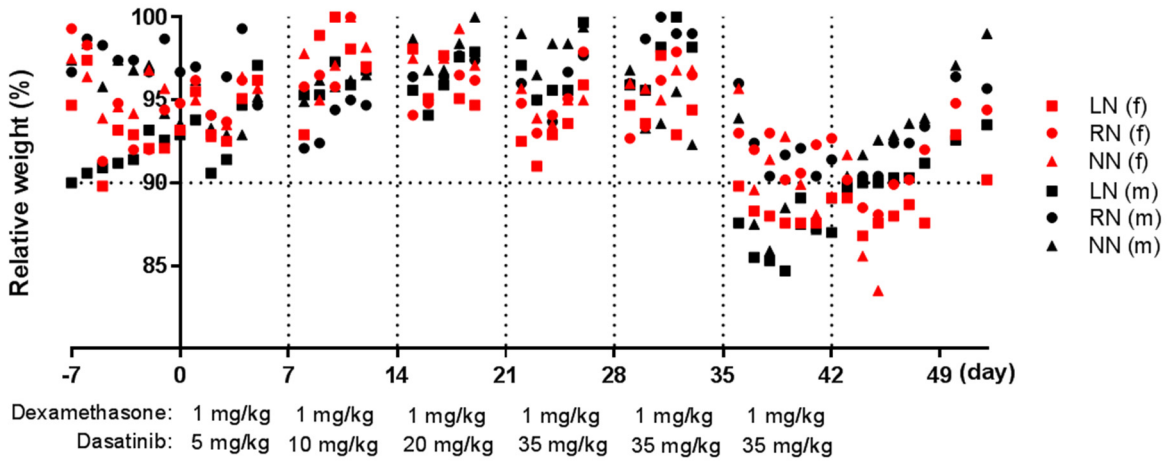

Figure 52. The weight monitoring and dosing timeline of six healthy mice in the toxicity study. Mice weights (f: female; m: male) were monitored daily for seven days before the toxicity study commenced. Both drugs, DEX and DAS, were were resuspended in distilled water and injected intraperitonealy. DEX was applied daily at 1 mg/kg throughout the study. DAS was dosed daily at 5 mg/kg for the 1st week, 10 mg/kg for the 2nd week, and 20 mg/kg for the 3rd week, and kept at 35 mg/kg for the following three weeks. Dosing was stopped after 6 weeks because significant weight loss was observed. The weights were monitored for another 10 days after stopping of the treatment in order to evaluate whether observed toxicity was reversible.

5.4.2 Study Design of a Murine phase-II-like Trial

To evaluate the efficacy of combination treatment, we used 10 T-ALL PDXs for a phase II-like trail in mice. All 10 PDXs were generated from NSG mice which had been injected with primary patient T-ALL samples previously. The survival time of those primary engrafted mice varied from 48 - 216 days (Appendix 4). For the murine phase-II like study, each PDX was intrafemorally injected into 4 NSG mice (40 mice in total). T-ALL engraftment was monitored weekly by tail bleeds (20 µl blood/mouse) and peripheral blood staining for hCD7, hCD45 and mCD45. The 4 mice derived from each PDX were randomised to receive the vehicle, DAS alone (35 mg/kg), DEX alone (1 mg/kg) or the combination treatment (35 mg/kg DAS plus 1 mg/kg DEX) by intraperitoneal injection beginning upon engraftment (defined as ≥ 0.5% peripheral

blood hCD45^{+} cells). Mice were dosed once daily from Monday to Friday. Treatment was given for two or three weeks depending on the rate of engraftment and progression. In cases where the PDXs engrafted very quickly, the mice were not kept alive for another weeks' dosing. In the end, mice of the same PDX were sacrificed at the same time to assess leukaemia progression and combination treatment efficacy (Figure 53). For analyses, mice blood, spleen, bone marrow, liver and CNS infiltration were harvested and tumour infiltration was determined by flow cytometry.

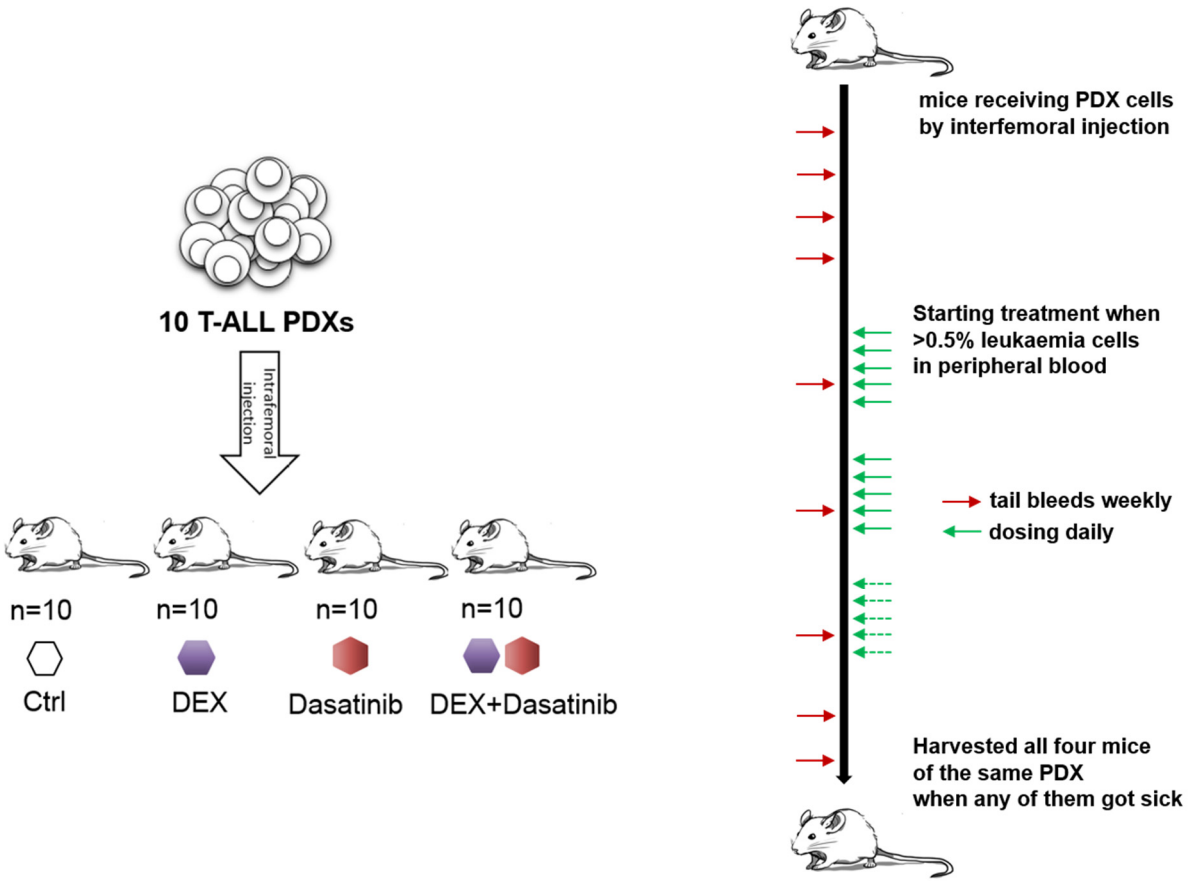

Figure 53. Schematic representation of the phase II-like clinical trial in mice. Ten T-ALL PDX samples were injected into 40 NSG mice (4 mice each PDX). Leukaemia engraftment was monitored by tail bleeds every week. Mice were randomised to receive control vehicle, DAS (35 mg/kg), DEX (1 mg/kg) or drug combination (DAS 35 mg/kg + DEX 1 mg/kg). The peripheral blood monitoring was continued during the dosing. Treatment was given for 2 or 3 weeks. When any of the four mice derived from 1 single PDX showed clinical symptoms, all four mice were killed and spleens, bone marrow, livers and CNS was isolated and assessed by flow cytometry for the engraftment.

5.4.3 Peripheral Blood Monitoring for Disease Progression and Treatment Effects

For peripheral blood engraftment monitoring, 20 µl of blood drawn from the mouse tail vein was stained weekly for hCD7, hCD45 and mCD45. Human leukaemia blast engraftment was shown by hCD45 or hCD7 cells in mouse blood. The dosing was commenced once > 1% (except L903 was started > 0.5%) peripheral blood engraftment was observed. The engraftment rate varied for different PDXs; LK080 and LK287 were dosed starting on the 3rd week after injection; L963 and LK203 were dosed starting on the 4th week after injection; L970 were dosed starting on the 6th week and L809, L903, LK290 and L907 were dosed starting on the 7th week. The dosing time was determined by clinical symptoms as observed in the mice. In order to determine the final peripheral blood engraftment, we collected mice blood right after euthanizing out of the eyeball after removing (Figure 54).

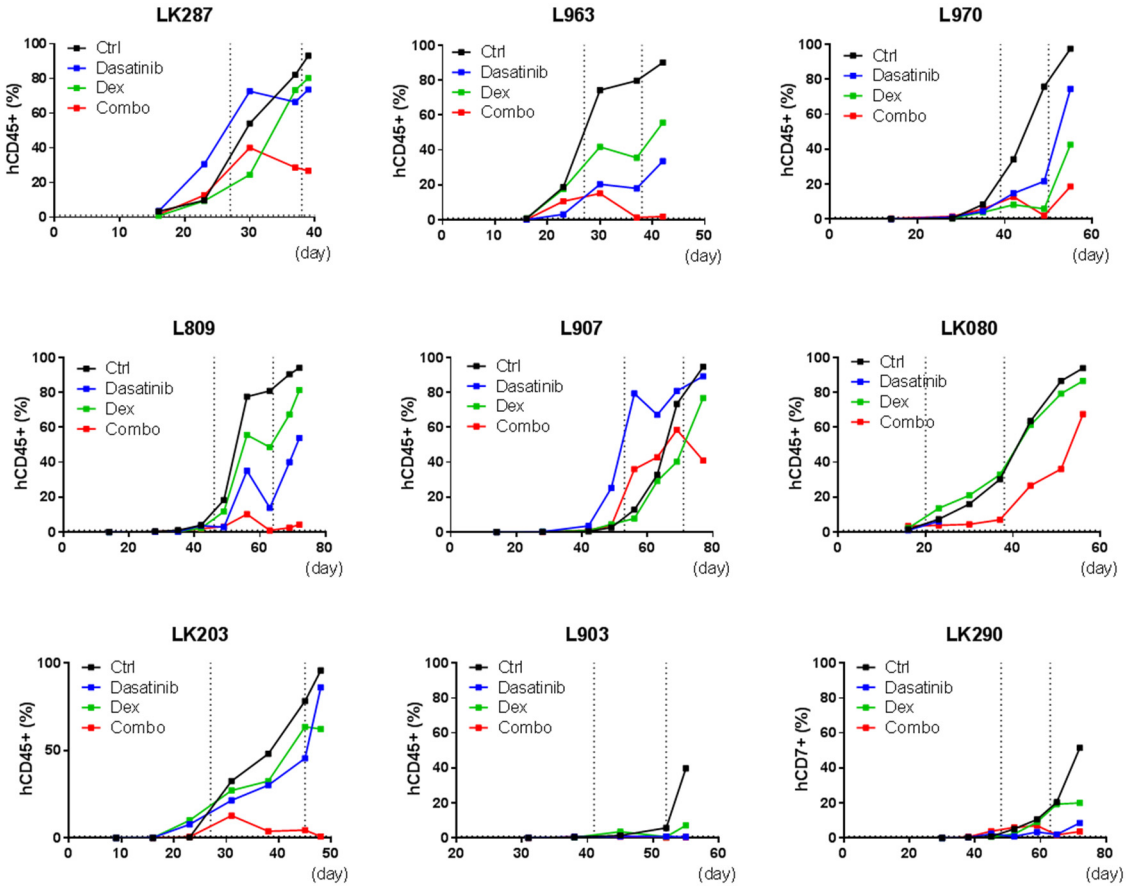

Figure 54. Peripheral blood monitoring in 35 mice derived from nine PDXs. Mouse tail vein blood was taken every week to monitor leukaemia engraftment *in vivo*. The four mice of each PDX was allocated to different treatment groups randomly: black, vehicle; blue, DAS; green, DEX; red, DEX in combination with DAS. The dosing

window was shown with dotted lines. Time (days after injection of leukaemia cells) was shown on the X-axis while the percentage of human cells ($hCD45^+$ or $hCD7^+$) in mouse blood was shown on the Y-axis.

5.4.4 Drug Efficacy in Mouse Bone Marrow, Spleen, and Liver Engraftment

It was very challenging to determine when to euthanise the mice for such an elaborate experiment. In most of the cases, such as LK080, L809, L963, LK287, LK203 and L970, the mice were harvested because the control vehicle mouse had high engraftment (> 70% $hCD7^+$/$hCD45^+$ cells) as established by peripheral blood staining. In the case of L903, the mice were harvested due to sickness of the mouse receiving the combinatorial treatment. For L907, the four mice were harvested because of high engraftment in the peripheral blood in the DAS treated mouse, which might have been due to higher engraftment rate prior to commencing dosing. For LK290, since the engraftment in the peripheral blood fluctuated (maximal 55% and 60%) in mice injected with the primary patient sample (n = 2), these mice were harvested when the control vehicle mouse reached 51% engraftment in peripheral blood. LK214 was excluded from the whole analysis because of experiment failure; this PDX samples engrafted so quickly that the mice had to be euthanised before treatment was commenced. At the end of the experiment, mice's peripheral blood, spleen, bone marrow and liver were analysed for 35 mice (the DAS mouse of LK080 died before the experiment commenced).

For the spleen samples, only PDXs that engrafted in the spleen as determined by enlarged spleens were taken into consideration for the analysis. Therefore, spleens derived from L903 and LK290 were excluded from the analysis. Spleen weights were recorded, and spleen sizes of 5 PDXs were captured in photos. Among the same PDX, the combination treated mouse displayed the smallest spleens compared to the control mouse or DEX/DAS single arm treated mice. Taken all the weights in statistical analysis, it turns out that control and single drug-treated mice had significantly more enlarged spleens than combination treatment mice (Figure 55).

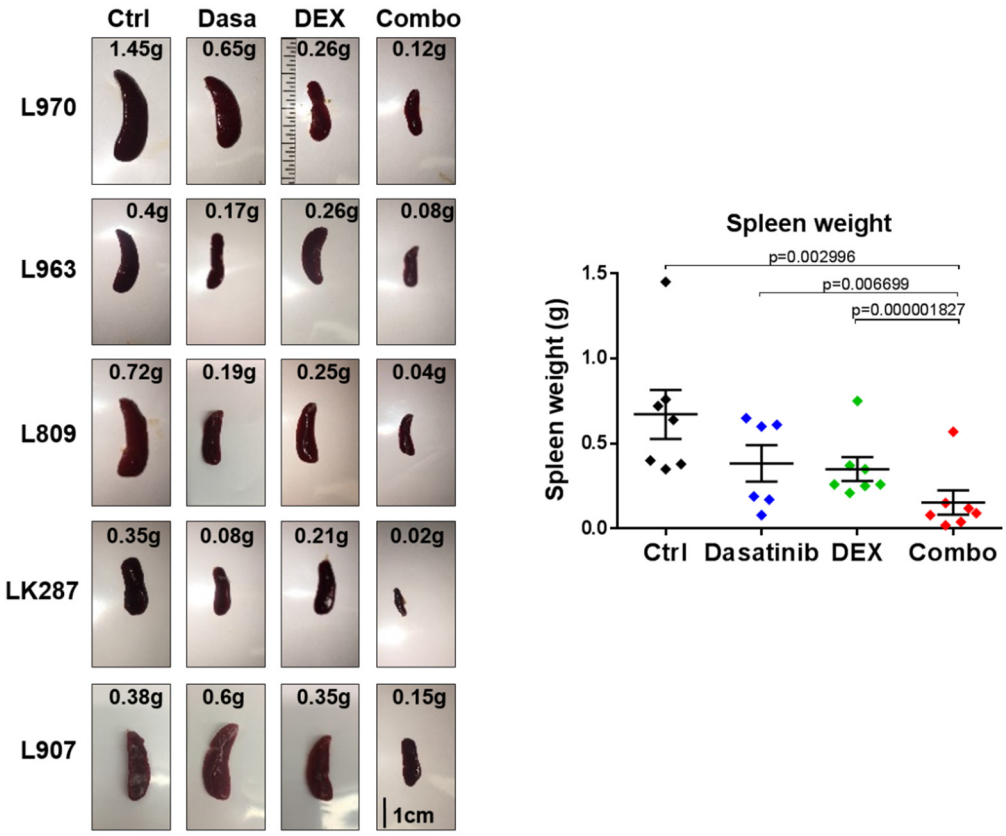

Figure 55. Spleen weights and size of spleens in the phase II-like murine trial. Mouse spleens of 5 PDXs were imaged at the same scale. Spleen weights are indicated. The dot plot shows spleen weights of all seven PDXs on the Y-axis with treatment arms on the X-axis. Statistical analysis was performed in R Studio by the linear mix model (Ctrl vs Combo, p = 0.00296; DAS vs Combo, p = 0.006699; DEX vs Combo, p = 0.000001827).

After homogenising material through a cell strainer with PBS, spleen and liver samples were stained with mCD45, hCD45 and hCD7. The end-point peripheral blood and bone marrow samples were also incubated with the same staining antibody cocktail. After (FSC/SSC) gating of singlets, doublets exclusion and exclusion of dead cells, flow cytometry dot plots were generated showing degree of PDX engraftment (mCD45 vs hCD7 or mCD45 vs hCD45; Figure 56).

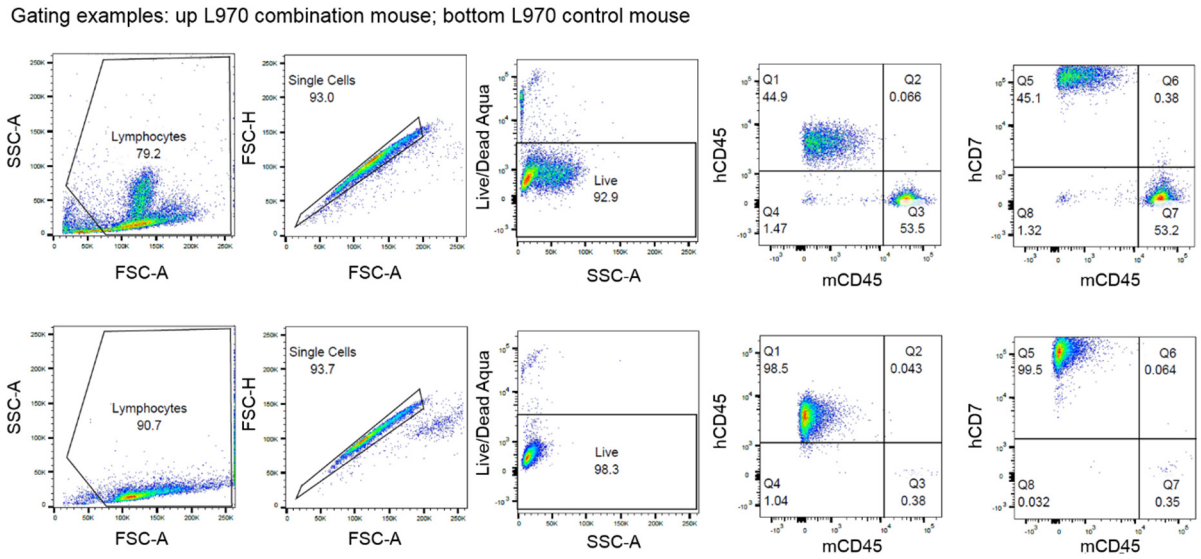

Figure 56. Gating strategy of flow cytometry data to assess human leukaemia cell engraftment in mouse spleens. Flowjo analysis was performed after acquiring samples on a BD FACSCanto II. Each sample was (i) gated according to their appearance in FSC vs SSC to exclude any debris, (ii) cleaned of doublets by FSC-A vs FSC-H and (iii) pruned of any dead cells by gating out Live/Dead Aqua positive cells. hCD45 or hCD7 positive cells in the live cell population were considered human leukaemia cells. In this example of L970, the leukaemia engraftment in the combination treatment mouse and the control mouse was 45% and 99% respectively.

Of nine T-ALL peripheral blood samples (round dots), the combination treatment group had significantly less engraftment judged by hCD7$^+$ cells compared to control ($p = 0.000001393$), DAS ($p = 0.00593$), or DEX-treated mice ($p = 0.0003794$). Seven PDXs were included in spleen engraftment analysis (squares). Also in spleen leukaemia progression was significantly impaired when combination treatment was applied. DAS and DEX in combination was substantially more effective than vehicle ($p = 0.0009869$) or single drug treatment ($p = 0.01104$ when compared with DAS and $p = 0.0003794$ when compared with DEX). NSG mice received PDX cells by interfemoral

injection. Bone marrow samples were harvested from both left and right femurs. In the final analysis (triangles) of 9 PDXs, the combination treatment significantly reduced leukaemia burden in bone marrow compared with control (p = 0.0000557), DAS (p = 0.008554) and DEX treatment (p = 0.00684). Initially, liver samples were not considered for analysis. However, it was observed that leukemia cells inflitrated to mouse livers, therefore liver samples had been also assessed, though no liver samples were collected from the first three PDXs. The remaining 6 PDXs were used to analyse liver engraftment. Consistent with the previous analyses in other organs, the combination treated mice had least liver engraftment among four treatment arms (Figure 57).

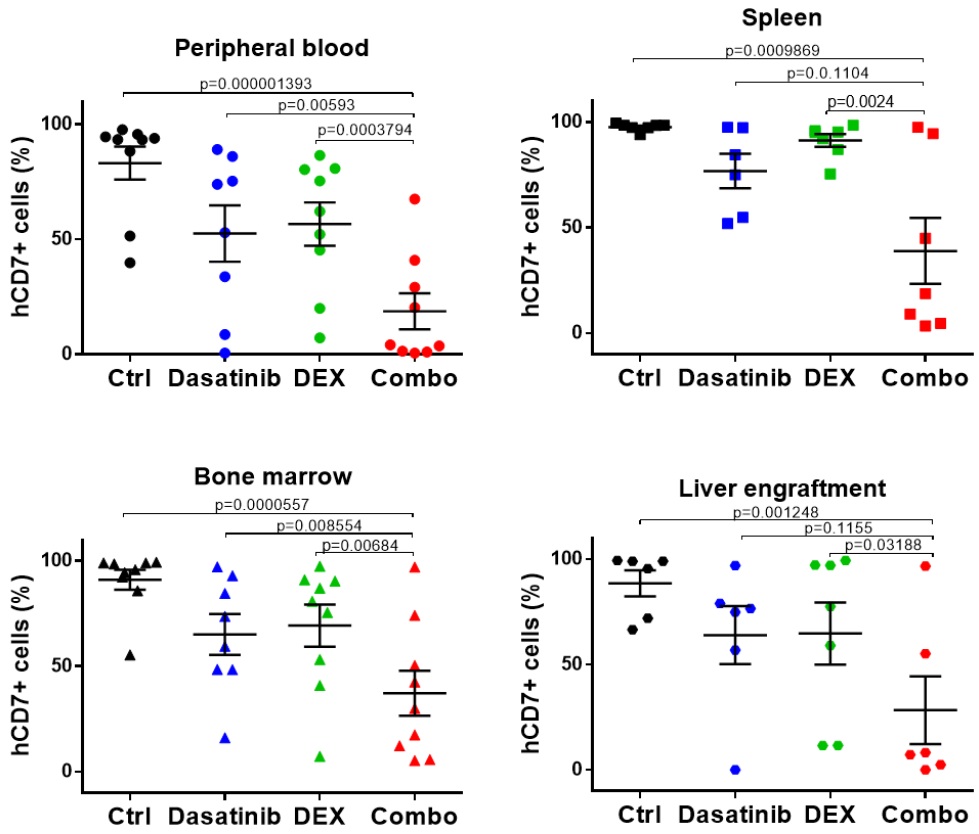

Figure 57. End-point analysis of human leukaemia engraftment (hCD7⁺) in NSG mice. Human leukaemia engraftment was determined by hCD7⁺ expression in peripheral blood (n = 9), spleen (n = 7), bone marrow (n = 9) and liver (n = 6) samples were plotted (black, control vehicle; blue, DAS; green, DEX; red, DEX in combination with DAS). Statistical analyses were performed by linear mix model using RStudio.

Similar analyses were performed using hCD45$^+$ cells as marker of human leukaemia engraftment. Seven out of nine PDXs expressed similar amounts of hCD45 and hCD7. LK290 had lower hCD45$^+$ expression than hCD7$^+$, while L970 had lower median expression of hCD45 compared with hCD7. However, overall the results of leukaemia engraftment remained similar, using either hCD45 or hCD7 as marker. In peripheral blood (n = 9), spleen (n = 6), bone marrow (n = 9) and liver (n = 6) samples, the combination treatment was significantly better than control or single drug treatments in impairing leukaemia engraftment (p values indicated in the graph) (Figure 58).

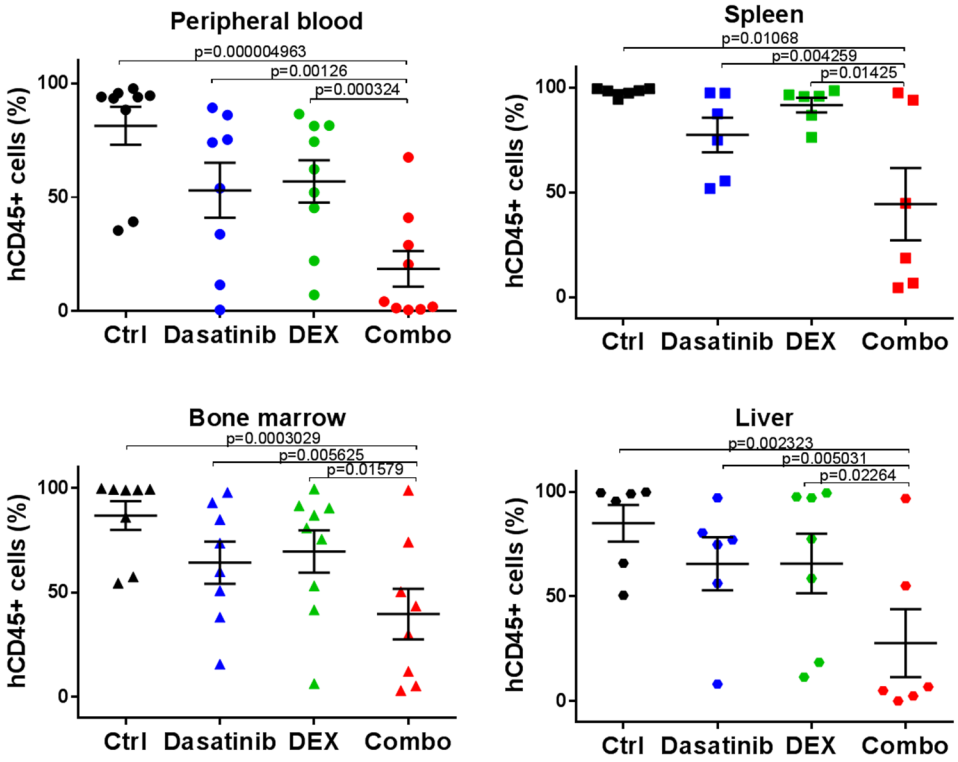

Figure 58. End-point analysis of human leukaemia engraftment (hCD45$^+$) in NSG mice. Samples examined in Figure 46 were assessed at the same time also for their hCD45 expression. Peripheral blood (n = 9), spleen (n = 6), bone marrow (n = 8) and liver (n = 6) samples were plotted (black, control vehicle; blue, DAS; green, DEX; red, DEX in combination with DAS). Statistical analysis were performed by linear mix model using RStudio.

All statistical analysis above were carried out with RStudio (Team, 2017) using a linear mixed effects model (Bates, 2014) with a varying intercept of PDX, and a fixed effect of drug treatments. P-values were obtained by likelihood ratio tests of the full model with the effect of PDX IDs against the model without the PDX IDs.

Although, in general, all mice included in this trial responded very similar according to their treatment arms, there were some outliers. The mice derived from PDX LK080 and L907 and treated with combination treatment had high leukaemia engraftment (the top two red dots of Figure 57 and Figure 58) in some organs similar to those of their control treated mice. There are several explanations for these observations: 1) LK080 derived mice were harvested three weeks after finishing drug treatments. Without being treated the leukaemia progressed very rapidly in these three weeks as shown by peripheral blood monitoring resulting in enlarged spleens (Ctrl 0.76 g, DEX 0.75 g, Combination 0.57 g) which were heavily infiltrated with leukaemia cells (Figure 54), 2) During the three week treatment window, PDX L907 had the least response to combination treatment compared with other T-ALLs. For example, after the complete dosing schedule the engraftment of the combination treated mouse versus the control treated mouse of L963 was 1.4% versus 79.7%, of LK287 was 28.7% versus 82.2%, of LK080 was 7.0% versus 30.2%, of L970 was 2.0% versus 75.8%, of L809 was 0.92% versus 80.9%, but for L907 it was 58.5% versus 73.4%. Although there was a difference in spleen weights of the combination treated mouse (0.15 g) versus the control mouse (0.38 g), no substantial difference in spleen engraftment was observed (Figure 54, Figure 57 and Figure 58). In addition, the DAS treated mouse of L907 had the quickest engraftment in the peripheral blood and most prominent spleen size among the four mice. This was possibly due to either higher engraftment at the beginning of dosing or L907 responding less to DAS compared with other PDXs.

5.4.5 Drug Efficacy in Mouse CNS

The CNS infiltration is common in T-ALL which makes the eradication of leukaemia from CNS is crucial for cure. To investigate how DEX+DAS affects the CNS leukaemia burden, whole brain-skull preparations from mice in the murine phase Ⅱ-like trial were made. The evaluation for CNS leukaemia engraftment was performed in collaboration of Dr Christina Halsey in University of Glasgow. Notably, PDX samples displayed considerable heterogeneity in overall CNS infiltration as indicated by the infiltration of control animals. In 7 out of 9 PDXs, DEX alone produced a reduction in CNS leukaemia infiltration while DAS alone affected 4 out of 8 PDXs. Notably, the DEX+DAS therapy was particularly effective, with complete removal of measurable CNS leukaemia engraftment in 5 PDXs and less engraftment in 3 out of 4 remaining PDXs. Statistical analysis of the cohort of 9 PDX samples, a significant reduction of leukaemia infiltration in CNS was shown only in DEX+DAS group (Figure 59). This demonstrates that on the one hand the high efficacy of DEX+DAS might overcome CNS engraftment of T-ALL, on the other hand, the maximum effect of DEX+DAS group might be simply due to the least leukaemia engraftment overall in NSG mice as demonstrated in spleen, bone marrow and liver samples previously.

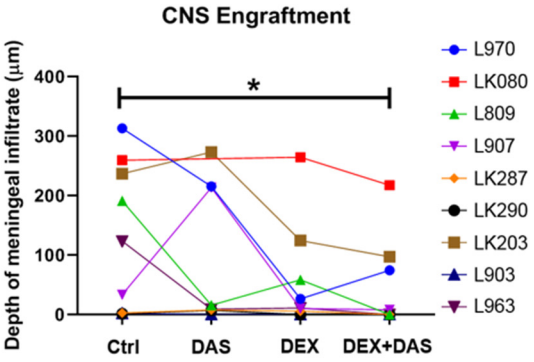

	Ctrl	DAS	DEX	DEX + DAS
L970	313.2	215.4	26.6	74.4
LK080	259.4	n/a	264.6	217.6
L809	191.2	15.8	58.4	0
L907	33.6	213.6	10.2	8
LK287	2.8	7.8	5.8	0
LK290	1.6	7.2	0	0
LK203	236.8	273	124.6	97
L903	2	0	0	0
L963	123.6	9	11.2	0

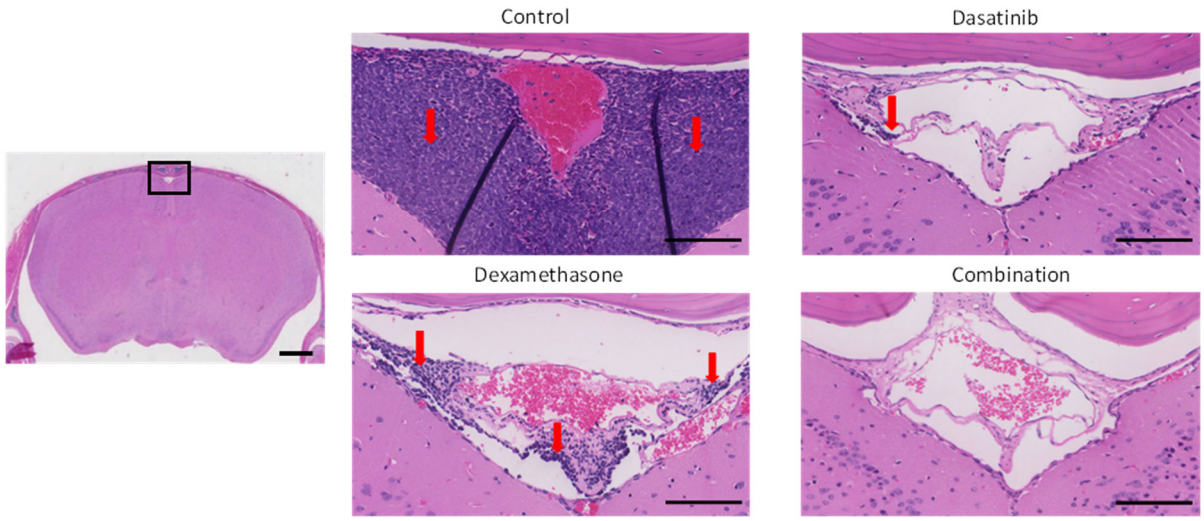

Figure 59. CNS engraftment in the murine phase II-like trial. Top, the average depth of CNS engraftment across 5 coronal sections per mouse analysed by paired t-test, significance level * $p < 0.05$. Means of the 5 individual measurements of the depth of each mouse are shown in the table. Bottom, Photomicrographs of whole brain-skull sections stained with hematoxylin and eosin from PDX L809, left panel – low power scout view of whole brain with an area shown in all other images is marked by a black box; centre and right panels – high power view (x 20 objective) of meninges around the central venous sinus, red arrows mark the leukemic infiltration. Scale bar marks 1 mm on scout view and 100 µm on high power images. These analysis have been performed in collaboration with Dr Christina Halsey in University of Glasgow.

5.4.6 DAS Inhibits LCK Activity *in vivo*

To investigate whether DAS could inhibit LCK *in vivo*, PDX L809 cells isolated from mouse spleens after three weeks of drug treatment in the phase II-like murine trial were harvested and examined by Western Blot analysis. DAS and DAS+DEX combination completely abolished LCK phosphorylation at Y394 and Y505. Also, total LCK was decreased substantially after three weeks of treatment compared to the control cells, treated with the vehicle alone (Figure 60). This data demonstrates that DAS, in presence or absence of DEX, affects both overall LCK levels and LCK activation phosphorylation resulting in an efficient inhibition of LCK *in vivo*.

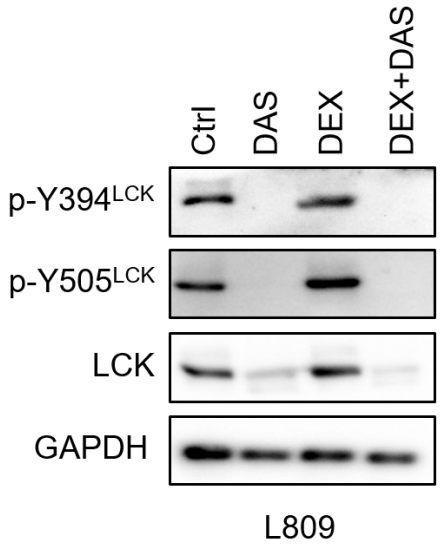

Figure 60. DAS diminishes LCK levels in L809 *in vivo*. L809 human leukaemia cells derived from the spleen of mice treated in the phase II-like murine trial were examined by western blotting of whole cell lysates for p-Y394^{LCK}, p-Y505^{LCK}, total LCK and GAPDH.

As shown previously *in vitro* short exposure to DAS for 24 hours led to p-Y394^{LCK} and p-Y505^{LCK} reduction, but no apparent change in total LCK in L809 (Figure 40). However, long term treatment of DAS or DAS+DEX combination for three weeks *in vivo*, also total LCK protein expression was substantially reduced (Figure 60). These results suggest that in the short exposure to DAS, its occupancy of the nucleotide-binding site of LCK abrogates the kinase activity without affecting total protein levels. How prolonged inhibition of LCK decreases total LCK expression is not understood so far.

5.5 Potential Mechanisms Underlying DAS and DEX Synergy

5.5.1 LCK Inhibition Enhances GILZ Expression after DEX Exposure

One gene target of GR signalling – Glucocorticoid-induced leucine zipper (*GILZ*, also known as *TSC22D3*) was used to evaluate drug synergy mechanisms of DAS and DEX. After knockdown of LCK, 100 nM DEX was applied to Jurkat cells (DEX-resistant). RNA samples were collected after 24-hour treatment, and *GILZ* expression was interrogated by qRT-PCR. In this experiment, the LCK knockdown level achieved was 72%. Whereas DEX treatment induced 27 fold induction of *GILZ* in control cells with normal LCK levels, knockdown of LCK induced an 80 fold increase of *GILZ* mRNA expression (Figure 61). This result suggests that LCK knockdown cells might be at least 3 fold more sensitive to DEX compared with control cells, indicating that LCK levels and/or activity supports DEX resistance at least in Jurkat cells.

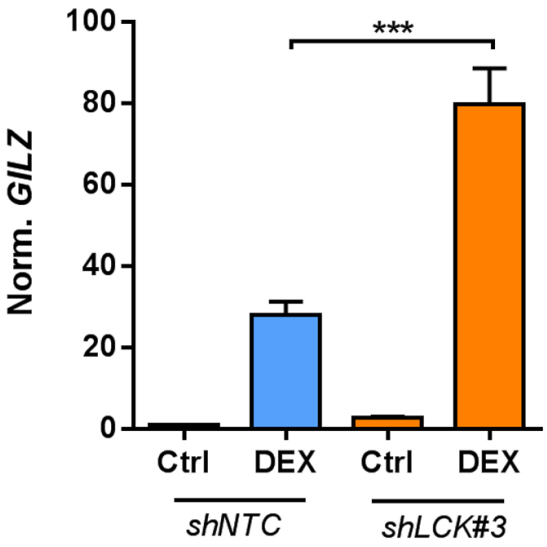

Figure 61. LCK depletion re-sensitises Jurkat cells to DEX. Jurkat cells were transduced with shNTC or shLCK#3 expression constructs. Stable knockdown cells were treated with DEX (100 nM) for 24 hours and analysed by qRT-PCR for GILZ expression levels, relative to GAPDH and normalised to shNTC control vehicle condition. Control cells (blue), LCK knockdown cells (orange). *** $p < 0.005$

LCK depletion-mediated re-sensitisation of cells to DEX was further assessed by using DAS. To evaluate this effect to a broader extent, six T-ALL cell lines that showed a strong synergistic effect of DEX+DAS in drug matrix analysis and five T-ALL PDXs were used in this experiment.

T-ALL cell lines were treated with 2 µM DAS and/or 100 nM DEX for 24 hours. RNA samples were collected, and *GILZ* expression was measured by qRT-PCR. Similar to LCK knockdown results, DAS alone could only induce 2 - 4 fold *GILZ* induction. DEX treatment led to 7 - 74 fold (CCRF-CEM 28 fold; CUTLL1 13 fold; Jurkat 7 fold; SUPT1 44 fold; MOLT16 23 fold; MOLT4 74 fold) induction of *GILZ* expression compared with the control sample. Strikingly, all T-ALL cell lines showed a substantial increase of *GILZ* expression after DEX and DAS combination treatment (CCRF-CEM 84 fold; CUTLL1 154 fold; Jurkat 216 fold; SUPT1 221 fold; MOLT16 293 fold; MOLT4 364 fold) (Figure 62). Taken together, in T-ALL cell lines, DAS and DEX synergistically induce substantial *GILZ* expression which might also apply to other DEX-targeted genes. Further investigations addressing DAS enhancing DEX-targeted genes will be performed in the future.

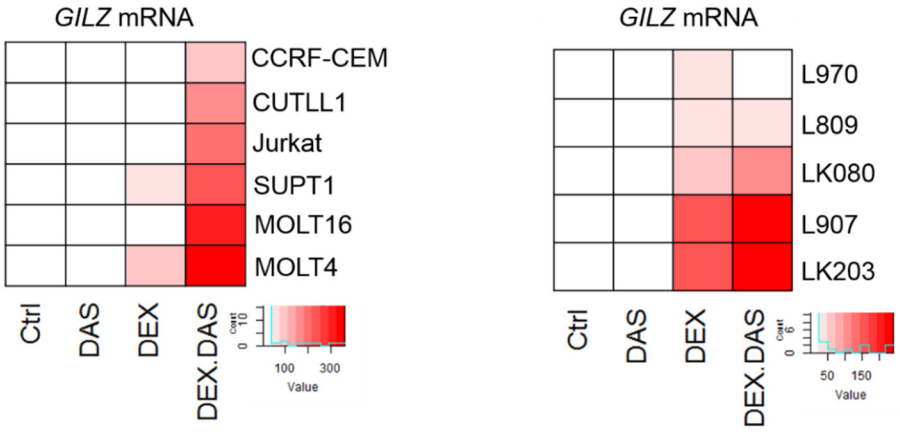

Figure 62. Heatmap demonstrating GILZ induction after DEX and/or DAS treatment in T-ALL cell lines and PDX cells. Six T-ALL cell lines (CCRF-CEM, CUTLL1, Jurkat, SUPT1, MOLT16 and MOLT4) were treated with 100 nM DEX and/or 2 µM DAS for 24 hours. GILZ expression (normalised to GAPDH expression) was determined by qRT-PCR (scale varying between 0 - 400 fold changes). Five T-ALL PDXs (L970, L809, LK080, L907 and LK203) were treated with 100 nM DEX and/or 1 µM DAS for 24 hours. GILZ expression (normalised to GAPDH expression) was determined by qRT-PCR with the scale of 0 - 200 fold.

T-ALL PDXs (L970, L809, LK080, L907 and LK203) after *in vitro* expansion were treated with 1 µM DAS and/or 100 nM DEX. After 24 hour treatment, RNA samples were collected. *GILZ* expression levels were examined by qRT-PCR. Consistently with T-ALL cell lines, DAS alone induced a 2 fold increase of *GILZ* expression, indicating that LCK inhibition itself did not alter *GILZ* expression substantially.

Regarding DEX+DAS effect, PDX samples showed varied effects of DAS and DEX combination. PDX LK080, L907 and LK203 showed a similar response to T-ALL cell lines. DEX treatment alone induced *GILZ* expression by 49, 167 and 162 fold, whilst DEX in combination with DAS induced *GILZ* by 105, 217 and 240 fold, respectively (Figure 62), however, PDX L809 treated with DEX+DAS showed a smaller increase in *GILZ* expression of 39 fold, which was similar to DEX only treatment (31 fold).

L970 was the only PDX that showed less *GILZ* induction after combination of DEX with DAS (Figure 62). Further investigation showed that DEX treatment induced a 70% reduction of *LCK* on mRNA expression levels. DEX+DAS sample had more than 90% reduction of *LCK* and even less *GILZ* induction compared with the DEX-treated sample (Figure 63). The decrease of LCK by DEX was only observed in L970 but no other T-ALL cells (Discussion chapter 6.2.5). These data indicate that LCK inhibition re-sensitises cells to DEX as shown by a substantial increase of DEX-targeted gene *GILZ*.

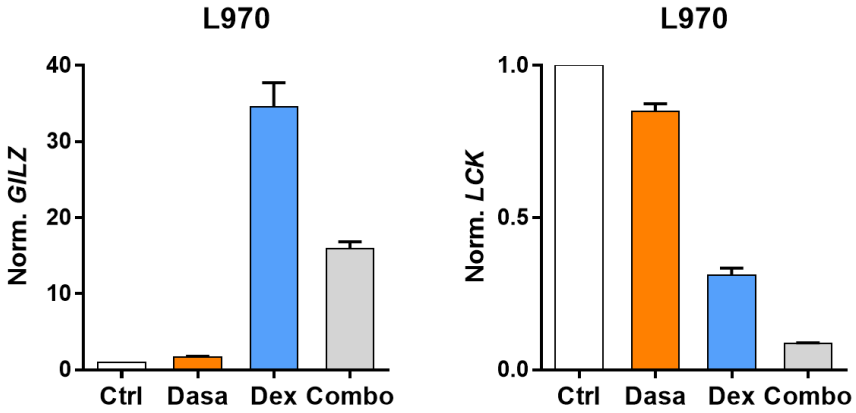

Figure 63. Transcriptional expression levels of GILZ and LCK in PDX L970 after drug treatment. L970 cells were treated with control vehicle (ctrl), DAS (1 µM), DEX (100 nM) and combination drugs for 24 hours. GILZ (left) and LCK (right) mRNA expression was determined by qRT-PCR relative to the housekeeper gene GAPDH.

5.5.2 The ERK Pathway Might Play a Role in DAS/DEX Synergy

To have more understanding of the mechanism underlying the observed drug synergy between DAS and DEX, the downstream signalling pathways of LCK were interrogated. Our previous RPPA analysis identified the ERK and AKT pathways as the predominant signalling pathways activated downstream of LCK in the T-ALL cell line CUTLL1. AKT has been shown to trap GR in the cytoplasm by regulating GR phosphorylation at Ser132 resulting in glucocorticoid resistance in T-ALL (Piovan et al., 2013). RAS mutations led to less sensitivity to prednisone in a cohort of 109 infant ALLs (Driessen et al., 2013). Also, steroid-resistant relapse might be conferred from a subpopulation of diagnostic samples with KRAS mutations (Irving et al., 2014).

The AKT inhibitor MK2206 and ERK1/2 inhibitor SCH772984 were used to examine if these pathways were involved in re-sensitising cells to DEX. In the presence of an inhibitor to LCK, AKT or ERK, there was minimal induction of *GILZ* mRNA expression in T-ALL cells. DEX-induced expression of *GILZ* was further increased when combined with DAS, MK2206, SCH772984, or both MK2206 and SCH772984 inhibitors. Notably, the combined effect of DEX with both the AKT and ERK inhibitors (DEX+AKTi+ERKi) induced more GILZ expression than using DEX+AKTi or DEX+ERKi, but this effect was still less pronounced when compared with the combination of DEX+DAS (Figure 64). LCK represents a proximal signalling node in the TCR signalling pathway. This observation might suggest that there might be signalling pathways downstream of LCK, other than AKT and ERK, also play a role in DEX+DAS synergy.

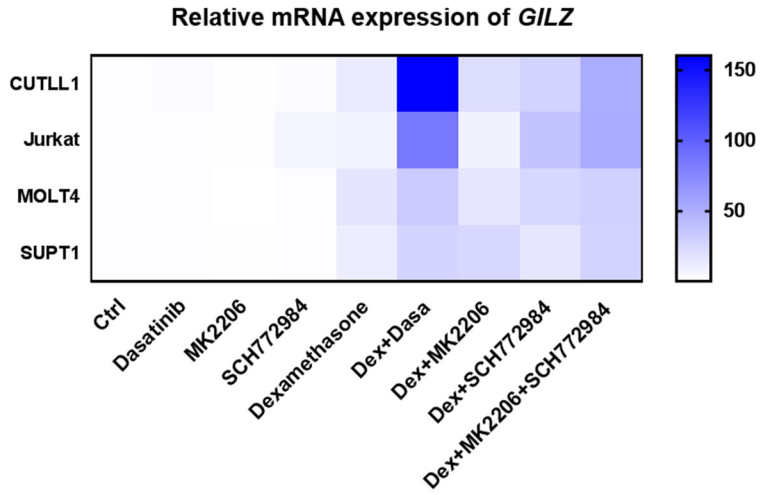

Figure 64. Heatmap of GILZ mRNA induction in T-ALL cell lines after the treatment with different drugs and drug combinations. The relative mRNA expression of GILZ was obtained by qRT-qPCR. T-ALL cell line CUTLL1, Jurkat, MOLT4 and SUPT1 were treated with the IC_{75} concentration of DAS, MK2206, SCH772984 (CUTLL1, 2.8 μM, 0.4 μM, 12.6 μM; Jurkat, 1.1 μM, 0.6 μM, 11 μM; MOLT4, 2.6 μM, 0.2 μM, 7.3 μM; SUPT1 0.3 μM, 3.6 μM, 18.7 μM), with or without DEX (100 nM) (combinations of DEX + DAS, DEX + MK2206, DEX + SCH772984, or DEX + MK2206 + SCH772984). The expression of GILZ was normalised to GAPDH and the non-treated control sample (Ctrl). The blue gradient bar graph on the right reflects the relative fold change of GILZ mRNA expression.

Chapter 6

Discussion

The event-free survival rate of paediatric T-ALL has exceeded 85%, but comes at a cost due to the use of high-dose, multi-agent chemotherapy, which is often accompanied by acute and chronic side effects. Also, there is virtually no cure for relapsed or refractory T-ALL (Bhojwani and Pui, 2013). These patients thus represent an unmet medical need. DEX is a core component of the intensive chemotherapy resulting in apoptosis. However, DEX-resistance has been associated with an increased risk of relapse and poor clinical outcome (Inaba and Pui, 2010). It is thus imperative to discover novel drug targets for T-ALL treatment and new strategies to overcome steroid resistance. T-ALL cells arise from the transformation of thymocyte progenitors to T-cell malignancies (Durinck et al., 2015). Development checkpoints are provided by the pTCR during β-selection and TCR in positive/negative selection (Li and Rudensky, 2016). To investigate the roles of pTCR/TCR complex components in T-ALL, a functional shRNA screen targeting pTCR/TCR signalling was performed in T-ALL cell lines and PDXs. We hypothesised that pathway components could provide new drug targets.

6.1 Targeted shRNA Screens Discovered a Role for LCK in Controlling T-ALL Growth

Our functional genomics approach identified LCK, an essential kinase in the pTCR/TCR signalling pathway, as a critical gene involved in T-ALL proliferation and maintenance. LCK is a central molecule in pTCR/TCR signalling transduction and has been shown to enhance tumourigenic BCR signalling in other lymphoid malignancies, namely CLL (Harr et al., 2010).

The screen library contained shRNAs targeting pTCR/TCR components (*PTCRA, LCK, FYN, ZAP70, LAT* and *CD3E*), ribosomal proteins (*RPL9* and *RPS29*), *PTEN*, and negative controls (NTC, *RUNX1/ETO*). The *in vitro* shRNA screens were carried out in four T-ALL cell lines (SUPT1, CUTLL1, MOLT4 and HPB-ALL). In general, the screening was successful because the performance of control shRNAs was consistent with our expectation; the negative controls were not depleted or enriched, knockdown of essential ribosomal proteins led to depletion, and cells with PTEN shRNAs were enriched as predicted. The screen identified crucial roles for LCK, ZAP70 or PTCRA for T-ALL proliferation (Figure 23). Notably, shRNAs targeting LCK were universally

depleted in all four cell lines with the highest significance, suggesting its essentiality for T-ALL maintenance.

6.1.1 *In vitro* Validation Demonstrated the Essentiality of LCK, but Not FYN

In vitro validation of the roles of pTCRα, LCK, and ZAP70 in T-ALL cell lines by competitive assays demonstrated the essentiality of the pTCR/TCR signalling complex in cell proliferation. LCK and ZAP70 showed the capacity to steer cell proliferation in 5 out of 6 cell lines that were tested (except for HPB-ALL) (Figure 31). Cell lines that only express pTCR (SUPT1 and MOLT4) are dependent on pTCRα. However, it is dispensable for $pTCR^{+}/TCR^{+}$ cell line CUTLL1 due to the possible redundant role of TCR to replace pTCR function. Remarkably, the impact of LCK on leukaemia propagation is further confirmed *in vivo* as demonstrated by the observation that shNTC cells outcompeted shLCK cells in MOLT4 transplanted mice. This effect was consistently observed in spleen, bone marrow and liver (Figure 34).

Interestingly, the other T-cell specific SFK (FYN) appeared to be non-essential for T-ALL cell proliferation or survival. No significant depletion or enrichment was observed in the targeted shRNA screens in SUPT1, MOLT4 and CUTLL1. *In vitro* depletion of LCK induced significant G_0/G_1 cell cycle arrest rather than apoptosis; however, knockdown (50% KD) of FYN by three shRNAs all failed to affect cell growth in MOLT4 and CUTLL1 for up to 40 days (Figure 29). Previous studies have shown that both Fyn and Lck are crucial for cell survival, but only Lck regulates cell proliferation in peripheral T cells (Seddon et al., 2000; Seddon and Zamoyska, 2002a). In these studies, it seemed that both LCK and FYN were dispensable for T-ALL cell survival. The regulation of cell survival by LCK and FYN in healthy T cells might be disturbed by the genetic lesions in T-ALL. Leukaemia cells are broadly considered immature T cells, which are usually more dependent on Lck rather than Fyn (Molina et al., 1998; Stein et al., 1992). Our data support the notion that LCK, rather than FYN, is imperative for T-ALL proliferation.

HPB-ALL is an unusal cell line in this project, as it behaved differently than all other cell lines tested. Both shLCK#1, #2, #3 and shFYN#1, #2 were significantly depleted in the targeted shRNA screen indicating its proliferation or survival is dependent on both LCK and FYN. However, we were not able to validate these initial findings in

follow up examinations. In the competitive assays, where we used shRNA constructs with GFP expression, several control shRNAs including shNTC and shRUNX1/ETO, were gradually lost at a similar speed as shLCK, shFYN, shPTCRA and shZAP70. It seems that HPB-ALL cannot retain GFP expression in general, which means that probably the un-transduced cells outcompeted GFP-transduced cells due to GFP toxicity. A similar phenomenon was observed in the repetition experiment. Other fluorescent proteins, such as RFP657 or dTomato, have not been tested. Perhaps using shRNA constructs with other fluorescent tags would work to evaluate the screen data. But no further investigations were carried out in HPB-ALL cells in this study.

6.1.2 Limited Screen in PDX L963 and LK080 *in vivo*

Followed by the success of targeted shRNA screens *in vitro*, a similar approach was expanded to PDX cells to address the importance of LCK *in vivo*. L963 and LK080 were chosen to perform this study.

In PDX L963, shLCK#3 was significantly depleted in spleen and bone marrow samples (Figure 28). Unlike T-ALL cell line data where shLCK#1 was also significantly depleted, shLCK#1 failed to reach the significance in L963 since it was lost in mouse 2, 4 and 5, but not the other three mice. Thus, shLCK#1 effect was discordant among different mice. Also, knockdown experiments performed *in vitro* in MOLT4 and CUTLL1 demonstrated shLCK#1 caused less reduction in *LCK* expression compared with shLCK#3, which makes it a less robust candidate for the depletion *in vivo*.

The relapsed sample LK080 showed clonal expansion in the *in vivo* shRNA screen with loss of library coverage. This made it difficult to interpret the functional role of individual shRNAs in this primary sample. However, LK080 was tested *in vitro* with the LCK inhibitor DAS. DAS abolished the activation of LCK and resulted in G_0/G_1 arrest in LK080, indicating its dependency on LCK (Figure 42). Also, a strong drug synergy was observed in LK080 drug matrix analyses *in vitro*, and it responded well to the DEX/DAS combination in the murine trial within the treatment window (Figure 54). LK080 is a GC-resistant sample both *in vitro* and *in vivo*, which could be used in the future to investigate how LCK inhibition improves DEX response. At the end-point analysis, there was little difference in leukaemia engraftment of the LK080 control mouse and the DEX+DAS mouse, since they were kept alive for an additional three

weeks after completing treatment. It is possible that continued dosing would have resulted in a significant impairment in leukaemia progression. Alternatively, this observation raised the assumption that DEX+DAS cannot eradicate leukaemia, at least in this primary sample. Further investigations into the mechanisms of DEX+DAS resistance might result in the development of a triple drug combination and enforce the application of targeted therapies.

6.2 LCK Regulation in T-ALL

6.2.1 Possible Mechanisms of LCK Activation in T-ALL

LCK in T-ALL exhibits non-oncogene addiction regulating cell proliferation *in vitro* and propagation *in vivo*. The cell growth of the HSB-2 cell line is dependent on LCK as it has a t(1; 7)(p34; q34) translocation, which places *LCK* under the control of the *TCRB* promoter (Wright et al., 1994). However, in T-ALL patients, it is infrequent to have mutations or translocations of the *LCK* locus. This raises the question of how LCK is (ab)normally activated or upregulated in T-ALL cells. Four scenarios might provide an explanation:

1. The most likely situation is that there is no abnormal activation or upregulation of LCK in T-ALL. Because LCK, and its activation, play a critical role in T-cell maintenance/tonic signalling (Li and Rudensky, 2016), it is present in levels that can be targeted/inhibited in T-ALL. To address this, comparisons of the expression and activation of LCK in healthy individuals and T-ALL patients are needed.

2. LCK might be activated because of genetic alterations upstream of pTCR/TCR, such as activation of the Notch pathway, which directly binds and upregulates *PTCRA* expression (Bene et al., 1995). Moreover, in T-ALL cell line Jurkat, LCK has been shown to interact with ICN and PI3K, which is necessary for ICN induced expression of anti-apoptotic proteins, such as BCL2, BCL-xL, and IAP-2. Enforced expression of ICN upregulates p-LCK in this cell line (Sade et al., 2004). Moreover, mouse studies on TCR reprogramming and engineering have demonstrated the oncogenic role of TCR signalling in T-cell malignancies. Firstly, in a mouse model in which mice were derived from a reprogrammed T-cell, half of the mice developed T-cell lymphomas. These lymphomas were dependent on TCR signalling as inhibition of TCR signalling, or lack of rearranged TCRα/β chains, would suppress lymphoma growth (Serwold et

al., 2010). In another mouse study which assessed engineered Sur-TCR-Tg (survivin-TCR-transgenic) in thymocytes, murine T-ALL occurred of 100% in cases in this model, which was dependent on TCR signalling resulting from the interaction of Sur-TCR-Tg and antigens (peptide 20-28 of survivin) (Cui et al., 2015).

3. Another possibility might be that LCK activation is aberrantly triggered either by the phosphorylation of Y394 or the dephosphorylation of Y505. Notably, alterations in the phosphatase CD45, which controls pY505^{LCK}, have been found in association with leukaemia. Particularly, mutations in the gene *PTPRC*, which encodes for CD45, has been found in T-ALL cell lines and patient samples concurrent with gene lesions in the IL-7R signalling pathway (Porcu et al., 2012). For example, the G863R mutant of *PTPRC* was found in combination with the *TCRB-LCK* translocation in HSB-2 cells. The R751* mutation was associated with JAK1 Y652H gain of function in a T-ALL patient, while the W764* mutation co-occurred with an insertion in IL-7R in the DND-41 cell line (Porcu et al., 2012). Also, it has been demonstrated that low or undetectable CD45 expression occurs in 3.7% of patients with childhood T-ALL (Ratei et al., 1998). In our cohort of ten PDXs, L970 and LK290 showed low CD45 expression on the cell surface. Future work will be carried out to investigate whether CD45 is downregulated by PTPRC mutations (or other mechanisms) and drives LCK activation in T-ALL cells.

4. Perhaps LCK expression is regulated by oncogenic super-enhancers recruiting core components of a major leukaemogenic transcriptional complex that contains for example TAL1, MYB, RUNX1 and GATA3 (Ferrando et al., 2002). In order to identify these super-enhancers, CRISPRa (Clustered Regularly Interspaced Short Palindromic Repeats activation) screens provide a robust tool to interrogate the enhancers that upregulate LCK in T-ALL. It has previously been used to identify IL-2R regulatory enhancers in T cells previously (Simeonov et al., 2017).

6.2.2 Dasatinib Inhibits LCK in T-ALL Cells

6.2.2.1 LCK as the Primary Target of DAS in T-ALL Cells

The dual ABL/SFKs inhibitor DAS has been approved for the treatment of CML and Ph$^+$ ALL (Squibb, 2009). In T-ALL, DAS eradicates LCK kinase activity as shown by the abolishment of pY394^{LCK}, Y493^{ZAP70} and Y783$^{PLC\gamma1}$ (Figure 40). The sensitivity to

DAS significantly correlates with $pY394^{LCK}$/LCK in T-ALL cell lines (IC_{50} from 23.8 nM to 19.7 μM) (Figure 44), which at least in part demonstrates the main target of DAS in T-ALL cells is LCK. This is in line with a previous study which showed that among 20 possible targets of DAS including ABL1, KIT, MAPAK5, EPHB2, EPHB4, SRC, YES, FGR, HCK, PDGFRα and PDGFRβ, LCK is the most abundantly expressed gene in T-ALL cell lines (Laukkanen et al., 2017). To further address the question around the main drug target of DAS, a more specific LCK inhibitor (Lowenberg et al., 2005) other than DAS could be used to confirm the role of LCK in T-ALL cell lines. The response of T-ALL to the SRC inhibitor KX2-391 correlates with DAS response, suggesting DAS acts via inhibiting the SRC pathway (Frismantas et al., 2017). A mutation of threonine (T) to methionine (M) at the gatekeeper residue T316 of LCK conferred resistance to DAS in T-cells (Lee et al., 2010). Overexpression of LCK^{T316M} in a *LCK* null background or the use of CRISPR/Cas9 to knock-in T316M into the human T-ALL genome, would allow us to address this notion elaborately and confirm that LCK is the likely primary target of DAS in T-ALL cells.

One of the limitations of this study was that there was no correlation between $pY394^{LCK}$/LCK and DAS response in primary samples (Figure 45). The high sensitivity to DAS (IC_{50} < 100 nM) in 30% of T-ALL patient samples (with the absence of ABL class mutations) was shown in an *in vitro* drug response profiling platform (Frismantas et al., 2017). In our study, 2 out of 6 PDXs (LK287 and L903) were highly sensitive to DAS with GI_{50} less than 100 nM, while the others showed GI_{50} > 1 μM. LK287 had a FIP1L1-PDGFRA fusion, which explained the high sensitivity to DAS. However, no known recurrent genetic abnormality could be identified in L903 to link with its high sensitivity to DAS. Only six PDXs were evaluated for $pY394^{LCK}$/LCK and DAS response in this study, which hinders the discovery of any correlations between them. Also, primary cells generally had problems with cell proliferation *in vitro*. Although we tried to co-culture PDXs with feeder cells for at least a week to support their proliferation before applying any drugs, the drug assays were performed without feeder cells, which would affect the evaluation of DAS response. In the future, developing a platform in which drug assays could be performed on PDXs co-cultured with feeder cells (Frismantas et al., 2017) would help to evaluate DAS response accurately.

6.2.2.2 DAS Reduces LCK Protein Expression in Some T-ALL Samples

DAS reduced LCK total protein levels in some cell lines and PDXs. For example, total LCK decreased after 24 h-treatment of DAS in SUPT1, MOLT4, CUTLL1, L907 and L963. But no substantial difference in LCK protein was shown in Jurkat, LK203, L970, L809 and LK080 (Figure 40). This variability is in line with their sensitivity to DAS based on IC_{50} and GI_{50} values observed in our study. Therefore, the reduction in LCK levels might differ according to the DAS dose or treatment duration employed. Another piece of evidence supporting this notion is the complete loss of LCK expression after long-term DAS treatment in L809 engrafted mice, which were exposed to DAS or DEX/DAS *in vivo* for three weeks. Further evaluations of the dosing and treatment duration effects of DAS on LCK are needed.

Interestingly, the transcriptional level of *LCK* in various T-ALLs remained unchanged after 24 h-DAS treatment. It is thus more likely that the half-life of LCK protein is affected by DAS. The RING finger E3 ubiquitin ligase CBL negatively regulated LCK function by ubiquitination and degradation through proteasome. Also, without phosphorylation at Y505, LCK was more susceptible to CBL-dependent ubiquitination and degradation (Rao et al., 2002). DAS inhibits the phosphorylation at Y394 and Y505 which might have an impact on ubiquitination of LCK. This question needs to be addressed in the future.

6.2.2.3 Comparison of LCK Knockdown and DAS Treatment

In general, DAS treatment and LCK KD produced similar effects, namely the induction of G_0/G_1 arrest in a panel of T-ALL cells and mild apoptosis induction in MOLT4 after shLCK and Jurkat after DAS treatment. The direct comparison of the degrees of cell cycle arrest or apoptosis generated by DAS inhibition and LCK knockdown is not straightforward. Because the maximal knockdown level of shLCK is around 70% in T-ALL cells which limited the LCK knockdown effects, however, presumably higher concentrations of DAS would induce more substantial effects. In line with this thought, the cell cycle arrest induced by DAS appeared slightly more pronounced than LCK knockdown. Alternatively, if DAS leads to increased G_0/G_1 arrest, this could be explained by the non-specific target inhibition of DAS. A more valid comparison would be provided by using a gene knockout, rather than knockdown, approach.

6.2.3 The Comparison of LCK Deficiency Induced Cell Cycle Arrest in Normal and Malignant T cells

One study reported that a murine LCK deficient T helper 2 (Th2) cell line increased expression of cyclin A, cyclin B, cdc2, accompanied by G_2/M cell cycle arrest compared with its parental cells. The upregulated cdc2 was highly phosphorylated, resulting in defects in cdc2 kinase activity (al-Ramadi et al., 1998). In contrast, in our study, knockdown or inhibition of LCK led to G_0/G_1, not G_2/M cell cycle arrest in human malignant T cells. RPPA data of the CUTLL1 cell line demonstrated that both CDK1 (also known as CDC2) and $pY15^{CDK1}$ were downregulated after LCK knockdown. Furthermore, RNA-seq data derived after 24 h DAS treatment in LK203 and LK080 showed a 30% reduction of *CDK1* expression. These data suggest that the cell cycle progression controlled by LCK differs between murine and human cells, or between normal and malignant T cells.

6.2.4 LCK Might Regulate Cell Survival or Proliferation in Different Subgroups of T-ALL

Knockdown of LCK leads to significant G_0/G_1 cell cycle arrest in MOLT4, SUPT1, Jurkat and CUTLL1. However, a mild apoptotic response was only observed in MOLT4 cells. This might illustrate that regulatory networks governed by LCK vary between T-ALL cell lines.

Based on my observation, DAS response profiling revealed three sub-groups of T-ALL cell lines. One group (DAS-hypersensitive) contained the hypersensitive cell lines with the IC_{50} in nM range, including HSB-2, KOPT-K1 and ALL-SIL; a second group (DAS-sensitive) was represented by the sensitive cell lines (IC_{50} < 10 µM) such as CUTLL1, MOLT4, and Jurkat, with a third one (DAS-resistant) consisting of the resistant cell lines (IC_{50} > 10 µM, e.g. CCRF-CEM and MOLT16).

I observed that single electroporation with LCK siRNA instantly induced apoptosis and G_0/G_1 arrest in HSB-2 (DAS-hypersensitive) cells, but no apoptosis nor cell cycle arrest was observed in MOLT4 (DAS-sensitive) and CCRF-CEM (DAS-resistant) cells. In my opinion, the transient knockdown of LCK is not sufficient to induce cell cycle arrest in DAS-sensitive and DAS-resistant cell lines. In line with this observation, transient knockdown of LCK in a NUP214-$ABL1^+$ T-ALL cell line ALL-SIL (DAS-

hypersensitive) led to substantial apoptosis and reduced proliferation while this was not seen in Jurkat (DAS-sensitive) and SUPT1 (DAS-sensitive) after single electroporation of siLCK (De Keersmaecker et al., 2014). Both HSB-2 and ALL-SIL are hypersensitive to dasatinib because of the presence of activated kinases and responded to the transient LCK knockdown by siRNA. However, the role of LCK in T-ALL cell cycle progression might be underestimated by the transient knockdown method itself. Based on our data, the essentiality of LCK for modulating cell proliferation and cell cycle progression was well characterised in DEX-sensitive cell lines, such as SUPT1, MOLT4, Jurkat and CUTLL1. This was achieved using a shRNA and lentiviral transduction approach, which generated stable cell lines with LCK knockdown for the long term. In this way, we discovered that LCK indeed modulates T-ALL cell cycle progression not only in DAS-hypersensitive group but also in DAS-sensitive group (Figure 37).

We have also shown that LCK is vital for cell cycle progression *in vitro* in co-cultured PDX L963 and LK203 cells. Knockdown of LCK by shRNA in L963 and LK203 induced G_0/G_1 cell cycle arrest. Moreover, cell proliferation assays of L963 with control or LCK shRNA after a two-week co-culture with feeder cells demonstrated that shLCK delayed cell division compared with shNTC cells (Figure 38). Notably, the GI_{50} of DAS in L963 and LK203 was 4 μM and 1 μM respectively, which was similar to the IC_{50} of DAS-sensitive cell lines. Consistent with the cell line data, single electroporation of siLCK did not induce G_0/G_1 arrest in L963 and LK203. However, cell cycle arrest appeared after the 2nd electroporation of siLCK and was further enhanced after the 3rd electroporation (Figure 39).

Collectively, these findings support the notion that LCK regulates different signalling networks in DAS-hypersensitive and DAS-sensitive cell lines by controlling cell proliferation and survival in DAS-hypersensitive group, while only regulating cell proliferation in DAS-sensitive T-ALL cell lines. The divergence needs to be further investigated.

6.2.5 DEX Downregulates LCK mRNA Expression in DEX-sensitive Cells

In practice, treatment of leukaemia needs a combination of drugs. In this study, DAS and DEX synergistically induce more significant cell death in T-ALLs (Figure 51). It is

reported that DEX downregulates LCK mRNA expression in DEX-sensitive cells such as thymocytes (S49.A2) and the murine T-lymphoma cells (WEHI7.2) (Harr et al., 2010). The mechanism underlying this response is currently unknown. Consistent with the literature, I found that PDX L970 was sensitive to DEX, and the mRNA expression of LCK was 60% downregulated upon DEX treatment (100 nM) (Figure 63). On the contrary, LCK downregulation was not observed in DEX-resistant T-ALL PDXs and cell lines.

However, this does not seem to affect DEX+DAS response. PDX L970 was included in the phase II-like murine trail. DEX treatment effectively reduced about 50% leukaemia engraftment in spleen and bone marrow. Although DAS treatment alone did not lead to substantial engraftment reduction, the DEX+DAS mouse had the most significant reduction in leukaemia blasts and this response was thus more effective than treatment with DEX alone.

6.3 A Phase II-like Murine Trial Demonstrates High Efficacy of DAS+DEX *in vivo*

The drug combination of DEX and DAS decreased the proliferation of physiological $CD3^+$ and virus-specific $CD8^+$ T cells without affecting cytokine production and cell viability (Nerreter et al., 2013). However, in malignant T cells, DAS synergises with DEX to induce more significant cell death in both DEX-sensitive and DEX-resistant patient samples (Figure 50). Significant enrichment of drug synergy can be observed at clinical-relevant C_{max} concentrations of DEX and DAS (Figure 49).

To evaluate the drug combination efficacy of DEX+DAS *in vitro*, a phase II-like murine trial was performed with ten primary samples. Each PDX was injected into four mice of the same gender and similar age. All four mice were randomised to the treatment of vehicle, DAS, DEX or DAS+DEX upon human leukaemia engraftment in the peripheral blood above 0.5%. Overall, DAS+DEX significantly reduced leukaemia engraftment in spleen (n=7), bone marrow (n=9), peripheral blood (n=9) and liver (n=6) samples (Figure 57).

The phase II-like clinical trials in mice allow not only fair comparison between treatment arms as the four mice receiving the same PDX, but also reflecting early phase clinical trials in humans as it includes heterogeneous biological samples. However, it was not simple and easy to implement. Firstly, the engraftment pattern of

these PDXs was different, causing the complication of determining when to start and when to stop the treatment. In line with other studies (Girardi et al., 2017; Jing et al., 2015), we decided to monitor peripheral blood engraftment weekly and commence dosing when the $hCD45^+$ cell count reached 1% (apart from L903 whose treatment started when engraftment > 0.5%). Secondly, the heterogeneity of different PDX samples made the final statistical analysis complicated. The general student t-test does not apply in this study, as four treatment arms were not independent. The drug efficiency comparison had to consider additional variables, for example PDX IDs. Therefore, a linear mixed effects model (Bates et al., 2015) was used with a varying intercept of PDX and a fixed effect of drug treatments and the p-values were obtained by likelihood ratio tests.

6.3.1 Exclusion of LK214 in the Final Analysis of the Murine Trial

PDX LK214 (n = 4 female mice) was excluded from the final analysis because of its rapid engraftment before the onset of treatment. Similar to other primary samples, treatment of LK214 was commenced after signs of engraftment in the peripheral blood. However, three out of four mice were unexpectedly found sudden death during the 1st week of treatment. Autopsy of these mice demonstrated heavy leukaemia burden with enlarged spleens (0.5 g), suggesting that these PDXs did not show peripheral blood engraftment although lymphoid organs had already heavily engrafted. A second attempt using LK214 was carried out in four male mice. This time dosing was commenced blindly without weekly tail bleed monitoring. Instead, treatment initiation (the 2nd week after injection of PDX cells) and duration (two-week dosing to avoid unexpected sudden death) were dictated by our previous experience with LK214. This time however, neither enlarged spleen (0.02 g) nor bone marrow or liver engraftment was detected when harvested on the 4th week after injection. Thus, LK214 was excluded from the final analysis of the phase II-like murine trial.

6.3.2 DEX+DAS Significantly Affected CNS Engraftment in the Murine Trial

CNS infiltration is frequently seen in T-ALL patients; therefore, novel therapies should aim for eradication of leukaemia cells from this sanctuary site. In our phase Ⅱ-like murine trial, DEX alone produced a reduction in CNS leukaemia infiltration in 7 PDXs,

while DAS alone affected 4 PDXs. Notably, a significant decrease in leukaemia infiltration in the CNS was shown in the DEX+DAS group of the cohort of 9 PDX samples (Figure 59), indicating that DEX+DAS might overcome CNS engraftment of T-ALL. It is also possible that the DEX+DAS group had the least leukaemia engraftment overall (spleen, bone marrow and liver) resulting in the least CNS engraftment. To address this, further experiments, including the evaluation of CNS infiltration prior to treatment initiation, would be useful. With regards to the mechanism underlying reduction in CNS infiltration, it has previously been shown that reduction in ZAP70, a downstream target of LCK, impairs leukaemic infiltration of the CNS (Alsadeq et al., 2017).

6.3.3 One Case of DEX+DAS Toxicity in the Murine Trial

The synergistic effect of DEX+DAS was evaluated in the phase Ⅱ-like trial in mice with ten PDXs. The DEX+DAS combination significantly reduced leukaemia burden compared with control or single-drug treated mice. The leukaemic engraftment in NSG mice was substantially impaired in the tissue of the spleen, bone marrow, liver and CNS. However, the potential toxicity of this drug combination was observed in one PDX sample L903. The four mice of L903 were harvested three days after completion of dosing (2 weeks) due to signs of illness of the DEX+DAS mouse. It was pale and reluctant to move; therefore, all four mice had to be collected. This PDX overall showed little engraftment in the spleen (about 4% $hCD7^+$ cells with the weights of 0.04 - 0.06 g) suggesting an early stage of leukaemia engraftment. Although the DEX+DAS mouse had the least engraftment in the blood, bone marrow and liver among all four arms of treatment, it showed general weakness, which might be due to the potential toxicity of this drug combination. In the case of human clinical trials, DAS was shown to be well tolerated in paediatric CML patients (McCafferty et al., 2018). However, some minor AEs (adverse events) were identified such as arthralgia, diarrhoea, and fatigue, haemorrhage, rash and vomiting. Interestingly, the DAS-treated mouse did not show any sickness signs. It might be that the combinatorial effect of DEX+DAS leads to toxicity in this particular sample. It is possible that DAS increased the plasma level of DEX and thus caused toxicity. Further investigation such as establishing the pharmacokinetics of DEX and DAS *in vivo* would be helpful to interrogate this issue.

As shown in a previous study, the C_{max} of mice dosed with 1 mg/kg DEX is approximately 100 nM which is similar to the C_{max} achieved in patients' serum (Yang et al., 2008). However, the blood concentrations of DAS and DEX after 35 mg/kg DAS and DEX+DAS administration remain unknown. Investigations will be carried out to identify the C_{max} of DAS and DEX and explore a dose which has the least toxicity but still synergises with DEX.

6.3.4 Identification of the Response Biomarker of DEX+DAS

Last year a paper described that pharmacological inhibition of LCK by DAS could reverse GC-resistance in PPR (prednisone-poor responders) patients with T-ALL (Serafin et al., 2017). When examining LCK phosphorylation status in 87 patient samples by phosphoproteomics, they identified high p-Y416^{SRC} and low p-Y505^{LCK} in PPR patients compared with PGR (prednisone-good responders) patients. However, I could not confirm the correlation between LCK activity and DEX response in our panel of T-ALL cell lines and PDXs in this study. Although my results suggest that LCK plays a role in DEX-resistance, it would be premature to conclude at this stage that DEX-resistance is caused by high LCK activation. The synergy between DAS and DEX is preserved in DEX-sensitive T-ALLs as well. However, it is possible that this inconsistency is due to the small sample size of PDXs in my study. Expanding the PDX sample size and understanding the LCK association with GC-resistance would be a primary focus in future research.

It is imperative to identify the biomarker of DEX+DAS response to stratify patients to receive this treatment in the clinic. One of the aims of conducting a phase Ⅱ-like murine trial was to identify a possible biomarker for DEX+DAS combination responsiveness. At least 7 out of 9 PDXs revealed an excellent response to DEX+DAS treatment in the murine trial, as shown by more than two-fold reduction in leukaemia engraftment in peripheral blood, spleen and bone marrow. Although this is an exciting observation, it makes it difficult to establish a response biomarker.

The therapeutic advantage of DEX+DAS was seen in LK080 during the treatment window as demonstrated by peripheral blood engraftment over time; however, this advantage was lost after the completion of the treatment because the DAS+DEX mouse had the same engraftment rates in spleen and bone marrow compared with its control mouse.

The least response to DEX+DAS was seen in L907 in the spleen, bone marrow and liver (4% - 40% reduction in leukaemia engraftment compared with the control mouse). Interestingly, DAS treatment alone did not provide benefit for this PDX sample, suggesting the little response to DEX+DAS might have been partially due to resistance to DAS. Up to now, this study has inadequate evidence to conclude on the identification of a biomarker for DEX+DAS response. DNA and RNA sequencing are ongoing to reveal the full mutational and transcriptomic landscape of these samples. These will be correlated with *in vitro* and *in vivo* treatment response in a further attempt to establish a response biomarker. In the future, this murine trial will be expanded to include relapsed T-ALL PDXs. Multivariate biomarker analysis will be performed to interrogate any association between differentiation stage, gene expression, mutational profiles, phosphoprotein profiles (including LCK) and treatment response.

6.4 Future Perspectives

6.4.1 Hypothesis for DEX+DAS Synergy

Our growing appreciation that LCK inhibition synergises with DEX response and the combined therapy DEX+DAS significantly improves leukaemia treatment *in vivo* has fuelled our interest in understanding the mechanism of DAS and DEX interaction. Several hypotheses could be formulated.

6.4.1.1 Pharmacokinetics of DEX and DAS

Pharmacokinetic (PK) studies of either DAS or DEX alone have been established (Liston and Davis, 2017; Yang et al., 2008). However, there is no investigation on the PK of either DAS or DEX when they are given together. It is possible that one drug somehow affects the metabolism or stability of the other drug *in vivo*, which augments its function. The normal phase HPLC (High-Performance Liquid Chromatography) assay for DEX (Samtani and Jusko, 2005) is well-established in the Drug Discovery group in NICR, while the HPLC-MS assay to quantify DAS levels needs to be developed (De Francia et al., 2009). In order to facilitate the development and optimisation of such an assay, a PK study incorporating numerous blood samples will be collected in healthy BALB/c mice treated with 35 mg/kg DAS and/or 1 mg/kg DEX by IP injection.

6.4.1.2 The ERK Pathway May Be Involved in DEX Resistance

Since LCK and GCs are molecules in signalling networks that interact and play various biological functions, it is likely that the interplays of downstream signalling play a crucial role in DEX+DAS synergy. It has been shown that DAS could facilitate DEX-induced BIM induction, which is a pro-apoptotic protein (Scherr et al., 2018). Another possibility could be that LCK downstream signalling pathways, such as ERK signalling, play a role in DEX-resistance (Polak et al., 2016). The combination of DEX and Selumetinib (MEK inhibitor) has been shown to synergise in the RAS pathway mutated ALL (Matheson et al., 2019). This combination is currently tested in an early phase clinical trial (UK, 2018). It is conceivable that DAS inhibits LCK and its downstream ERK signalling, thereby sensitising cells to DEX. Our preliminary data have demonstrated that an ERK inhibitor could substantially augment DEX-induced *GILZ* gene expression in CUTLL1 and Jurkat (Figure 64), suggesting that the ERK pathway is implicated in DEX-resistance.

6.4.1.3 LCK and GC Interaction

The interplay between TCR and GR has been shown in healthy T cells, and GR translocation is not directly affected by TCR in healthy T cells (Zacharchuk et al., 1990). However, the effect of TCR activity on GR localisation remains an open question and needs to be interrogated in T-ALL cells. There is the possibility that LCK knockdown enhances DEX-induced GR translocation in malignant T cells, as has been shown in a similar fashion for AKT inhibition (Piovan et al., 2013). GR is a part of a multiprotein complex linked with TCR which contains LCK and HSP90. The binding of GC to the GR leads to rapid disassociation of LCK and FYN from this complex; therefore attenuating TCR signalling (Lowenberg et al., 2006). One hypothesis to explain the mechanism underlying DEX-resistance would be that in DEX-resistant T-ALL cells, the GR is tightly associated with this complex, which forbids GR disassociation and subsequently translocation into the nucleus after GC stimulus. Inhibition or knockdown of LCK would facilitate the release of GR and augment GR induced apoptosis. To address this question, I plan to perform co-immunoprecipitation of GR and LCK and assess the translocation of GR from the cytoplasm to nucleus after DEX+DAS treatment. A more comprehensive understanding could be achieved by high-throughput mass spectrometry analysis of the LCK interactome, particularly

when comparing this interactome in healthy T-cells versus malignant T-cells, as well as in DEX-resistant T-ALLs versus DEX-sensitive T-ALLs.

6.4.2 The Rationale of Performing Functional Genomic Studies for DEX+DAS Synergy and Resistance

As I mentioned before, it looks like we can explore the observed drug synergy mechanism from many angles. However, the number of essential genes involved in regulating DEX+DAS synergy is easily underestimated. I propose to perform a genome-wide CRISPR/Cas9 screen under selection pressure from four different arms of treatment (Ctrl, DAS, DEX, DEX+DAS) to facilitate the identification of genes that are essential in leukaemia survival vulnerability, drug synergy and therapy resistance in a systematic manner. DAS sensitises DEX in multiple T-ALL cell lines and PDXs, which represent different genetic subtypes, leukemogenic stages and differentiation stages. Performing this genome-wide screen in a large and diverse panel of cell lines/PDXs would increase the chance to find universal mechanisms of drug synergy and resistance relevant to T-ALL.

6.4.2.1 Identification of DAS-target Genes and DEX-resistance Associated Genes

In a first analysis, differentially expressed sgRNAs in single drug-treated samples, compared to control cells, could answer several questions:

1) Differentially enriched sgRNAs in DAS-treated cells demonstrate DAS targeted genes. After knockout of these genes, cells become resistant to DAS and have high abundance in the pool. By analysing these genes, we could cross-reference whether these genes are DAS targets or LCK-signalling associated genes.

2) Differentially depleted sgRNAs in DEX-treated cells, but not in control samples, point towards genes related to GC-resistance, as these knockout cells are only depleted when treated with DEX. Identification of these genes allows us to gain a comprehensive insight into understanding steroid-resistance in T-ALL, which might be beneficial for future clinical application.

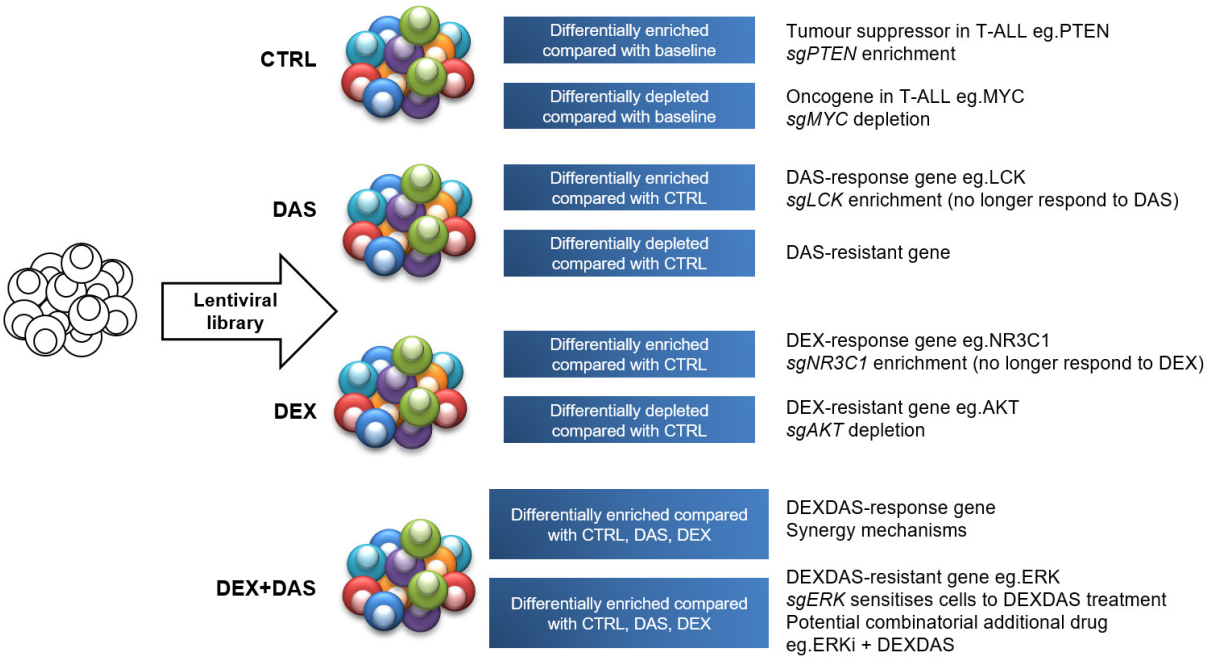

Figure 65. Principle of genome-wide CRISPR/Cas9 screening analysis. After lentiviral library transduction, cells will be treated with control vehicle (CTRL), DAS, DEX and DEX+DAS arms. CTRL samples will be compared with baselines to identify genes that suppress or promote leukaemia cell proliferation/survival, such as enrichment of *sgPTEN* and depletion of *sgMYC*. The DAS (DEX) treated arm will be compared with CTRL arm to identify differentially expressed sgRNAs. DAS impairs cell proliferation via inhibiting LCK; thus, *sgLCK* is expected to be enriched in DAS-treated arm. DEX induces apoptosis via activating NR3C1, thus knockout of NR3C1 (*sgNR3C1*) is expected to cause DEX resistance. AKT has been shown to antagonise DEX response. Therefore, *sgAKT* will sensitise cells to DEX response, which will be depleted in the DEX-treated arm. Similar principles apply to DEX+DAS arm. sgRNAs that are differentially enriched in DEX+DAS treated cells demonstrating DEX+DAS synergy-related genes. On the contrary, differentially depleted sgRNAs in DEX+DAS samples are genes that cause DEX+DAS resistance. For example, loss of function of ERK would sensitise cells to DEX+DAS treatment leading to the reduction of this *sgERK* clone. This will facilitate to develop more powerful multi-drug combination to eradicate leukaemia cells.

6.4.2.2 Identification of Genes for DEX+DAS Synergy

The integrated analysis of DAS-targeted genes and DEX-resistance related genes would facilitate the discovery of possible mechanisms underlying DAS sensitising the DEX response in T-ALL. More importantly, these genes can be further examined in cells receiving the combined DEX+DAS treatment arm.

The discovery of sgRNAs that are only differentially expressed in the DEX+DAS-treated cells, but not control or single treatment samples, would enable us to identify genes involved in both synergy with DEX+DAS and resistance to DEX+DAS. 3) sgRNAs that are enriched explicitly in DEX+DAS group suggest these genes contribute to drug synergy. Such essentiality might point to novel cytoplasm-nucleus transporters that affect GR translocation, chaperones involved in GR-LCK interaction, phosphatases regulating LCK signalling, transcription factors or cofactors differentially associated with GR, as well as BH3 proteins with pro-apoptotic or anti-apoptotic roles. Overall, the global vision of DEX+DAS synergy-related genes would allow us to identify novel mechanisms of how LCK or TCR signalling modulates DEX response.

6.4.2.3 Discovery of Genes for DEX+DAS Resistance

4) In the murine phase Ⅱ-like clinical trial, the engraftment of leukaemia cells of PDX LK080 was impaired during the three-week dosing with DEX+DAS. Peripheral blood monitor revealed a substantial reduction of leukaemia engraftment in the DEX+DAS mouse. However, as soon as the treatment was completed, the leukaemia progressed and eventually reached similar engraftment levels as observed in the control mouse, suggesting potential resistant mechanisms to the combination of DEX+DAS.

Any differentially depleted sgRNAs in the DEX+DAS treatment group would provide potential drug targets to synergise with DEX+DAS. Perhaps other activated kinases causing resistance to the DEX+DAS treatment will be identified. If so, it would be sensible to explore other kinase inhibitors and design more efficient combinatorial therapies. More intriguingly, the genes underlying DEX+DAS resistance might be metabolic regulators, cytokines, as well as surface receptors that can be targeted. In this case, it would be feasible to combine a metabolism inhibitor, antibody therapy, or immunotherapy with DEX+DAS. Once the resistance genes are identified, validation can be done by investigation of these genes in cell lines that do not show synergy with DEX+DAS (such as RPMI8402) or in artificially generated DEX+DAS-resistant cell

lines. Another approach is to manipulate these newly identified genes to drive cells to DEX+DAS resistance. The ultimate aim of identifying drug resistance mechanisms is to develop novel triple/quadruple drug combinations to assess the efficacy *in vitro* and *in vivo* against T-ALL.

Using a whole-genome screen approach to investigate DEX+DAS synergy and resistance mechanisms would offer a global view of genes and pathways interacting or cooperating with LCK and GC regulated networks, to aid the development of a more robust drug combination to eradicate leukaemia cells and improve patient outcomes completely.

6.4.3 RNA-Seq to Identify Auxiliary Survival Pathways

We have received the RNA-seq data for two PDX samples (LK203 and LK080) treated with Ctrl, DAS, DEX and DEX/DAS *in vitro* for 24 hours. These data will provide insight into biological processes induced by DEX+DAS treatment and hint towards the activation of potential auxiliary survival pathways. Shortly, more samples of PDXs treated *in vivo* in murine phase Ⅱ-like clinical trials will be sent for RNA sequencing to increase this data set. Analysis and interpretation of this dataset would provide some insight into genes that are associated with DEX resistancy and DEX+DAS sensitisation.

6.4.4 Perform Phase II-like Trial with Novel Multi-Drug Combination Leading to Early Phase Clinical Trial

Once DEX+DAS resistance mechanisms had been identified, a novel triple/quadruple drug combination could be designed. Depending on the type of mediator, a kinase inhibitor, metabolism inhibitor, chemotherapy drug, or immunotherapy could be used to explore the combinatorial drug efficacy *in vitro*. For *in vivo* evaluation, the maximal tolerated dose and pharmacokinetics of this drug combination will be assessed. In order to increase the success rate of translation of preclinical trials into the clinical setting, the novel triple/quadruple drug combination will be validated in randomised phase II-like murine trials whose principle and methodology will be similar to what we have done in this study.

To summarise, this study I have identified a novel drug target in T-ALL, namely LCK, which universally modulates cell cycle progression, moreover, I have developed an efficient drug combination of DEX/DAS that could substantially reduce leukaemia burden in a murine phase II-like clinical trial. Future work will focus on unravelling the synergy and DEX/DAS resistance mechanisms to develop a robust multi-drug combination for T-ALL patients and translate this into clinical care.

Chapter 7

Conclusion

In summary, we hypothesised that the pTCR/TCR signalling pathway has an essential function in promoting cell proliferation and survival in T-ALL cells. The *in vitro* targeted shRNA screen identified *LCK*, *ZAP70* and *PTCRA* as crucial genes for cell proliferation in T-ALL cell lines. These data have been validated *in vitro* by shRNA-mediated gene silencing and *in vivo* using a competitive assay with MOLT4 cells, in which the shNTC population outcompeted *LCK* knockdown cells demonstrating LCK is required for leukaemia propagation. Notably, the *in vivo* screening of PDX L963 in which all six mice showed significant depletion of shLCK#3 in both spleen and bone marrow samples, further confirms the essentiality of LCK in T-ALL cell maintenance.

Phenotypically, knockdown of LCK primarily induced G_0/G_1 arrest and reduced the rate of cell division. The dual ABL/SFKs inhibitor DAS effectively inhibited LCK kinase activity, as demonstrated by the abolishment of p-Y394^{LCK} and p-Y783$^{PLC\gamma1}$. Treatment of DAS caused substantial cell cycle arrest in cell lines and PDXs. Moreover, the sensitivity of T-ALL cell lines to DAS was significantly correlated with p-Y394^{LCK}/LCK.

The broad impact of DEX on the induction of apoptosis in lymphoid malignancies suggests a rationale to explore its efficacy in LCK knockdown cells. Excitingly, SUPT1 and CUTLL1 cells were re-sensitised to DEX after LCK depletion. Pharmacological inhibition of LCK by DAS synergised with DEX to induce greater cell death in both DEX sensitive and resistant T-ALLs *in vitro*. Bioinformatics analysis of integrated drug matrix data revealed significant enrichment of drug synergy around the clinically-relevant concentrations of DAS and DEX.

Evidence is emerging that murine trials using acute leukaemia PDXs, that mimic human randomised clinical trials, can assess drug efficacy. We first determined the maximum tolerated doses of the DEX/DAS combination, and then performed a phase Ⅱ-like clinical trial in mice with ten T-ALL PDXs. Collectively, the DEX/DAS combination proved to be an efficient leukaemia treatment and significantly delayed the engraftment of primary patient samples in bone marrow, spleen, and liver compared with control mice and single-drug treatment groups. DEX/DAS also considerably reduced or delayed the CNS infiltration of leukaemia cells, which was achieved less effectively by DEX or DAS alone.

The presented evidence endeavours to highlight the crucial role of LCK in T-ALL cell proliferation and steroid resistance. Inhibition of LCK blocks cell proliferation and could

re-sensitise leukaemia cells to DEX. The synergistic effects and the high efficacy of DAS and DEX in triggering apoptosis *in vivo* might provide a novel treatment strategy for T-ALL patients, particularly for the refractory and relapsed T-ALL cases.

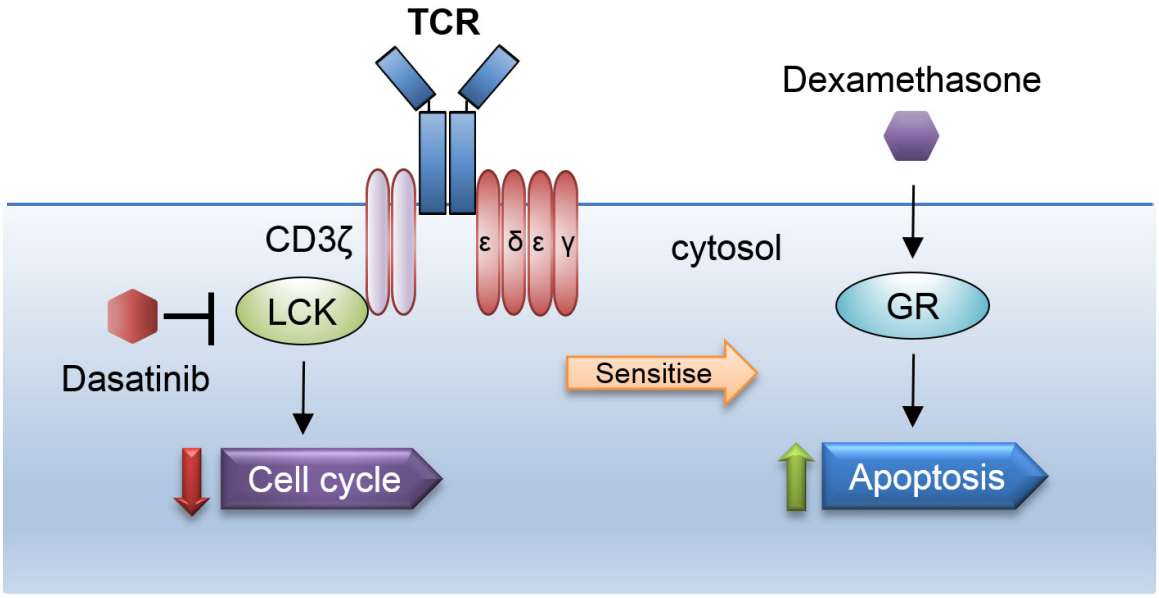

Figure 66. The proposed model of LCK modulating cell cycle progression and steroid resistance in leukemic cells. LCK is constitutively activated in T cells resulting in tonic TCR signalling that promotes cell cycle progression. DAS effectively inhibits LCK kinase activity and induces cell cycle arrest. DEX activates GR upon binding, and GR subsequently translocates to the nucleus to induce apoptosis. The interplay between TCR and GR signalling is affected by LCK depletion or DAS treatment, which could sensitise cells to DEX-induced cell death. In this way, DAS and DEX can be combined to impair leukaemia proliferation *in vitro* and propagation *in vivo* synergistically.

Appendix

Table 6. Barcoding reverse primers used in the targeted shRNA screen.

Name	Sequences	Primer Seq	Read
1	CAAGCAGAAGACGGCATACGAGATCGTGATATTTATACCATTTTAATTCAGCTTTGT	CGTGAT	ATCACG
2	CAAGCAGAAGACGGCATACGAGATACATCGATTTATACCATTTTAATTCAGCTTTGT	ACATCG	CGATGT
3	CAAGCAGAAGACGGCATACGAGATGCCTAAATTTATACCATTTTAATTCAGCTTTGT	GCCTAA	TTAGGC
4	CAAGCAGAAGACGGCATACGAGATTGGTCAATTTATACCATTTTAATTCAGCTTTGT	TGGTCA	TGACCA
5	CAAGCAGAAGACGGCATACGAGATCACTGTATTTATACCATTTTAATTCAGCTTTGT	CACTGT	ACAGTG
6	CAAGCAGAAGACGGCATACGAGATATTGGCATTTATACCATTTTAATTCAGCTTTGT	ATTGGC	GCCAAT
7	CAAGCAGAAGACGGCATACGAGATGATCTGATTTATACCATTTTAATTCAGCTTTGT	GATCTG	CAGATC
8	CAAGCAGAAGACGGCATACGAGATTCAAGTATTTATACCATTTTAATTCAGCTTTGT	TCAAGT	ACTTGA
9	CAAGCAGAAGACGGCATACGAGATCTGATCATTTATACCATTTTAATTCAGCTTTGT	CTGATC	GATCAG
10	CAAGCAGAAGACGGCATACGAGATAAGCTAATTTATACCATTTTAATTCAGCTTTGT	AAGCTA	TAGCTT
11	CAAGCAGAAGACGGCATACGAGATGTAGCCATTTATACCATTTTAATTCAGCTTTGT	GTAGCC	GGCTAC
12	CAAGCAGAAGACGGCATACGAGATTACAAGATTTATACCATTTTAATTCAGCTTTGT	TACAAG	CTTGTA
13	CAAGCAGAAGACGGCATACGAGATTTGACTATTTATACCATTTTAATTCAGCTTTGT	TTGACT	AGTCAA
14	CAAGCAGAAGACGGCATACGAGATGGAACTATTTATACCATTTTAATTCAGCTTTGT	GGAACT	AGTTCC
15	CAAGCAGAAGACGGCATACGAGATTGACATATTTATACCATTTTAATTCAGCTTTGT	TGACAT	ATGTCA
16	CAAGCAGAAGACGGCATACGAGATGGACGGATTTATACCATTTTAATTCAGCTTTGT	GGACGG	CCGTCC

17	CAAGCAGAAGACGGCATACGAGATCTCTACATTTATACCATTTTAATTCAGCTTTGT	CTCTAC	GTAGAG
18	CAAGCAGAAGACGGCATACGAGATGCGGACATTTATACCATTTTAATTCAGCTTTGT	GCGGAC	GTCCGC
19	CAAGCAGAAGACGGCATACGAGATTTTCACATTTATACCATTTTAATTCAGCTTTGT	TTTCAC	GTGAAA
20	CAAGCAGAAGACGGCATACGAGATGTGGCCATTTATACCATTTTAATTCAGCTTTGT	GTGGCC	GTGGCC
21	CAAGCAGAAGACGGCATACGAGATCGAAACATTTATACCATTTTAATTCAGCTTTGT	CGAAAC	GTTTCG
22	CAAGCAGAAGACGGCATACGAGATCGTACGATTTATACCATTTTAATTCAGCTTTGT	CGTACG	CGTACG
23	CAAGCAGAAGACGGCATACGAGATCCACTCATTTATACCATTTTAATTCAGCTTTGT	CCACTC	GAGTGG
24	CAAGCAGAAGACGGCATACGAGATGCTACCATTTATACCATTTTAATTCAGCTTTGT	GCTACC	GGTAGC
25	CAAGCAGAAGACGGCATACGAGATATCAGTATTTATACCATTTTAATTCAGCTTTGT	ATCAGT	ACTGAT
26	CAAGCAGAAGACGGCATACGAGATGCTCATATTTATACCATTTTAATTCAGCTTTGT	GCTCAT	ATGAGC
27	CAAGCAGAAGACGGCATACGAGATAGGAATATTTATACCATTTTAATTCAGCTTTGT	AGGAAT	ATTCCT
28	CAAGCAGAAGACGGCATACGAGATCTTTTGATTTATACCATTTTAATTCAGCTTTGT	CTTTTG	CAAAAG
29	CAAGCAGAAGACGGCATACGAGATTAGTTGATTTATACCATTTTAATTCAGCTTTGT	TAGTTG	CAACTA
30	CAAGCAGAAGACGGCATACGAGATCCGGTGATTTATACCATTTTAATTCAGCTTTGT	CCGGTG	CACCGG
31	CAAGCAGAAGACGGCATACGAGATATCGTGATTTATACCATTTTAATTCAGCTTTGT	ATCGTG	CACGAT
32	CAAGCAGAAGACGGCATACGAGATTGAGTGATTTATACCATTTTAATTCAGCTTTGT	TGAGTG	CACTCA
33	CAAGCAGAAGACGGCATACGAGATGCGGACATTTATACCATTTTAATTCAGCTTTGT	GCGGAC	GCGGAC
	* same with No. 18, not used in this study		
34	CAAGCAGAAGACGGCATACGAGATGCCATGATTTATACCATTTTAATTCAGCTTTGT	GCCATG	CATGGC
35	CAAGCAGAAGACGGCATACGAGATAAAATGATTTATACCATTTTAATTCAGCTTTGT	AAAATG	CATTTT
36	CAAGCAGAAGACGGCATACGAGATTGTTGGATTTATACCATTTTAATTCAGCTTTGT	TGTTGG	CCAACA

37	CAAGCAGAAGACGGCATACGAGATATTCCGATTTATACCATTTTAATTCAGCTTTGT	ATTCCG	CGGAAT
38	CAAGCAGAAGACGGCATACGAGATAGCTAGATTTATACCATTTTAATTCAGCTTTGT	AGCTAG	CTAGCT
39	CAAGCAGAAGACGGCATACGAGATGTATAGATTTATACCATTTTAATTCAGCTTTGT	GTATAG	CTATAC
40	CAAGCAGAAGACGGCATACGAGATTCTGAGATTTATACCATTTTAATTCAGCTTTGT	TCTGAG	CTCAGA
41	CAAGCAGAAGACGGCATACGAGATGTCGTCATTTATACCATTTTAATTCAGCTTTGT	GTCGTC	GACGAC
42	CAAGCAGAAGACGGCATACGAGATCGATTAATTTATACCATTTTAATTCAGCTTTGT	CGATTA	TAATCG
43	CAAGCAGAAGACGGCATACGAGATGCTGTAATTTATACCATTTTAATTCAGCTTTGT	GCTGTA	TACAGC
44	CAAGCAGAAGACGGCATACGAGATATTATAATTTATACCATTTTAATTCAGCTTTGT	ATTATA	TATAAT
45	CAAGCAGAAGACGGCATACGAGATGAATGAATTTATACCATTTTAATTCAGCTTTGT	GAATGA	TCATTC
46	CAAGCAGAAGACGGCATACGAGATTCGGGAATTTATACCATTTTAATTCAGCTTTGT	TCGGGA	TCCCGA
47	CAAGCAGAAGACGGCATACGAGATCTTCGAATTTATACCATTTTAATTCAGCTTTGT	CTTCGA	TCGAAG
48	CAAGCAGAAGACGGCATACGAGATTGCCGAATTTATACCATTTTAATTCAGCTTTGT	TGCCGA	TCGGCA
49	CAAGCAGAAGACGGCATACGAGATTAGCGCATTTATACCATTTTAATTCAGCTTTGT	TAGCGC	GCGCTA
50	CAAGCAGAAGACGGCATACGAGATGTGTTTATTTATACCATTTTAATTCAGCTTTGT	GTGTTT	AAACAC
51	CAAGCAGAAGACGGCATACGAGATCCTTCAATTTATACCATTTTAATTCAGCTTTGT	CCTTCA	TGAAGG
52	CAAGCAGAAGACGGCATACGAGATTATGTTATTTATACCATTTTAATTCAGCTTTGT	TATGTT	AACATA
53	CAAGCAGAAGACGGCATACGAGATGACGCGATTTATACCATTTTAATTCAGCTTTGT	GACGCG	CGCGTC
54	CAAGCAGAAGACGGCATACGAGATTGTATCATTTATACCATTTTAATTCAGCTTTGT	TGTATC	GATACA
55	CAAGCAGAAGACGGCATACGAGATCACACCATTTATACCATTTTAATTCAGCTTTGT	CACACC	GGTGTG
56	CAAGCAGAAGACGGCATACGAGATTTCTTAATTTATACCATTTTAATTCAGCTTTGT	TTCTTA	TAAGAA
57	CAAGCAGAAGACGGCATACGAGATCTCGCTATTTATACCATTTTAATTCAGCTTTGT	CTCGCT	AGCGAG

58	CAAGCAGAAGACGGCATACGAGATTAACCGATTTATACCATTTTAATTCAGCTTTGT	TAACCG	CGGTTA
59	CAAGCAGAAGACGGCATACGAGATAAAGCTATTTATACCATTTTAATTCAGCTTTGT	AAAGCT	AGCTTT
60	CAAGCAGAAGACGGCATACGAGATAGACCAATTTATACCATTTTAATTCAGCTTTGT	AGACCA	TGGTCT
61	CAAGCAGAAGACGGCATACGAGATGGGATAATTTATACCATTTTAATTCAGCTTTGT	GGGATA	TATCCC
62	CAAGCAGAAGACGGCATACGAGATACGACAATTTATACCATTTTAATTCAGCTTTGT	ACGACA	TGTCGT
63	CAAGCAGAAGACGGCATACGAGATGTGGGGATTTATACCATTTTAATTCAGCTTTGT	GTGGGG	CCCCAC
64	CAAGCAGAAGACGGCATACGAGATTCGTATATTTATACCATTTTAATTCAGCTTTGT	TCGTAT	ATACGA
65	CAAGCAGAAGACGGCATACGAGATCAAGGGATTTATACCATTTTAATTCAGCTTTGT	CAAGGG	CCCTTG
66	CAAGCAGAAGACGGCATACGAGATGCCGGTATTTATACCATTTTAATTCAGCTTTGT	GCCGGT	ACCGGC
67	CAAGCAGAAGACGGCATACGAGATCAGTAAATTTATACCATTTTAATTCAGCTTTGT	CAGTAA	TTACTG
68	CAAGCAGAAGACGGCATACGAGATAGTTCCATTTATACCATTTTAATTCAGCTTTGT	AGTTCC	GGAACT
69	CAAGCAGAAGACGGCATACGAGATAATAACATTTATACCATTTTAATTCAGCTTTGT	AATAAC	GTTATT
70	CAAGCAGAAGACGGCATACGAGATACTTTTATTTATACCATTTTAATTCAGCTTTGT	ACTTTT	AAAAGT
71	CAAGCAGAAGACGGCATACGAGATTCCCTTATTTATACCATTTTAATTCAGCTTTGT	TCCCTT	AAGGGA
72	CAAGCAGAAGACGGCATACGAGATATACTTATTTATACCATTTTAATTCAGCTTTGT	ATACTT	AAGTAT
73	CAAGCAGAAGACGGCATACGAGATAGATGTATTTATACCATTTTAATTCAGCTTTGT	AGATGT	ACATCT
74	CAAGCAGAAGACGGCATACGAGATAATCGTATTTATACCATTTTAATTCAGCTTTGT	AATCGT	ACGATT
75	CAAGCAGAAGACGGCATACGAGATCGGCGTATTTATACCATTTTAATTCAGCTTTGT	CGGCGT	ACGCCG
76	CAAGCAGAAGACGGCATACGAGATGAGAGTATTTATACCATTTTAATTCAGCTTTGT	GAGAGT	ACTCTC
77	CAAGCAGAAGACGGCATACGAGATGATTCTATTTATACCATTTTAATTCAGCTTTGT	GATTCT	AGAATC
78	CAAGCAGAAGACGGCATACGAGATCCCAATATTTATACCATTTTAATTCAGCTTTGT	CCCAAT	ATTGGG

79	CAAGCAGAAGACGGCATACGAGATACGCGGATTTATACCATTTTAATTCAGCTTTGT	ACGCGG	CCGCGT
80	CAAGCAGAAGACGGCATACGAGATAGGGCGATTTATACCATTTTAATTCAGCTTTGT	AGGGCG	CGCCCT
81	CAAGCAGAAGACGGCATACGAGATCTGCAGATTTATACCATTTTAATTCAGCTTTGT	CTGCAG	CTGCAG
82	CAAGCAGAAGACGGCATACGAGATAACTTCATTTATACCATTTTAATTCAGCTTTGT	AACTTC	GAAGTT
83	CAAGCAGAAGACGGCATACGAGATGGGTGCATTTATACCATTTTAATTCAGCTTTGT	GGGTGC	GCACCC
84	CAAGCAGAAGACGGCATACGAGATTCCTGCATTTATACCATTTTAATTCAGCTTTGT	TCCTGC	GCAGGA
85	CAAGCAGAAGACGGCATACGAGATCGCGGCATTTATACCATTTTAATTCAGCTTTGT	CGCGGC	GCCGCG
86	CAAGCAGAAGACGGCATACGAGATACCGCCATTTATACCATTTTAATTCAGCTTTGT	ACCGCC	GGCGGT
87	CAAGCAGAAGACGGCATACGAGATTAATACATTTATACCATTTTAATTCAGCTTTGT	TAATAC	GTATTA
88	CAAGCAGAAGACGGCATACGAGATCACGTAATTTATACCATTTTAATTCAGCTTTGT	CACGTA	TACGTG
89	CAAGCAGAAGACGGCATACGAGATATGTGAATTTATACCATTTTAATTCAGCTTTGT	ATGTGA	TCACAT

Name	Sequences
NGS-F3	AATGATACGGCGACCACCGAGATCTACACTCTTTCCCTACACGACGCTCTTCCGATCTNNNNCATGGACGAGCTGTACAAGT
	Forward amplification primer used in the targeted shRNA screen
NGS-F2	AATGATACGGCGACCACCGAGATCTACACTCTTTCCCTACACGACGCTCTTCCGATCTNNNNATGCCCGAAGGCTACGTCC
NGS-F1	AATGATACGGCGACCACCGAGATCTACACTCTTTCCCTACACGACGCTCTTCCGATCTNNNNCTCGGCATGGACGAGCTG

Table 7. The sample annotation and quantification of the targeted shRNA screen.

No.	Barcode	Sample				ng/ul
1	1	Spleen	T-ALL9	2411 LN	L963	13.6
2	2	Spleen	T-ALL9	2411 RN	L963	3.24
3	3	Spleen	T-ALL9	2411 NN	L963	8.25
4	4	Spleen	T-ALL9	2410 LN	L963	6.58
5	5	Spleen	T-ALL9	2413 LN	L963	12.5
6	6	Spleen	T-ALL9	2413 NN	L963	6.6
7	7	Bone marrow	T-ALL9	2411 LN	L963	4.12
8	8	Bone marrow	T-ALL9	2411 RN	L963	7.56
9	9	Bone marrow	T-ALL9	2411 NN	L963	7.16
10	10	Bone marrow	T-ALL9	2410 LN	L963	7.44
11	11	Bone marrow	T-ALL9	2413 LN	L963	10.9
12	12	Bone marrow	T-ALL9	2413 NN	L963	7.36
13	13	Spleen	T-ALL13	2544 NN	LK080	25.6
14	14	Spleen	T-ALL13	2544 LN	LK080	14
15	15	Spleen	T-ALL13	2544 RN	LK080	3.54
16	16	Spleen	T-ALL13	2543 NN	LK080	8.88
18	18	Spleen	T-ALL13	2543 RN	LK080	38.8
19	19	Bone marrow	T-ALL13	2544 NN	LK080	34.8
20	20	Bone marrow	T-ALL13	2544 LN	LK080	27.8
21	21	Bone marrow	T-ALL13	2544 RN	LK080	42.8
22	22	Bone marrow	T-ALL13	2543 NN	LK080	7.92
23	23	Bone marrow	T-ALL13	2543 LN	LK080	25.6
24	24	Bone marrow	T-ALL13	2543 RN	LK080	23.8
25	25	Spleen	T-ALL3	3343 LN	LK203	11.5
26	26	Spleen	T-ALL3	3343 RN	LK203	5.72
27	27	Spleen	T-ALL3	3343 NN	LK203	10.8
28	88	Spleen	T-ALL3	3343 BN	LK203	7.12
29	29	Spleen	T-ALL3	3343 2LN	LK203	10.3
30	30	Spleen	T-ALL3	3343 2RN	LK203	7.32
31	31	Bone marrow	T-ALL3	3343 LN	LK203	23
32	32	Bone marrow	T-ALL3	3343 RN	LK203	12.8
33	83	Bone marrow	T-ALL3	3343 NN	LK203	12.4
34	34	Bone marrow	T-ALL3	3343 BN	LK203	7.4
35	35	Bone marrow	T-ALL3	3343 2LN	LK203	8.98
36	36	Bone marrow	T-ALL3	3343 2RN	LK203	18.9
37	37		T-ALL13	d16 in vitro	LK080	10.8
38	38		T-ALL13	d30 in vitro	LK080	7.18
39	39		T-ALL3	d16 in vitro	LK203	17.2
40	40		T-ALL3	d30 -MSC	LK203	10.9
41	41		T-ALL3	d30 +MSC	LK203	11.3
42	42		T-ALL9	L963	baseline	24

43	43	T-ALL9	L963	baseline	27
44	44	T-ALL9	L963	baseline	24.2
45	45	T-ALL13	LK080	baseline	27
46	46	T-ALL13	LK080	baseline	25.8
47	47	T-ALL13	LK080	baseline	25.8
48	48	T-ALL3	LK203	baseline	31.2
49	49	T-ALL3	LK203	baseline	21.8
50	50	T-ALL3	LK203	baseline	26.6
51	51	SUPT1	Lib 1	d16	12.5
52	52	SUPT1	Lib 2	d16	30.6
53	53	SUPT1	Lib 1	d30	16
54	54	SUPT1	Lib 2	d30	25.2
55	55	SUPT1	Lib 1	d40	15.3
56	56	SUPT1	Lib 2	d40	25
57	57	CUTLL1	Lib 1	d16	20.2
58	58	CUTLL1	Lib 2	d16	30.2
59	59	CUTLL1	Lib 1	d30	18.5
60	60	CUTLL1	Lib 2	d30	27.4
61	61	CUTLL1	Lib 1	d40	22
62	62	CUTLL1	Lib 2	d40	32.4
63	63	MOLT4	Lib 1	d16	23.2
64	64	MOLT4	Lib 2	d16	28
65	65	MOLT4	Lib 1	d30	20.6
66	66	MOLT4	Lib 2	d30	19.9
67	67	MOLT4	Lib 1	d40	18.6
68	68	MOLT4	Lib 2	d40	18.5
69	69	HPB-ALL	Lib 1	d16	17.2
70	70	HPB-ALL	Lib 2	d16	26
71	71	HPB-ALL	Lib1	d30	12
72	72	HPB-ALL	Lib2	d30	25.8
73	73	HPB-ALL	Lib 1	d40	23.2
74	74	HPB-ALL	Lib 2	d40	25.4
75	75	SUPT1	Lib 1	baseline	19.3
76	76	SUPT1	Lib 2	baseline	30
77	77	CUTLL1	Lib 1	baseline	24
78	78	CUTLL1	Lib 2	baseline	40.4
79	79	MOLT4	Lib 1	baseline	24.2
80	80	MOLT4	Lib 2	baseline	12.4
81	81	HPB-ALL	Lib 1	baseline	16
82	82	HPB-ALL	Lib 2	baseline	20.8

Table 8. The raw data of shRNA screens.

SUPT1

shRNA	gene	slope	logCPM	LR	PValue	FDR
shRPS29#1	RPS29	-0.53123	14.29437	72.14488	2.00E-17	7.20E-16
shRPL9#1	RPL9	-0.55786	13.85047	67.01331	2.70E-16	4.85E-15
shLCK#3	LCK	-0.61735	13.94143	52.16641	5.10E-13	6.12E-12
shPTCRA#2	PTCRA	-0.54271	13.57462	46.17613	1.08E-11	9.73E-11
shPTEN#2	PTEN	0.282258	15.35395	35.02909	3.25E-09	2.34E-08
shPTEN#3	PTEN	0.424263	15.38662	32.73342	1.06E-08	6.34E-08
shZAP70#1	ZAP70	-0.37416	13.77377	31.02042	2.55E-08	1.31E-07
shLCK#1	LCK	-0.34628	14.26935	25.45437	4.53E-07	2.04E-06
shPTEN#1	PTEN	0.289544	15.57128	20.91663	4.80E-06	1.92E-05
shCD3e#1	CD3e	-0.24225	14.39331	19.64187	9.34E-06	3.36E-05
shLAT#2	LAT	0.273	14.31746	14.00058	0.000183	0.000598
shRPL9#2	RPL9	-0.18126	14.89238	12.83435	0.00034	0.001021
shTRPM7#2	TRPM7	-0.19066	14.65694	12.51527	0.000404	0.001118
shPTCRA#3	PTCRA	-0.35518	14.13973	12.15597	0.000489	0.001258
shRPS29#2	RPS29	0.628086	12.66522	8.708742	0.003167	0.007601
shKLHL7	KLHL7	0.162163	15.11518	8.211222	0.004163	0.009367
shCD3e#2	CD3e	-0.14202	14.55194	6.734616	0.009456	0.020024
shCD19#2	CD19	0.12862	14.4973	5.898472	0.015154	0.030308
shSESN2	SESN2	0.129881	14.83796	5.430274	0.019791	0.037498
shCD3e#3	CD3e	-0.09928	14.71464	3.841146	0.050009	0.090017
shZAP70#3	ZAP70	0.121387	14.66767	3.03661	0.081406	0.139553
shFYN#3	FYN	0.08937	14.62285	2.836867	0.092124	0.150748
shDDB2	DDB2	0.08035	15.58186	2.732132	0.098348	0.153936
shFYN#1	FYN	-0.07978	14.72385	2.471572	0.115922	0.173883
shERGIC3	ERGIC3	0.065503	14.82244	1.627733	0.202017	0.28986
shLCK#2	LCK	-0.06171	15.14572	1.575962	0.209343	0.28986
shNTC	NTC	0.062558	15.05358	1.325919	0.249533	0.33271
shCD19#1	CD19	-0.04584	14.65114	0.636513	0.424976	0.546398
shLAT#3	LAT	-0.04232	14.63143	0.364078	0.54625	0.678104
shFYN#2	FYN	0.027577	15.02277	0.293038	0.58828	0.705936
shPTCRA#1	PTCRA	-0.07778	12.83142	0.260297	0.609916	0.70829
shFLG	FLG	0.018123	15.83752	0.129273	0.719188	0.809086
shZAP70#2	ZAP70	0.02048	15.15053	0.069517	0.792042	0.842413
shRUNX1/ETO	Run1	0.012942	15.29902	0.067097	0.795612	0.842413
shLAT#1	LAT	-0.01131	14.34605	0.043935	0.833974	0.857802
shTRPM7#1	TRPM7	-0.00974	15.0676	0.025845	0.87228	0.87228

MOLT4

shRNA	gene	slope	logCPM	LR	PValue	FDR
shLCK#3	LCK	-0.49393	14.57817	37.60301	8.67E-10	3.12E-08
shRPS29#1	RPS29	-0.32417	14.50428	13.0007	0.000311	0.005605
shPTCRA#2	PTCRA	-0.19116	14.18089	7.283953	0.006957	0.083488
shERGIC3	ERGIC3	0.1602	14.77733	5.377864	0.020394	0.183544
shKLHL7	KLHL7	0.130125	14.88374	4.360828	0.036774	0.231921
shLCK#1	LCK	-0.13122	14.76446	4.085409	0.043255	0.231921
shPTEN#2	PTEN	0.109527	14.80355	4.015054	0.045096	0.231921
shZAP70#2	ZAP70	0.136615	15.01813	3.505103	0.06118	0.27531
shLCK#2	LCK	-0.16797	15.34151	3.129431	0.076891	0.275791
shZAP70#3	ZAP70	0.347658	14.31406	3.121749	0.077254	0.275791
shNTC	NTC	0.214847	14.77209	2.980575	0.084269	0.275791
shFYN#3	FYN	0.104816	14.56482	2.537008	0.111205	0.310058
shCD19#2	CD19	0.304433	14.16582	2.526258	0.111965	0.310058
shLAT#2	LAT	0.420649	13.73192	2.350098	0.125275	0.316841
shSESN2	SESN2	0.119695	14.52444	2.268625	0.132017	0.316841
shFYN#2	FYN	-0.11644	15.07516	1.8726	0.171178	0.38515
shCD3e#3	CD3e	0.097748	14.92095	1.407473	0.235476	0.484078
shCD19#1	CD19	0.076676	14.63632	1.36868	0.242039	0.484078
shZAP70#1	ZAP70	-0.06882	14.24169	1.04734	0.30612	0.580018
shTRPM7#2	TRPM7	0.073465	14.78222	0.850954	0.356283	0.641309
shLAT#3	LAT	-0.0557	14.45989	0.731144	0.392513	0.654138
shLAT#1	LAT	-0.05618	14.38549	0.709075	0.399751	0.654138
shRPS29#2	RPS29	0.455703	11.59586	0.554487	0.45649	0.714506
shPTEN#3	PTEN	0.037494	14.68379	0.428577	0.512688	0.734676
shTRPM7#1	TRPM7	-0.04328	15.18369	0.357437	0.549933	0.734676
shRUNX1/ETO	Run1	-0.04558	15.46496	0.32547	0.568339	0.734676
shPTEN#1	PTEN	0.030015	15.12332	0.320785	0.571136	0.734676
shCD3e#1	CD3e	0.053084	14.7422	0.320321	0.571415	0.734676
shPTCRA#3	PTCRA	-0.03215	14.61697	0.239374	0.624659	0.775439
shPTCRA#1	PTCRA	0.267687	12.7532	0.208158	0.648215	0.777858
shDDB2	DDB2	-0.01769	15.59403	0.083688	0.77236	0.896935
shRPL9#1	RPL9	-0.01118	14.45504	0.023847	0.877274	0.948472
shFYN#1	FYN	0.007742	14.81366	0.018907	0.890633	0.948472
shRPL9#2	RPL9	0.007072	15.13202	0.01716	0.895779	0.948472
shFLG	FLG	0.003909	15.84047	0.005994	0.938291	0.965099
shCD3e#2	CD3e	0.000262	14.94729	1.06E-05	0.997398	0.997398

CUTLL1

shRNA	gene	slope	logCPM	LR	PValue	FDR
shLCK#3	LCK	-0.35675	14.29463	132.3253	1.27E-30	4.57E-29
shPTEN#3	PTEN	0.270945	14.94674	89.43219	3.17E-21	5.71E-20
shTRPM7#2	TRPM7	-0.24783	14.66783	74.99375	4.72E-18	5.67E-17
shPTEN#1	PTEN	0.233804	15.29035	71.80669	2.37E-17	2.14E-16
shRPS29#2	RPS29	0.287987	13.31127	41.1585	1.40E-10	1.01E-09
shZAP70#1	ZAP70	-0.14383	14.17178	19.57463	9.67E-06	5.80E-05
shTRPM7#1	TRPM7	-0.13288	14.8739	18.39057	1.80E-05	9.25E-05
shPTCRA#1	PTCRA	0.144236	14.12509	14.74569	0.000123	0.000554
shPTEN#2	PTEN	0.10558	14.9605	12.22175	0.000472	0.001889
shSESN2	SESN2	0.080821	14.62455	7.360335	0.006668	0.024004
shRPL9#2	RPL9	-0.06889	15.13805	5.806092	0.015971	0.052268
shLCK#1	LCK	-0.05504	14.65581	3.562372	0.059103	0.173345
shZAP70#2	ZAP70	-0.05783	15.04069	3.467211	0.062597	0.173345
shPTCRA#2	PTCRA	0.04774	14.35548	2.492345	0.114401	0.286763
shRPS29#1	RPS29	-0.04414	14.94927	2.424066	0.119484	0.286763
shLAT#2	LAT	0.049563	14.24421	2.267049	0.132151	0.29734
shFYN#2	FYN	-0.03946	14.81744	1.948541	0.162744	0.344635
shRPL9#1	RPL9	-0.03939	14.58448	1.841226	0.174807	0.349615
shFYN#1	FYN	-0.03403	14.6642	1.363196	0.242984	0.460391
shNTC	NTC	0.026824	14.92501	0.916581	0.338374	0.609074
shFYN#3	FYN	0.021791	14.52647	0.547283	0.45943	0.787594
shLCK#2	LCK	-0.01924	15.03996	0.410081	0.521928	0.787689
shCD3e#3	CD3e	0.017933	14.88124	0.403658	0.525206	0.787689
shFLG	FLG	-0.01381	15.7347	0.258837	0.61092	0.787689
shKLHL7	KLHL7	0.014446	14.82185	0.258797	0.610948	0.787689
shCD19#2	CD19	0.01455	14.51295	0.233252	0.629123	0.787689
shCD19#1	CD19	-0.01426	14.71381	0.229565	0.631846	0.787689
shERGIC3	ERGIC3	-0.01392	14.61057	0.229422	0.631952	0.787689
shCD3e#2	CD3e	-0.01372	14.76283	0.225394	0.63496	0.787689
shZAP70#3	ZAP70	0.01156	14.50116	0.149549	0.698967	0.787689
shLAT#1	LAT	0.012082	14.28583	0.142321	0.705985	0.787689
shLAT#3	LAT	0.011454	14.41083	0.137908	0.71037	0.787689
shRUNX1/ETO	Run1	0.009921	15.20024	0.126539	0.722048	0.787689
shCD3e#1	CD3e	-0.00759	14.72741	0.066942	0.795843	0.842657
shPTCRA#3	PTCRA	-0.00638	14.61162	0.044858	0.832265	0.856044
shDDB2	DDB2	0.00466	15.3542	0.028696	0.865483	0.865483

HPB-ALL

shRNA	gene	slope	logCPM	LR	PValue	FDR
shRPS29#2	RPS29	1.390155	11.19096	116.9687	2.92E-27	1.05E-25
shPTCRA#1	PTCRA	1.162686	12.44823	97.1251	6.51E-23	1.17E-21
shRPL9#1	RPL9	-1.21206	13.30871	93.49248	4.08E-22	4.89E-21
shLAT#2	LAT	0.448203	13.41074	82.51448	1.05E-19	9.44E-19
shLCK#3	LCK	-0.30854	14.80821	71.77447	2.41E-17	1.74E-16
shPTEN#3	PTEN	0.324605	15.09946	68.71281	1.14E-16	6.83E-16
shPTEN#2	PTEN	0.360431	15.34098	60.10506	8.99E-15	4.62E-14
shRPL9#2	RPL9	-0.54714	14.65503	57.88878	2.77E-14	1.25E-13
shZAP70#3	ZAP70	0.307299	14.0987	40.39811	2.07E-10	8.29E-10
shPTEN#1	PTEN	0.192277	15.38286	23.49149	1.25E-06	4.52E-06
shLCK#2	LCK	-0.16964	15.37185	20.91965	4.79E-06	1.57E-05
shNTC	NTC	0.142722	14.67407	16.20187	5.69E-05	0.000171
shCD19#2	CD19	0.322201	14.00891	15.24878	9.42E-05	0.000261
shZAP70#1	ZAP70	-0.14588	14.20112	12.15537	0.000489	0.001231
shRPS29#1	RPS29	-0.1659	15.04966	12.06883	0.000513	0.001231
shLCK#1	LCK	-0.12064	14.80174	10.8718	0.000976	0.002181
shFYN#2	FYN	-0.1498	15.14792	10.77279	0.00103	0.002181
shFYN#1	FYN	-0.1067	14.72682	8.761949	0.003076	0.00609
shERGIC3	ERGIC3	0.149835	14.66639	8.681668	0.003214	0.00609
shCD3e#3	CD3e	0.110724	14.81066	5.815661	0.015884	0.028591
shPTCRA#2	PTCRA	-0.09302	14.33642	5.450512	0.019563	0.033536
shDDB2	DDB2	-0.07671	15.54087	4.91949	0.026555	0.043454
shTRPM7#1	TRPM7	-0.07996	15.19215	4.631726	0.031386	0.04911
shLAT#1	LAT	-0.07844	14.33617	4.559337	0.03274	0.04911
shKLHL7	KLHL7	0.094138	14.73021	3.918114	0.047768	0.068787
shLAT#3	LAT	-0.08526	14.49881	3.410346	0.064789	0.089708
shRUNX1/ETO	Run1	-0.05371	15.45031	2.394155	0.12179	0.162386
shFYN#3	FYN	0.052444	14.53822	1.91671	0.16622	0.213711
shZAP70#2	ZAP70	0.060226	15.03983	1.719252	0.189789	0.235601
shPTCRA#3	PTCRA	0.045001	14.68605	1.3185	0.250862	0.301034
shFLG	FLG	-0.03314	15.809	0.840896	0.359141	0.417067
shCD3e#1	CD3e	0.074454	14.68732	0.737249	0.390543	0.438663
shSESN2	SESN2	0.05198	14.32832	0.702013	0.402108	0.438663
shCD3e#2	CD3e	-0.02839	14.99087	0.530497	0.466398	0.493833
shCD19#1	CD19	-0.02494	14.61324	0.360766	0.548081	0.563741
shTRPM7#2	TRPM7	-0.01993	14.77305	0.300749	0.583413	0.583413

LK203 *in vitro*

shRNA	logFC	logCPM	LR	PValue	FDR
shRPL9#2	-2.34442	14.34755	57.47394	3.42E-14	1.23E-12
shRPS29#1	-3.28914	13.91702	18.12502	2.07E-05	0.0003
shSESN2	1.058582	14.68708	17.23154	3.31E-05	0.0003
shERGIC3	1.769788	15.65966	17.22071	3.33E-05	0.0003
shPTEN#3	0.97378	15.07812	15.42601	8.58E-05	0.000618
shLCK#1	-0.77115	14.55244	10.42664	0.001242	0.007453
shLAT#1	-0.79255	14.38541	10.03618	1.53E-03	0.007894
shZAP70#3	0.913031	14.12767	8.893602	0.002862	0.012878
shLCK#2	-0.67921	15.12368	7.527476	0.006076	0.022739
shLAT#3	-0.81492	14.37636	7.457751	0.006316	0.022739
shRPL9#1	-1.72479	13.97955	5.985659	0.014423	0.047201
shLCK#3	-0.65503	15.0903	5.812054	0.015917	0.04775
shPTEN#2	0.577326	15.27768	4.590465	0.03215	0.086249
shTRPM7#2	-0.69319	14.87496	4.517927	0.033541	0.086249
shCD19#2	0.563898	14.21015	3.744642	0.052977	0.122818
shPTEN#1	0.513298	14.97789	3.6947	0.054586	0.122818
shTRPM7#1	0.619672	15.45041	3.558532	0.05924	0.12545
shPTCRA#3	-0.53497	14.5679	3.154093	0.075737	0.151474
shNTC	0.43134	14.77022	2.861392	0.090729	0.171907
shFYN#1	-0.45909	14.66029	2.5511	0.110218	0.198392
shPTCRA#2	-0.94997	14.01477	2.396064	0.121641	0.208527
shCD3E#3	0.350878	14.81547	2.265706	0.132266	0.216245
shFYN#2	-0.36781	15.08274	2.198372	0.138157	0.216245
shCD3E#2	0.363319	15.12521	1.809009	0.178627	0.267941
shPTCRA#1	0.764157	13.1688	1.504773	2.20E-01	0.316711
shCD3E#1	0.284976	14.5903	1.312212	0.251995	0.343891
shRPS29#2	0.792341	10.99167	1.273523	2.59E-01	3.44E-01
shKLHL7	0.278821	14.20479	1.229674	2.67E-01	0.343891
shRUNX1/ETO	-0.26394	15.47563	1.101449	0.293948	0.364901
shDDB2	-0.24191	15.4647	0.99148	0.319381	0.383257
shZAP70#1	-0.2403	14.2102	0.766361	3.81E-01	0.442853
shCD19#1	0.151835	14.9887	0.447914	0.503327	0.566243
shFYN#3	0.134089	14.51175	0.32771	0.567011	0.618557
shLAT#2	0.173499	13.50733	0.187032	0.665398	0.704539
shFLG	0.026086	15.75399	0.011679	0.913942	0.9148
shZAP70#2	-0.02632	15.0016	0.011446	0.9148	0.9148

L963 *in vivo* spleen

shRNA	logFC	logCPM	LR	PValue	FDR
shLCK#3	-8.03321	12.38082	31.3336	2.17E-08	7.82E-07
shRPL9#1	-6.10375	11.56515	10.30905	0.001324	0.023828
shCD19#2	-3.204	12.52308	5.983788	0.014438	0.173256
shFYN#1	-1.84535	13.22957	3.100858	0.078251	0.70426
shPTEN#3	-2.03758	12.77494	2.452733	0.11732	0.844707
shERGIC3	2.276879	16.74306	2.167813	0.140927	0.845559
shPTEN#1	-1.68258	16.29354	1.21885	0.269586	0.97833
shZAP70#1	-1.7052	13.5309	1.21095	0.271144	0.97833
shRUNX1/ETO	-1.24494	13.95386	1.073682	0.300115	0.97833
shSESN2	-1.19801	14.09281	0.952131	0.329178	0.97833
shLAT#3	-1.22223	13.02144	0.900891	0.342543	0.97833
shPTCRA#2	1.322231	16.3038	0.800911	0.370821	0.97833
shKLHL7	-1.08219	14.4175	0.763621	0.382198	0.97833
shCD3E#2	-1.11341	13.91845	0.727283	0.393765	0.97833
shLAT#1	1.335508	15.05768	0.68568	0.407638	0.97833
shLAT#2	-0.97306	12.92357	0.572829	0.449137	0.983201
shCD19#1	1.115446	15.03059	0.441655	0.506325	0.983201
shCD3E#3	-0.60982	14.28719	0.219188	0.63966	0.983201
shDDB2	0.588038	16.93928	0.207383	0.648827	0.983201
shFYN#3	0.565636	14.69092	0.16716	0.682649	0.983201
shNTC	0.412178	14.50807	0.165008	0.684587	0.983201
shLCK#1	-0.76202	14.11903	0.157834	0.691159	0.983201
shCD3E#1	-0.43304	15.02011	0.143895	0.704439	0.983201
shFYN#2	-0.49307	14.25891	0.119843	0.729204	0.983201
shFLG	-0.38268	15.06153	0.093593	0.759658	0.983201
shPTCRA#1	-0.34852	12.41615	0.050705	0.821841	0.983201
shTRPM7#1	0.316594	16.76503	0.044782	0.832406	0.983201
shPTCRA#3	-0.23218	13.87086	0.042135	0.837362	0.983201
shZAP70#2	0.20482	14.9653	0.0318	0.858466	0.983201
shTRPM7#2	-0.15276	14.70756	0.012512	0.910937	0.983201
shPTEN#2	0.157617	14.2727	0.011548	0.914423	0.983201
shLCK#2	0.12677	15.19829	0.010496	0.918399	0.983201
shRPL9#2	-0.12975	14.19795	0.008017	0.928657	0.983201
shZAP70#3	0.053671	14.20344	0.001976	0.964547	0.983201
shRPS29#1	0.037446	14.52556	0.000707	0.978787	0.983201
shRPS29#2	-0.04447	10.95056	0.000443	0.983201	0.983201

L963 *in vivo* bone marrow

shRNA	logFC	logCPM	LR	PValue	FDR
shLCK#3	-8.57718	12.38082	26.24361	3.01E-07	1.08E-05
shRPL9#1	-6.49117	11.56515	9.817988	0.001728	0.031106
shCD19#2	-3.25763	12.52308	6.059984	0.013828	0.160969
shERGIC3	4.058343	16.74306	5.607333	0.017885	0.160969
shPTEN#1	-2.94281	16.29354	3.816812	0.050741	0.365333
shPTEN#3	-2.59947	12.77494	3.110715	0.077779	0.390707
shLAT#3	-2.39486	13.02144	3.075171	0.079496	0.390707
shLAT#2	-1.92967	12.92357	2.9323	0.086824	0.390707
shPTCRA#2	1.95272	16.3038	1.774488	0.182828	0.731311
shKLHL7	-1.47015	14.4175	1.514979	0.218381	0.762553
shFYN#1	-1.3497	13.22957	1.422439	0.233002	0.762553
shDDB2	1.461431	16.93928	1.028954	0.310405	0.906671
shCD3E#2	-1.28722	13.91845	0.959119	0.327409	0.906671
shCD3E#3	-1.04132	14.28719	0.636985	0.424805	0.922599
shZAP70#3	1.02018	14.20344	0.618771	0.431504	0.922599
shSESN2	-0.82483	14.09281	0.494419	0.481963	0.922599
shLCK#2	0.795998	15.19829	0.363831	0.546386	0.922599
shRUNX1/ETO	-0.78189	13.95386	0.338049	5.61E-01	9.23E-01
shZAP70#2	-0.53391	14.9653	0.236764	0.626553	0.922599
shTRPM7#1	-0.6809	16.76503	0.20726	0.648923	0.922599
shNTC	0.408758	14.50807	0.155089	0.693718	0.922599
shLCK#1	0.737421	14.11903	0.153269	0.695431	0.922599
shCD19#1	0.678317	15.03059	0.145387	0.702983	0.922599
shZAP70#1	-0.68116	13.5309	0.126603	0.721981	0.922599
shFYN#3	0.510772	14.69092	0.11697	0.732345	0.922599
shRPS29#1	-0.44438	14.52556	0.095859	0.756857	0.922599
shRPL9#2	0.47237	14.19795	0.091172	0.762693	0.922599
shFLG	-0.37716	15.06153	0.081228	0.775641	0.922599
shFYN#2	-0.41495	14.25891	0.079526	0.777941	0.922599
shLAT#1	0.35956	15.05768	0.050328	0.822494	0.922599
shPTCRA#3	-0.26426	13.87086	0.047526	0.827426	0.922599
shTRPM7#2	-0.26199	14.70756	0.03781	0.845825	0.922599
shPTEN#2	-0.24905	14.2727	0.027004	0.869473	0.922599
shPTCRA#1	-0.2584	12.41615	0.026229	0.871343	0.922599
shCD3E#1	0.050404	15.02011	0.001907	0.965171	0.965706
shRPS29#2	0.08799	10.95056	0.001849	0.965706	0.965706

Table 9. The average life span of mice engrafted with T-ALL PDXs.

PDX	Lifespan of primary mice
LK214	48
LK203	52
L903	62
LK287	64
L963	87
LK080	105
L970	123
L809	151
L907	216

Conference Abstract

The European Hematology Association (EHA) 2018, Stockholm
Acute lymphoblastic leukemia – Biology & Translational Research EHA-3362

AN ESSENTIAL ROLE OF LCK IN T-ALL CELL PROLIFERATION AND SURVIVAL

Yuzhe Shi[*1], Melanie Beckett[1], Helen Blair[1], Olaf Heidenreich[1], Anja Krippner-Heidenreich[1], Frederik van Delft[1]*

[1]Wolfson Childhood Cancer Research Centre, Northern Institute for Cancer Research, Newcastle University, Newcastle upon Tyne, United Kingdom

Background: T-cell Acute Lymphoblastic Leukemia (T-ALL) is caused by malignant transformation of T cells showing differentiation arrest and uncontrolled proliferation. The checkpoints during T-cell development are dominated by pre-T-cell receptor (pTCR) for β-selection and T-cell receptor (TCR) for positive/negative selection. Gene lesions with proximity to these checkpoints are found in T-ALL such as *NOTCH, FBXW7, PTEN* and *NRAS*. As shown in B-cell Precursor Leukemia, kinases of the pre-B-cell receptor signaling complex (SYK and BTK) have been validated as drug targets, but whether critical components of the pTCR/TCR signaling such as LCK or ZAP70 play a similar role in T-ALL remains unclear. LCK (lymphocyte-specific kinase) is a central molecule in pTCR/TCR signaling transduction. The important role for LCK has been shown in Chronic Lymphoblastic Leukemia, however, the role of LCK in T-ALL has not been studied.

Aims: To investigate the importance of pTCR/TCR complex for T-ALL cell proliferation and survival.

Methods: We performed limited screens targeting six components of the pTCR/TCR signaling complex *in vitro* and *in vivo* in 4 TALL cell lines and 2 T-ALL patient-derived xenografts (PDXs). To validate the screening results we conducted gene knockdown experiments in T-ALL cell lines using GFP-expressing lentiviral shRNA vectors and evaluated cell proliferation by competitive assays *in vitro* and *in vivo*. The activation and expression of LCK were determined in 11 T-ALL cell lines and 10 PDXs by qPCR, western blotting and Phosflow. The kinase activity of LCK was abrogated using Dasatinib. Synergism between Dexamethasone and Dasatinib was evaluated by drug matrix assays. The *ex-vivo* expansion of PDXs was achieved by co-culture with OP9-DL1 feeder cells and proliferation was assessed by Cell Trace Violet.

Results: A targeted *in vitro* and *in vivo* shRNA screen targeting central components of the pTCR/TCR signalling complex (*PTCRA, CD3ε, LCK, FYN, ZAP70* and *LAT*) in T-ALL cell lines and PDXs identified LCK to be crucial for T-ALL maintenance and engraftment. Knockdown of LCK in SUP-T1, CUTLL1 and MOLT4 cells revealed a significant loss of at least 50% of GFP^+/*LCK* shRNA transduced cells over a time period of 2-3 weeks. This was also confirmed *in vivo* in competitive assays with MOLT4 cells showing a growth advantage of control shNTC cells over LCK knockdown cells in bone marrow, spleen and liver. Mechanistic analyses indicate that knockdown or inhibition of LCK by Dasatinib impairs cell proliferation by inducing G1/G0 arrest in both TALL cell lines and PDXs, but has little effect on the induction of cell death. The sensitivity of T-ALL cell lines towards Dasatinib seems to correlate positively with activated LCK (LCK p-Y394). Moreover, *LCK* knockdown significantly sensitizes T-ALL cells to Dexamethasone (Dex) and strong synergistic lethal effects between Dex and Dasatinib have been observed in various T-ALL cell lines and PDXs. Importantly, both Dex-sensitive and Dex-resistant T-ALLs are highly sensitive to Dex/Dasatinib combination treatment. To evaluate this further we currently perform a randomized phase-Ⅱ like mini-trial in NSG mice with 10 PDXs comparing four treatment arms including control, Dex, Dasatinib and combination.

Summary/Conclusion: Overall, our data demonstrate that LCK plays a critical role in T-ALL cell proliferation and engraftment.
LCK inhibition with Dasatinib, in conjunction with Dex, reverses glucocorticoid resistance and induces cell death. The Dex/Dasatinib combination might provide a novel treatment strategy for refractory and relapsed T-ALL patients.

Keywords: Cell cycle progression, Drug resistance, Screening, Synergy

STOCKHOLM
23RD CONGRESS
JUNE 14 - 17 | 2018
European Hematology Association

An Essential Role for LCK in T-ALL Cell Proliferation and Survival

Yuzhe Shi* [1], Melanie Beckett[1], Helen Blair[1], Olaf Heidenreich[1], Anja Krippner-Heidenreich[1], Frederik van Delft[1]
[1]Wolfson Childhood Cancer Research Centre, Northern Institute For Cancer Research, Newcastle University, Newcastle upon Tyne, U.K.

China Scholarship Council · Newcastle University Northern Institute for Cancer Research · North of England Children's Cancer Research · JGW Patterson Foundation

INTRODUCTION

T-ALL (T-cell Acute Lymphoblastic Leukaemia) accounts for 15% of paediatric leukaemia. Although the overall outcome is favourable, this is achieved by intensive chemotherapy along with long-term and short-term side effects. Moreover, 20% of paediatric T-ALLs are refractory or relapse; their outcome is very poor. Therefore, it is urgent to develop novel drug targets and combinatorial therapies for T-ALL patients.

The pre-T cell receptor (pTCR) and T-cell Receptor (TCR) signalling complexes are crucial for T-cell development, survival and proliferation. Genetic characterisation has identified mutations that occur both up and downstream of pTCR/TCR signalling. LCK (Lymphocyte-specific kinase) is a central component of both signalling complexes. The pTCR/TCR and pBCR/BCR complexes share many similarities. SYK and BTK (two central kinases of pBCR signalling) have been validated as promising drug targets in BCP-ALL. However, whether key components of pTCR/TCR signalling are critical for T-ALL maintenance remains unclear.

RESULT

Targeted shRNA screens identify LCK as a key component for leukaemia propagation.

(A-C) Depleted and enriched shRNAs during T-ALL cell line propagation (p-value vs slope (changes over time)).
(D) Heatmap of depleted and enriched individual shRNA in four T-ALL cell lines.
(E) Schematic of the *in vivo* limited screen in patient-derived xenograft (PDX) L963.
(F-H) The *in vivo* screen identified shLCK#3 as the most significantly depleted construct in bone marrow and spleen.

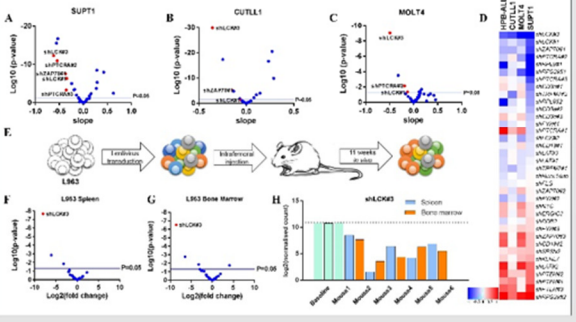

RESULT

Verification of LCK as a critical factor for the maintenance of T-ALL cells *in vitro* and *in vivo*. Knockdown or inhibition of LCK leads to G0/G1 arrest in T-ALL cells.

(A,B) Efficient knockdown of *LCK* in T-ALL cell lines results in LCK protein reduction and diminishes LCK activation (p-Y394).
(C) Knockdown of LCK, ZAP70 or pTCRα leads to proliferation reduction in T-ALL cell lines.
(D) *In vivo* competitive engraftment assay demonstrates that LCK plays a critical role in leukaemia propagation.

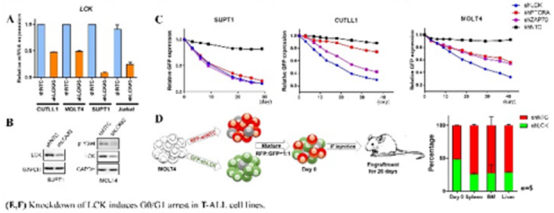

(F,F) Knockdown of LCK induces G0/G1 arrest in T-ALL cell lines.
(G) A reduction of *CCND3* can be observed after LCK knockdown.
(H-J) Knockdown of LCK in PDX L963 leads to the reduction of S phase over time and cell proliferation *ex vivo*.

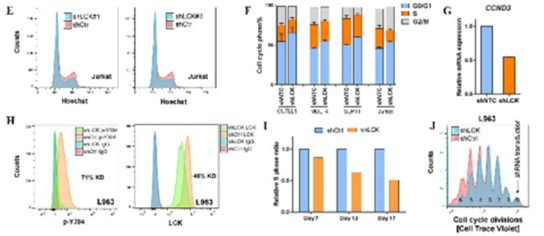

(K) The Src-family kinase inhibitor Dasatinib diminishes LCK activation (p-Y394) and induces cell cycle arrest in T-ALL cells.
(L) Dasatinib treatment reduces *CCND3* mRNA expression.
(M) In T-ALL cell lines, LCK activation (p-Y394) is positively correlated with Dasatinib sensitivity.

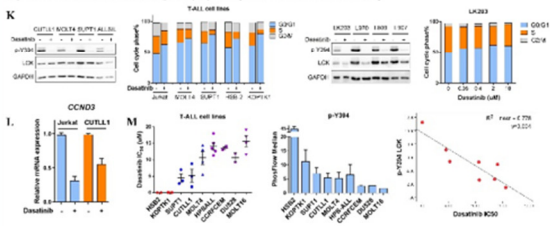

RESULT

The combination of Dasatinib and Dexamethasone shows strong synergism in T-ALL cells.

(A) LCK knockdown cells are re-sensitised to Dexamethasone (DEX) and show greater *GILZ* induction after DEX treatment.
(B) 72h drug matrix assays reveal synergy between Dasatinib and Dexamethasone at clinical relevant concentrations.
(C,D) Drug matrix analyses indicate that both DEX-sensitive and DEX-resistant PDXs respond synergistically to Dasatinib/DEX treatment.

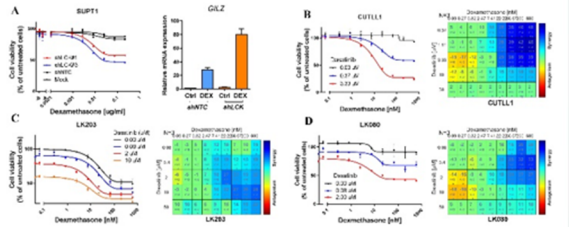

A Phasel-like Trial in mice demonstrates Dasatinib and Dexamethasone synergistically impair leukaemia progression *in vivo* (work in progress).

(A) Schematic of randomised mini-trial. 10 PDXs are each injected into 4 mice , 1 mouse per randomly assigned treatment arm.
(B) The combination of Dasatinib and DEX significantly reduces leukaemia burden in peripheral blood (end-point), bone marrow and spleen.
(C) Mouse spleen weight for 5 PDX samples across 4 treatment arms.
(D) Peripheral blood monitoring of leukaemic engraftment over time. Dasatinib and DEX synergistically impair leukaemia engraftment.

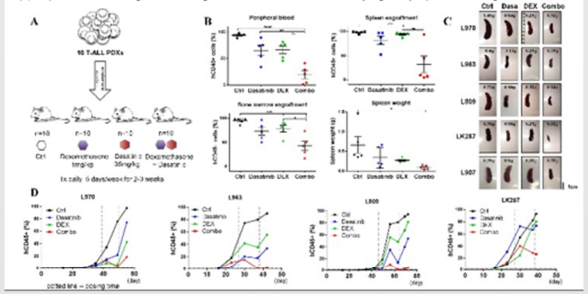

CONCLUSION

LCK plays an important role in T-ALL proliferation and maintenance as shown by targeted shRNA screen of TCR components and competitive assays *in vitro* and *in vivo*. Knockdown of LCK or inhibition by Dasatinib impairs cell proliferation by inducing G0/G1 arrest. Combination treatment with Dasatinib and Dexamethasone reveals strong synergistic effects on *in vitro* and *in vivo* survival of DFX-sensitive and DEX-resistant T-ALLs. Overall, our data identify a crucial role for LCK in T-ALL proliferation and propagation. The *in vivo* synergism between Dexamethasone and Dasatinib indicates the potential for the development of combination therapies.

Phase II-like murine trial identifies synergy between Dexamethasone and Dasatinib in T-cell Acute Lymphoblastic Leukemia

Yuzhe Shi[1], Melanie C Beckett[1], Helen J Blair[1], Ricky Tirtakusuma[1], Sirintra Nakjang[1], Amir Enshaei[1], Christina Halsey[2], Josef Vormoor[3], Olaf Heidenreich[1,3], Anja Krippner-Heidenreich[3]* and Frederik W van Delft[1]*

[1]Wolfson Childhood Cancer Research Centre, Northern Institute for Cancer Research, Newcastle University, Herschel Building, Brewery Lane, Newcastle upon Tyne, United Kingdom

[2]Wolfson Wohl Cancer Research Centre, Institute of Cancer Sciences, College of Medical, Veterinary and Life Sciences, University of Glasgow, Glasgow, United Kingdom

[3]Prinses Máxima Centrum voor Kinderoncologie, Utrecht, The Netherlands

*AKH and FWvD contributed equally to this work and are joint corresponding authors.

Anja Krippner-Heidenreich PhD

E: A.Krippner@prinsesmaximacentrum.nl

Phone +31 8897 25063

Frederik W van Delft MD PhD FRCPCH

E: Frederik.van-Delft@newcastle.ac.uk

Phone + 44 191 208 2231

Running title DEX and DAS impair *in vivo* T-ALL propagation

Main body of text word count 4,009 words

Figure count 7

Supplemental pdf file 1

Reference count 35

Abstract

T-cell Acute Lymphoblastic Leukemia (T-ALL) is frequently characterized by glucocorticoid (GC) resistance, which is associated with inferior outcomes, thus highlighting the need for novel therapeutic approaches for GC resistant T-ALL. The pTCR/TCR signaling pathways play a critical role in cell fate decisions during physiological thymocyte development, with an interplay between TCR and glucocorticoid receptor (GR) signaling determining the T-lymphocyte selection process. We performed an shRNA screen *in vitro* and *in vivo* in T-ALL cell lines and patient derived xenograft (PDX) samples to identify vulnerabilities in the pTCR/TCR pathway and identified a critical role for the kinase LCK in cell proliferation. LCK knockdown or inhibition with dasatinib (DAS) caused cell cycle arrest. Combination of DAS with dexamethasone (DEX) resulted in significant drug synergy leading to cell death. The efficacy of this drug combination was underscored in a randomized phase II-like murine trial, recapitulating an early phase human clinical trial. T-ALL expansion in immunocompromised mice was significantly impaired using this drug combination, relative to mice receiving control vehicle or single drug treatment, highlighting the immediate clinical relevance of this drug combination for high risk T-ALL patients. Our results thus provide a strategy to improve the efficacy of current chemotherapy platforms and circumvent GC resistance.

Introduction

Current minimal residual disease (MRD) stratified chemotherapy protocols for patients with T-ALL result in 5-year event free survival rates of 80% and 50% for pediatric and adult patients respectively (1, 2). Induction failure, early relapse and isolated central nervous system involvement are more common in T than B-lineage ALL (3). Moreover, resistance to conventional chemotherapy including GC is a frequent feature of relapsed and refractory T-ALL, reducing the second remission rate and long term outcomes (4). GC are an instrumental component of ALL therapy and induce apoptosis in lymphoid malignancies (5-7). Resistance to GC is a critical factor influencing treatment response and outcome (5, 8-11). Amongst ALL subtypes, GC resistance is more frequently observed in infant ALL and T-ALL (5, 9, 11, 12).

Endogenous GC can induce apoptosis during the selection process of T-lymphocytes in the thymus, an effect which can be constrained by crosstalk with T cell receptor (TCR) signaling (13, 14). Whilst mature T-cell maintenance requires tonic TCR signaling, inappropriate TCR expression has been shown to give rise to T-cell malignancies in mouse model systems (15, 16).

The immature pre T-cell receptor (pTCR) consists of a complex of alpha (pTCRα) and beta (TCRβ) peptide chains complexed with CD3□□ and CD3□□ heterodimers. Activation of this complex occurs through the Src family kinase (SFK) members Lymphocyte Cell-Specific Protein-Tyrosine Kinase (LCK) and FYN. They are critical modulators of T-cell development and activation (17). LCK phosphorylates the plasma membrane associated TCR complex (18) and ZAP70 (19). ZAP70 in turn phosphorylates the linker for activation of T-cells (LAT) leading to the activation of downstream signaling cascades. The overall activity of LCK is regulated by the phosphorylation status of the activating and inhibitory tyrosine residues 394 and 505 respectively (20). LCK activation correlates with SrcY416 phosphorylation, as the latter overrides the inhibitory effects of Y505 phosphorylation (21).

We hypothesized therefore that T-ALL continues to rely on proliferative and survival stimuli inherent to the TCR signaling pathway, which, if inhibited, may enhance GC sensitivity. A targeted shRNA screen directed against components of the TCR signaling initiation complex identified a crucial role for LCK in T-ALL proliferation, both *in vitro* and *in vivo*. The anti-proliferative effects of LCK knockdown could be replicated by using the small molecule inhibitor DAS. Drug synergy was observed using DAS in combination with DEX on patient derived xenograft (PDX) cell survival *in vitro.* Mirroring the design of early phase human trials, a murine phase II-like trial demonstrated significantly impaired leukemia progression *in vivo* using combination treatment. Our results present a clear rationale for using DAS in conjunction with DEX to enhance conventional chemotherapeutic treatment and revert glucocorticoid resistance in pediatric T-ALL patients.

Methods

Patient samples

The patient derived material was collected as part of diagnostic investigations of patients at the Great North Children's Hospital, Department of Paediatric Haematology and Oncology, Newcastle upon Tyne, United Kingdom. The material was collected and stored with informed consent obtained from all subjects in accordance with the Declaration of Helsinki.

Samples with explicit written consent for *in vivo* studies were requested from the Newcastle Biomedicine Biobank, Newcastle University, United Kingdom and used according to approvals given by the Newcastle Biomedicine Biobank (NHB application NHB-008) and the local institutional review board Newcastle & North Tyneside Ethics Committee (REC reference: 07/H0906/109).

Patient-derived xenografts (PDXs) were harvested from the NOD.Cg-PrkdcscidIl2rgtm1wjl/SzJ (NSG, Charles River labs and bred in-house) mice after the engraftment of patient samples. PDXs were co-cultured *ex vivo* with OP9-DL1 in StemSpan Serum-Free Expansion Medium II (STEMCELL, UK) supplemented with human IL7 (10 ng/ml) and SCF (100 ng/ml) (both PeproTech, UK).

Drug matrix assays

Dasatinib (9 nM – 30 μM) (DC Chemicals, Shanghai, China) was titrated on T-ALL cell lines (4 x 10^4/well) in 96-well plates (Corning, NY, USA). Cell viability was assessed after 3 days using Cell Counting Kit 8 (NBS Biologicals, Cambridgeshire, UK). The absorbance was measured at OD450 nm using a POLARstar Omega plate reader (BMG LABTECH, Bucks, UK). IC_{50} values were determined by GraphPad Prism. Assays were performed in triplicate and at least 3 independent repeats were performed.

For DAS/DEX combination treatments DAS (80 nM – 50 μM) and DEX (0.09 nM – 600 nM) were titrated in 2-dimensions on T-ALL cell lines (4 x 10^4 cells / 96-well) or *ex vivo* expanded PDX cells (8 x 10^4 cells / 96-well). *Ex vivo* expansion was achieved after co-culture with OP9-DL1 for 1 week, after which cells were separated from their feeders by repetitive transfer and subsequently plated. After 72h of culture, the plates were developed as above. Drug synergy was determined using Combenefit software (v2.021) (22).

Phase II-like Murine Trial

For each of the 10 patient derived xenograft (PDX) samples, 8 x 10^6 cells were intrafemorally (IF) injected into 4 NSG mice (40 mice in total) under isoflurane anesthesia. The 4 NSG mice derived from one PDX sample were matched for gender and age. T-ALL engraftment in mouse peripheral blood was monitored weekly by tail vein bleeds (20 µl blood/mouse). The four mice of each PDX were randomized to receive control vehicle, DAS (35 mg/kg), DEX (1 mg/kg) or DEX/DAS combination by intraperitoneal (IP) injection upon engraftment, defined as ≥ 0.5% peripheral blood hCD45+/hCD7+ cells. The median treatment duration of these mice was 15 days, depending on the clinical status. When any of the four mice displayed signs of ill health or weight loss, all four mice derived from this PDX were killed at the same time to assess leukemia engraftment in bone marrow, blood, spleen, liver and central nervous system (CNS). Spleen size and weight were recorded. Statistical analyses were performed using RStudio (MA, USA) with linear mix model. The final analysis excluded the 4 mice derived from patient sample LK214, as all mice succumbed to T-ALL before treatment was initiated.

See online supplemental file for further methods.

Results

A targeted shRNA screen of TCR pathway components identifies an essential role for LCK in T-ALL cell line and PDX proliferation *in vitro*

To explore the importance of the pTCR/TCR signaling complex in proliferation and survival of malignant T-cells, we performed a limited shRNA screen targeting 6 genes with 3 shRNAs per gene, including *LCK*, *ZAP70*, *PTCRA*, *FYN*, *CD3E* and *LAT* in 4 T-ALL cell lines (HPB-ALL, CUTLL1, MOLT4, SUPT1), and included 18 control shRNAs (see Supplementary Methods)(Supplementary Table 1). *In silico* analysis, using the Cancer Cell Line Encyclopedia (CCLE), demonstrated that these 6 genes are highly expressed in a panel of T-ALL cell lines (Supplementary Figure 1A). *LCK* and *PTCRA* expression was confirmed by targeted gene expression analysis in T-ALL cell lines and patient samples (Figure 1B)(Supplementary Figure 1B). The limited shRNA screen revealed the shLCK#3 construct targeting *LCK* was the only construct

significantly depleted in all 4 cell lines, when compared with base line shRNA integration, underlining an important role for LCK in T-ALL cell line proliferation and/or survival (Figure 1A)(Supplementary Figure 1C-D). The shLCK#1, shZAP70#1 and shPTCRA#2 constructs were lost in 3 out of 4 cell lines. Constructs targeting *FYN*, *CD3E*, or *LAT* were significantly depleted in one cell line only, suggesting that these molecules do not play an universal role in T-ALL cell proliferation. ShRNAs against essential ribosomal genes were predictably depleted, whilst all 3 shRNA constructs targeting the tumor suppressor *PTEN* were enriched as expected. Repeated sampling at 16, 30 and 40 days after transduction demonstrated progressive depletion of shRNA constructs targeting *LCK* and *ZAP70* (Supplementary Figure 1E)(Supplementary Table 2). PDX LK203 showed good viability (≥75%) and proliferation potential (Td = 2.8 days) in co-culture with human Mesenchymal Stem Cells (hMSC), hence subjected to shRNA screening. ShRNA sequencing 30 days after transduction confirmed all constructs targeting LCK were significantly depleted (Figure 1)(Supplementary Figure 1F)(Supplementary Table 3).

Knockdown of LCK in T-ALL cell lines confirms an essential role for LCK *in vitro* propagation.

To confirm the role of LCK and other components of the pTCR/TCR signaling complex in cell proliferation, competitive outgrowth assays were performed. SUPT1, MOLT4 and CUTLL1 cells were transduced with lentiviral shRNAs targeting *LCK*, *ZAP70*, *FYN*, *PTCRA* or non-targeting control shRNAs. Successfully transduced cells expressing green fluorescence protein (GFP) were seeded in a 1:1 ratio with parental cells.

Three shRNAs were used to silence LCK, of which shLCK#3 achieved the greatest degree of knockdown. Lentiviral knockdown with shLCK#3 led to significant reduction in mRNA in SUPT1 (75%KD), MOLT4 (55% KD) and CUTLL1 (45% KD) cells (Figure 2A). Generally, greater knockdown was associated with more pronounced impairment of *in vitro* proliferation (Figure 2B). *LCK* expression was confirmed at protein level, demonstrating ubiquitous expression of LCK in cell lines (Supplementary Figure 1G). In line with mRNA downregulation, knockdown of *LCK* led to decreased total LCK protein expression (Figure 2A). Non-transduced cells consistently outcompeted LCK

knockdown cells resulting in a pronounced loss of over 70% transduced GFP$^+$ cells in all 3 cell lines, underlining the critical and universal role of LCK in T-ALL cell line maintenance (Figure 2B)(Supplementary Figure 2A).

A similar, but less significant, observation was made for *ZAP70* knockdown in SUPT1, MOLT4 and CUTLL1 cells. Efficient *ZAP70* knockdown correlated with a pronounced proliferation defect (Supplementary Figure 2A). Knockdown of *PTCRA* affected proliferation in pTCRα$^+$ MOLT4 and SUPT1, but not in pTCRa$^-$ CUTLL1 (Supplementary Figure 2A). Moreover, *FYN* knockdown did not affect proliferation in any of the cells lines despite efficient knockdown (Supplementary Figure 2B).

Knockdown of LCK in T-ALL cell lines and PDX samples impairs leukemia propagation *in vivo*.

To confirm a functional role for LCK *in vivo*, PDX L963 cells were transduced with our shRNA library and transplanted into 6 NSG mice (Figure 3A)(Supplementary Figure 3A). Genomic DNA (gDNA) was extracted from L963 cells isolated from bone marrow and spleen after mice became symptomatic (week 11). ShRNA sequencing indicated that shLCK#3 represented the most significantly depleted shRNA construct *in vivo* (Figure 3A)(Supplementary Figure 3B)(Supplementary Table 3).

To assess the effect of LCK knockdown on engraftment fitness, MOLT4 cells were transduced with lentiviral vectors encoding either red fluorescent protein RFP/shNTC (non-targeting control) or GFP/shLCK#3. Equal proportions of cell populations were transplanted into NSG mice (n = 5). Leukemia cells were isolated from spleen, bone marrow and liver once mice were symptomatic (day 26). Flow cytometric analysis of the leukemic cell population established that cells carrying shNTC had a clear competitive engraftment advantage over cells with LCK knockdown in all mice tissues sampled (Figure 3B)(Supplementary Figure 3C).

Knockdown of LCK leads to cell cycle arrest in T-ALL cell lines and PDX samples

Next we investigated the mechanisms underlying the defect in proliferation, survival and engraftment observed after LCK knockdown. Jurkat, MOLT4 and SUPT1 cells

were transduced with shLCK#1/#3 and cell cycle analyses performed. In all cell lines, we observed significant cell cycle arrest with an increase in G_0/G_1 phase and decrease in S phase after LCK knockdown (Figure 4A-C) (Supplementary Figure 4A).

ShLCK#3 led to decreased protein levels of total LCK and activated p-Y416^{Src} in cell lines, suggesting activation status of LCK is associated with cell cycle arrest. In PDX L963, LCK knockdown led to a 45% reduction in total LCK expression, as well as 71% reduction in p-Y416^{Src} as assessed by Phosflow (Figure 4D). This knockdown resulted in a decrease in S phase over time compared to control (Supplementary Figure 4B). The proliferative behavior of PDX cells was analyzed after labeling with cell trace violet (CTV). PDX L963 cells were transduced with shRNA constructs targeting LCK or a non-targeting control (NTC) and co-cultured with OP9-DL1 feeder cells for 13 days. The LCK knockdown cells showed restricted proliferation compared to the control cells (Figure 4E). Confirmatory siRNA knockdown of LCK was undertaken in PDX samples LK203 and L963. Knockdown of total and activated LCK was confirmed by Phosflow. Corroborating our earlier findings, cell cycle arrest was observed (Supplementary Figure 4C-D).

Knockdown of LCK was analyzed for early apoptosis induction in CUTLL1, MOLT4, SUPT1 and Jurkat. Although a clear increase in Annexin V staining was observed in MOLT4, suggesting LCK knockdown led to apoptosis, this was not observed in CUTLL1, Jurkat or SUPT1 (Supplementary Figure 4E). This suggests that cell cycle arrest, rather than apoptosis induction, is the predominant effect leading to diminished cell expansion *in vitro* and reduced propagation *in vivo* after LCK knockdown.

The tyrosine kinase inhibitor DAS blocks LCK function and leads to cell cycle arrest. LCK activation levels predict response to LCK inhibition.

The tyrosine kinase inhibitor DAS is a dual SRC/ABL inhibitor known to effectively inhibit LCK (21). The effect of DAS on LCK protein expression and activation status was assessed by Western Blot, after demonstrating near universal LCK activation as evidenced by tyrosine residue 416 phosphorylation in cell lines (Supplementary Figure 1G). We confirmed that DAS effectively abolished activated p-Y416^{Src} in all 4 T-ALL cell lines tested, whilst slightly decreasing total LCK protein levels. Furthermore, dephosphorylation of inhibitory p-Y505^{LCK} was noted, as well as a decrease in p-

Y783$^{PLC\gamma1}$ and p-Y493^{ZAP70}, two downstream targets of LCK (Figure 5A)(Supplementary Figure 5A). As knockdown of LCK leads to cell cycle arrest, we performed cell cycle analyses after administration of DAS. Cell cycle arrest was observed in all 6 T-ALL cell lines tested, with a significant increase in G_0/G_1 and decrease in S phase (Figure 5A)(Supplementary Figure 5B). In parallel, PDX cells supported by *in vitro* co-culture with OP9-DL1 were exposed to DAS. In line with our cell line data, DAS abolished activated p-Y416^{Src} levels in all 6 PDX samples (Figure 5B)(Supplementary Figure 5C) and cell cycle arrest was observed in all 3 PDX samples tested (Figure 5B)(Supplementary Figure 5D).

The *in vitro* sensitivity of a panel of 9 T-ALL cell lines to DAS was determined. The IC_{50} observed ranged from 5 nM (HSB2) to 15 µM (MOLT16) (Figure 5C). The cell line HSB2 not only demonstrated the highest sensitivity to DAS but also the highest p-Y416^{Src} activation level as determined by Phosflow. This observation can be explained by the presence of a t(1;7)(p34;q34) translocation leading to LCK activation by T cell receptor beta (TRB) enhancer elements in HSB2 (Figure 5C). We thus hypothesized that the level of activated LCK might represent a biomarker for DAS responsiveness. Phosflow was used to quantify and calculate the ratio between p-Y416^{Src} and total LCK (Figure 5C). A strong and significant correlation was observed between the IC_{50} for DAS and the ratio of activated Y416^{Src} in T-ALL cell lines (R^2=0.778, p=0.004) (Figure 5C). The sensitivity of PDX cells to DAS ranged from GI_{50} of 23.8 nM to 19.7 µM (median of 1.2 µM). However, in this setting, no significant correlation between the GI_{50} and p-Y416^{Src}/LCK ratio was identified, suggesting that DAS sensitivity of patient-derived cells is dependent on additional factors (Supplementary Figure 5E).

DAS re-sensitizes DEX resistance in T-ALL cell lines and PDX samples

DAS leads to complete inhibition of p-Y416^{Src} and cell cycle arrest in T-ALL cell lines and PDX cells, suggesting that DAS treatment of T-ALL has a cytostatic effect. In clinical practice, effective eradication of T-ALL relies on the application of combinatorial treatment. LCK inhibition has previously been shown to sensitize chronic lymphoid leukemia (CLL) to DEX and induce cell death (23). We thus went on to investigate potential synergy between LCK inhibition and DEX, as DEX is universally used for treatment of ALL. The cell viability of SUPT1 and CUTLL1, in the presence of

DEX, was evaluated after knockdown of LCK. Whereas the cell viability of mock transduced and non-targeting control cells was minimally affected by DEX treatment, LCK knockdown increased DEX sensitivity suggesting that LCK protein and/or activity levels play a crucial role in glucocorticoid resistance (Figure 6A)(Supplementary Figure 6A).

A more detailed analysis of the potency of the combination of DEX and LCK inhibition was examined by using DAS instead of the LCK knockdown. DEX (0-600 nM) and DAS (0-50 μM) were titrated along a dose matrix and cell viability was determined. Synergy for individual drug combinations was determined using Combenefit (22). The matrix revealed drug synergy at concentrations which are clinically achieved, i.e. 100 nM for DEX and 264 nM for DAS (Figure 6B)(Supplementary Figure 6B) (24, 25). Bioinformatic analysis of all 10 T-ALL cell lines revealed a statistically significant enrichment of drug synergy at clinically relevant concentrations. This synergy was observed at 8-110 nM of DEX and 0.223-4.5 μM of DAS (Supplementary Figure 6C-D).

Subsequently, PDX cells were expanded *ex vivo* for 1 week and exposed to the same drug combinations in dose matrices. These assays verified the synergistic action of DEX+DAS in a wide range of PDX cells, whilst confirming that increased DAS concentrations and resultant LCK inhibition augmented the response to DEX (Figure 6C)(Supplementary Figure 6E). Combined analysis of all drug matrices with PDX cells again revealed a statistically significant enrichment of drug synergy at clinically relevant concentrations (Supplementary Figure 6F). Moreover, the combination of DEX+DAS induced more cell death compared with control vehicle or single drugs as revealed by Annexin V/PI staining (Figure 6C).

DEX has a wide range of actions, including genomic and non-genomic effects. Genomic effects are the result of nuclear translocation of the glucocorticoid receptor and subsequent transactivation or repression of genes containing a glucocorticoid response element (GRE), as exemplified by the *Glucocorticoid-Induced Leucine Zipper* (*GILZ*) gene. Accordingly, we observed strong induction of *GILZ* gene expression after DEX exposure in the T-ALL cell line Jurkat and 5 PDX samples tested (Figure 6D)(Supplementary Figure 6G). This response was significantly enhanced when combining DEX with knockdown of LCK (Figure 6D, left) or DEX+DAS in a range

of T-ALL cell lines and PDX samples, suggesting that LCK inactivation augments DEX-induced gene transcription and reverses DEX resistance (Figure 6D)(Supplementary Figure 6G).

Phase II-like trial *in vivo* demonstrates significant reduction in leukemia burden after combination treatment with DEX and DAS

To test the efficacy of DEX and DAS *in vivo*, we conducted a phase II-like trial in mice (Figure 7A) (26). Ten PDXs were engrafted in 4 mice each. The 4 mice derived from 1 single patient sample were randomly assigned to treatment arms, namely control vehicle, DEX (1 mg/kg), DAS (35 mg/kg) or DEX+DAS (1 mg/kg DEX + 35 mg/kg DAS). After IF injection, mice tail vein blood was monitored weekly for human CD7/CD45 and murine CD45 expression to monitor peripheral blood engraftment. Representative PDX L809 commenced treatment 46 days after injection for a total duration of 3 weeks; the 4 mice were culled 72 days after injection (Figure 7B). L809 cells engrafted in the spleens of the 4 mice showed greatly reduced levels of total LCK and dephosphorylation of LCK (p-Y416^{Src} and p-Y505) after DAS or DEX+DAS combination treatment (Figure 7C). Western analysis of positively selected viable human cells again demonstrated decreased protein expression of LCK and p-Y416^{Src} after DAS treatment. The number of residual viable human cells after effective DEX+DAS treatment was not sufficient to categorically confirm reduced protein expression (Supplementary Figure 7F). One mouse in DAS arm (LK080) developed uterine prolapse before dosing commenced and the mice derived from PDX LK214 succumbed during first week of treatment. These 5 were excluded from final analysis. Combining the results of 35 mice derived from 9 patient samples, DEX+DAS treatment significantly impaired leukemia progression more than single drug DEX, DAS or control vehicle as measured by hCD45 or hCD7 engraftment in peripheral blood, bone marrow, spleen and CNS (Figure 7D-F)(Supplementary Figure 7A). Single agent DEX reduced CNS leukemia burden in 7/9 samples, reflecting its proven efficacy in reducing CNS relapses (27), whilst DAS showed some reduction in CNS burden in 4/8 samples (Supplementary Figure 7B). Combination therapy was particularly effective, with complete eradication of measurable CNS leukemia in 5 patient samples and evidence of an additive effect with DEX in 3 out of 4 of the remaining patient samples

(Supplementary Figure 7B). When considering the cohort of nine patient samples overall, combination treatment significantly reduced leukemic infiltrates compared to control (p=0.02). Representative histology images are shown in Figure 7G. Spleen weight was substantially reduced in mice receiving combination treatment, compared with the single or control treatment arms (Supplementary Figure 7C-D). DEX+DAS also significantly reduced $hCD45^+$ or $hCD7^+$ leukemia cell engraftment in liver tissue of all 6 PDX samples analyzed (Supplementary Figure 7E). The initial therapeutic advantage of DEX+DAS in mice derived from PDX LK080 was lost at the end of the experiment, most likely because these mice were kept alive for 3 weeks after completion of treatment. In the case of L907 however, the benefit of combination treatment was not observed until the last time point (Supplementary Figure 7G).

Discussion

Using a phase II-like murine trial, we demonstrate here the efficacy of the drug combination DEX+DAS in impairing expansion of human T-ALL samples. This effect is apparent in an unselected, biologically heterogeneous, cohort of PDX samples. This trial format recapitulates early phase human clinical trials and indicates that this drug combination could be widely applicable in the treatment of T-ALL. Studies by Serafin *et al* first proposed a role for this drug combination (28). Our murine trial extends these initial observations with an extensive cohort consisting of 9 different PDXs demonstrating treatment advantage for both DEX sensitive and resistant T-ALL.

Significant superiority of DEX+DAS was demonstrated even after exclusion of mice, who reached their clinical end points prematurely. These untoward events highlight the practicalities of performing murine trials.

We propose that the impaired *in vivo* expansion results from a combination of cell cycle arrest as well as cell death. Several mechanisms could provide plausible explanations for the occurrence of cell cycle arrest. DAS is a protein tyrosine kinase inhibitor which targets Abl and SFK family members. We have confirmed that DAS effectively inhibits activity of the SFK member LCK by preventing phosphorylation, leading to G_0/G_1 arrest. DAS has previously been shown to inhibit cyclin dependent kinase 1 (CDK1), which plays a central role in G_1/S and G_2/M transition (29).

Furthermore, G_1 cell cycle arrest, through upregulation of the cyclin-dependent kinase inhibitors $p21^{CIP1}$ (CDKN1A) and $p27^{KIP1}$ (CDKN1B), has been observed after DAS treatment in AML (30). We propose that LCK is the predominant target of DAS in this disease setting, as our shRNA screen identified a critical role for LCK in cell proliferation in cell lines and PDX samples. Moreover, LCK is the proposed DAS target when blocking T-cell activation (21). Competitive assays confirmed defective proliferation of T-ALL cells after LCK knockdown *in vitro* and *in vivo*. We have shown that LCK knockdown leads to G_0/G_1 cell cycle arrest in cell lines and PDXs. This effect was more pronounced using DAS, a finding which could potentially be explained by incomplete knockdown of LCK or the wide spectrum of kinases targeted by DAS.

As reported earlier and confirmed in our studies, DAS is cytotoxic to a small subset of T-ALL samples with IC_{50} values in the low nanomolar range (31). These observations were made in T-ALL samples with kinase activating mutations, which are seen very infrequently in T-ALL. To the best of our knowledge, our cohort includes only one PDX with such an activating genetic lesion (LK287, FIP1L1-PDGFRA). Cytotoxicity to DAS is significantly increased upon combination with DEX. Our data indicate drug synergy between DAS and DEX at clinically relevant concentrations. A previous, mostly *in vitro*, study advocated the use of DEX+DAS in GC resistant T-ALL (28). Our extended studies indicate DEX+DAS act synergistically in the majority of cell lines and PDXs tested independent of their prior sensitivity to DEX. The potential of DEX+DAS to revert GC resistance is an exciting observation. GC resistance is frequently observed in relapsed / refractory T-ALL (4), and DEX+DAS provide a clinically actionable approach to re-sensitize resistant T-ALL to DEX.

The implementation of DAS into clinical management would benefit from the identification of a reliable response biomarker. Although LCK activation status (ratio p-$Y416^{Src}$/LCK) strongly correlates with DAS sensitivity in cell lines, we were unable to corroborate this observation in PDX cells. Sample size and intricacies of *in vitro* assays using PDX cells could provide possible explanations for these inconsistencies. Nevertheless, *in vivo* drug synergy was observed in the majority of samples tested. Of interest, drug response profiling of T-ALL samples suggested SRC pathway activation may represent a response biomarker (31).

The mechanism underlying the observed drug synergy remains to be fully elucidated. T-cell activation can be blocked by using clinically relevant concentrations of the tyrosine kinase inhibitor DAS, which binds to the ATP-binding pocket of LCK thereby preventing the phosphorylation of the activating loop of the kinase domain p-Y416 (21, 32). When DEX is combined with DAS, physiological CD3+ T-cell proliferation is reduced in an additive way (33, 34). Furthermore, it has been previously suggested that the Calcineurin/NFAT/IL-4 axis is activated in patients exhibiting a prednisone poor response (28). We have shown here that combination of DEX+DAS significantly increases *GILZ* gene expression, reflecting increased transcriptional activity of the GC receptor. We thus hypothesize that inhibition of LCK disrupts the TCR-GR complex and established crosstalk between the TCR and GR pathways leading to dissociation and transcriptional activation of the GR (13).

To conclude, drug resistant T-ALL continues to represent an unmet clinical need. We provide further support for the inclusion of DAS in the treatment of T-ALL. It has been reported that DAS in combination with conventional chemotherapy is safe and well tolerated in children and young adults, although hematologic toxicity was significant (35). Thus, the DEX+DAS combination should be considered in early phase setting to evaluate toxicity and efficacy in patients with GC resistant disease with or without cerebral spinal fluid (CSF) involvement.

Authorship

F.W.v.D., A.K.H., Y.S. designed the research; Y.S. performed the research; Y.S., M.C.B., H.J.B. O.H. and R.T. designed and performed the *in vivo* experiments; F.W.v.D., A.K.H. and Y.S. analyzed the data and wrote the paper; S.N. and A.E. performed the bioinformatics analysis; C.H. performed brain histology and imaging; J.V., O.H. and C.H. reviewed the manuscript.

Acknowledgements

The authors would like to thank patients, parents, and hospital staff at the Great North Children’s Hospital, Newcastle upon Tyne, United Kingdom, for their valuable collaboration.

This work was supported by a Newcastle University Research Fellowship (F.W.v.D.), Chinese Scholarship Council (CSC) (Y.S.), JGW Patterson Foundation (M.C.B.), North of England Children's Cancer Research, Action Medical Research (F.W.v.D.).

The authors would like to thank Lynn Stevenson and Clare Orange, University of Glasgow, for brain histology and imaging. The brain histology slides were scanned by Glasgow University slide scanning and image analysis service at the Queen Elizabeth University Hospital, Glasgow. C.H. was funded by the Chief Scientist Office (ETM/374).

Disclosure of Conflicts of interest

The authors declare that they have no conflict of interest.

References

1. Marks DI, Paietta EM, Moorman AV, et al. T-cell acute lymphoblastic leukemia in adults: clinical features, immunophenotype, cytogenetics, and outcome from the large randomized prospective trial (UKALL XII/ECOG 2993). Blood. 2009;114(25):5136-45.

2. Patrick K, Wade R, Goulden N, et al. Outcome for children and young people with Early T-cell precursor acute lymphoblastic leukaemia treated on a contemporary protocol, UKALL 2003. Br J Haematol. 2014;166(3):421-4.

3. Goldberg JM, Silverman LB, Levy DE, et al. Childhood T-cell acute lymphoblastic leukemia: the Dana-Farber Cancer Institute acute lymphoblastic leukemia consortium experience. J Clin Oncol. 2003;21(19):3616-22.

4. Raetz EA, Borowitz MJ, Devidas M, et al. Reinduction platform for children with first marrow relapse of acute lymphoblastic Leukemia: A Children's Oncology Group Study[corrected]. J Clin Oncol. 2008;26(24):3971-8.

5. Inaba H, Pui CH. Glucocorticoid use in acute lymphoblastic leukaemia. Lancet Oncol. 2010;11(11):1096-106.

6. Pui CH, Carroll WL, Meshinchi S, Arceci RJ. Biology, risk stratification, and therapy of pediatric acute leukemias: an update. J Clin Oncol. 2011;29(5):551-65.

7. Pui CH, Mullighan CG, Evans WE, Relling MV. Pediatric acute lymphoblastic leukemia: where are we going and how do we get there? Blood. 2012;120(6):1165-74.

8. Dordelmann M, Reiter A, Borkhardt A, et al. Prednisone response is the strongest predictor of treatment outcome in infant acute lymphoblastic leukemia. Blood. 1999;94(4):1209-17.

9. Hongo T, Yajima S, Sakurai M, Horikoshi Y, Hanada R. In vitro drug sensitivity testing can predict induction failure and early relapse of childhood acute lymphoblastic leukemia. Blood. 1997;89(8):2959-65.

10. Kaspers GJ, Wijnands JJ, Hartmann R, et al. Immunophenotypic cell lineage and in vitro cellular drug resistance in childhood relapsed acute lymphoblastic leukaemia. Eur J Cancer. 2005;41(9):1300-3.

11. Klumper E, Pieters R, Veerman AJ, et al. In vitro cellular drug resistance in children with relapsed/refractory acute lymphoblastic leukemia. Blood. 1995;86(10):3861-8.

12. Pieters R, den Boer ML, Durian M, et al. Relation between age, immunophenotype and in vitro drug resistance in 395 children with acute lymphoblastic leukemia--implications for treatment of infants. Leukemia. 1998;12(9):1344-8.

13. Jamieson CA, Yamamoto KR. Crosstalk pathway for inhibition of glucocorticoid-induced apoptosis by T cell receptor signaling. Proc Natl Acad Sci U S A. 2000;97(13):7319-24.

14. Ashwell JD, King LB, Vacchio MS. Cross-talk between the T cell antigen receptor and the glucocorticoid receptor regulates thymocyte development. Stem Cells. 1996;14(5):490-500.

15. Cui Y, Onozawa M, Garber HR, et al. Thymic expression of a T-cell receptor targeting a tumor-associated antigen coexpressed in the thymus induces T-ALL. Blood. 2015;125(19):2958-67.

16. Serwold T, Hochedlinger K, Swindle J, Hedgpeth J, Jaenisch R, Weissman IL. T-cell receptor-driven lymphomagenesis in mice derived from a reprogrammed T cell. Proc Natl Acad Sci U S A. 2010;107(44):18939-43.

17. Palacios EH, Weiss A. Function of the Src-family kinases, Lck and Fyn, in T-cell development and activation. Oncogene. 2004;23(48):7990-8000.

18. Iwashima M, Irving BA, van Oers NS, Chan AC, Weiss A. Sequential interactions of the TCR with two distinct cytoplasmic tyrosine kinases. Science. 1994;263(5150):1136-9.

19. van Oers NS, Killeen N, Weiss A. Lck regulates the tyrosine phosphorylation of the T cell receptor subunits and ZAP-70 in murine thymocytes. J Exp Med. 1996;183(3):1053-62.

20. Nyakeriga AM, Garg H, Joshi A. TCR-induced T cell activation leads to simultaneous phosphorylation at Y505 and Y394 of p56(lck) residues. Cytometry A. 2012;81(9):797-805.

21. Lee KC, Ouwehand I, Giannini AL, Thomas NS, Dibb NJ, Bijlmakers MJ. Lck is a key target of imatinib and dasatinib in T-cell activation. Leukemia. 2010;24(4):896-900.

22. Di Veroli GY, Fornari C, Wang D, etal. Combenefit: an interactive platform for the analysis and visualization of drug combinations. Bioinformatics. 2016;32(18):2866-8.

23. Harr MW, Caimi PF, McColl KS, et al. Inhibition of Lck enhances glucocorticoid sensitivity and apoptosis in lymphoid cell lines and in chronic lymphocytic leukemia. Cell Death Differ. 2010;17(9):1381-91.

24. Liston DR, Davis M. Clinically Relevant Concentrations of Anticancer Drugs: A Guide for Nonclinical Studies. Clin Cancer Res. 2017;23(14):3489-3498.

25. Yang L, Panetta JC, Cai X, et al. Asparaginase may influence dexamethasone pharmacokinetics in acute lymphoblastic leukemia. J Clin Oncol. 2008;26(12):1932-9.

26. Townsend EC, Murakami MA, Christodoulou A, et al. The Public Repository of Xenografts Enables Discovery and Randomized Phase II-like Trials in Mice. Cancer Cell. 2016;30(1):183.

27. Mitchell CD, Richards SM, Kinsey SE, Lilleyman J, Vora A, Eden TO, Medical Research Council Childhood Leukaemia Working P. Benefit of dexamethasone compared with prednisolone for childhood acute lymphoblastic leukaemia: results of the UK Medical Research Council ALL97 randomized trial. Br J Haematol. 2005;129(6):734-45.

28. Serafin V, Capuzzo G, Milani G, et al. Glucocorticoid resistance is reverted by LCK inhibition in pediatric T-cell acute lymphoblastic leukemia. Blood. 2017;130(25):2750-2761.

29. Kruewel T, Schenone S, Radi M, et al. Molecular characterization of c-Abl/c-Src kinase inhibitors targeted against murine tumour progenitor cells that express stem cell markers. PLoS One. 2010;5(11):e14143.

30. Guerrouahen BS, Futami M, Vaklavas C, et al. Dasatinib inhibits the growth of molecularly heterogeneous myeloid leukemias. Clin Cancer Res. 2010;16(4):1149-58.

31. Frismantas V, Dobay MP, Rinaldi A, et al. Ex vivo drug response profiling detects recurrent sensitivity patterns in drug-resistant acute lymphoblastic leukemia. Blood. 2017;129(11):e26-e37.

32. Schade AE, Schieven GL, Townsend R, et al. Dasatinib, a small-molecule protein tyrosine kinase inhibitor, inhibits T-cell activation and proliferation. Blood. 2008;111(3):1366-77.

33. Nerreter T, Distler E, Kochel C, Einsele H, Herr W, Seggewiss-Bernhardt R. Combining dasatinib with dexamethasone long-term leads to maintenance of antiviral and antileukemia specific cytotoxic T cell responses in vitro. Exp Hematol. 2013;41(7):604-614 e4.

34. Smith LK, Cidlowski JA. Glucocorticoid-induced apoptosis of healthy and malignant lymphocytes. Prog Brain Res. 2010;182:1-30.

35. Slayton WB, Schultz KR, Kairalla JA, et al. Dasatinib Plus Intensive Chemotherapy in Children, Adolescents, and Young Adults With Philadelphia Chromosome-Positive Acute Lymphoblastic Leukemia: Results of Children's Oncology Group Trial AALL0622. J Clin Oncol. 2018;36(22):2306-2314.

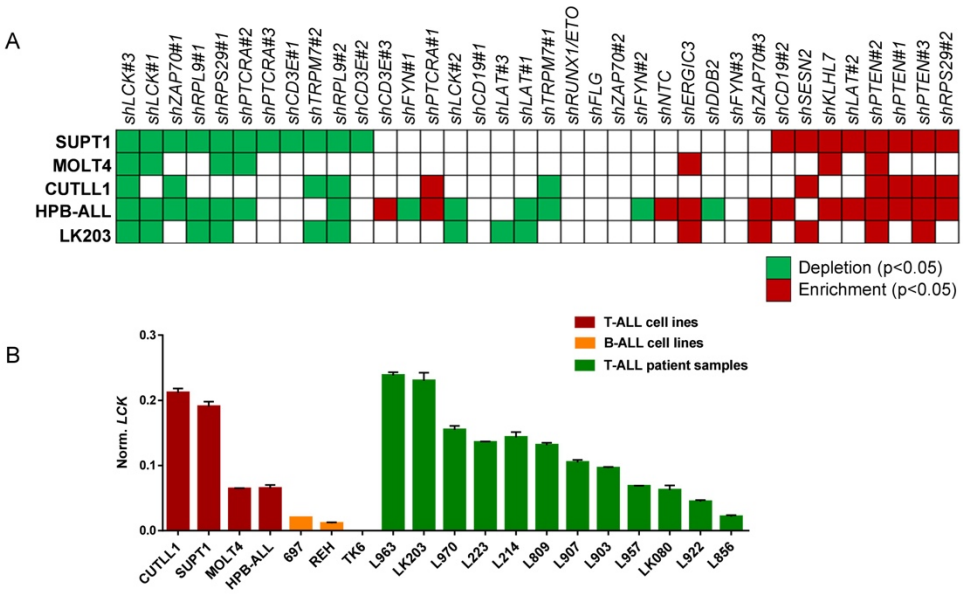

Figure 1. A targeted shRNA screen reveals LCK is essential for *in vitro* proliferative potential. (A) T-ALL cell lines (SUPT1, MOLT4, HBP-ALL, CUTLL1) and PDX LK203 were subjected to a functional screen using a pLKO5-shRNA library containing 36 constructs targeting selected pTCR/TCR signaling complex components (PTCRA, CD3E, FYN, ZAP70, LCK, LAT), positive (PTEN, RPS29, RPL9), negative controls (KLHL7, CD19, DDB2, ERGIC3, FLG, RUNX1-ETO, SESN2, TRPM7) and a non-targeting control (NTC). Genomic DNA was sampled and barcoded. Enriched and depleted shRNAs were identified by next generation sequencing (NGS). The heatmap depicts statistically significant gains (red) or losses (green) of shRNA constructs after *in vitro* culture of 4 T-ALL cell lines (40 days) and PDX LK203 (30 days). (B) Relative gene expression of LCK in 4 cell lines and 12 PDX samples. LCK expression was determined in 4 T-ALL cell lines, 697 and REH (B-lineage ALL cell lines), TK6 (lymphoblastoid cell line) and 12 PDX samples by real time qPCR. GAPDH served as reference gene for normalization.

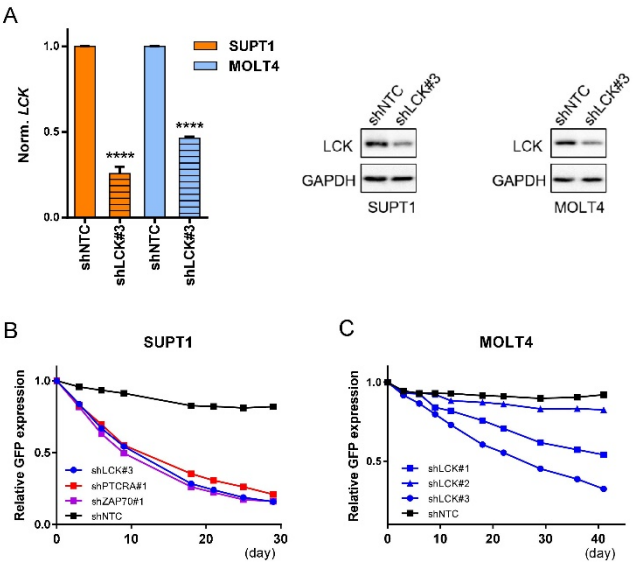

Figure 2. Knockdown of LCK reduces propagation of T-ALL cell lines *in vitro*. SUPT1 (A and B) and MOLT4 (A and C) cells were lentivirally transduced with shNTC (non-targeting control), shLCK#1, shLCK#2, shLCK#3, shPTCRA#1, or shZAP70#1 expression constructs. (A) Knockdown efficiency of LCK at mRNA level (left) and protein level (right) after 6 days. Whole cell lysates were probed for total LCK and GAPDH in Western Blot analysis. (B and C) T-ALL cell lines SUPT1 (B) and MOLT4 (C) transduced with GFP-expressing shLCK (blue), shZAP70 (purple), shPTCRA (red) or shNTC (black) constructs were seeded in a 1:1 ratio with non-transduced parental cells *in vitro*. Cells were cultured and analyzed repetitively by flow cytometry for the presence of GFP+ cells over a time period of 30 and 40 days for SUPT1 and MOLT4, respectively. A relative GFP expression of 1 denotes a mixture of 50% GFP+ cells with 50% parental cells (ratio 1:1). A value of 0.5 refers to 25% of GFP+ cells and 75% parental cells (ratio 1:4). Student t-test; *p<0.05, ** p<0.01, *** p<0.005, **** p<0.001.

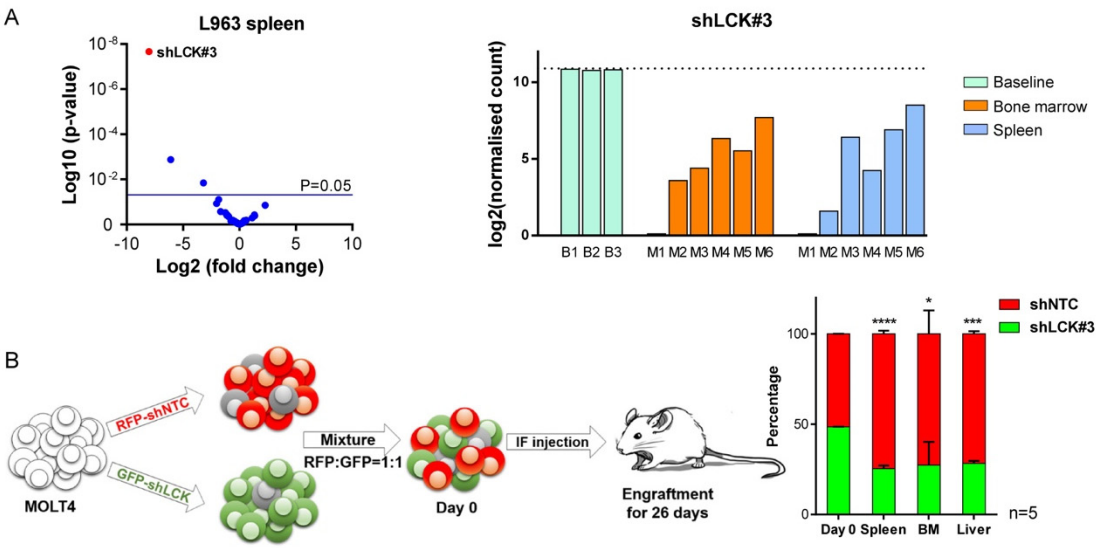

Figure 3. Loss of LCK negatively effects propagation potential of the T-ALL cell line MOLT4 and PDX L963 *in vivo*. (A) Volcano plot derived from the functional *in vivo* screen representing the magnitude of the fold change (log2) in shRNA abundance derived from leukemia cells isolated from the spleen of PDX L963 on the x-axis. Each dot represents an individual shRNA construct. The y-axis represents the significance in enrichment or depletion of shRNA constructs (log10 scale). 3 dots (shLCK#3, shRPL9#1 and shCD19#2) above the blue line are significantly depleted ($p<0.05$). Bar plot of the normalized shLCK#3 sequencing reads (log2) in leukemic cells derived from the bone marrow (orange) or spleen (blue) of 6 individual mice (M1-6), relative to the frequency of these reads before transplantation (green, base line B1-3). (B) Schematic representation of the *in vivo* competitive outgrowth assay. MOLT4 cells were lentivirally transduced with shNTC (red fluorescent protein, RFP) or shLCK#3 (GFP) and intrafemorally injected into 5 NSG mice in a 1:1 ratio. Mice were culled once symptomatic and the ratio of RFP : GFP positive human leukemic cells in spleen (n=5), bone marrow (n=3) or liver (n=3) determined by flow cytometry. In all mice the MOLT4 cells carrying shLCK#3 were outcompeted by shNTC cells during engraftment in spleen, marrow and liver. Student t-test; *$p<0.05$, ** $p<0.01$, *** $p<0.005$, **** $p<0.001$.

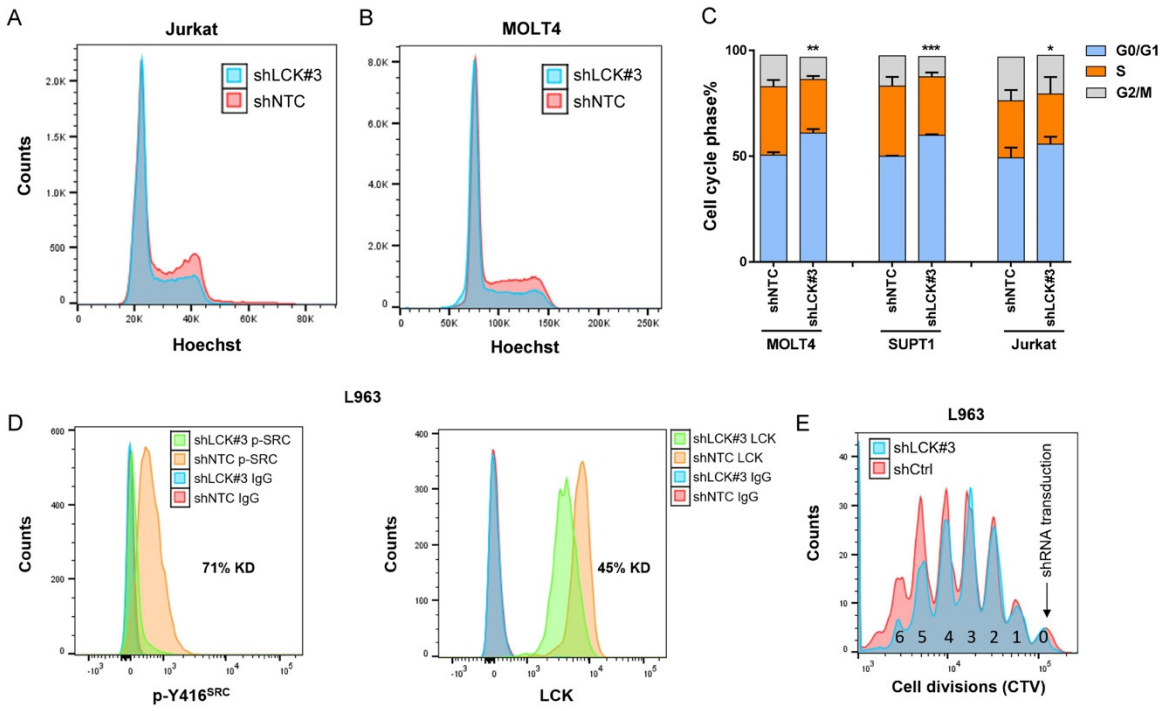

Figure 4. LCK knockdown leads to cell cycle arrest in T-ALL cell lines and PDX cells. (A - C) Cell cycle status was determined by flow cytometry using Hoechst 33342 in cell lines Jurkat (A and C), MOLT4 (B and C) and SUPT1 (C) 7 days after transduction with shLCK#3 or shNTC expression vectors. (D) PDX L963 cells were lentivirally transduced with shLCK#3 or shNTC expression constructs. Phosflow analysis of total LCK and p-Y416^{Src} was performed 8 days later. (E) shLCK#3 and shNTC transduced PDX L963 cells were loaded with CTV and cultured for 13 days. Flow cytometric analysis of CTV incorporation (cell divisions) was performed and demonstrated progressive reduction in cell number after 4-6 cell divisions after LCK knockdown relative to control knockdown. Student t-test; *p<0.05, ** p<0.01, *** p<0.005.

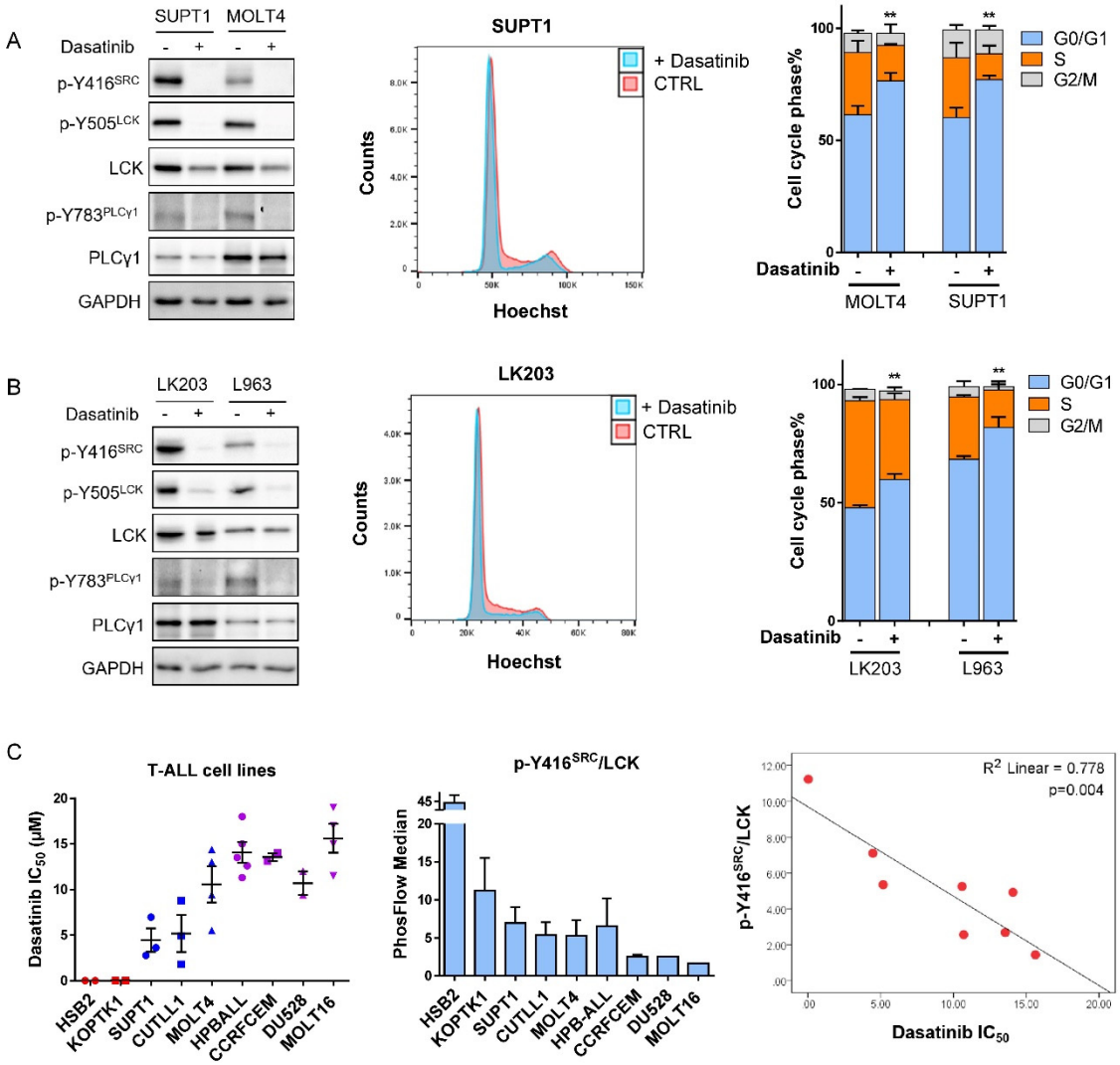

Figure 5. DAS inhibits LCK and leads to cell cycle arrest. (A) SUPT1 and MOLT4 cells were treated with vehicle control or DAS (2 μM) for 24 h and expression of total LCK, activated p-Y416^{Src}, total PLCy1 and activated p-Y783^{PLCγ1} was assessed in Western Blot analysis (left) or cells were stained with Hoechst and analyzed for cell cycle status (middle and right). (B) PDX LK203 and L963 cells were treated for 24 h with 1 μM of DAS. LCK and PLCγ1 total protein and activating phospho-sites at Y416 and Y783 were assessed in Western Blot analyses or PDXs were stained with Hoechst and analyzed for cell cycle status. (C) The *in vitro* sensitivity of a panel of T-ALL cell lines to DAS was investigated and IC_{50} calculated. Phosflow was used to determine the ratio of activated p-Y416^{Src} / total LCK. This ratio was correlated with *in vitro* sensitivity to DAS (R^2=0.778, p=0.004). Student t-test; *p<0.05, ** p<0.01. NB HSB2 was excluded from this analysis, as the extreme sensitivity to dasatinib was caused by the presence of a unique translocation absent in all other sensitive cell lines.

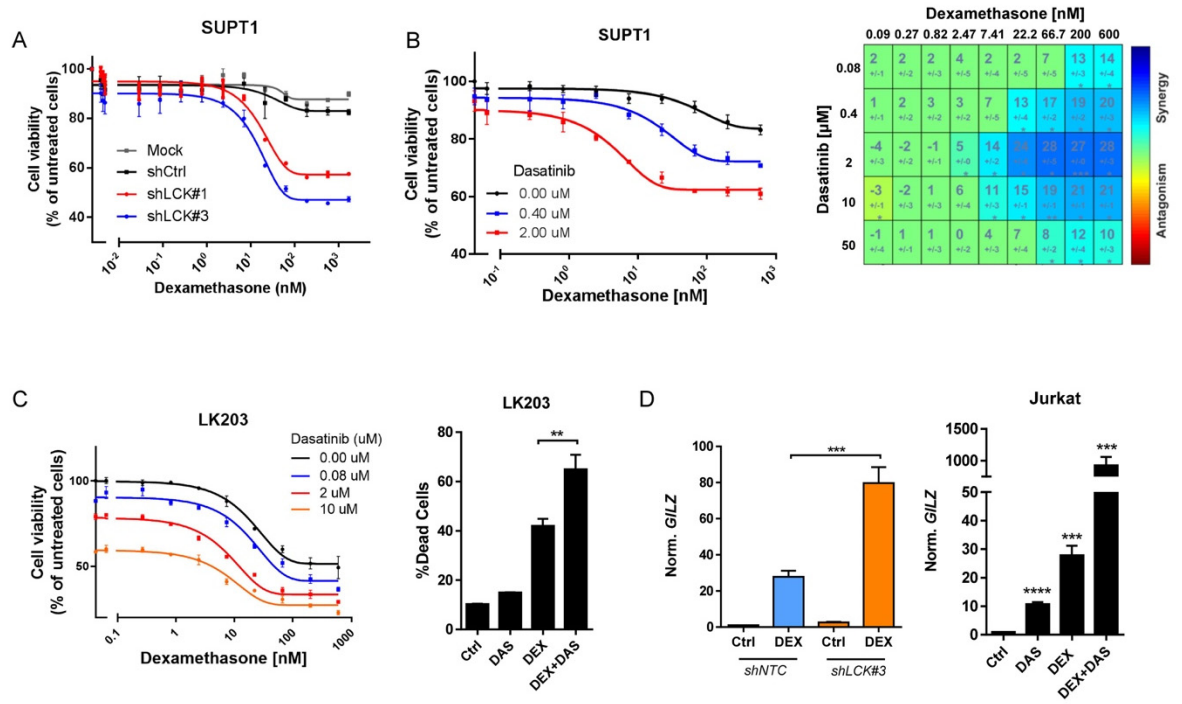

682

683 **Figure 6. DEX and DAS act synergistically to induce cell death in T-ALL.** (A) Cell
684 viability of parental SUPT1 cells (mock), shCtrl (NTC), shLCK#1 or shLCK#3
685 transduced SUPT1 cells upon treatment with increasing DEX concentrations (0-1699
686 nM). (B) Cell viability of SUPT1 with and without DAS (left; black line, no DAS; blue
687 line, 0.4 μM; red line, 2.0 μM) in combination with increasing concentrations of DEX
688 (0-600 nM) as derived from the drug matrix with titration of DEX (0-600 nM) and DAS
689 (0.08-50 uM; right). (Right) Combenefit analysis of drug matrix demonstrates drug
690 synergy in SUPT1 cells at clinically relevant drug concentrations. (C) (Left) LK203 cells
691 were expanded *ex vivo* on OP9-DL1 feeder cells for 1 week prior to treatment with and
692 without DAS (black line, no DAS; blue line, 0.08 μM; red line, 2.0 μM; orange line, 10
693 μM) in combination with increasing concentrations of DEX (0-600 nM) as derived from
694 a drug matrix with DEX (0-600 nM) and DAS (0.08-50 uM)(Supplementary Figure 6E).
695 (Right) Cell death analysis in LK203 cells exposed to control (Ctrl) conditions, DAS (1
696 μM), DEX (100 nM) or DAS+DEX combination treatment. (D) (Left) Normalized *GILZ*
697 mRNA expression in Jurkat cells after transduction with shNTC or shLCK#3 with or
698 without DEX exposure (100 nM). (Right) Normalized *GILZ* mRNA expression in Jurkat
699 cells after exposure to control (Ctrl) conditions, DAS (2 μM), DEX (100 nM) or
700 DAS+DEX combination treatment at the same concentrations. Student t-test; *p<0.05,
701 ** p<0.01, *** p<0.005, **** p<0.001.

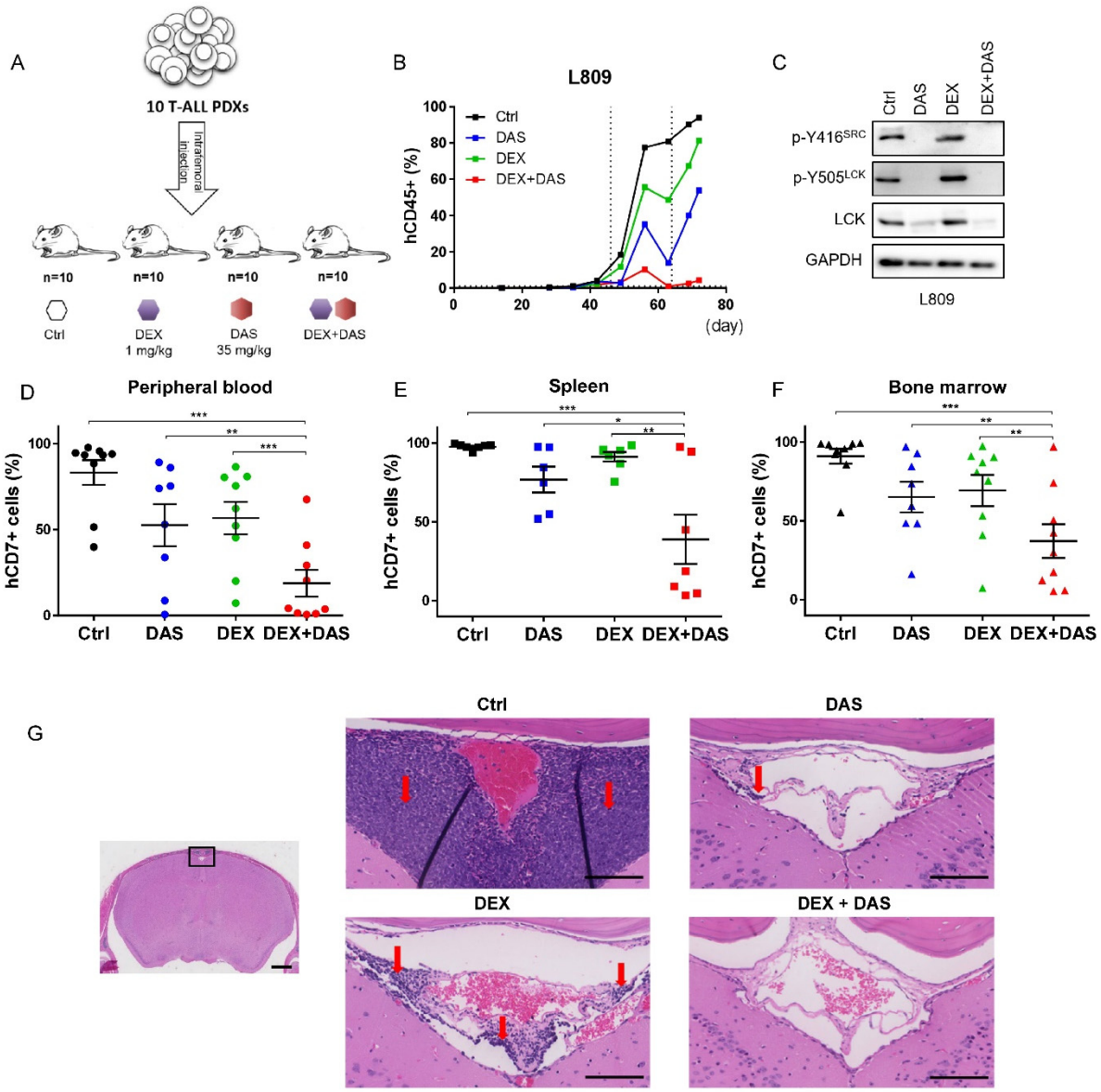

Figure 7. DEX + DAS synergize to impair leukemia engraftment in a Phase II-like murine trial. (A) Layout of the *in vivo* trial using 10 different PDX samples. PDX samples were engrafted into 4 mice each and treated with control vehicle (Ctrl), DEX (1mg/kg), DAS (35mg/kg) or DEX+DAS (1mg/kg DEX + 35mg/kg DAS). Mice were dosed once daily, 5 times per week, for 2 – 3 weeks depending on clinical status of the mice. (B) Engraftment of hCD45+ cells (%) was determined weekly in peripheral blood derived from 4 mice injected with PDX L809. Engraftment levels are shown starting from day of injection (day 0) in mice receiving control vehicle (Ctrl, black), DAS (blue), DEX (green) or DEX+DAS (red). The vertical dotted lines indicate the treatment window (3 weeks) starting on day 46 and completing on day 64. Mice were culled on day 72 and analyzed for hCD45/hCD7 engraftment. (C) Western blotting of total and

phosphorylated LCK protein levels of whole cell lysates derived from the spleens of 4 mice injected with PDX L809 under 4 different treatment arms (Ctrl, DAS, DEX or DEX+DAS) relative to the housekeeper GAPDH. (D - F) Summary of final human CD7+ engraftment (%) in peripheral blood (D), spleen (E) and bone marrow (F) of mice treated with Ctrl (black), DAS (blue), DEX (green) or DEX+DAS (red). Significance levels;*$p<0.05$, ** $p<0.01$, *** $p<0.001$. (G) Photomicrographs of whole brain-skull sections stained with hematoxylin and eosin from PDX L809. (Left) Low power scout view of whole brain with area shown in all other images marked by black box. (Centre and Right) High power view (x20 objective) of meninges around the central venous sinus in mice receiving Ctrl, DAS, DEX or DEX+DAS treatment. Red arrows mark the leukemic infiltrate. Scale bar marks 1mm on scout view and 100μm on high power images.

References:

Abate-Shen, C. (2002). Deregulated homeobox gene expression in cancer: cause or consequence? Nat Rev Cancer *2*, 777-785.

Abraham, K. M., Levin, S. D., Marth, J. D., Forbush, K. A., and Perlmutter, R. M. (1991). Thymic tumorigenesis induced by overexpression of p56lck. Proc Natl Acad Sci U S A *88*, 3977-3981.

Adolfsson, J., Mansson, R., Buza-Vidas, N., Hultquist, A., Liuba, K., Jensen, C. T., Bryder, D., Yang, L., Borge, O. J., Thoren, L. A.*, et al.* (2005). Identification of Flt3+ lympho-myeloid stem cells lacking erythro-megakaryocytic potential a revised road map for adult blood lineage commitment. Cell *121*, 295-306.

Aifantis, I., Raetz, E., and Buonamici, S. (2008). Molecular pathogenesis of T-cell leukaemia and lymphoma. Nat Rev Immunol *8*, 380-390.

Akashi, K., Kondo, M., and Weissman, I. L. (1998). Role of interleukin-7 in T-cell development from hematopoietic stem cells. Immunol Rev *165*, 13-28.

al-Ramadi, B. K., Zhang, H., and Bothwell, A. L. (1998). Cell-cycle arrest and apoptosis hypersusceptibility as a consequence of Lck deficiency in nontransformed T lymphocytes. Proc Natl Acad Sci U S A *95*, 12498-12503.

Allman, D., Karnell, F. G., Punt, J. A., Bakkour, S., Xu, L., Myung, P., Koretzky, G. A., Pui, J. C., Aster, J. C., and Pear, W. S. (2001). Separation of Notch1 promoted lineage commitment and expansion/transformation in developing T cells. J Exp Med *194*, 99-106.

Allman, D., Sambandam, A., Kim, S., Miller, J. P., Pagan, A., Well, D., Meraz, A., and Bhandoola, A. (2003). Thymopoiesis independent of common lymphoid progenitors. Nat Immunol *4*, 168-174.

Alsadeq, A., Fedders, H., Vokuhl, C., Belau, N. M., Zimmermann, M., Wirbelauer, T., Spielberg, S., Vossen-Gajcy, M., Cario, G., Schrappe, M., and Schewe, D. M. (2017). The role of ZAP70 kinase in acute lymphoblastic leukemia infiltration into the central nervous system. Haematologica *102*, 346-355.

Anderson, M. K., Weiss, A. H., Hernandez-Hoyos, G., Dionne, C. J., and Rothenberg, E. V. (2002). Constitutive expression of PU.1 in fetal hematopoietic progenitors blocks T cell development at the pro-T cell stage. Immunity *16*, 285-296.

Appleby, M. W., Gross, J. A., Cooke, M. P., Levin, S. D., Qian, X., and Perlmutter, R. M. (1992). Defective T cell receptor signaling in mice lacking the thymic isoform of p59fyn. Cell *70*, 751-763.

Arifin, W. N., and Zahiruddin, W. M. (2017). Sample Size Calculation in Animal Studies Using Resource Equation Approach. Malays J Med Sci *24*, 101-105.

Ashwell, J. D., Lu, F. W., and Vacchio, M. S. (2000). Glucocorticoids in T cell development and function*. Annu Rev Immunol *18*, 309-345.

Asnafi, V., Radford-Weiss, I., Dastugue, N., Bayle, C., Leboeuf, D., Charrin, C., Garand, R., Lafage-Pochitaloff, M., Delabesse, E., Buzyn, A.*, et al.* (2003). CALM-AF10 is a common fusion transcript in T-ALL and is specific to the TCRgammadelta lineage. Blood *102*, 1000-1006.

Asselin-Labat, M. L., David, M., Biola-Vidamment, A., Lecoeuche, D., Zennaro, M. C., Bertoglio, J., and Pallardy, M. (2004). GILZ, a new target for the transcription factor FoxO3, protects T lymphocytes from interleukin-2 withdrawal-induced apoptosis. Blood *104*, 215-223.

Ayroldi, E., Migliorati, G., Bruscoli, S., Marchetti, C., Zollo, O., Cannarile, L., D'Adamio, F., and Riccardi, C. (2001). Modulation of T-cell activation by the glucocorticoid-induced leucine zipper factor via inhibition of nuclear factor kappaB. Blood *98*, 743-753.

Baer, R. (1993). TAL1, TAL2 and LYL1: a family of basic helix-loop-helix proteins implicated in T cell acute leukaemia. Semin Cancer Biol *4*, 341-347.

Baldus, C. D., Burmeister, T., Martus, P., Schwartz, S., Gokbuget, N., Bloomfield, C. D., Hoelzer, D., Thiel, E., and Hofmann, W. K. (2006). High expression of the ETS transcription factor ERG predicts adverse outcome in acute T-lymphoblastic leukemia in adults. J Clin Oncol *24*, 4714-4720.

Ballerini, P., Blaise, A., Busson-Le Coniat, M., Su, X. Y., Zucman-Rossi, J., Adam, M., van den Akker, J., Perot, C., Pellegrino, B., Landman-Parker, J.*, et al.* (2002). HOX11L2 expression defines a clinical subtype of pediatric T-ALL associated with poor prognosis. Blood *100*, 991-997.

Bamberger, C. M., Bamberger, A. M., de Castro, M., and Chrousos, G. P. (1995). Glucocorticoid receptor beta, a potential endogenous inhibitor of glucocorticoid action in humans. J Clin Invest *95*, 2435-2441.

Ban, K., Gao, Y., Amin, H. M., Howard, A., Miller, C., Lin, Q., Leng, X., Munsell, M., Bar-Eli, M., Arlinghaus, R. B., and Chandra, J. (2008). BCR-ABL1 mediates up-regulation of Fyn in chronic myelogenous leukemia. Blood *111*, 2904-2908.

Bandi, S. R., Brandts, C., Rensinghoff, M., Grundler, R., Tickenbrock, L., Kohler, G., Duyster, J., Berdel, W. E., Muller-Tidow, C., Serve, H.*, et al.* (2009). E3 ligase-defective Cbl mutants lead to a generalized mastocytosis and myeloproliferative disease. Blood *114*, 4197-4208.

Bates, D. (2014). Fitting linear mixed-effects models using lme4. arXiv preprint arXiv *1406*.

Bates, D., Machler, M., Bolker, B. M., and Walker, S. C. (2015). Fitting Linear Mixed-Effects Models Using lme4. J Stat Softw *67*, 1-48.

Batista, A., Barata, J. T., Raderschall, E., Sallan, S. E., Carlesso, N., Nadler, L. M., and Cardoso, A. A. (2011). Targeting of active mTOR inhibits primary leukemia T cells and synergizes with cytotoxic drugs and signaling inhibitors. Exp Hematol *39*, 457-472 e453.

Begley, C. G., and Green, A. R. (1999). The SCL gene: from case report to critical hematopoietic regulator. Blood *93*, 2760-2770.

Belver, L., and Ferrando, A. (2016). The genetics and mechanisms of T cell acute lymphoblastic leukaemia. Nat Rev Cancer *16*, 494-507.

Ben Abdelali, R., Asnafi, V., Petit, A., Micol, J. B., Callens, C., Villarese, P., Delabesse, E., Reman, O., Lepretre, S., Cahn, J. Y.*, et al.* (2013). The prognosis of CALM-AF10-positive adult T-cell acute lymphoblastic leukemias depends on the stage of maturation arrest. Haematologica *98*, 1711-1717.

Ben Abdelali, R., Roggy, A., Leguay, T., Cieslak, A., Renneville, A., Touzart, A., Banos, A., Randriamalala, E., Caillot, D., Lioure, B.*, et al.* (2014). SET-NUP214 is a recurrent gammadelta lineage-specific fusion transcript associated with corticosteroid/chemotherapy resistance in adult T-ALL. Blood *123*, 1860-1863.

Bene, M. C., Castoldi, G., Knapp, W., Ludwig, W. D., Matutes, E., Orfao, A., and van't Veer, M. B. (1995). Proposals for the immunological classification of acute leukemias. European Group for the Immunological Characterization of Leukemias (EGIL). Leukemia *9*, 1783-1786.

Benyoucef, A., Palii, C. G., Wang, C., Porter, C. J., Chu, A., Dai, F., Tremblay, V., Rakopoulos, P., Singh, K., Huang, S.*, et al.* (2016). UTX inhibition as selective

epigenetic therapy against TAL1-driven T-cell acute lymphoblastic leukemia. Genes Dev *30*, 508-521.

Benz, C., and Bleul, C. C. (2005). A multipotent precursor in the thymus maps to the branching point of the T versus B lineage decision. J Exp Med *202*, 21-31.

Bhandoola, A., and Sambandam, A. (2006). From stem cell to T cell: one route or many? Nat Rev Immunol *6*, 117-126.

Bhandoola, A., von Boehmer, H., Petrie, H. T., and Zuniga-Pflucker, J. C. (2007). Commitment and developmental potential of extrathymic and intrathymic T cell precursors: plenty to choose from. Immunity *26*, 678-689.

Bhojwani, D., and Pui, C. H. (2013). Relapsed childhood acute lymphoblastic leukaemia. Lancet Oncol *14*, e205-217.

Boehm, T., Foroni, L., Kaneko, Y., Perutz, M. F., and Rabbitts, T. H. (1991). The rhombotin family of cysteine-rich LIM-domain oncogenes: distinct members are involved in T-cell translocations to human chromosomes 11p15 and 11p13. Proc Natl Acad Sci U S A *88*, 4367-4371.

Brdicka, T., Kadlecek, T. A., Roose, J. P., Pastuszak, A. W., and Weiss, A. (2005). Intramolecular regulatory switch in ZAP-70: analogy with receptor tyrosine kinases. Mol Cell Biol *25*, 4924-4933.

Brownlie, R. J., and Zamoyska, R. (2013). T cell receptor signalling networks: branched, diversified and bounded. Nat Rev Immunol *13*, 257-269.

Bunda, S., Kang, M. W., Sybingco, S. S., Weng, J., Favre, H., Shin, D. H., Irwin, M. S., Loh, M. L., and Ohh, M. (2013). Inhibition of SRC corrects GM-CSF hypersensitivity that underlies juvenile myelomonocytic leukemia. Cancer Res *73*, 2540-2550.

Cantley, L. C. (2002). The phosphoinositide 3-kinase pathway. Science *296*, 1655-1657.

Chen, L., Huynh, L., Apgar, J., Tang, L., Rassenti, L., Weiss, A., and Kipps, T. J. (2008). ZAP-70 enhances IgM signaling independent of its kinase activity in chronic lymphocytic leukemia. Blood *111*, 2685-2692.

Chen, Z., Shojaee, S., Buchner, M., Geng, H., Lee, J. W., Klemm, L., Titz, B., Graeber, T. G., Park, E., Tan, Y. X.*, et al.* (2015). Signalling thresholds and negative B-cell selection in acute lymphoblastic leukaemia. Nature *521*, 357-361.

Cheng, Y., Zhang, Z., Slape, C., and Aplan, P. D. (2007). Cre-loxP-mediated recombination between the SIL and SCL genes leads to a block in T-cell development at the CD4- CD8- to CD4+ CD8+ transition. Neoplasia *9*, 315-321.

Chervinsky, D. S., Zhao, X. F., Lam, D. H., Ellsworth, M., Gross, K. W., and Aplan, P. D. (1999). Disordered T-cell development and T-cell malignancies in SCL LMO1 double-transgenic mice: parallels with E2A-deficient mice. Mol Cell Biol *19*, 5025-5035.

Cohen, J. J., and Duke, R. C. (1984). Glucocorticoid activation of a calcium-dependent endonuclease in thymocyte nuclei leads to cell death. J Immunol *132*, 38-42.

Condorelli, G. L., Facchiano, F., Valtieri, M., Proietti, E., Vitelli, L., Lulli, V., Huebner, K., Peschle, C., and Croce, C. M. (1996). T-cell-directed TAL-1 expression induces T-cell malignancies in transgenic mice. Cancer Res *56*, 5113-5119.

Contri, A., Brunati, A. M., Trentin, L., Cabrelle, A., Miorin, M., Cesaro, L., Pinna, L. A., Zambello, R., Semenzato, G., and Donella-Deana, A. (2005). Chronic lymphocytic leukemia B cells contain anomalous Lyn tyrosine kinase, a putative contribution to defective apoptosis. J Clin Invest *115*, 369-378.

Cooke, M. P., Abraham, K. M., Forbush, K. A., and Perlmutter, R. M. (1991). Regulation of T cell receptor signaling by a src family protein-tyrosine kinase (p59fyn). Cell *65*, 281-291.

Coustan-Smith, E., Mullighan, C. G., Onciu, M., Behm, F. G., Raimondi, S. C., Pei, D., Cheng, C., Su, X., Rubnitz, J. E., Basso, G.*, et al.* (2009). Early T-cell precursor leukaemia: a subtype of very high-risk acute lymphoblastic leukaemia. Lancet Oncol *10*, 147-156.

Cui, Y., Onozawa, M., Garber, H. R., Samsel, L., Wang, Z., McCoy, J. P., Burkett, S., Wu, X., Aplan, P. D., and Mackall, C. L. (2015). Thymic expression of a T-cell receptor targeting a tumor-associated antigen coexpressed in the thymus induces T-ALL. Blood *125*, 2958-2967.

Curtis, D. J., Robb, L., Strasser, A., and Begley, C. G. (1997). The CD2-scl transgene alters the phenotype and frequency of T-lymphomas in N-ras transgenic or p53 deficient mice. Oncogene *15*, 2975-2983.

D'Adamio, F., Zollo, O., Moraca, R., Ayroldi, E., Bruscoli, S., Bartoli, A., Cannarile, L., Migliorati, G., and Riccardi, C. (1997). A new dexamethasone-induced gene of the leucine zipper family protects T lymphocytes from TCR/CD3-activated cell death. Immunity *7*, 803-812.

Dai, Z., Sheridan, J. M., Gearing, L. J., Moore, D. L., Su, S., Wormald, S., Wilcox, S., O'Connor, L., Dickins, R. A., Blewitt, M. E., and Ritchie, M. E. (2014). edgeR: a

versatile tool for the analysis of shRNA-seq and CRISPR-Cas9 genetic screens. F1000Res *3*, 95.

De Francia, S., D'Avolio, A., De Martino, F., Pirro, E., Baietto, L., Siccardi, M., Simiele, M., Racca, S., Saglio, G., Di Carlo, F., and Di Perri, G. (2009). New HPLC-MS method for the simultaneous quantification of the antileukemia drugs imatinib, dasatinib, and nilotinib in human plasma. J Chromatogr B Analyt Technol Biomed Life Sci *877*, 1721-1726.

De Keersmaecker, K., Graux, C., Odero, M. D., Mentens, N., Somers, R., Maertens, J., Wlodarska, I., Vandenberghe, P., Hagemeijer, A., Marynen, P., and Cools, J. (2005). Fusion of EML1 to ABL1 in T-cell acute lymphoblastic leukemia with cryptic t(9;14)(q34;q32). Blood *105*, 4849-4852.

De Keersmaecker, K., Porcu, M., Cox, L., Girardi, T., Vandepoel, R., de Beeck, J. O., Gielen, O., Mentens, N., Bennett, K. L., and Hantschel, O. (2014). NUP214-ABL1-mediated cell proliferation in T-cell acute lymphoblastic leukemia is dependent on the LCK kinase and various interacting proteins. Haematologica *99*, 85-93.

De Keersmaecker, K., Real, P. J., Gatta, G. D., Palomero, T., Sulis, M. L., Tosello, V., Van Vlierberghe, P., Barnes, K., Castillo, M., Sole, X.*, et al.* (2010). The TLX1 oncogene drives aneuploidy in T cell transformation. Nat Med *16*, 1321-1327.

De Keersmaecker, K., Rocnik, J. L., Bernad, R., Lee, B. H., Leeman, D., Gielen, O., Verachtert, H., Folens, C., Munck, S., Marynen, P.*, et al.* (2008). Kinase activation and transformation by NUP214-ABL1 is dependent on the context of the nuclear pore. Mol Cell *31*, 134-142.

De Smedt, M., Hoebeke, I., Reynvoet, K., Leclercq, G., and Plum, J. (2005). Different thresholds of Notch signaling bias human precursor cells toward B-, NK-, monocytic/dendritic-, or T-cell lineage in thymus microenvironment. Blood *106*, 3498-3506.

De Smedt, M., Reynvoet, K., Kerre, T., Taghon, T., Verhasselt, B., Vandekerckhove, B., Leclercq, G., and Plum, J. (2002). Active form of Notch imposes T cell fate in human progenitor cells. J Immunol *169*, 3021-3029.

Deftos, M. L., He, Y. W., Ojala, E. W., and Bevan, M. J. (1998). Correlating notch signaling with thymocyte maturation. Immunity *9*, 777-786.

Della Gatta, G., Palomero, T., Perez-Garcia, A., Ambesi-Impiombato, A., Bansal, M., Carpenter, Z. W., De Keersmaecker, K., Sole, X., Xu, L., Paietta, E.*, et al.* (2012).

Reverse engineering of TLX oncogenic transcriptional networks identifies RUNX1 as tumor suppressor in T-ALL. Nat Med *18*, 436-440.

Di Veroli, G. Y., Fornari, C., Wang, D., Mollard, S., Bramhall, J. L., Richards, F. M., and Jodrell, D. I. (2016). Combenefit: an interactive platform for the analysis and visualization of drug combinations. Bioinformatics *32*, 2866-2868.

Ding, Q., Xia, W., Liu, J. C., Yang, J. Y., Lee, D. F., Xia, J., Bartholomeusz, G., Li, Y., Pan, Y., Li, Z.*, et al.* (2005). Erk associates with and primes GSK-3beta for its inactivation resulting in upregulation of beta-catenin. Mol Cell *19*, 159-170.

Dordelmann, M., Reiter, A., Borkhardt, A., Ludwig, W. D., Gotz, N., Viehmann, S., Gadner, H., Riehm, H., and Schrappe, M. (1999). Prednisone response is the strongest predictor of treatment outcome in infant acute lymphoblastic leukemia. Blood *94*, 1209-1217.

Dos Santos, C., McDonald, T., Ho, Y. W., Liu, H., Lin, A., Forman, S. J., Kuo, Y. H., and Bhatia, R. (2013). The Src and c-Kit kinase inhibitor dasatinib enhances p53-mediated targeting of human acute myeloid leukemia stem cells by chemotherapeutic agents. Blood *122*, 1900-1913.

Driessen, E. M., van Roon, E. H., Spijkers-Hagelstein, J. A., Schneider, P., de Lorenzo, P., Valsecchi, M. G., Pieters, R., and Stam, R. W. (2013). Frequencies and prognostic impact of RAS mutations in MLL-rearranged acute lymphoblastic leukemia in infants. Haematologica *98*, 937-944.

Duong, V. H., Jaglal, M. V., Zhang, L., Kale, V., Lancet, J. E., Komrokji, R. S., and List, A. F. (2013). Phase II pilot study of oral dasatinib in patients with higher-risk myelodysplastic syndrome (MDS) who failed conventional therapy. Leuk Res *37*, 300-304.

Durinck, K., Goossens, S., Peirs, S., Wallaert, A., Van Loocke, W., Matthijssens, F., Pieters, T., Milani, G., Lammens, T., Rondou, P.*, et al.* (2015). Novel biological insights in T-cell acute lymphoblastic leukemia. Exp Hematol *43*, 625-639.

Durum, S. K., Candeias, S., Nakajima, H., Leonard, W. J., Baird, A. M., Berg, L. J., and Muegge, K. (1998). Interleukin 7 receptor control of T cell receptor gamma gene rearrangement: role of receptor-associated chains and locus accessibility. J Exp Med *188*, 2233-2241.

Eck, M. J., Atwell, S. K., Shoelson, S. E., and Harrison, S. C. (1994). Structure of the regulatory domains of the Src-family tyrosine kinase Lck. Nature *368*, 764-769.

El Zawily, A., McEwen, E., Toosi, B., Vizeacoumar, F. S., Freywald, T., Vizeacoumar, F. J., and Freywald, A. (2017). The EphB6 receptor is overexpressed in pediatric T cell acute lymphoblastic leukemia and increases its sensitivity to doxorubicin treatment. Sci Rep *7*, 14767.

Ellisen, L. W., Bird, J., West, D. C., Soreng, A. L., Reynolds, T. C., Smith, S. D., and Sklar, J. (1991). TAN-1, the human homolog of the Drosophila notch gene, is broken by chromosomal translocations in T lymphoblastic neoplasms. Cell *66*, 649-661.

Elwood, N. J., and Begley, C. G. (1995). Reconstitution of mice with bone marrow cells expressing the SCL gene is insufficient to cause leukemia. Cell Growth Differ *6*, 19-25.

Fehse, B., Kustikova, O. S., Bubenheim, M., and Baum, C. (2004). Pois(s)on--it's a question of dose. Gene Ther *11*, 879-881.

Ferrando, A. A., and Look, A. T. (2000). Clinical implications of recurring chromosomal and associated molecular abnormalities in acute lymphoblastic leukemia. Semin Hematol *37*, 381-395.

Ferrando, A. A., Neuberg, D. S., Staunton, J., Loh, M. L., Huard, C., Raimondi, S. C., Behm, F. G., Pui, C. H., Downing, J. R., Gilliland, D. G.*, et al.* (2002). Gene expression signatures define novel oncogenic pathways in T cell acute lymphoblastic leukemia. Cancer Cell *1*, 75-87.

Filipp, D., Leung, B. L., Zhang, J., Veillette, A., and Julius, M. (2004). Enrichment of lck in lipid rafts regulates colocalized fyn activation and the initiation of proximal signals through TCR alpha beta. J Immunol *172*, 4266-4274.

Flemming, A., Brummer, T., Reth, M., and Jumaa, H. (2003). The adaptor protein SLP-65 acts as a tumor suppressor that limits pre-B cell expansion. Nat Immunol *4*, 38-43.

Flex, E., Petrangeli, V., Stella, L., Chiaretti, S., Hornakova, T., Knoops, L., Ariola, C., Fodale, V., Clappier, E., Paoloni, F.*, et al.* (2008). Somatically acquired JAK1 mutations in adult acute lymphoblastic leukemia. J Exp Med *205*, 751-758.

Frey, J. R., Ernst, B., Surh, C. D., and Sprent, J. (1992). Thymus-grafted SCID mice show transient thymopoiesis and limited depletion of V beta 11+ T cells. J Exp Med *175*, 1067-1071.

Frismantas, V., Dobay, M. P., Rinaldi, A., Tchinda, J., Dunn, S. H., Kunz, J., Richter-Pechanska, P., Marovca, B., Pail, O., Jenni, S.*, et al.* (2017). Ex vivo drug response profiling detects recurrent sensitivity patterns in drug-resistant acute lymphoblastic leukemia. Blood *129*, e26-e37.

Gamas, P., Marchetti, S., Puissant, A., Grosso, S., Jacquel, A., Colosetti, P., Pasquet, J. M., Mahon, F. X., Cassuto, J. P., and Auberger, P. (2009). Inhibition of imatinib-mediated apoptosis by the caspase-cleaved form of the tyrosine kinase Lyn in chronic myelogenous leukemia cells. Leukemia *23*, 1500-1506.

Garcia-Peydro, M., de Yebenes, V. G., and Toribio, M. L. (2006). Notch1 and IL-7 receptor interplay maintains proliferation of human thymic progenitors while suppressing non-T cell fates. J Immunol *177*, 3711-3720.

Garvin, A. M., Abraham, K. M., Forbush, K. A., Farr, A. G., Davison, B. L., and Perlmutter, R. M. (1990). Disruption of thymocyte development and lymphomagenesis induced by SV40 T-antigen. Int Immunol *2*, 173-180.

Geng, H., Hurtz, C., Lenz, K. B., Chen, Z., Baumjohann, D., Thompson, S., Goloviznina, N. A., Chen, W. Y., Huan, J., LaTocha, D.*, et al.* (2015). Self-enforcing feedback activation between BCL6 and pre-B cell receptor signaling defines a distinct subtype of acute lymphoblastic leukemia. Cancer Cell *27*, 409-425.

Gioia, R., Leroy, C., Drullion, C., Lagarde, V., Etienne, G., Dulucq, S., Lippert, E., Roche, S., Mahon, F. X., and Pasquet, J. M. (2011). Quantitative phosphoproteomics revealed interplay between Syk and Lyn in the resistance to nilotinib in chronic myeloid leukemia cells. Blood *118*, 2211-2221.

Girardi, T., Vicente, C., Cools, J., and De Keersmaecker, K. (2017). The genetics and molecular biology of T-ALL. Blood *129*, 1113-1123.

Gonzalez-Garcia, S., Garcia-Peydro, M., Alcain, J., and Toribio, M. L. (2012). Notch1 and IL-7 receptor signalling in early T-cell development and leukaemia. Curr Top Microbiol Immunol *360*, 47-73.

Gonzalez-Garcia, S., Garcia-Peydro, M., Martin-Gayo, E., Ballestar, E., Esteller, M., Bornstein, R., de la Pompa, J. L., Ferrando, A. A., and Toribio, M. L. (2009). CSL-MAML-dependent Notch1 signaling controls T lineage-specific IL-7R{alpha} gene expression in early human thymopoiesis and leukemia. J Exp Med *206*, 779-791.

Goossens, S., Radaelli, E., Blanchet, O., Durinck, K., Van der Meulen, J., Peirs, S., Taghon, T., Tremblay, C. S., Costa, M., Farhang Ghahremani, M.*, et al.* (2015). ZEB2 drives immature T-cell lymphoblastic leukaemia development via enhanced tumour-initiating potential and IL-7 receptor signalling. Nat Commun *6*, 5794.

Graux, C., Cools, J., Melotte, C., Quentmeier, H., Ferrando, A., Levine, R., Vermeesch, J. R., Stul, M., Dutta, B., Boeckx, N.*, et al.* (2004). Fusion of NUP214 to

ABL1 on amplified episomes in T-cell acute lymphoblastic leukemia. Nat Genet *36*, 1084-1089.

Gregorj, C., Ricciardi, M. R., Petrucci, M. T., Scerpa, M. C., De Cave, F., Fazi, P., Vignetti, M., Vitale, A., Mancini, M., Cimino, G.*, et al.* (2007). ERK1/2 phosphorylation is an independent predictor of complete remission in newly diagnosed adult acute lymphoblastic leukemia. Blood *109*, 5473-5476.

Gupta-Rossi, N., Le Bail, O., Gonen, H., Brou, C., Logeat, F., Six, E., Ciechanover, A., and Israel, A. (2001). Functional interaction between SEL-10, an F-box protein, and the nuclear form of activated Notch1 receptor. J Biol Chem *276*, 34371-34378.

Gutierrez, A., Sanda, T., Grebliunaite, R., Carracedo, A., Salmena, L., Ahn, Y., Dahlberg, S., Neuberg, D., Moreau, L. A., Winter, S. S.*, et al.* (2009). High frequency of PTEN, PI3K, and AKT abnormalities in T-cell acute lymphoblastic leukemia. Blood *114*, 647-650.

Haarman, E. G., Kaspers, G. J., Pieters, R., Rottier, M. M., and Veerman, A. J. (2004). Glucocorticoid receptor alpha, beta and gamma expression vs in vitro glucocorticod resistance in childhood leukemia. Leukemia *18*, 530-537.

Harr, M. W., Caimi, P. F., McColl, K. S., Zhong, F., Patel, S. N., Barr, P. M., and Distelhorst, C. W. (2010). Inhibition of Lck enhances glucocorticoid sensitivity and apoptosis in lymphoid cell lines and in chronic lymphocytic leukemia. Cell Death Differ *17*, 1381-1391.

Helmberg, A., Auphan, N., Caelles, C., and Karin, M. (1995). Glucocorticoid-induced apoptosis of human leukemic cells is caused by the repressive function of the glucocorticoid receptor. EMBO J *14*, 452-460.

Hendriks, R. W., and Middendorp, S. (2004). The pre-BCR checkpoint as a cell-autonomous proliferation switch. Trends Immunol *25*, 249-256.

Hermiston, M. L., Xu, Z., and Weiss, A. (2003). CD45: a critical regulator of signaling thresholds in immune cells. Annu Rev Immunol *21*, 107-137.

Hernandez-Hoyos, G., Sohn, S. J., Rothenberg, E. V., and Alberola-Ila, J. (2000). Lck activity controls CD4/CD8 T cell lineage commitment. Immunity *12*, 313-322.

Hockenbery, D. M., Zutter, M., Hickey, W., Nahm, M., and Korsmeyer, S. J. (1991). BCL2 protein is topographically restricted in tissues characterized by apoptotic cell death. Proc Natl Acad Sci U S A *88*, 6961-6965.

Holmfeldt, L., Wei, L., Diaz-Flores, E., Walsh, M., Zhang, J., Ding, L., Payne-Turner, D., Churchman, M., Andersson, A., Chen, S. C.*, et al.* (2013). The genomic landscape of hypodiploid acute lymphoblastic leukemia. Nat Genet *45*, 242-252.

Hosoya, T., Kuroha, T., Moriguchi, T., Cummings, D., Maillard, I., Lim, K. C., and Engel, J. D. (2009). GATA-3 is required for early T lineage progenitor development. J Exp Med *206*, 2987-3000.

Hu, Y., Liu, Y., Pelletier, S., Buchdunger, E., Warmuth, M., Fabbro, D., Hallek, M., Van Etten, R. A., and Li, S. (2004). Requirement of Src kinases Lyn, Hck and Fgr for BCR-ABL1-induced B-lymphoblastic leukemia but not chronic myeloid leukemia. Nat Genet *36*, 453-461.

Huang, Y., Thoms, J. A., Tursky, M. L., Knezevic, K., Beck, D., Chandrakanthan, V., Suryani, S., Olivier, J., Boulton, A., Glaros, E. N.*, et al.* (2016). MAPK/ERK2 phosphorylates ERG at serine 283 in leukemic cells and promotes stem cell signatures and cell proliferation. Leukemia *30*, 1552-1561.

Huntington, N. D., and Tarlinton, D. M. (2004). CD45: direct and indirect government of immune regulation. Immunol Lett *94*, 167-174.

Igarashi, H., Gregory, S. C., Yokota, T., Sakaguchi, N., and Kincade, P. W. (2002). Transcription from the RAG1 locus marks the earliest lymphocyte progenitors in bone marrow. Immunity *17*, 117-130.

Ikawa, T., Hirose, S., Masuda, K., Kakugawa, K., Satoh, R., Shibano-Satoh, A., Kominami, R., Katsura, Y., and Kawamoto, H. (2010). An essential developmental checkpoint for production of the T cell lineage. Science *329*, 93-96.

Imai, E., Miner, J. N., Mitchell, J. A., Yamamoto, K. R., and Granner, D. K. (1993). Glucocorticoid receptor-cAMP response element-binding protein interaction and the response of the phosphoenolpyruvate carboxykinase gene to glucocorticoids. J Biol Chem *268*, 5353-5356.

Inaba, H., and Pui, C. H. (2010). Glucocorticoid use in acute lymphoblastic leukaemia. Lancet Oncol *11*, 1096-1106.

Irving, J., Matheson, E., Minto, L., Blair, H., Case, M., Halsey, C., Swidenbank, I., Ponthan, F., Kirschner-Schwabe, R., Groeneveld-Krentz, S.*, et al.* (2014). Ras pathway mutations are prevalent in relapsed childhood acute lymphoblastic leukemia and confer sensitivity to MEK inhibition. Blood *124*, 3420-3430.

Jamieson, C. A., and Yamamoto, K. R. (2000). Crosstalk pathway for inhibition of glucocorticoid-induced apoptosis by T cell receptor signaling. Proc Natl Acad Sci U S A *97*, 7319-7324.

Jing, D., Bhadri, V. A., Beck, D., Thoms, J. A., Yakob, N. A., Wong, J. W., Knezevic, K., Pimanda, J. E., and Lock, R. B. (2015). Opposing regulation of BIM and BCL2 controls glucocorticoid-induced apoptosis of pediatric acute lymphoblastic leukemia cells. Blood *125*, 273-283.

Jing, D., Huang, Y., Liu, X., Sia, K. C. S., Zhang, J. C., Tai, X., Wang, M., Toscan, C. E., McCalmont, H., Evans, K.*, et al.* (2018). Lymphocyte-Specific Chromatin Accessibility Pre-determines Glucocorticoid Resistance in Acute Lymphoblastic Leukemia. Cancer Cell *34*, 906-921 e908.

Kalaitzidis, D., Sykes, S. M., Wang, Z., Punt, N., Tang, Y., Ragu, C., Sinha, A. U., Lane, S. W., Souza, A. L., Clish, C. B.*, et al.* (2012). mTOR complex 1 plays critical roles in hematopoiesis and Pten-loss-evoked leukemogenesis. Cell Stem Cell *11*, 429-439.

Kang, J., Volkmann, A., and Raulet, D. H. (2001). Evidence that gammadelta versus alphabeta T cell fate determination is initiated independently of T cell receptor signaling. J Exp Med *193*, 689-698.

Katsura, Y. (2002). Redefinition of lymphoid progenitors. Nat Rev Immunol *2*, 127-132.

Kawamoto, H., Ikawa, T., Ohmura, K., Fujimoto, S., and Katsura, Y. (2000). T cell progenitors emerge earlier than B cell progenitors in the murine fetal liver. Immunity *12*, 441-450.

Kfir-Erenfeld, S., Sionov, R. V., Spokoini, R., Cohen, O., and Yefenof, E. (2010). Protein kinase networks regulating glucocorticoid-induced apoptosis of hematopoietic cancer cells: fundamental aspects and practical considerations. Leuk Lymphoma *51*, 1968-2005.

Kindler, T., Cornejo, M. G., Scholl, C., Liu, J., Leeman, D. S., Haydu, J. E., Frohling, S., Lee, B. H., and Gilliland, D. G. (2008). K-RasG12D-induced T-cell lymphoblastic lymphoma/leukemias harbor Notch1 mutations and are sensitive to gamma-secretase inhibitors. Blood *112*, 3373-3382.

King, A. G., Kondo, M., Scherer, D. C., and Weissman, I. L. (2002). Lineage infidelity in myeloid cells with TCR gene rearrangement: a latent developmental potential of proT cells revealed by ectopic cytokine receptor signaling. Proc Natl Acad Sci U S A *99*, 4508-4513.

King, L. B., Vacchio, M. S., Dixon, K., Hunziker, R., Margulies, D. H., and Ashwell, J. D. (1995). A targeted glucocorticoid receptor antisense transgene increases thymocyte apoptosis and alters thymocyte development. Immunity *3*, 647-656.

Klein, F., Feldhahn, N., Harder, L., Wang, H., Wartenberg, M., Hofmann, W. K., Wernet, P., Siebert, R., and Muschen, M. (2004). The BCR-ABL1 kinase bypasses selection for the expression of a pre-B cell receptor in pre-B acute lymphoblastic leukemia cells. J Exp Med *199*, 673-685.

Kleppe, M., Soulier, J., Asnafi, V., Mentens, N., Hornakova, T., Knoops, L., Constantinescu, S., Sigaux, F., Meijerink, J. P., Vandenberghe, P.*, et al.* (2011). PTPN2 negatively regulates oncogenic JAK1 in T-cell acute lymphoblastic leukemia. Blood *117*, 7090-7098.

Knoechel, B., Roderick, J. E., Williamson, K. E., Zhu, J., Lohr, J. G., Cotton, M. J., Gillespie, S. M., Fernandez, D., Ku, M., Wang, H.*, et al.* (2014). An epigenetic mechanism of resistance to targeted therapy in T cell acute lymphoblastic leukemia. Nat Genet *46*, 364-370.

Kondo, M., Weissman, I. L., and Akashi, K. (1997). Identification of clonogenic common lymphoid progenitors in mouse bone marrow. Cell *91*, 661-672.

Kopan, R., and Ilagan, M. X. (2009). The canonical Notch signaling pathway: unfolding the activation mechanism. Cell *137*, 216-233.

Krstic, M. D., Rogatsky, I., Yamamoto, K. R., and Garabedian, M. J. (1997). Mitogen-activated and cyclin-dependent protein kinases selectively and differentially modulate transcriptional enhancement by the glucocorticoid receptor. Mol Cell Biol *17*, 3947-3954.

Krueger, A., Willenzon, S., Lyszkiewicz, M., Kremmer, E., and Forster, R. (2010). CC chemokine receptor 7 and 9 double-deficient hematopoietic progenitors are severely impaired in seeding the adult thymus. Blood *115*, 1906-1912.

Ku, M., Wall, M., MacKinnon, R. N., Walkley, C. R., Purton, L. E., Tam, C., Izon, D., Campbell, L., Cheng, H. C., and Nandurkar, H. (2015). Src family kinases and their role in hematological malignancies. Leuk Lymphoma *56*, 577-586.

Kullmann, M., Schneikert, J., Moll, J., Heck, S., Zeiner, M., Gehring, U., and Cato, A. C. (1998). RAP46 is a negative regulator of glucocorticoid receptor action and hormone-induced apoptosis. J Biol Chem *273*, 14620-14625.

Kusy, S., Gerby, B., Goardon, N., Gault, N., Ferri, F., Gerard, D., Armstrong, F., Ballerini, P., Cayuela, J. M., Baruchel, A.*, et al.* (2010). NKX3.1 is a direct TAL1 target

gene that mediates proliferation of TAL1-expressing human T cell acute lymphoblastic leukemia. J Exp Med *207*, 2141-2156.

Lai, E. C. (2004). Notch signaling: control of cell communication and cell fate. Development *131*, 965-973.

Langmead, B., and Salzberg, S. L. (2012). Fast gapped-read alignment with Bowtie 2. Nat Methods *9*, 357-359.

Larson, R. C., Lavenir, I., Larson, T. A., Baer, R., Warren, A. J., Wadman, I., Nottage, K., and Rabbitts, T. H. (1996). Protein dimerization between Lmo2 (Rbtn2) and Tal1 alters thymocyte development and potentiates T cell tumorigenesis in transgenic mice. EMBO J *15*, 1021-1027.

Laukkanen, S., Gronroos, T., Polonen, P., Kuusanmaki, H., Mehtonen, J., Cloos, J., Ossenkoppele, G., Gjertsen, B., Oystein, B., Heckman, C.*, et al.* (2017). In silico and preclinical drug screening identifies dasatinib as a targeted therapy for T-ALL. Blood Cancer J *7*, e604.

Lauten, M., Beger, C., Gerdes, K., Asgedom, G., Kardinal, C., Welte, K., and Schrappe, M. (2003). Expression of heat-shock protein 90 in glucocorticoid-sensitive and -resistant childhood acute lymphoblastic leukaemia. Leukemia *17*, 1551-1556.

Lee, K. C., Ouwehand, I., Giannini, A. L., Thomas, N. S., Dibb, N. J., and Bijlmakers, M. J. (2010). Lck is a key target of imatinib and dasatinib in T-cell activation. Leukemia *24*, 896-900.

Legname, G., Seddon, B., Lovatt, M., Tomlinson, P., Sarner, N., Tolaini, M., Williams, K., Norton, T., Kioussis, D., and Zamoyska, R. (2000). Inducible expression of a p56Lck transgene reveals a central role for Lck in the differentiation of CD4 SP thymocytes. Immunity *12*, 537-546.

Leung, D. Y., Hamid, Q., Vottero, A., Szefler, S. J., Surs, W., Minshall, E., Chrousos, G. P., and Klemm, D. J. (1997). Association of glucocorticoid insensitivity with increased expression of glucocorticoid receptor beta. J Exp Med *186*, 1567-1574.

Levin, S. D., Anderson, S. J., Forbush, K. A., and Perlmutter, R. M. (1993). A dominant-negative transgene defines a role for p56lck in thymopoiesis. EMBO J *12*, 1671-1680.

Ley, R., Balmanno, K., Hadfield, K., Weston, C., and Cook, S. J. (2003). Activation of the ERK1/2 signaling pathway promotes phosphorylation and proteasome-dependent degradation of the BH3-only protein, Bim. J Biol Chem *278*, 18811-18816.

Ley, S. C., Marsh, M., Bebbington, C. R., Proudfoot, K., and Jordan, P. (1994). Distinct intracellular localization of Lck and Fyn protein tyrosine kinases in human T lymphocytes. J Cell Biol *125*, 639-649.

Li, L., Leid, M., and Rothenberg, E. V. (2010a). An early T cell lineage commitment checkpoint dependent on the transcription factor Bcl11b. Science *329*, 89-93.

Li, M. O., and Rudensky, A. Y. (2016). T cell receptor signalling in the control of regulatory T cell differentiation and function. Nat Rev Immunol *16*, 220-233.

Li, P., Burke, S., Wang, J., Chen, X., Ortiz, M., Lee, S. C., Lu, D., Campos, L., Goulding, D., Ng, B. L.*, et al.* (2010b). Reprogramming of T cells to natural killer-like cells upon Bcl11b deletion. Science *329*, 85-89.

Li, W. Q., Jiang, Q., Aleem, E., Kaldis, P., Khaled, A. R., and Durum, S. K. (2006). IL-7 promotes T cell proliferation through destabilization of p27Kip1. J Exp Med *203*, 573-582.

Li, Y., Buijs-Gladdines, J. G., Cante-Barrett, K., Stubbs, A. P., Vroegindeweij, E. M., Smits, W. K., van Marion, R., Dinjens, W. N., Horstmann, M., Kuiper, R. P.*, et al.* (2016). IL-7 Receptor Mutations and Steroid Resistance in Pediatric T cell Acute Lymphoblastic Leukemia: A Genome Sequencing Study. PLoS Med *13*, e1002200.

Lin, K., Longo, N. S., Wang, X., Hewitt, J. A., and Abraham, K. M. (2000). Lck domains differentially contribute to pre-T cell receptor (TCR)- and TCR-alpha/beta-regulated developmental transitions. J Exp Med *191*, 703-716.

Liston, D. R., and Davis, M. (2017). Clinically Relevant Concentrations of Anticancer Drugs: A Guide for Nonclinical Studies. Clin Cancer Res *23*, 3489-3498.

Livak, K. J., and Schmittgen, T. D. (2001). Analysis of relative gene expression data using real-time quantitative PCR and the 2(-Delta Delta C(T)) Method. Methods *25*, 402-408.

Loewe, S. (1926). Effects of combinations: mathematical basis of problem. Arch Exp Pathol Pharmakol *114*, 313-326.

Lowenberg, M., Tuynman, J., Bilderbeek, J., Gaber, T., Buttgereit, F., van Deventer, S., Peppelenbosch, M., and Hommes, D. (2005). Rapid immunosuppressive effects of glucocorticoids mediated through Lck and Fyn. Blood *106*, 1703-1710.

Lowenberg, M., Verhaar, A. P., Bilderbeek, J., Marle, J., Buttgereit, F., Peppelenbosch, M. P., van Deventer, S. J., and Hommes, D. W. (2006). Glucocorticoids cause rapid dissociation of a T-cell-receptor-associated protein complex containing LCK and FYN. EMBO Rep *7*, 1023-1029.

Mahon, F. X., Hayette, S., Lagarde, V., Belloc, F., Turcq, B., Nicolini, F., Belanger, C., Manley, P. W., Leroy, C., Etienne, G.*, et al.* (2008). Evidence that resistance to nilotinib may be due to BCR-ABL, Pgp, or Src kinase overexpression. Cancer Res *68*, 9809-9816.

Mansour, M. R., Abraham, B. J., Anders, L., Berezovskaya, A., Gutierrez, A., Durbin, A. D., Etchin, J., Lawton, L., Sallan, S. E., Silverman, L. B.*, et al.* (2014). Oncogene regulation. An oncogenic super-enhancer formed through somatic mutation of a noncoding intergenic element. Science *346*, 1373-1377.

Martelli, A. M., Tabellini, G., Ricci, F., Evangelisti, C., Chiarini, F., Bortul, R., McCubrey, J. A., and Manzoli, F. A. (2012). PI3K/AKT/mTORC1 and MEK/ERK signaling in T-cell acute lymphoblastic leukemia: new options for targeted therapy. Adv Biol Regul *52*, 214-227.

Marth, J. D., Cooper, J. A., King, C. S., Ziegler, S. F., Tinker, D. A., Overell, R. W., Krebs, E. G., and Perlmutter, R. M. (1988). Neoplastic transformation induced by an activated lymphocyte-specific protein tyrosine kinase (pp56lck). Mol Cell Biol *8*, 540-550.

Martin, C. H., Aifantis, I., Scimone, M. L., von Andrian, U. H., Reizis, B., von Boehmer, H., and Gounari, F. (2003). Efficient thymic immigration of B220+ lymphoid-restricted bone marrow cells with T precursor potential. Nat Immunol *4*, 866-873.

Matheson, E. C., Thomas, H., Case, M., Blair, H., Jackson, R. K., Masic, D., Veal, G., Halsey, C., Newell, D. R., Vormoor, J., and Irving, J. A. E. (2019). Glucocorticoids and selumetinib are highly synergistic in RAS pathway mutated childhood acute lymphoblastic leukemia through upregulation of BIM. Haematologica.

Mavrakis, K. J., Wolfe, A. L., Oricchio, E., Palomero, T., de Keersmaecker, K., McJunkin, K., Zuber, J., James, T., Khan, A. A., Leslie, C. S.*, et al.* (2010). Genome-wide RNA-mediated interference screen identifies miR-19 targets in Notch-induced T-cell acute lymphoblastic leukaemia. Nat Cell Biol *12*, 372-379.

McCafferty, E. H., Dhillon, S., and Deeks, E. D. (2018). Dasatinib: A Review in Pediatric Chronic Myeloid Leukemia. Paediatr Drugs *20*, 593-600.

Mege, D., Di Bartolo, V., Germain, V., Tuosto, L., Michel, F., and Acuto, O. (1996). Mutation of tyrosines 492/493 in the kinase domain of ZAP-70 affects multiple T-cell receptor signaling pathways. J Biol Chem *271*, 32644-32652.

Mellentin, J. D., Smith, S. D., and Cleary, M. L. (1989). lyl-1, a novel gene altered by chromosomal translocation in T cell leukemia, codes for a protein with a helix-loop-helix DNA binding motif. Cell *58*, 77-83.

Mestermann, K., Giavridis, T., Weber, J., Rydzek, J., Frenz, S., Nerreter, T., Mades, A., Sadelain, M., Einsele, H., and Hudecek, M. (2019). The tyrosine kinase inhibitor dasatinib acts as a pharmacologic on/off switch for CAR T cells. Sci Transl Med *11*.

Meyer, S. C., and Levine, R. L. (2014). Molecular pathways: molecular basis for sensitivity and resistance to JAK kinase inhibitors. Clin Cancer Res *20*, 2051-2059.

Michie, A. M., Carlyle, J. R., and Zuniga-Pflucker, J. C. (1998). Early intrathymic precursor cells acquire a CD4(low) phenotype. J Immunol *160*, 1735-1741.

Miller, J. F., and Osoba, D. (1967). Current concepts of the immunological function of the thymus. Physiol Rev *47*, 437-520.

Moellering, R. E., Cornejo, M., Davis, T. N., Del Bianco, C., Aster, J. C., Blacklow, S. C., Kung, A. L., Gilliland, D. G., Verdine, G. L., and Bradner, J. E. (2009). Direct inhibition of the NOTCH transcription factor complex. Nature *462*, 182-188.

Molina, T. J., Kishihara, K., Siderovski, D. P., van Ewijk, W., Narendran, A., Timms, E., Wakeham, A., Paige, C. J., Hartmann, K. U., Veillette, A., and et al. (1992). Profound block in thymocyte development in mice lacking p56lck. Nature *357*, 161-164.

Molina, T. J., Perrot, J. Y., Penninger, J., Ramos, A., Audouin, J., Briand, P., Mak, T. W., and Diebold, J. (1998). Differential requirement for p56lck in fetal and adult thymopoiesis. J Immunol *160*, 3828-3834.

Mori, S., Shortman, K., and Wu, L. (2001). Characterization of thymus-seeding precursor cells from mouse bone marrow. Blood *98*, 696-704.

Mullighan, C. G., Zhang, J., Kasper, L. H., Lerach, S., Payne-Turner, D., Phillips, L. A., Heatley, S. L., Holmfeldt, L., Collins-Underwood, J. R., Ma, J.*, et al.* (2011). CREBBP mutations in relapsed acute lymphoblastic leukaemia. Nature *471*, 235-239.

Nerreter, T., Distler, E., Kochel, C., Einsele, H., Herr, W., and Seggewiss-Bernhardt, R. (2013). Combining dasatinib with dexamethasone long-term leads to maintenance of antiviral and antileukemia specific cytotoxic T cell responses in vitro. Exp Hematol *41*, 604-614 e604.

Nika, K., Soldani, C., Salek, M., Paster, W., Gray, A., Etzensperger, R., Fugger, L., Polzella, P., Cerundolo, V., Dushek, O.*, et al.* (2010). Constitutively active Lck kinase in T cells drives antigen receptor signal transduction. Immunity *32*, 766-777.

Northrop, J. P., Crabtree, G. R., and Mattila, P. S. (1992). Negative regulation of interleukin 2 transcription by the glucocorticoid receptor. J Exp Med *175*, 1235-1245.
Ntziachristos, P., Tsirigos, A., Van Vlierberghe, P., Nedjic, J., Trimarchi, T., Flaherty, M. S., Ferres-Marco, D., da Ros, V., Tang, Z., Siegle, J.*, et al.* (2012). Genetic inactivation of the polycomb repressive complex 2 in T cell acute lymphoblastic leukemia. Nat Med *18*, 298-301.
Ntziachristos, P., Tsirigos, A., Welstead, G. G., Trimarchi, T., Bakogianni, S., Xu, L., Loizou, E., Holmfeldt, L., Strikoudis, A., King, B.*, et al.* (2014). Contrasting roles of histone 3 lysine 27 demethylases in acute lymphoblastic leukaemia. Nature *514*, 513-517.
O'Neil, J., Grim, J., Strack, P., Rao, S., Tibbitts, D., Winter, C., Hardwick, J., Welcker, M., Meijerink, J. P., Pieters, R.*, et al.* (2007). FBW7 mutations in leukemic cells mediate NOTCH pathway activation and resistance to gamma-secretase inhibitors. J Exp Med *204*, 1813-1824.
O'Neil, J., Shank, J., Cusson, N., Murre, C., and Kelliher, M. (2004). TAL1/SCL induces leukemia by inhibiting the transcriptional activity of E47/HEB. Cancer Cell *5*, 587-596.
Okabe, S., Tauchi, T., Tanaka, Y., and Ohyashiki, K. (2011). Dasatinib preferentially induces apoptosis by inhibiting Lyn kinase in nilotinib-resistant chronic myeloid leukemia cell line. J Hematol Oncol *4*, 32.
Okamoto, M., Hayakawa, F., Miyata, Y., Watamoto, K., Emi, N., Abe, A., Kiyoi, H., Towatari, M., and Naoe, T. (2007). Lyn is an important component of the signal transduction pathway specific to FLT3/ITD and can be a therapeutic target in the treatment of AML with FLT3/ITD. Leukemia *21*, 403-410.
Paliogianni, F., Raptis, A., Ahuja, S. S., Najjar, S. M., and Boumpas, D. T. (1993). Negative transcriptional regulation of human interleukin 2 (IL-2) gene by glucocorticoids through interference with nuclear transcription factors AP-1 and NF-AT. J Clin Invest *91*, 1481-1489.
Palomero, T., Lim, W. K., Odom, D. T., Sulis, M. L., Real, P. J., Margolin, A., Barnes, K. C., O'Neil, J., Neuberg, D., Weng, A. P.*, et al.* (2006). NOTCH1 directly regulates c-MYC and activates a feed-forward-loop transcriptional network promoting leukemic cell growth. Proc Natl Acad Sci U S A *103*, 18261-18266.
Paugh, S. W., Bonten, E. J., Savic, D., Ramsey, L. B., Thierfelder, W. E., Gurung, P., Malireddi, R. K., Actis, M., Mayasundari, A., Min, J.*, et al.* (2015). NALP3

inflammasome upregulation and CASP1 cleavage of the glucocorticoid receptor cause glucocorticoid resistance in leukemia cells. Nat Genet *47*, 607-614.

Pazirandeh, A., Xue, Y., Rafter, I., Sjovall, J., Jondal, M., and Okret, S. (1999). Paracrine glucocorticoid activity produced by mouse thymic epithelial cells. FASEB J *13*, 893-901.

Pear, W. S., Aster, J. C., Scott, M. L., Hasserjian, R. P., Soffer, B., Sklar, J., and Baltimore, D. (1996). Exclusive development of T cell neoplasms in mice transplanted with bone marrow expressing activated Notch alleles. J Exp Med *183*, 2283-2291.

Pene-Dumitrescu, T., and Smithgall, T. E. (2010). Expression of a Src family kinase in chronic myelogenous leukemia cells induces resistance to imatinib in a kinase-dependent manner. J Biol Chem *285*, 21446-21457.

Piovan, E., Yu, J., Tosello, V., Herranz, D., Ambesi-Impiombato, A., Da Silva, A. C., Sanchez-Martin, M., Perez-Garcia, A., Rigo, I., Castillo, M.*, et al.* (2013). Direct reversal of glucocorticoid resistance by AKT inhibition in acute lymphoblastic leukemia. Cancer Cell *24*, 766-776.

Pitcher, L. A., Young, J. A., Mathis, M. A., Wrage, P. C., Bartok, B., and van Oers, N. S. (2003). The formation and functions of the 21- and 23-kDa tyrosine-phosphorylated TCR zeta subunits. Immunol Rev *191*, 47-61.

Polak, A., Kiliszek, P., Sewastianik, T., Szydlowski, M., Jablonska, E., Bialopiotrowicz, E., Gorniak, P., Markowicz, S., Nowak, E., Grygorowicz, M. A.*, et al.* (2016). MEK Inhibition Sensitizes Precursor B-Cell Acute Lymphoblastic Leukemia (B-ALL) Cells to Dexamethasone through Modulation of mTOR Activity and Stimulation of Autophagy. PLoS One *11*, e0155893.

Porcu, M., Kleppe, M., Gianfelici, V., Geerdens, E., De Keersmaecker, K., Tartaglia, M., Foa, R., Soulier, J., Cauwelier, B., Uyttebroeck, A.*, et al.* (2012). Mutation of the receptor tyrosine phosphatase PTPRC (CD45) in T-cell acute lymphoblastic leukemia. Blood *119*, 4476-4479.

Porkka, K., Koskenvesa, P., Lundan, T., Rimpilainen, J., Mustjoki, S., Smykla, R., Wild, R., Luo, R., Arnan, M., Brethon, B.*, et al.* (2008). Dasatinib crosses the blood-brain barrier and is an efficient therapy for central nervous system Philadelphia chromosome-positive leukemia. Blood *112*, 1005-1012.

Pui, C. H., Robison, L. L., and Look, A. T. (2008). Acute lymphoblastic leukaemia. Lancet *371*, 1030-1043.

Pui, J. C., Allman, D., Xu, L., DeRocco, S., Karnell, F. G., Bakkour, S., Lee, J. Y., Kadesch, T., Hardy, R. R., Aster, J. C., and Pear, W. S. (1999). Notch1 expression in early lymphopoiesis influences B versus T lineage determination. Immunity *11*, 299-308.

R. Mead, S. G. G., A. Mead (2012). Statistical Principles for the Design of Experiments. Cambridge University Press.

Radtke, F., Wilson, A., Stark, G., Bauer, M., van Meerwijk, J., MacDonald, H. R., and Aguet, M. (1999). Deficient T cell fate specification in mice with an induced inactivation of Notch1. Immunity *10*, 547-558.

Raetz, E. A., and Teachey, D. T. (2016). T-cell acute lymphoblastic leukemia. Hematology Am Soc Hematol Educ Program *2016*, 580-588.

Rakowski, L. A., Lehotzky, E. A., and Chiang, M. Y. (2011). Transient responses to NOTCH and TLX1/HOX11 inhibition in T-cell acute lymphoblastic leukemia/lymphoma. PLoS One *6*, e16761.

Rao, N., Miyake, S., Reddi, A. L., Douillard, P., Ghosh, A. K., Dodge, I. L., Zhou, P., Fernandes, N. D., and Band, H. (2002). Negative regulation of Lck by Cbl ubiquitin ligase. Proc Natl Acad Sci U S A *99*, 3794-3799.

Ratei, R., Sperling, C., Karawajew, L., Schott, G., Schrappe, M., Harbott, J., Riehm, H., and Ludwig, W. D. (1998). Immunophenotype and clinical characteristics of CD45-negative and CD45-positive childhood acute lymphoblastic leukemia. Ann Hematol *77*, 107-114.

Real, P. J., Tosello, V., Palomero, T., Castillo, M., Hernando, E., de Stanchina, E., Sulis, M. L., Barnes, K., Sawai, C., Homminga, I.*, et al.* (2009). Gamma-secretase inhibitors reverse glucocorticoid resistance in T cell acute lymphoblastic leukemia. Nat Med *15*, 50-58.

Reichardt, H. M., Kaestner, K. H., Tuckermann, J., Kretz, O., Wessely, O., Bock, R., Gass, P., Schmid, W., Herrlich, P., Angel, P., and Schutz, G. (1998). DNA binding of the glucocorticoid receptor is not essential for survival. Cell *93*, 531-541.

Reizis, B., and Leder, P. (2002). Direct induction of T lymphocyte-specific gene expression by the mammalian Notch signaling pathway. Genes Dev *16*, 295-300.

Reth, M., and Brummer, T. (2004). Feedback regulation of lymphocyte signalling. Nat Rev Immunol *4*, 269-277.

Rickert, R. C. (2013). New insights into pre-BCR and BCR signalling with relevance to B cell malignancies. Nat Rev Immunol *13*, 578-591.

Risso, D., Ngai, J., Speed, T. P., and Dudoit, S. (2014). Normalization of RNA-seq data using factor analysis of control genes or samples. Nat Biotechnol *32*, 896-902.

Robinson, M. D., McCarthy, D. J., and Smyth, G. K. (2010). edgeR: a Bioconductor package for differential expression analysis of digital gene expression data. Bioinformatics *26*, 139-140.

Roginskaya, V., Zuo, S., Caudell, E., Nambudiri, G., Kraker, A. J., and Corey, S. J. (1999). Therapeutic targeting of Src-kinase Lyn in myeloid leukemic cell growth. Leukemia *13*, 855-861.

Rothenberg, E. V., and Taghon, T. (2005). Molecular genetics of T cell development. Annu Rev Immunol *23*, 601-649.

Rubbi, L., Titz, B., Brown, L., Galvan, E., Komisopoulou, E., Chen, S. S., Low, T., Tahmasian, M., Skaggs, B., Muschen, M.*, et al.* (2011). Global phosphoproteomics reveals crosstalk between Bcr-Abl and negative feedback mechanisms controlling Src signaling. Sci Signal *4*, ra18.

Rubnitz, J. E., Behm, F. G., Curcio-Brint, A. M., Pinheiro, R. P., Carroll, A. J., Raimondi, S. C., Shurtleff, S. A., and Downing, J. R. (1996). Molecular analysis of t(11;19) breakpoints in childhood acute leukemias. Blood *87*, 4804-4808.

Sade, H., Krishna, S., and Sarin, A. (2004). The anti-apoptotic effect of Notch-1 requires p56lck-dependent, Akt/PKB-mediated signaling in T cells. J Biol Chem *279*, 2937-2944.

Saint-Ruf, C., Panigada, M., Azogui, O., Debey, P., von Boehmer, H., and Grassi, F. (2000). Different initiation of pre-TCR and gammadeltaTCR signalling. Nature *406*, 524-527.

Sambandam, A., Maillard, I., Zediak, V. P., Xu, L., Gerstein, R. M., Aster, J. C., Pear, W. S., and Bhandoola, A. (2005). Notch signaling controls the generation and differentiation of early T lineage progenitors. Nat Immunol *6*, 663-670.

Samtani, M. N., and Jusko, W. J. (2005). Comparison of dexamethasone pharmacokinetics in female rats after intravenous and intramuscular administration. Biopharm Drug Dispos *26*, 85-91.

Sanda, T., Lawton, L. N., Barrasa, M. I., Fan, Z. P., Kohlhammer, H., Gutierrez, A., Ma, W., Tatarek, J., Ahn, Y., Kelliher, M. A.*, et al.* (2012). Core transcriptional regulatory circuit controlled by the TAL1 complex in human T cell acute lymphoblastic leukemia. Cancer Cell *22*, 209-221.

Sanda, T., Tyner, J. W., Gutierrez, A., Ngo, V. N., Glover, J., Chang, B. H., Yost, A., Ma, W., Fleischman, A. G., Zhou, W.*, et al.* (2013). TYK2-STAT1-BCL2 pathway dependence in T-cell acute lymphoblastic leukemia. Cancer Discov *3*, 564-577.

Schade, A. E., Schieven, G. L., Townsend, R., Jankowska, A. M., Susulic, V., Zhang, R., Szpurka, H., and Maciejewski, J. P. (2008). Dasatinib, a small-molecule protein tyrosine kinase inhibitor, inhibits T-cell activation and proliferation. Blood *111*, 1366-1377.

Schamel, W. W., and Reth, M. (2007). The TCR binding site does move. Proc Natl Acad Sci U S A *104*, 16398-16399.

Scheinman, R. I., Gualberto, A., Jewell, C. M., Cidlowski, J. A., and Baldwin, A. S., Jr. (1995). Characterization of mechanisms involved in transrepression of NF-kappa B by activated glucocorticoid receptors. Mol Cell Biol *15*, 943-953.

Scherr, M., Kirchhoff, H., Battmer, K., Wohlan, K., Lee, C. W., Ricke-Hoch, M., Erschow, S., Law, E., Kloos, A., Heuser, M.*, et al.* (2018). Optimized induction of mitochondrial apoptosis for chemotherapy-free treatment of BCR-ABL+acute lymphoblastic leukemia. Leukemia.

Schluns, K. S., Kieper, W. C., Jameson, S. C., and Lefrancois, L. (2000). Interleukin-7 mediates the homeostasis of naive and memory CD8 T cells in vivo. Nat Immunol *1*, 426-432.

Schmedt, C., Saijo, K., Niidome, T., Kuhn, R., Aizawa, S., and Tarakhovsky, A. (1998). Csk controls antigen receptor-mediated development and selection of T-lineage cells. Nature *394*, 901-904.

Schwarz, B. A., and Bhandoola, A. (2004). Circulating hematopoietic progenitors with T lineage potential. Nat Immunol *5*, 953-960.

Schwarzer, A., Emmrich, S., Schmidt, F., Beck, D., Ng, M., Reimer, C., Adams, F. F., Grasedieck, S., Witte, D., Kabler, S.*, et al.* (2017). The non-coding RNA landscape of human hematopoiesis and leukemia. Nat Commun *8*, 218.

Scollay, R., Smith, J., and Stauffer, V. (1986). Dynamics of early T cells: prothymocyte migration and proliferation in the adult mouse thymus. Immunol Rev *91*, 129-157.

Seavitt, J. R., White, L. S., Murphy, K. M., Loh, D. Y., Perlmutter, R. M., and Thomas, M. L. (1999). Expression of the p56(Lck) Y505F mutation in CD45-deficient mice rescues thymocyte development. Mol Cell Biol *19*, 4200-4208.

Seddon, B., Legname, G., Tomlinson, P., and Zamoyska, R. (2000). Long-term survival but impaired homeostatic proliferation of Naive T cells in the absence of p56lck. Science *290*, 127-131.

Seddon, B., and Zamoyska, R. (2002a). TCR and IL-7 receptor signals can operate independently or synergize to promote lymphopenia-induced expansion of naive T cells. J Immunol *169*, 3752-3759.

Seddon, B., and Zamoyska, R. (2002b). TCR signals mediated by Src family kinases are essential for the survival of naive T cells. J Immunol *169*, 2997-3005.

Seong, R. H., Chamberlain, J. W., and Parnes, J. R. (1992). Signal for T-cell differentiation to a CD4 cell lineage is delivered by CD4 transmembrane region and/or cytoplasmic tail. Nature *356*, 718-720.

Serafin, V., Capuzzo, G., Milani, G., Minuzzo, S. A., Pinazza, M., Bortolozzi, R., Bresolin, S., Porcu, E., Frasson, C., Indraccolo, S.*, et al.* (2017). Glucocorticoid resistance is reverted by LCK inhibition in pediatric T-cell acute lymphoblastic leukemia. Blood *130*, 2750-2761.

Serwold, T., Hochedlinger, K., Swindle, J., Hedgpeth, J., Jaenisch, R., and Weissman, I. L. (2010). T-cell receptor-driven lymphomagenesis in mice derived from a reprogrammed T cell. Proc Natl Acad Sci U S A *107*, 18939-18943.

Shibata, H., Spencer, T. E., Onate, S. A., Jenster, G., Tsai, S. Y., Tsai, M. J., and O'Malley, B. W. (1997). Role of co-activators and co-repressors in the mechanism of steroid/thyroid receptor action. Recent Prog Horm Res *52*, 141-164; discussion 164-145.

Sicheri, F., and Kuriyan, J. (1997). Structures of Src-family tyrosine kinases. Curr Opin Struct Biol *7*, 777-785.

Sicinska, E., Aifantis, I., Le Cam, L., Swat, W., Borowski, C., Yu, Q., Ferrando, A. A., Levin, S. D., Geng, Y., von Boehmer, H., and Sicinski, P. (2003). Requirement for cyclin D3 in lymphocyte development and T cell leukemias. Cancer Cell *4*, 451-461.

Silverman, L. B., Gelber, R. D., Dalton, V. K., Asselin, B. L., Barr, R. D., Clavell, L. A., Hurwitz, C. A., Moghrabi, A., Samson, Y., Schorin, M. A.*, et al.* (2001). Improved outcome for children with acute lymphoblastic leukemia: results of Dana-Farber Consortium Protocol 91-01. Blood *97*, 1211-1218.

Simeonov, D. R., Gowen, B. G., Boontanrart, M., Roth, T. L., Gagnon, J. D., Mumbach, M. R., Satpathy, A. T., Lee, Y., Bray, N. L., Chan, A. Y.*, et al.* (2017). Discovery of

stimulation-responsive immune enhancers with CRISPR activation. Nature *549*, 111-115.

Sims, D., Mendes-Pereira, A. M., Frankum, J., Burgess, D., Cerone, M. A., Lombardelli, C., Mitsopoulos, C., Hakas, J., Murugaesu, N., Isacke, C. M.*, et al.* (2011). High-throughput RNA interference screening using pooled shRNA libraries and next generation sequencing. Genome Biol *12*, R104.

Sionov, R. V., Spokoini, R., Kfir-Erenfeld, S., Cohen, O., and Yefenof, E. (2008). Mechanisms regulating the susceptibility of hematopoietic malignancies to glucocorticoid-induced apoptosis. Adv Cancer Res *101*, 127-248.

Soulier, J., Clappier, E., Cayuela, J. M., Regnault, A., Garcia-Peydro, M., Dombret, H., Baruchel, A., Toribio, M. L., and Sigaux, F. (2005). HOXA genes are included in genetic and biologic networks defining human acute T-cell leukemia (T-ALL). Blood *106*, 274-286.

Squibb, B.-M. (2009). FDA Grants Full Approval for SPRYCEL® (dasatinib) for the Treatment of Adults with Chronic Myeloid Leukemia Who Are Resistant or Intolerant to Prior Therapies Including Gleevec.

Stefanova, I., Dorfman, J. R., and Germain, R. N. (2002). Self-recognition promotes the foreign antigen sensitivity of naive T lymphocytes. Nature *420*, 429-434.

Stein, P. L., Lee, H. M., Rich, S., and Soriano, P. (1992). pp59fyn mutant mice display differential signaling in thymocytes and peripheral T cells. Cell *70*, 741-750.

Stocklin, E., Wissler, M., Gouilleux, F., and Groner, B. (1996). Functional interactions between Stat5 and the glucocorticoid receptor. Nature *383*, 726-728.

Taghon, T., Yui, M. A., and Rothenberg, E. V. (2007). Mast cell lineage diversion of T lineage precursors by the essential T cell transcription factor GATA-3. Nat Immunol *8*, 845-855.

Talab, F., Allen, J. C., Thompson, V., Lin, K., and Slupsky, J. R. (2013). LCK is an important mediator of B-cell receptor signaling in chronic lymphocytic leukemia cells. Mol Cancer Res *11*, 541-554.

Team, R. C. (2017). R: a language and environment for statistical computing. R Found. Stat Comput Vienna, Austria.

Teh, H. S., Kisielow, P., Scott, B., Kishi, H., Uematsu, Y., Bluthmann, H., and von Boehmer, H. (1988). Thymic major histocompatibility complex antigens and the alpha beta T-cell receptor determine the CD4/CD8 phenotype of T cells. Nature *335*, 229-233.

Thomas, M. L. (1989). The leukocyte common antigen family. Annu Rev Immunol *7*, 339-369.

Thompson, B. J., Buonamici, S., Sulis, M. L., Palomero, T., Vilimas, T., Basso, G., Ferrando, A., and Aifantis, I. (2007). The SCFFBW7 ubiquitin ligase complex as a tumor suppressor in T cell leukemia. J Exp Med *204*, 1825-1835.

Thoms, J. A., Birger, Y., Foster, S., Knezevic, K., Kirschenbaum, Y., Chandrakanthan, V., Jonquieres, G., Spensberger, D., Wong, J. W., Oram, S. H.*, et al.* (2011). ERG promotes T-acute lymphoblastic leukemia and is transcriptionally regulated in leukemic cells by a stem cell enhancer. Blood *117*, 7079-7089.

Tibaldi, E., Brunati, A. M., Zonta, F., Frezzato, F., Gattazzo, C., Zambello, R., Gringeri, E., Semenzato, G., Pagano, M. A., and Trentin, L. (2011). Lyn-mediated SHP-1 recruitment to CD5 contributes to resistance to apoptosis of B-cell chronic lymphocytic leukemia cells. Leukemia *25*, 1768-1781.

Ting, C. N., Olson, M. C., Barton, K. P., and Leiden, J. M. (1996). Transcription factor GATA-3 is required for development of the T-cell lineage. Nature *384*, 474-478.

Tissing, W. J., Lauten, M., Meijerink, J. P., den Boer, M. L., Koper, J. W., Sonneveld, P., and Pieters, R. (2005a). Expression of the glucocorticoid receptor and its isoforms in relation to glucocorticoid resistance in childhood acute lymphocytic leukemia. Haematologica *90*, 1279-1281.

Tissing, W. J., Meijerink, J. P., den Boer, M. L., Brinkhof, B., and Pieters, R. (2005b). mRNA expression levels of (co)chaperone molecules of the glucocorticoid receptor are not involved in glucocorticoid resistance in pediatric ALL. Leukemia *19*, 727-733.

Tobler, A., Meier, R., Seitz, M., Dewald, B., Baggiolini, M., and Fey, M. F. (1992). Glucocorticoids downregulate gene expression of GM-CSF, NAP-1/IL-8, and IL-6, but not of M-CSF in human fibroblasts. Blood *79*, 45-51.

Tokarski, J. S., Newitt, J. A., Chang, C. Y., Cheng, J. D., Wittekind, M., Kiefer, S. E., Kish, K., Lee, F. Y., Borzillerri, R., Lombardo, L. J.*, et al.* (2006). The structure of Dasatinib (BMS-354825) bound to activated ABL kinase domain elucidates its inhibitory activity against imatinib-resistant ABL mutants. Cancer Res *66*, 5790-5797.

Torgersen, K. M., Vang, T., Abrahamsen, H., Yaqub, S., Horejsi, V., Schraven, B., Rolstad, B., Mustelin, T., and Tasken, K. (2001). Release from tonic inhibition of T cell activation through transient displacement of C-terminal Src kinase (Csk) from lipid rafts. J Biol Chem *276*, 29313-29318.

Tosello, V., Mansour, M. R., Barnes, K., Paganin, M., Sulis, M. L., Jenkinson, S., Allen, C. G., Gale, R. E., Linch, D. C., Palomero, T.*, et al.* (2009). WT1 mutations in T-ALL. Blood *114*, 1038-1045.

Townsend, E. C., Murakami, M. A., Christodoulou, A., Christie, A. L., Koster, J., DeSouza, T. A., Morgan, E. A., Kallgren, S. P., Liu, H., Wu, S. C.*, et al.* (2016). The Public Repository of Xenografts Enables Discovery and Randomized Phase II-like Trials in Mice. Cancer Cell *29*, 574-586.

Trageser, D., Iacobucci, I., Nahar, R., Duy, C., von Levetzow, G., Klemm, L., Park, E., Schuh, W., Gruber, T., Herzog, S.*, et al.* (2009). Pre-B cell receptor-mediated cell cycle arrest in Philadelphia chromosome-positive acute lymphoblastic leukemia requires IKAROS function. J Exp Med *206*, 1739-1753.

Tremblay, C. S., Brown, F. C., Collett, M., Saw, J., Chiu, S. K., Sonderegger, S. E., Lucas, S. E., Alserihi, R., Chau, N., Toribio, M. L.*, et al.* (2016). Loss-of-function mutations of Dynamin 2 promote T-ALL by enhancing IL-7 signalling. Leukemia *30*, 1993-2001.

Trentin, L., Frasson, M., Donella-Deana, A., Frezzato, F., Pagano, M. A., Tibaldi, E., Gattazzo, C., Zambello, R., Semenzato, G., and Brunati, A. M. (2008). Geldanamycin-induced Lyn dissociation from aberrant Hsp90-stabilized cytosolic complex is an early event in apoptotic mechanisms in B-chronic lymphocytic leukemia. Blood *112*, 4665-4674.

Trimarchi, T., Bilal, E., Ntziachristos, P., Fabbri, G., Dalla-Favera, R., Tsirigos, A., and Aifantis, I. (2014). Genome-wide mapping and characterization of Notch-regulated long noncoding RNAs in acute leukemia. Cell *158*, 593-606.

Turner, J. M., Brodsky, M. H., Irving, B. A., Levin, S. D., Perlmutter, R. M., and Littman, D. R. (1990). Interaction of the unique N-terminal region of tyrosine kinase p56lck with cytoplasmic domains of CD4 and CD8 is mediated by cysteine motifs. Cell *60*, 755-765.

UK, C. R. (2018). A trial looking at selumetinib and dexamethasone for acute lymphoblastic leukaemia (SeluDex). In.

Vacchio, M. S., and Ashwell, J. D. (1997). Thymus-derived glucocorticoids regulate antigen-specific positive selection. J Exp Med *185*, 2033-2038.

Van Laethem, F., Baus, E., Smyth, L. A., Andris, F., Bex, F., Urbain, J., Kioussis, D., and Leo, O. (2001). Glucocorticoids attenuate T cell receptor signaling. J Exp Med *193*, 803-814.

Van Limbergen, H., Beverloo, H. B., van Drunen, E., Janssens, A., Hahlen, K., Poppe, B., Van Roy, N., Marynen, P., De Paepe, A., Slater, R., and Speleman, F. (2001). Molecular cytogenetic and clinical findings in ETV6/ABL1-positive leukemia. Genes Chromosomes Cancer *30*, 274-282.

van Oers, N. S., Tao, W., Watts, J. D., Johnson, P., Aebersold, R., and Teh, H. S. (1993). Constitutive tyrosine phosphorylation of the T-cell receptor (TCR) zeta subunit: regulation of TCR-associated protein tyrosine kinase activity by TCR zeta. Mol Cell Biol *13*, 5771-5780.

Van Vlierberghe, P., and Ferrando, A. (2012). The molecular basis of T cell acute lymphoblastic leukemia. J Clin Invest *122*, 3398-3406.

Van Vlierberghe, P., Palomero, T., Khiabanian, H., Van der Meulen, J., Castillo, M., Van Roy, N., De Moerloose, B., Philippe, J., Gonzalez-Garcia, S., Toribio, M. L.*, et al.* (2010). PHF6 mutations in T-cell acute lymphoblastic leukemia. Nat Genet *42*, 338-342.

Van Vlierberghe, P., van Grotel, M., Tchinda, J., Lee, C., Beverloo, H. B., van der Spek, P. J., Stubbs, A., Cools, J., Nagata, K., Fornerod, M.*, et al.* (2008). The recurrent SET-NUP214 fusion as a new HOXA activation mechanism in pediatric T-cell acute lymphoblastic leukemia. Blood *111*, 4668-4680.

Verbeek, S., Izon, D., Hofhuis, F., Robanus-Maandag, E., te Riele, H., van de Wetering, M., Oosterwegel, M., Wilson, A., MacDonald, H. R., and Clevers, H. (1995). An HMG-box-containing T-cell factor required for thymocyte differentiation. Nature *374*, 70-74.

von Boehmer, H. (2005). Unique features of the pre-T-cell receptor alpha-chain: not just a surrogate. Nat Rev Immunol *5*, 571-577.

von Boehmer, H., and Fehling, H. J. (1997). Structure and function of the pre-T cell receptor. Annu Rev Immunol *15*, 433-452.

Wagner, D. H., Jr., Hagman, J., Linsley, P. S., Hodsdon, W., Freed, J. H., and Newell, M. K. (1996). Rescue of thymocytes from glucocorticoid-induced cell death mediated by CD28/CTLA-4 costimulatory interactions with B7-1/B7-2. J Exp Med *184*, 1631-1638.

Wakabayashi, Y., Watanabe, H., Inoue, J., Takeda, N., Sakata, J., Mishima, Y., Hitomi, J., Yamamoto, T., Utsuyama, M., Niwa, O.*, et al.* (2003). Bcl11b is required for differentiation and survival of alphabeta T lymphocytes. Nat Immunol *4*, 533-539.

Wan, R., Wu, J., Ouyang, M., Lei, L., Wei, J., Peng, Q., Harrison, R., Wu, Y., Cheng, B., Li, K.*, et al.* (2019). Biophysical basis underlying dynamic Lck activation visualized by ZapLck FRET biosensor. Sci Adv *5*, eaau2001.

Wang, J., Liu, Y., Tan, L. X., Lo, J. C., Du, J., Ryu, M. J., Ranheim, E. A., and Zhang, J. (2011). Distinct requirements of hematopoietic stem cell activity and Nras G12D signaling in different cell types during leukemogenesis. Cell Cycle *10*, 2836-2839.

Weber, B. N., Chi, A. W., Chavez, A., Yashiro-Ohtani, Y., Yang, Q., Shestova, O., and Bhandoola, A. (2011). A critical role for TCF-1 in T-lineage specification and differentiation. Nature *476*, 63-68.

Wei, G., Abraham, B. J., Yagi, R., Jothi, R., Cui, K., Sharma, S., Narlikar, L., Northrup, D. L., Tang, Q., Paul, W. E.*, et al.* (2011). Genome-wide analyses of transcription factor GATA3-mediated gene regulation in distinct T cell types. Immunity *35*, 299-311.

Wei, G., Twomey, D., Lamb, J., Schlis, K., Agarwal, J., Stam, R. W., Opferman, J. T., Sallan, S. E., den Boer, M. L., Pieters, R.*, et al.* (2006). Gene expression-based chemical genomics identifies rapamycin as a modulator of MCL1 and glucocorticoid resistance. Cancer Cell *10*, 331-342.

Weng, A. P., Ferrando, A. A., Lee, W., Morris, J. P. t., Silverman, L. B., Sanchez-Irizarry, C., Blacklow, S. C., Look, A. T., and Aster, J. C. (2004). Activating mutations of NOTCH1 in human T cell acute lymphoblastic leukemia. Science *306*, 269-271.

Williams, B. L., Schreiber, K. L., Zhang, W., Wange, R. L., Samelson, L. E., Leibson, P. J., and Abraham, R. T. (1998). Genetic evidence for differential coupling of Syk family kinases to the T-cell receptor: reconstitution studies in a ZAP-70-deficient Jurkat T-cell line. Mol Cell Biol *18*, 1388-1399.

Woodgett, J. R., and Ohashi, P. S. (2005). GSK3: an in-Toll-erant protein kinase? Nat Immunol *6*, 751-752.

Wossning, T., Herzog, S., Kohler, F., Meixlsperger, S., Kulathu, Y., Mittler, G., Abe, A., Fuchs, U., Borkhardt, A., and Jumaa, H. (2006). Deregulated Syk inhibits differentiation and induces growth factor-independent proliferation of pre-B cells. J Exp Med *203*, 2829-2840.

Wright, D. D., Sefton, B. M., and Kamps, M. P. (1994). Oncogenic activation of the Lck protein accompanies translocation of the LCK gene in the human HSB2 T-cell leukemia. Mol Cell Biol *14*, 2429-2437.

Xie, M., Yang, A., Ma, J., Wu, M., Xu, H., Wu, K., Jin, Y., and Xie, Y. (2019). Akt2 mediates glucocorticoid resistance in lymphoid malignancies through FoxO3a/Bim axis and serves as a direct target for resistance reversal. Cell Death Dis *9*, 1013.

Xiong, H., Maraver, A., Latkowski, J. A., Henderson, T., Schlessinger, K., Ding, Y., Shen, J., Tadokoro, C. E., and Lafaille, J. J. (2013). Characterization of two distinct lymphoproliferative diseases caused by ectopic expression of the Notch ligand DLL4 on T cells. PLoS One *8*, e84841.

Yamasaki, S., and Saito, T. (2007). Molecular basis for pre-TCR-mediated autonomous signaling. Trends Immunol *28*, 39-43.

Yang-Yen, H. F., Chambard, J. C., Sun, Y. L., Smeal, T., Schmidt, T. J., Drouin, J., and Karin, M. (1990). Transcriptional interference between c-Jun and the glucocorticoid receptor: mutual inhibition of DNA binding due to direct protein-protein interaction. Cell *62*, 1205-1215.

Yang, L., Panetta, J. C., Cai, X., Yang, W., Pei, D., Cheng, C., Kornegay, N., Pui, C. H., and Relling, M. V. (2008). Asparaginase may influence dexamethasone pharmacokinetics in acute lymphoblastic leukemia. J Clin Oncol *26*, 1932-1939.

Zacharchuk, C. M., Mercep, M., Chakraborti, P. K., Simons, S. S., Jr., and Ashwell, J. D. (1990). Programmed T lymphocyte death. Cell activation- and steroid-induced pathways are mutually antagonistic. J Immunol *145*, 4037-4045.

Zamoyska, R., Basson, A., Filby, A., Legname, G., Lovatt, M., and Seddon, B. (2003). The influence of the src-family kinases, Lck and Fyn, on T cell differentiation, survival and activation. Immunol Rev *191*, 107-118.

Zeiner, M., and Gehring, U. (1995). A protein that interacts with members of the nuclear hormone receptor family: identification and cDNA cloning. Proc Natl Acad Sci U S A *92*, 11465-11469.

Zenatti, P. P., Ribeiro, D., Li, W., Zuurbier, L., Silva, M. C., Paganin, M., Tritapoe, J., Hixon, J. A., Silveira, A. B., Cardoso, B. A.*, et al.* (2011). Oncogenic IL7R gain-of-function mutations in childhood T-cell acute lymphoblastic leukemia. Nat Genet *43*, 932-939.

Zhang, G., Zhang, L., and Duff, G. W. (1997). A negative regulatory region containing a glucocorticosteroid response element (nGRE) in the human interleukin-1beta gene. DNA Cell Biol *16*, 145-152.

Zhang, J., Grindley, J. C., Yin, T., Jayasinghe, S., He, X. C., Ross, J. T., Haug, J. S., Rupp, D., Porter-Westpfahl, K. S., Wiedemann, L. M.*, et al.* (2006). PTEN maintains

haematopoietic stem cells and acts in lineage choice and leukaemia prevention. Nature *441*, 518-522.

Zhang, J. A., Mortazavi, A., Williams, B. A., Wold, B. J., and Rothenberg, E. V. (2012). Dynamic transformations of genome-wide epigenetic marking and transcriptional control establish T cell identity. Cell *149*, 467-482.

Zhao, Y., Tozawa, Y., Iseki, R., Mukai, M., and Iwata, M. (1995). Calcineurin activation protects T cells from glucocorticoid-induced apoptosis. J Immunol *154*, 6346-6354.

Zhong, Y., Jiang, L., Hiai, H., Toyokuni, S., and Yamada, Y. (2007). Overexpression of a transcription factor LYL1 induces T- and B-cell lymphoma in mice. Oncogene *26*, 6937-6947.

Zuurbier, L., Petricoin, E. F., 3rd, Vuerhard, M. J., Calvert, V., Kooi, C., Buijs-Gladdines, J. G., Smits, W. K., Sonneveld, E., Veerman, A. J., Kamps, W. A.*, et al.* (2012). The significance of PTEN and AKT aberrations in pediatric T-cell acute lymphoblastic leukemia. Haematologica *97*, 1405-1413.

Zwaan, C. M., Rizzari, C., Mechinaud, F., Lancaster, D. L., Lehrnbecher, T., van der Velden, V. H., Beverloo, B. B., den Boer, M. L., Pieters, R., Reinhardt, D.*, et al.* (2013). Dasatinib in children and adolescents with relapsed or refractory leukemia: results of the CA180-018 phase I dose-escalation study of the Innovative Therapies for Children with Cancer Consortium. J Clin Oncol *31*, 2460-2468.